

INAUGURAL-DISSERTATION

ZUR ERLANGUNG DER DOKTORWÜRDE
DER GESAMTFAKULTÄT FÜR MATHEMATIK,
INGENIEUR- UND NATURWISSENSCHAFTEN
DER RUPRECHT-KARLS-UNIVERSITÄT
HEIDELBERG

Vorgelegt von

Simon Alexander Hammerich

Tag der mündlichen Prüfung: 25.10.2024

CHARACTERIZATION OF
URANIUM OXIDE MICROPARTICLES
FOR QUALITY CONTROL
IN NUCLEAR SAFEGUARDS APPLICATIONS

Gutachter:

Prof. Dr. Axel K. Schmitt

Prof. Dr. Mario Trieloff

September 2024

Abstract

The International Atomic Energy Agency's (IAEA) main goal is the support and development of nuclear technology for non-military purposes. This includes the verification of peaceful use of nuclear material and technologies within the Treaty on the Non-Proliferation of Nuclear Weapons (NPT). Therefore, technical measures – the IAEA Safeguards – were introduced to assure the compliance with the treaty by its member states. Among other safeguards measures, the IAEA conducts inspections of nuclear facilities during which environmental swipe samples are taken by the delegates. The dust grains in these environmental samples are shipped to the IAEA Safeguards Analytical Services' Environmental Sampling Laboratory (SGAS-ESL) and IAEA's worldwide partners in the Network of Analytical Laboratories (NWAL) for isotopic abundance analysis using mass-spectrometric techniques such as Large Geometry-Secondary Ion Mass Spectrometry (LG-SIMS). The goal of these analyses is either to confirm the handling of nuclear material according to the member state's declarations to the IAEA or to reveal undeclared activities.

To ensure the quality of these measurements, microparticle reference materials that are similar to the environmental samples in shape and size as well as elemental and isotopic composition are of dire need. In the safeguards laboratories of Forschungszentrum Jülich (FZJ), an aerosol-based process is used for the production of potential uranium oxide microparticle reference materials. However, capacities for characterization measurements of potential reference materials are limited. Thus, the microparticles produced in FZJ are analyzed in the Heidelberg Ion Probe (HIP) laboratories at the Institute of Earth Sciences, Heidelberg University as part of a cooperation program.

In this thesis, the implementation of a transparent and effective measurement setup at the HIP lab is described. First approaches built up on an already prevalent configuration yielded promising results for the isotopic abundance measurements of single particles, but were not suitable for the characterization of an entire particle population with the CAMECA-developed Automated Particle Measurement (APM) software. A second approach based on the IAEA SGAS-ESL measurement protocol resulted in satisfying results for both single particle analyses and measurements of entire particle planchets with the APM software. The functionality of this setup was confirmed by the measurement of FZJ-produced aerosol-generated uranium oxide microparticles and certified reference materials from New Brunswick Laboratory's (NBL) "CRM U" series.

Within the work of this thesis, three IAEA-requested batches of microparticulate reference materials were characterized using LG-SIMS. The characterization process of two batches, FZJ-3050P and FZJ-3090P is described here. The measurements confirmed the compliance with the IAEA requirements for potential reference materials. The isotopic composition of a pre-defined number of random single particles measurements was in good agreement with the certificate values of the source material. APM measurements excluded the possibility of contamination with material of different uranium isotopic composition and confirmed the requested number of particles on a sample planchet as well as their homogeneous distribution. The results for both particle batches together with quality control measurements for the cleaning step used in the FZJ safeguards laboratories verified the suitability and high-quality standards of the aerosol-based microparticle production process used by the particle producers of FZJ.

A core requirement for a potential microparticulate reference material is the assurance of a practical shelf-life. Previous studies of uranium oxide microparticles produced with an aerosol-based process demonstrated possible alteration leading to the formation of uranium hydroxides like schoepite. To address these issues, a comprehensive shelf-life investigation of uranium oxide microparticles was conducted. Particle stability in three different potentially suitable atmospheric storage conditions with an additional sample in an unrealistically harsh fourth environment to accelerate possible alteration was investigated. Accordingly, particle shelf-life in dispersions with four alcoholic potential long-term storage media was examined. After more than one year, the investigations confirmed the hypothesis that the microparticle shelf-life heavily depends on the amount of water in the respective storage conditions. Continuous storage in a water-saturated atmosphere lead to alteration, formation of uranyl hydroperoxides, uranium mobilization and fractionation and therefore rendered the particles useless for the purpose as reference material. The other three conditions kept the particles stable over the course of the investigation with an inert argon atmosphere showing the most promising results. Accordingly, the isotopic abundance in all four alcoholic storage media remained unchanged over the course of nearly two years. Particles stored in *tert*-butanol showed the highest stability.

Some additional insights for the measurement of uranium oxide microparticles could be obtained in measurement sessions over the course of three years. Examples are the possible influence of secondary ion beam aberrations, measurement dependency on sample stage focus and sample area signal. This leads to the conclusion, that a reliable measurement setup for uranium microparticles needs continuous review and development.

Zusammenfassung

Das Ziel der Internationalen Atomenergieorganisation (IAEA) ist es, die nichtmilitärische Nutzung der Kerntechnologie zu fördern. Dazu gehört die Verifizierung der im Atomwaffensperrvertrag (NPT) festgehaltene friedliche Verwendung von Kernmaterial und Kerntechnologien. Daher wurden technische Maßnahmen – die IAEA Safeguards – eingeführt, um die Vertragseinhaltung durch seine Mitgliedsstaaten zu gewährleisten. Unter anderem führt die IAEA deshalb Inspektionen von Nuklearanlagen durch, im Zuge derer auch Umweltproben genommen werden. Die dabei beprobten Staubkörner werden zur massenspektrometrischen Bestimmung der Isotopie unter anderem durch Large Geometry-Sekundärionenmassenspektrometrie (LG-SIMS) zum IAEA-eigenen Safeguards Analytical Services Environmental Sampling Laboratory (SGAS-ESL) sowie den weltweiten Partnern im Network of Analytical Laboratories (NWAL) versandt. Ziel dieser Analysen ist der Nachweis des vertragsgerechten Umgangs mit Kernmaterial oder die Enthüllung nicht deklarerter Aktivitäten des Mitgliedsstaates.

Für hochqualitative Messungen werden Referenzmaterialien benötigt, die den gesammelten Umweltproben in Form und Größe sowie Isotopenzusammensetzung ähnlich sind. In den Safeguards-Laboratorien des Forschungszentrums Jülich (FZJ) werden potentielle Uranoxid-Mikropartikelreferenzmaterialien in einem Aerosol-basierten Prozess hergestellt. Allerdings sind die Kapazitäten für Charakterisierungsmessungen der potentiellen Referenzmaterialien begrenzt. Daher werden im FZJ hergestellte Mikropartikel im Zuge eines Kooperationsprogramms an der Heidelberg Ion Probe (HIP) am Institut für Geowissenschaften der Universität Heidelberg analysiert.

In dieser Arbeit wird die Implementierung eines transparenten und effektiven Messprozesses an der HIP dargestellt. Erste, auf der bereits bestehenden Konfiguration aufbauende Ansätze lieferten vielversprechende Ergebnisse der Isotopiemessungen, konnten allerdings nicht für die Charakterisierung des Partikelbestands einer Probe mithilfe der von CAMECA entwickelten Automated Particle Measurement (APM)-Software genutzt werden. Ein zweiter, auf dem Messprotokoll des SGAS-ESL basierender Ansatz erbrachte sowohl bei den Einzelpartikelmessungen als auch bei APM-Messungen des gesamten Partikelbestands zufriedenstellende Ergebnisse. Die Funktionalität dieses Setups konnte durch Messungen von in Jülich hergestellten Uranoxid-Mikropartikeln sowie von zertifizierten Referenzmaterialien der New Brunswick Laboratory (NBL) „CRM U“-Serie bestätigt werden.

Im Zuge dieser Arbeit wurden drei von der IAEA bestellte Referenzpartikel-Batches durch LG-SIMS-Messungen charakterisiert. Der Charakterisierungsprozess der beiden Batches FZJ-3050P und FZJ-3090P wird hier erläutert. In den Messungen konnte die Einhaltung der IAEA-Vorgaben bestätigt werden. Die Isotopie einer vorher definierten Anzahl zufällig ausgewählter Partikel entsprach den Zertifikatswerten des bei der Produktion verwendeten Ausgangsmaterials. Durch APM-Messungen konnte eine mögliche Kontamination mit Partikeln abweichender Isotopie ausgeschlossen und die gewünschte Partikelanzahl und -verteilung bestätigt werden. Die Messergebnisse beider Batches und zusätzliche Kontrollmessungen zur Überprüfung des im FZJ verwendeten Reinigungsprozesses konnten die Eignung und Qualität des in Jülich verwendeten Aerosol-basierten Herstellungsprozesses bestätigen.

Eine garantierte Haltbarkeitsdauer ist von zentraler Bedeutung für ein potentielles Mikropartikel-Referenzmaterial. In vorherigen Studien zeigten Uranoxid-Mikropartikel, die in einem aerosol-basierten Prozess hergestellt wurden, mögliche Anzeichen von Alteration bis hin zur Bildung von Uran-Hydroxiden wie zum Beispiel Schoepit. Zur näheren Beleuchtung dieser Aspekte wurde eine umfassende Haltbarkeitsstudie der Uranoxid-Mikropartikel durchgeführt. Die Partikel wurden unter drei ausgewählten Schutzatmosphären und als Referenz unter absichtlich alterierenden Bedingungen gelagert. Außerdem wurden die Partikel in vier verschiedenen Alkanolen in Dispersion gebracht und regelmäßig untersucht. Nach mehr als einem Jahr Lagerdauer bestätigte sich die Hypothese, dass die Haltbarkeit der Mikropartikel stark vom Wassergehalt abhängig ist. Anhaltende Lagerung in einer wassergesättigten Umgebung führte zu Alteration, Bildung von Uran-Hydroperoxiden sowie Uranmobilisierung und -fraktionierung und beeinträchtigte die Eignung der Partikel als Referenzmaterialien immens bis hin zur Unbenutzbarkeit. Unter den anderen drei Bedingungen blieben die Partikel stabil, wobei die Lagerung in Argon die besten Ergebnisse erzielte. Entsprechend dazu blieb die Isotopie der Partikel in allen vier Alkanol-Dispersionen über eine Lagerzeit von fast zwei Jahren unverändert. Die höchste Stabilität zeigten Partikel in *tert*-Butanol.

Im Zuge der über drei Jahre verteilten Messkampagnen konnten einige zusätzliche Erkenntnisse zur Messung von Uranoxid-Mikropartikeln gewonnen werden. Beispiele hierfür sind ein möglicher Einfluss von Aberrationen im Sekundärionenstrahl sowie die Abhängigkeit der Messergebnisse vom Fokuspunkt der Probenbühne und von der Fläche des gemessenen Signals auf der Probenoberfläche. Daher lässt sich schlussfolgern, dass ein verlässlicher Prozess zur Messung von Uran-Mikropartikeln regelmäßiger Überprüfung und Weiterentwicklung bedarf.

Table of Contents

Abstract	III
Zusammenfassung	V
Table of Contents	VII
1 Introduction	1
2 Scientific and historical background.....	5
2.1 Production of uranium oxide microparticles	5
2.1.1 Overview of production approaches	5
2.1.2 Production approach at IEK-6.....	6
2.2 Structural investigation.....	8
2.3 Mass-spectrometric measurement of uranium enrichment	11
3 Materials and Methods	15
3.1 Particle production at FZJ using a VOAG	15
3.2 Particle deposition.....	17
3.2.1 Direct collection	17
3.2.2 Dispersion step.....	19
3.3 Isotopic abundance measurements using SIMS	20
3.3.1 Microparticle measurements.....	22
3.3.2 Automated Particle Measurement (APM)	23
3.4 Shelf-life investigation	24
3.4.1 Storage conditions.....	24
3.4.1.1 Atmospheric shelf-life study	24
3.4.1.2 Dispersion shelf-life study	25
3.4.2 Scanning Electron Microscopy	25
3.4.3 μ -Raman spectroscopy	26
4 Results and Discussion	27
4.1 SIMS measurements.....	27
4.1.1 First steps using a mixed EM and FC detector setup	27
4.1.2 Full EM detector setup	31

Table of Contents

4.1.3	Uranium isotopic composition of <i>Lanthanide</i> -doped microparticles	42
4.1.4	APM verification.....	44
4.2	SIMS characterization of IAEA-requested uranium microparticles.....	49
4.2.1	Glassy Carbon Disk blank.....	49
4.2.2	LG-SIMS measurements of FZJ-3050P	50
4.2.2.1	Microparticle measurements.....	51
4.2.2.2	APM measurements.....	54
4.2.3	LG-SIMS measurements of FZJ-3090P	57
4.2.3.1	Microparticle measurements.....	57
4.2.3.2	APM measurements.....	59
4.2.4	Cleaning process verification.....	63
4.2.4.1	FZJ-3050P blank.....	63
4.2.4.2	Intentional contamination	65
4.3	Uranium microparticle shelf-life.....	70
4.3.1	Atmospheric shelf-life investigation.....	70
4.3.1.1	SEM investigation	70
4.3.1.2	μ -Raman spectroscopy	73
4.3.1.3	SIMS ion images.....	80
4.3.1.4	Uranium isotopic abundance of microparticles stored in different atmospheres 84	
4.3.2	Particle shelf-life in alcoholic dispersion.....	88
4.3.2.1	Ethanol	90
4.3.2.2	2-Propanol.....	92
4.3.2.3	<i>n</i> -Butanol.....	94
4.3.2.4	<i>tert</i> -Butanol.....	96
4.3.2.5	Uranium isotopic abundance of microparticles stored in different alcoholic solvents 98	
4.4	Insights for SIMS measurement setup.....	100
4.4.1	Secondary ion beam aberrations	100

4.4.2	Influence of Z-axis centering on APM measurements	104
4.4.3	Signal size in sputtered area	106
5	Conclusion and Outlook.....	109
6	Appendices.....	112
6.1	Detailed μ -Raman spectra	112
6.2	Additional Isotopic Abundance Measurements.....	118
6.2.1	Atmospheric Shelf-Life Investigation.....	118
6.2.2	Dispersion Shelf-Life Investigation	120
	List of Tables.....	122
	List of Figures.....	123
	List of Abbreviations	127
	Acknowledgements	130
	Literature	132

1 Introduction

The International Atomic Energy Agency (IAEA) is an international organization that promotes the peaceful use of nuclear energy (a list with all abbreviations can be found at the end). In the Statute of the IAEA, its objectives are described as follows:

“The Agency shall seek to accelerate and enlarge the contribution of atomic energy to peace, health and prosperity throughout the world. It shall ensure, so far as it is able, that assistance provided by it or at its request or under its supervision or control is not used in such a way as to further any military purpose.”

(IAEA Statute, 23 October 1956 [1])

Within these objectives, the IAEA seeks to regulate the use of nuclear material to prevent military use through various international treaties. The most important one for this task is the Treaty on the Non-Proliferation of Nuclear Weapons (NPT) [2]. The treaty was signed by 191 member nations and was extended indefinitely in 1995 [3]. The member states declare not to pursue obtaining nuclear weapons and to use nuclear technologies only for peaceful purposes. To verify that the member states comply with these obligations, the IAEA is allowed to implement a set of measures – the IAEA safeguards [4]. In 2024, 182 non-nuclear weapon states who are signing nations of the treaty have comprehensive safeguard agreements (CSA) with the IAEA to allow IAEA safeguards inspectors to verify the fulfilment of their safeguards obligations and to ensure the peaceful use of nuclear materials and technology [3]. CSAs with four more nations are in process.

One part of the verification measures for nuclear safeguards is the on-site investigation of IAEA safeguards inspectors in nuclear facilities of the NPT member states. In a first step, the IAEA inspectors verify the reports provided by the member state. The nuclear material present is reviewed with a wide spectrum of non-destructive analysis methods on-site, for example item counting, weighing, and the use of radiation detectors such as gamma spectrometers. During these inspections, there are also samples taken from the nuclear inventory and shipped to the IAEA laboratories for a very accurate determination of the concentration of nuclear material in a destructive assay [5]. These samples are measured in the Nuclear Material Laboratory (NML) in the facilities of the Safeguards Analytical Services (SGAS) in Seibersdorf, Austria [6].

Analysis of the nuclear material may yield information about the material declared by the member state, but it does not verify the absence of undeclared activity. The IAEA made this experience in the early 1990s, when both the Iraq and the Democratic People’s Republic of Korea were found to conduct undeclared nuclear activities, although both countries had ongoing

safeguards agreements with the IAEA [7]. In 1993, the IAEA started a new program to enhance its ability to detect undeclared nuclear material and to strengthen the IAEA safeguards. This led to the introduction of the Additional Protocol (AP) for member states that have a CSA with the IAEA in 1997. Within this AP, the IAEA's inspectors gain expanded rights and access to information about nuclear facilities of the signing states. In 2024, 141 states and the European Atomic Energy Community Euratom have brought APs into force with another 14 APs signed but not yet implemented [8].

Besides the early provision of design information and the use of satellite imagery, environmental sampling is a powerful tool to exclude the possibility of undeclared activity. Environmental samples are samples of air, water, vegetation, soil or smears that assist the IAEA to verify the absence of undeclared nuclear activity. The majority are smear samples consisting of dust taken with cotton swipes from specific locations inside nuclear facilities (Figure 1).



Figure 1: Inspectors taking a swipe sample at a nuclear facility. Photo: IAEA Department of Safeguards, Copyright IAEA, 2016 [9].

Within the entirety of the dust particles on the cotton swipes, traces of nuclear activities conducted in the member states' facility are present in the form of microparticulate dust grains. The samples are shipped to the Environmental Sampling Laboratory (ESL) of the SGAS in Seibersdorf, Austria [10]. They can be investigated either using bulk analysis or particle analysis tools [11; 12]. For bulk analysis, all material collected on the swipe sample is dissolved and the

bulk isotopic composition of the nuclear material is determined. Any deviation from declared enrichment values can indicate undeclared activity.

In particle analysis, single dust particles on the cotton swipes are identified and their isotopic composition is measured individually with different mass-spectrometric techniques [13]. One of the methods universally used for microparticle analysis in nuclear safeguards is Large Geometry-Secondary Ion Mass Spectrometry (LG-SIMS) [13-16]. Using LG-SIMS single particle analysis, even slightest traces of undeclared nuclear activities such as uranium enrichment above values usually necessary for civilian energy production can be identified, as it was demonstrated in the IAEA inspection activities in Iran in the Joint Comprehensive Plan of Action released in 2015, despite the politically-driven retreat from the agreement by the government of Iran in 2020. In fact, implemented IAEA safeguards did prove the enrichment to weapons-grade uranium [17].

Because the capacities of the IAEA SGAS-ESL are insufficient for all the swipe samples collected, the IAEA coordinates and operates with a worldwide Network of Analytical Laboratories (NWAL) [18]. Besides NWAL facilities using other analysis methods, there are currently seven laboratories world-wide qualified by the IAEA to support the NWAL with LG-SIMS measurements on environmental samples in 2023 (pers. information, Marc Humphrey, IAEA).

Both the NWAL facilities as well as the IAEA SGAS-ESL are dependent on Quality Control (QC) measurements to ensure the provision of reliable results. For LG-SIMS, QC measurements have to be conducted on a daily basis to monitor the measurements quality and to obtain data that is essential for the measurement of unknown samples and to observe changes in the instrument calibration [15; 19]. These QC measurements can only be conducted with well-defined and well-characterized reference materials that are similar in composition, size and shape to the unknown sample materials [14]. Until the late 2010s the only Certified Reference Materials (CRMs) in use suitable for this task were the "NBL CRM U" series of U_3O_8 powders representing a wide range of ^{235}U enrichment. However, these CRMs were produced and certified in the 1970s [20]. The supply of these reference materials is limited and they are not suitable for every measurement. Therefore, the nuclear safeguards community with all the analytical laboratories is in dire need of new, tailor-made reference materials that can be used for QC tasks that are urgent today and a production process that can provide reference materials that can easily be adjusted for new tasks in the future [21; 22]. Other requirements for a possible reference material are a monodisperse size distribution for analysis technique development, sample-to-sample homogeneity and structural and chemical stability over the intended duration of use.

The safeguards laboratories at the Institute of Energy and Climate Research – Nuclear Waste Management and Reactor Safety (IEK-6) at Forschungszentrum Jülich (FZJ), Germany, have

developed and refined a process to produce monodisperse uranium oxide microparticles that are intended as future reference materials by the IAEA and its NWAL member states. However, the production of reference materials is just half of the IAEA requirements. The IAEA requires a potential reference material to be well-characterized concerning its shape, structure, size, chemical composition and most importantly isotopic abundance. It has to be guaranteed that the provided uranium microparticle batches consist of homogeneous particles and do not show any signs of chemical or isotopic contamination. In addition, it is essential to provide an estimation about the particles' stability and to investigate different storage conditions [23]. This led to challenges for the FZJ safeguards laboratories, because they are not in possession of suitable mass-spectrometric analysis tools to analyze single microparticles such as LG-SIMS.

Because of the extensive amount of regular field samples from safeguards inspectors (the IAEA SGAS-ESL alone currently measures approximately 400 field samples per year [10]), the IAEA and the NWAL member laboratories lack the capacities to support potential reference material providers in the characterization of their produced microparticles. In order to still be able to deliver well-characterized microparticles as potential reference materials, the IEK-6 of FZJ and the Heidelberg Ion Probe (HIP) group of the Institute of Earth Sciences, Heidelberg University, Germany, have combined their resources to provide a comprehensive particle characterization in a cooperation program.

The first aim of this work is to document the successful implementation of a uranium measurement setup at the HIP laboratories. This contains the screening-mode analysis of whole particle populations on a sample planchet as well as the targeted measurement of single uranium particles with different isotopic abundances. The successful implementation is a prerequisite for subsequent characterization of various uranium microparticle productions provided by the FZJ safeguards laboratories in an adequate way to finish the particle batches for the distribution as potential reference materials.

In a second part of this thesis research, the physical, chemical, structural and isotopic stability of uranium oxide microparticles provided by FZJ under different storage conditions were investigated. A comprehensive shelf-life study was carried out to assess structural and chemical integrity of particles stored in different environments with the goal to provide users of the potential particle reference materials with robust recommendations concerning storage conditions and storage time.

2 Scientific and historical background

2.1 Production of uranium oxide microparticles

2.1.1 Overview of production approaches

The IAEA is in urgent need of qualified and well-characterized microparticle reference materials [21]. To meet the demand, several different approaches for the production of microparticles have been investigated before [24-26]. One possible approach was blending of borosilicate powder with certified U_3O_8 powders to create uranium glass. This glass was later grinded and milled and provided sharp-edged, irregular particles with a size of 20–30 μm [27]. The resulting glasses were later certified as reference materials for uranium isotopic abundance [28]. At the Joint Research Centre – Institute for Reference Materials and Measurements (JRC-IRMM), Kips *et al.* [29] used hydrolysis of certified UF_6 to produce uranium oxifluoride particles and collect them on glassy carbon disks (GCDs). Scanning Electron Microscope (SEM) and SIMS investigations later revealed, that the produced particles are inhomogeneous and tend to form particle agglomerations [30-32].

Research groups from both Pacific Northwest National Lab (PNNL), Richland, USA [33; 34] and Institut de Chimie Séparative de Marcoule (ICSM), Commissariat à l'Énergie Atomique (CEA), Marcoule, France [35-37] have been using a wet chemical approach for the production of uranium microparticulate reference materials. The pH of an aqueous solution containing uranium compounds is changed to trigger the precipitation of uranium microparticles. Further hydrothermal treatment led to the formation of well-designed high-purity uranium microparticles in remarkable quantities of up to milligrams.

At the Technical Research Center of Finland VTT, an Atomizer aerosol generator fed with an actinide nitrate solution was used to produce polydisperse actinide microparticles using spray pyrolysis [24]. Unfortunately, these particles were not suitable for safeguards purposes because particle analysis was impossible due to the used adhesive. A similar approach was investigated by the UK Safeguards Support Programme to the IAEA [38]. A spinning-top aerosol generator was fueled with uranium-containing solution. Unwanted droplet sizes were removed to guarantee mono-dispersity and the remaining uranium solution droplets were heated up to 1200 °C to produce uranium oxide particles. Although this was a promising approach and led to the production of $\sim 1 \mu m$ sized uranium oxide microparticles, the particles showed tendencies

towards alteration, disintegration and formed particle agglomerations. Nevertheless, they were used for the production of IAEA QC materials and for Interlaboratory Comparison (ILC) exercises.

The JRC Institute for Transuranium Elements (JRC-ITU) also pursued an approach using spray pyrolysis [39; 40]. Existing uranium oxide powder standards were dissolved in HNO₃ and the resulting solution diluted with isopropanol and water. The resulting solution was fed into a Vibrating Orifice Aerosol Generator (VOAG) to create aerosol droplets. The droplets were heated to uranium particles and collected on Nucleopore filters. The particle morphology, shape, size distribution and uranium isotopic composition was later investigated [41]. Some batches produced were investigated for the amount of uranium in a single particle using Isotope Dilution-Thermal Ionization Mass Spectrometry (ID-TIMS). It was stated, that the molecular composition of the particles remains unknown, although a mix of different uranium oxides appears probable [42].

2.1.2 Production approach at IEK-6

The spray pyrolysis approach used by the JRC-ITU provided promising results concerning mono-dispersity of produced particles and easily adjustable uranium isotopic composition by using a different feeding solution. It was also possible to measure single particles produced with this approach using TIMS [16]. Therefore, this approach was used by different research groups to produce particles simulating the release of sub-micrometer-sized radioactive particles [43] and as reference material for fission track analysis [44]. These good results make the spray pyrolysis approach using a VOAG the method of choice for a microparticle production setup to provide mono-disperse uranium microparticles as reference materials. It was therefore first implemented by IEK-6 at FZJ [45] in a joint program with the IAEA-SGAS starting 2012. The aims of this cooperation were to develop and establish a reproducible production process for particles suitable as reference materials for QC purposes and the subsequent delivery of said particles as well as the provision of FZJ laboratory and QC capabilities for the production of tailor-made reference microparticles with a qualification for a membership in the IAEA's NWAL [26].

In FZJ, a monodisperse aerosol is generated using a VOAG, Model 3450, TSI Inc., USA. A schematic overview of the initial setup is shown in Figure 2 [45]. Uranyl nitrate solution is fed into the aerosol generator where an orifice vibrating at a certain resonance frequency generates monodisperse droplets. The isotopic composition of the particles is determined by the composition of the feeding solution. The droplet volume is controlled by the volume flow through the orifice and the vibration frequency. An airstream with a certain flux disperses the droplets

and prevents coagulation of single droplets. The droplets pass the drying column evaporating the volatile aerosol components and creating precursor particles. The proto-particles are then guided into an aerosol heater (Dekati Pressurized Air Heater, Dekati Ltd., Finland) and heated up to 600°C. This heating leads to a phase transformation of the proto-particles into oxide form. The airstream containing the particles then enters a cooling pipe and is directed into a vacuum impactor (Sturm, Austria). Within this vacuum impactor, the particles can be collected on flat substrates like GCDs or quartz disks with a diameter of up to 2.54 cm (1 inch), depending on the intended use of the particles.

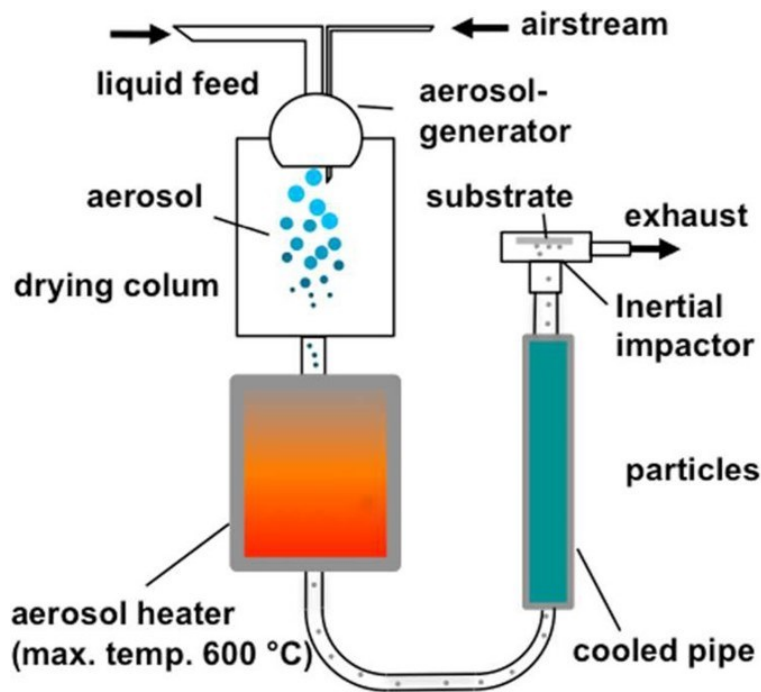


Figure 2: Schematic overview of the microparticle production system using spray pyrolysis. Reprinted with permission from [45]. Copyright 2017, American Chemical Society.

This production approach allows for bringing the microparticles into suspension for either long-term storage or as an intermediate step for a more homogeneous distribution on the particle planchet [46-49]. Ethanol is mainly used as a solvent for the intermediate suspension. The particles collected with the vacuum impactor are detached from the substrate with ethanol and afterwards transferred on a new substrate. The solvent is evaporated by heating the substrate to typically 50 °C leaving the particles homogeneously spread over the planchet surface and preventing coagulation [47; 50].

2.2 Structural investigation

Comprehensive knowledge about the formation process and the resulting structure of VOAG-produced uranium microparticles is essential to predict alteration behavior and incorporation of possible dopants. To answer structural questions concerning the internal structure of the produced microparticles as well as the exact composition of uranium oxide phases, several investigations were launched.

Previous studies have shown the major influence of the chemical composition of the feeding solution on the particle morphology [51]. Different solvents used for the production of the feeding solution usually result in different physicochemical processes during evaporation of the solvent and subsequent particle formation in the VOAG [45]. The availability of well characterized CRMs makes uranyl nitrate a perfect candidate for the production of uranium microparticles, despite its complex thermal decomposition [52]. In theory, a feeding solution containing uranyl acetate or uranyl chloride is also suitable, but dissolution of available U_3O_8 reference materials in nitric acid is far simpler to achieve than dissolution in acetic acid [26] and particles derived from uranyl chloride showed irregular shapes and high porosity [45].

The mainly produced microparticles derived from a uranyl nitrate solution have been characterized by different analytical techniques in previous studies. SEM investigations of particles heated to 500°C including particle size distribution analysis reveal the formation of well-rounded microspheres with a diameter of $\sim 1.2 \mu\text{m}$ (Figure 3) [48]. Simultaneously, in-SEM Energy Dispersive X-ray Spectroscopy (EDS) to determine elemental composition and μ -Raman Spectrometry to characterize the chemical phases was carried out. EDS spectra confirm the formation of Uranium oxides [25; 45; 48].

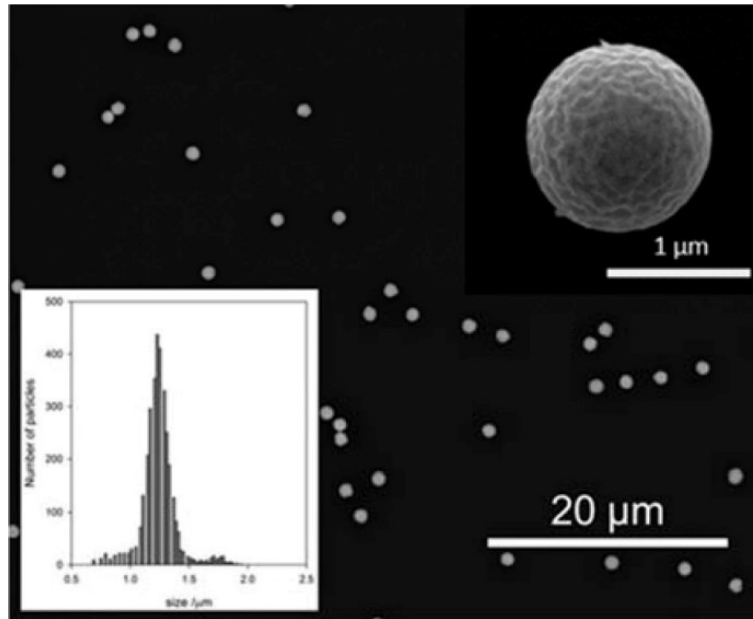


Figure 3: SEM images of U-oxide microparticles distributed on a glassy carbon substrate with high-resolution SEM image included. Inset: Particle size distribution of collected particles showing highest abundance at $\sim 1.2 \mu\text{m}$. Image reprinted from Kegler *et al.* [48], [CC BY 4.0](https://creativecommons.org/licenses/by/4.0/).

Middendorp *et al.* [45] compared the Raman spectra of particles derived from uranyl nitrate, uranyl acetate and uranyl chloride with previously recorded spectra of U_3O_8 microparticles [53] and a particle derived from a uranium ore concentrate (UOC) from South Dakota described as $\text{UO}_2(\text{OH})_2$ [54]. Considering their measurement results using $\mu\text{-XRD}$, they concluded a particle composition of mainly U_3O_8 with some surficial uranium hydroxide (Figure 4).

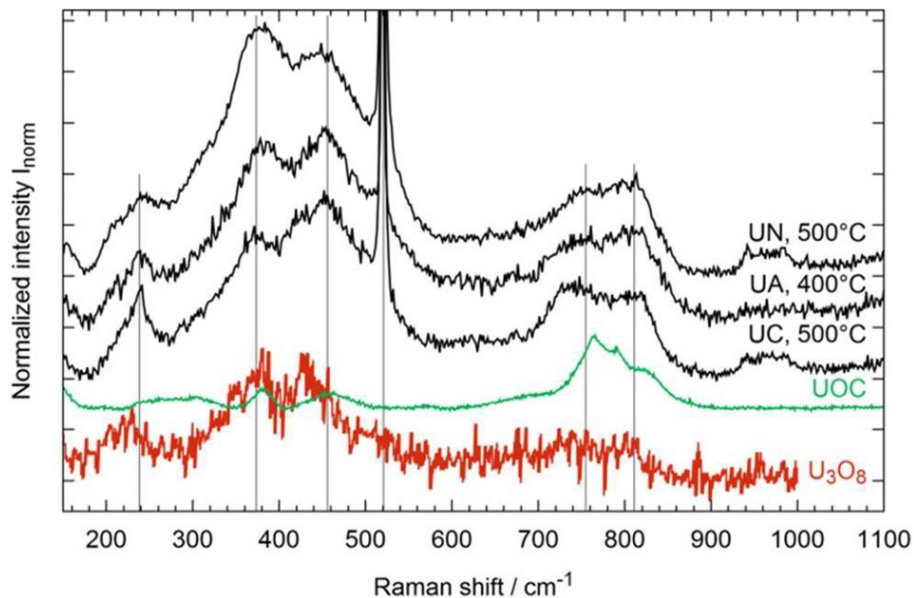


Figure 4: Raman spectra of microparticles produced using uranyl nitrate (UN), uranyl acetate (UA) and uranyl chloride (UC) compared to the spectrum of a micrometer-sized U_3O_8 particle and the spectrum of a uranium ore concentrate (UOC) from South Dakota. The line at $\sim 521 \text{ cm}^{-1}$ is an interference from the Si substrate. Reprinted with permission from [45]. Copyright 2017, American Chemical Society.

A subsequent comprehensive structural investigation of the uranium microparticles concluded that the particles mainly consist of a mix of uranium oxides [48]. Figure 5 shows the representative Raman spectrum of a particle stored in laboratory air for two years. The spectrum was characterized as mainly U_3O_8 mixed with minor UO_2 phase and the uranium hydroxide schoepite ($[(UO_2)_4O|(OH)_6] \cdot 6H_2O$). It was also concluded, that this hydration is probably a result of the long storage time and is uncharacteristic for freshly produced particles.

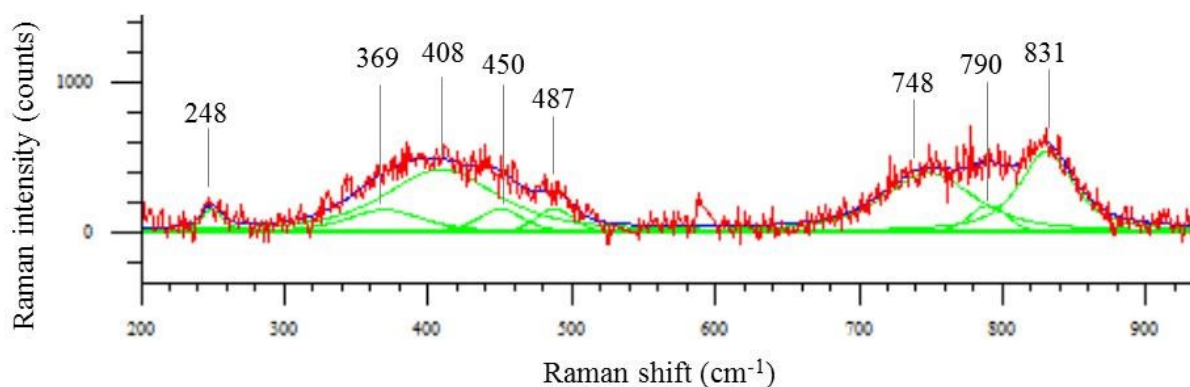


Figure 5: Background subtracted Raman spectrum of an individual uranium oxide particle stored for two years under laboratory atmosphere. Image reprinted from Kegler *et al.* [48], [CC BY 4.0](https://creativecommons.org/licenses/by/4.0/).

In the same study, the particles were investigated using high resolution X-ray absorption near-edge structure spectrometry (HR-XANES) (Figure 6). The particles in question were stored for 10 months. The obtained spectra were compared to uranium compound reference spectra [55; 56]. It was concluded, that the uranium in the particles is mostly present in pentavalent state with fluorite-type coordination. Nonetheless, the obtained spectrum shows a coexistence with small amounts of $U(IV)O_2$ and uranyl-type species like schoepite, confirming the results from Raman spectrometry.

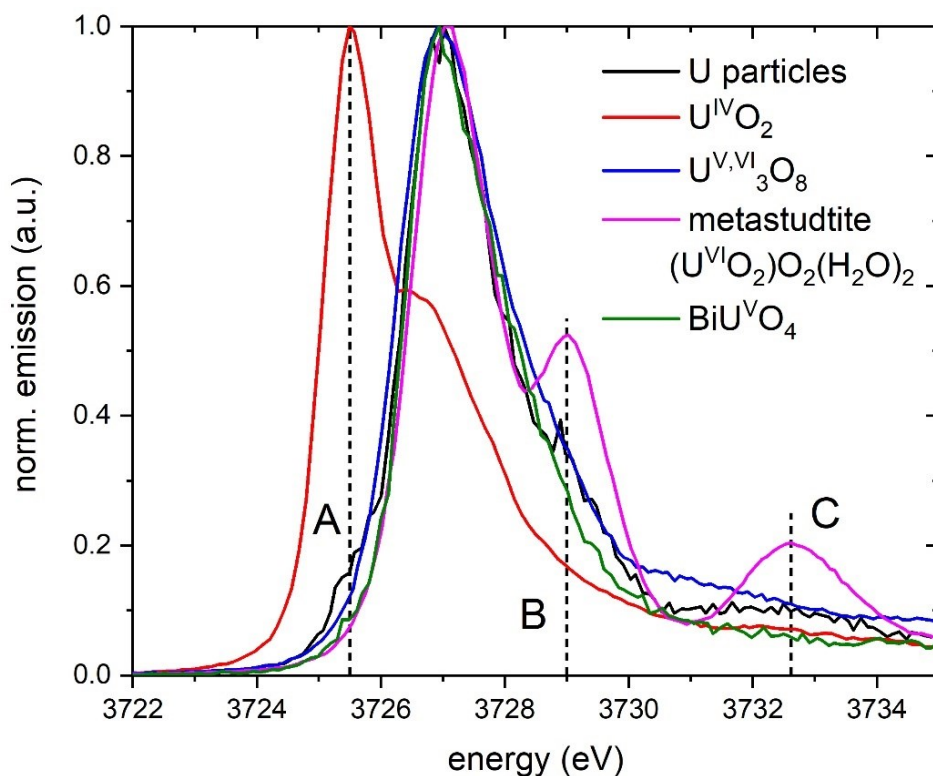


Figure 6: Normalized U M₄ HR-XANES spectra of uranium microparticles in comparison to uranium reference compounds. Image reprinted from Kegler *et al.* [48], [CC BY 4.0](https://creativecommons.org/licenses/by/4.0/).

However, XANES measurements on the L₃-edge from the same study showed a domination of uranium in tetravalent form pointing towards U(IV)O₂ as primary phase. In contrast to the HR-XANES measurements, the particles measured on the L₃-edge were newly produced. It was concluded, that the older particles underwent gradual uranium oxidation. The difference to the results from Raman spectrometry can be explained by the fact, that Raman spectrometry is a surface sensitive technique and therefore overestimates the fraction of uranium hydroxide compared to XANES, where the whole volume of the particle is taken into consideration. These initial results underscore that alteration of the particles during ambient storage needs to be further investigated.

2.3 Mass-spectrometric measurement of uranium enrichment

During the aftermath of the second Gulf War and the discovery of the clandestine program to produce nuclear weapons in Iraq, the IAEA and its member states concluded that environmental sampling with the characterization of individual radioactive particles is essential to detect undeclared nuclear activities as part of the IAEA safeguards system [7; 13; 39]. Single particle analysis requires high sensitivity instrumentation to detect small amounts of isotopes as well as

high accuracy to distinguish between natural background and anthropogenic components of enrichment [13]. In addition, the method of choice should provide precise abundances for the minor isotopes ^{234}U and ^{236}U . Simultaneous multi-element measurements are advantageous.

Several different mass-spectrometric approaches were investigated as a method of choice to characterize single micrometer-sized uranium particles and identify their ^{235}U enrichment [57]. Among the methods vetted, there were approaches using time-of-flight mass spectrometry [58-62], quadrupole ion trap mass spectrometers [63], fission track analysis [40; 64-67], Laser Ablation-Inductively Coupled Plasma-Mass Spectrometry (LA-ICP-MS) [13; 68-71] or TIMS [66; 72-74]. For Nuclear Safeguards purposes it is very common to use a combination of these different analytical techniques or chose an approach based on the samples' characteristics. Figure 7 shows a general analytical scheme with different analytical approaches for environmental samples as it is used by the IAEA and the NWAL [75].

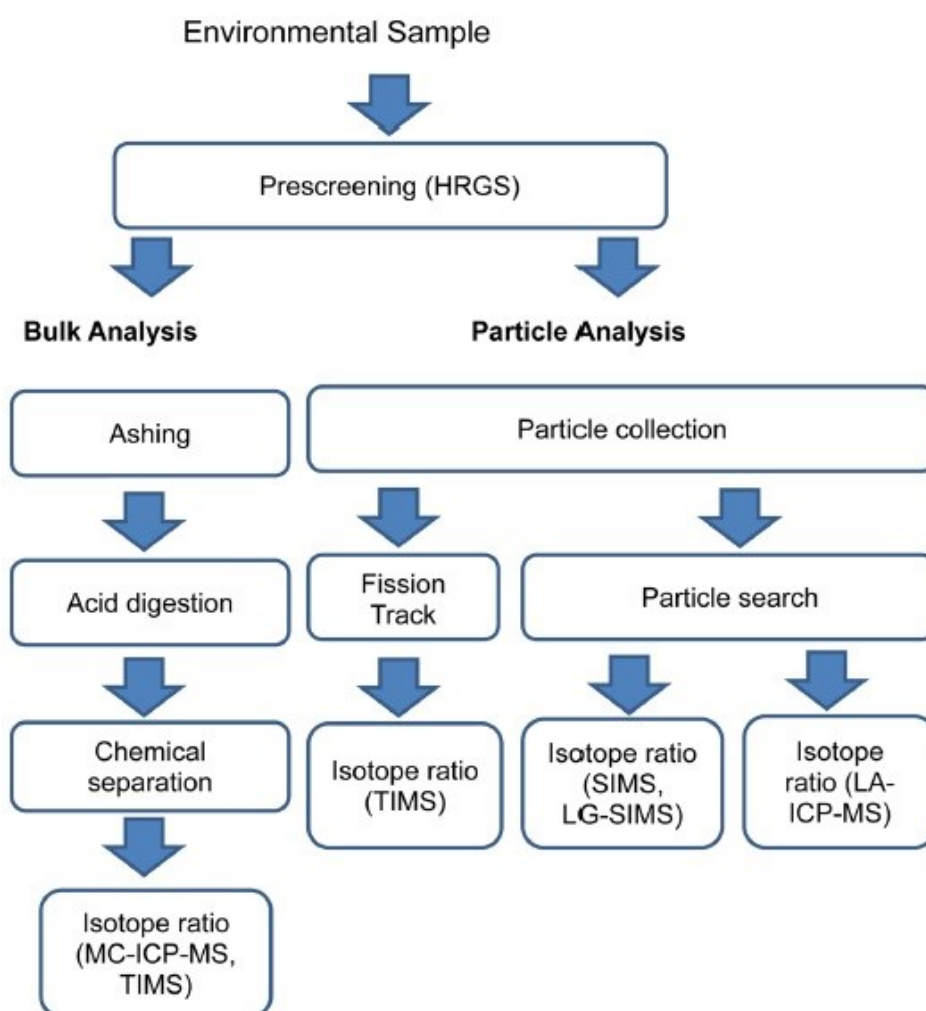


Figure 7: Schematic flow chart for widely used analytical procedures for nuclear safeguards samples showing the area of application for different measurement techniques. Image reprinted from Song *et al.* [75], [CC BY-NC 4.0](https://creativecommons.org/licenses/by-nc/4.0/).

One of the most promising techniques proved to be the analysis of single microparticles to detect impurities and the isotopic composition regarding uranium and plutonium using SIMS [76-81]. Compared to the other approaches for the analysis of single uranium particles, SIMS yielded the best precision in a comprehensive case study [82] and is therefore widely used in the field of particle analysis.

In a process developed in the mid-2000s together with the Japanese Atomic Energy Agency (JAEA), the particles of interest are transferred from the sample collecting medium (cotton swipe) directly onto a GCD using a vacuum impactor in a clean room environment [13]. Another IAEA requirement was the possibility to locate single particles yielding an isotopic signature of interest within the bulk of the particles on the sample. To achieve this, the United States Department of Energy (DoE) and Charles Evans & Associates developed a software using SIMS as a scanning ion microscope for the purpose of particle screening called P-Search [83].

The widespread Small Geometry-SIMS (SG-SIMS) instruments such as the CAMECA IMS 4f, used for particle analysis in the mid-2000s had the disadvantage that they had to be operated at low mass resolution if the operator wanted to achieve an acceptable transmission. For natural samples this led to the problem that interferences on ^{234}U and ^{236}U caused by PbAl and PbSi polyatomic ions could not be resolved [14]. In addition, the SG-SIMS had to be operated in the so-called peak-hopping mode measuring the mass peaks of interest sequentially. This implicates that isotope ratios have to be calculated based on time-interpolated signals. During the SIMS analysis of a small sample like a uranium microparticle, most of the particle volume is consumed. Moreover, the particle matter is not sputtered uniformly, which leads to potentially large signal variation during the particle analysis process and therefore large uncertainty for the calculation of the isotope ratios. In addition, the electronics of the CAMECA IMS 4f successors (5f, 6f and 7f) are not compatible with the P-Search screening software, leaving particle analysts operating outdated instruments [13].

To address these problems, SIMS particle analysts turned towards the use of LG-SIMS. CAMECA developed the first LG-SIMS in the early 1990s [84]. The implementation of the CAMECA IMS 1270 and its successor IMS 1280 for particle analysis in nuclear safeguards was tested in the mid- to late-2000s by a wide range of operators such as the Analytical Microscopy group at the National Institute of Standards and Technology (NIST), the NORDSIM facility in Stockholm, the CAMECA Application Laboratory and the ion probe facilities at UCLA (USA), University of Western Australia (Australia) and Edinburgh University (United Kingdom). The larger mass dispersion coefficient of the LG-SIMS compared to SG-SIMS allows for a much higher mass resolution power (MRP) while the instrument is still operating at full transmission. This opens the possibility to measure the minor uranium isotopes in small particles. In addition, state-of-the-art LG-SIMS

instruments are usually capable of analyzing several masses simultaneously [13]. Eventually, all of the LG-SIMS operators reported a huge performance gain for microparticle analysis compared to SG-SIMS [16]. To address the problem of particle location, CAMECA developed the Automated Particle Measurement (APM) software in 2009 in cooperation with Magnus Hedberg at JRC-ITU Karlsruhe, Germany [85; 86]. The APM software allows the user to locate single uranium microparticles on a sample planchet within the entirety of dust grains of a sample and to determine its preliminary uranium enrichment. It is also used on the predecessor models CAMECA 1280-HR and IMS-1300-HR³. The IAEA operates LG-SIMS in its own SGAS-ESL [87].

The use of LG-SIMS increased the useful yield, defined as the relative number of ions counted versus atoms sputtered, for uranium to up to 1.12 % for widely used O₂⁺ primary beams [15] compared to useful yields of a few ‰ for SG-SIMS [14]. The latest improvements using a Hyperion-II radio-frequency plasma ion sources even suggest useful yields of up to 4.7 % with an O₃⁻ primary beam [88]. However, other SIMS operators reported that they were not able to produce a necessary amount of O₃⁻ ions with their RF source (Axel Schmitt, Curtin University, pers. comm.; Johannes Grimm, IAEA SGAS-ESL, pers. comm.). Another benefit of the LG-SIMS instruments is the improved vacuum system, which leads to a better abundance sensitivity and the formation of fewer hydrides.

All of these improvements lead to greatly improved uncertainty for the uranium isotopes measured. ²³⁵U is generally reported with 1–2 % uncertainty, and ²³⁴U with 2–6 % uncertainty. Perfect measurement conditions such as large and homogeneous particles result in uncertainties of up to 0.4 % and 0.8 %, respectively [13]. Results within these typical uncertainties were achieved in the ILC NUSIMEP-7 [89].

3 Materials and Methods

3.1 Particle production at FZJ using a VOAG

In the following chapter the production process of uranium oxide microparticles in the safeguards laboratories is summarized. The exact amount of material used and the production conditions of the VOAG are typical for a generic uranium oxide microparticle production using a solution derived from the certified reference material NBL CRM 129-A [90]. The following pictures were taken at the FZJ safeguards laboratories during a particle production of microparticles doped with lanthanides to resemble the rare earth element (REE) signature of the natural Happy Jack uraninite [91; 92]. These microparticles were however not used for LG-SIMS measurements in this thesis. Nonetheless, they give an impression of the typical production process. Detailed information about the development of the production process can be found in the theses of Alexander Knott [24] and Ronald Middendorp [25]. The production processes of IAEA-requested particle productions characterized in this thesis is described by Neumeier *et al.* [93; 94] and Richter *et al.* [95].

The dilution and mixing of the prepared solutions took place on a laminar flow bench inside the controlled area of the FZJ nuclear safeguards laboratories (Figure 8). In the first step, a prepared uranyl nitrate solution derived from CRM 129-A with a uranium concentration of $c(\text{U})=9.58 \text{ mg/g}$ was diluted using ultrapure water ($\geq 18.2 \text{ M}\Omega \times \text{cm}$) until a uranium concentration of $c(\text{U})=200 \text{ }\mu\text{g/g}$ is achieved, in this example the dilution factor was 47.9. For the preparation of a volume of feeding solution that can be used for a whole day of particle production this is equal to 0.7 ml of the original uranyl nitrate solution diluted by 32.83 ml of ultrapure water. As a standard procedure, an aliquot of 1 ml of the aqueous uranyl nitrate solution is taken for QC using Solution Mode-ICP-MS. To prevent evaporation, the 50:50 vol% aqueous/ethanol nitrate solution is only prepared shortly before particle production. In this case, the 32.53 ml aqueous uranyl nitrate solution is mixed with 32.53 ml of 99.9% ethanol (Merck KGaA). Because ethanol has a density of $\rho(\text{EtOH})=0.789 \text{ g/ml}$, the volume of the finished feeding solution equals a mass of 58.1962 g leading to a uranium concentration of $c(\text{U})=115.2 \text{ }\mu\text{g/g}$. This value is within the desired concentration of 100 – 120 $\mu\text{g/g}$ [24; 45; 49].

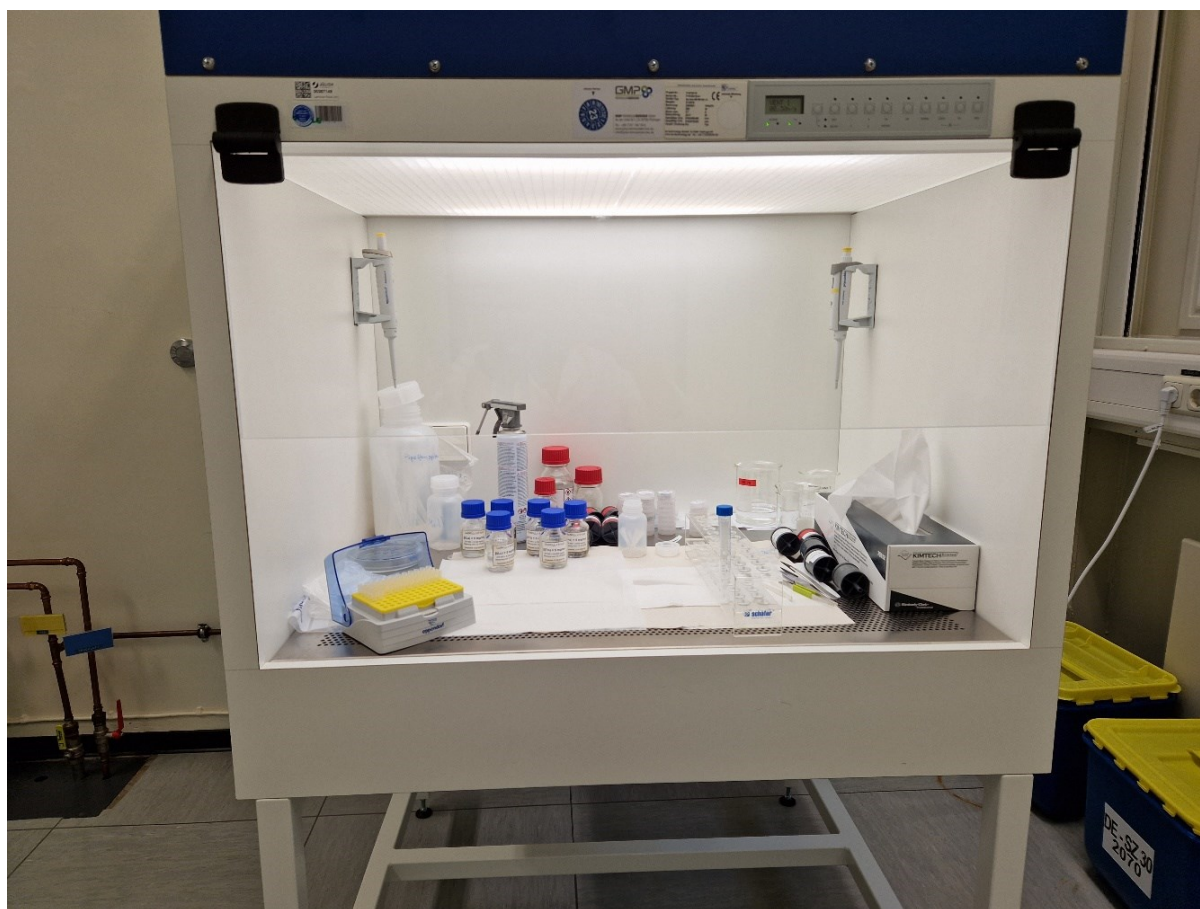


Figure 8: Laminar flow bench for the preparation of uranyl nitrate feeding solutions for the VOAG in the FZJ safeguards laboratories.

The feeding solution was degassed in an ultrasonic bath for 2 minutes and afterwards a syringe with a 60 ml aliquot of the produced feeding solution attached to the VOAG (Figure 9). To produce uranium microparticles in the range of $\sim 1.2 \mu\text{m}$, the VOAG was operated with a $20 \mu\text{m}$ orifice at a frequency of $f=70 \text{ kHz}$. To start the generation of droplets in the aerosol jet, the feeding solution was pumped into the top of the aerosol generator at a feeding rate of approximately $4.2 \times 10^{-4} \text{ cm/s}$ (for schematic view see Figure 2). After passing down the drying column, the particles were heated to $T=500 \text{ }^\circ\text{C}$, cooled and directed into the vacuum impactor.



Figure 9: VOAG in the FZJ safeguards laboratories. The syringe with the feeding solution is placed on the top left side, the vacuum impactors with the substrates are on the right side of the drying column.

3.2 Particle deposition

The deposition of the particles on the substrates for further analysis can be performed in two different ways: either in direct collection on the substrates and in an optional dispersion step. The two possibilities are described using the same example as for the production step.

3.2.1 Direct collection

The air stream with the particles was directed into the inert vacuum impactor after passing the cooling pipes [96]. Figure 10 shows a vacuum impactor in use during the production process. Inside the vacuum impactor the particles were deposited onto a substrate like a GCD, an Si-wafer

or a quartz disk with a flow rate of 4 l/min. In this specific production, the particles were deposited on one Si-wafer for a duration of 15 min. This wafer was used for SEM investigations. Afterwards two GCDs (each 30 min) for SIMS measurements and 4 quartz disks (60 min) for Raman measurements were prepared. The longer the substrates are in the vacuum impactor, the more microparticles are deposited. The duration for this specific case was chosen, because microparticles are hard to identify using Raman spectroscopy and therefore a high particle concentration on the substrates should be achieved.

When a substrate is sufficiently loaded with particles, a valve in front of the vacuum impactor was closed forcing the air stream containing particles through a bypass (Figure 10). The vacuum impactor containing the loaded substrate was removed and another prepared impactor containing the next substrate was attached to the tube system of the VOAG. The valve was opened again and particles were deposited onto the next substrate. Subsequently, the previously removed impactor was disassembled and the substrate was removed and labelled. The substrate was now ready for shipping or analysis.



Figure 10: Vacuum impactor containing a substrate (left) within the VOAG setup of the FZJ safeguards laboratories. Bypass for substrate change is on the right.

3.2.2 Dispersion step

While direct deposition leads to a very high particle yield on the substrate, the microparticles are heterogeneously distributed across the substrate surface. They tend to form a ring with a high particle concentration and areas of lower particle numbers in the middle and near the substrate edges (Figure 11). To achieve a homogeneous particle distribution across the sample planchet, members of FZJ IEK-6 developed a second, optional particle dispersion step [26; 47].

The collection planchets from the impactors were transferred into vials filled with either 5 or 10 ml 99.9% ethanol (Merck KGaA) and treated in ultrasonic baths for a few minutes. The collection planchets were then removed and the dispersion was filled in vessels ready to be used. An unused or cleaned sample planchet was put into a petri dish and placed on a first heater at a temperature of 60 °C. For a normal production 300 µl of the prepared dispersion is brought onto the sample planchet with an Eppendorf pipette. The petri dish with the substrate remained on the heater until the ethanol was completely evaporated. Subsequently, it was placed on a second heater at 300 °C for 5 min. This should guarantee the removal of remaining organic components. Afterwards, the sample was cooled for 15 min, labeled and packed.

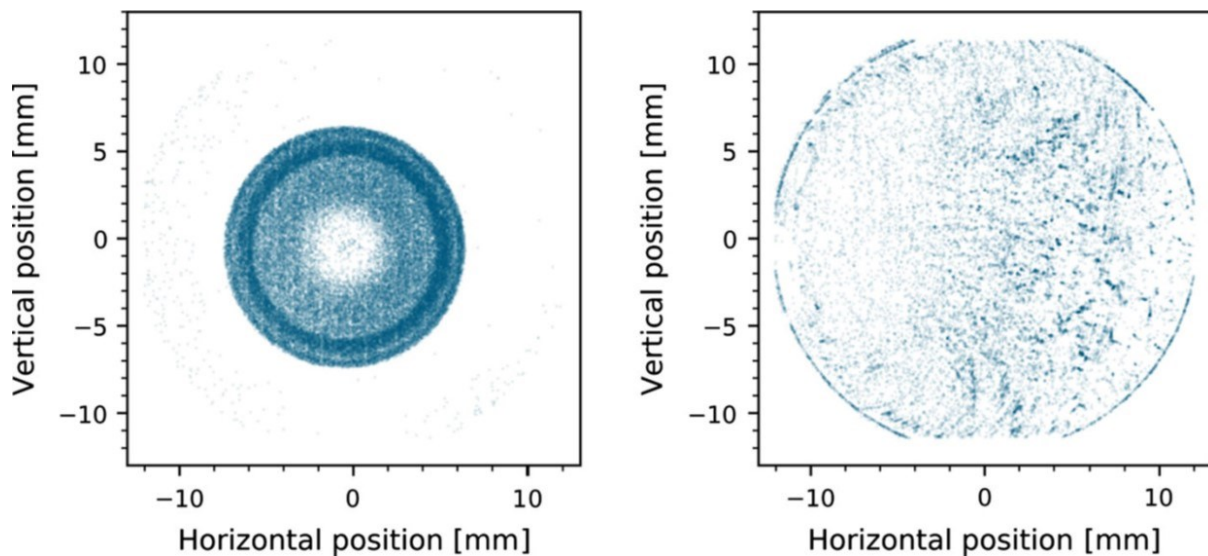


Figure 11: Distribution of uranium oxide microparticles on GCDs analyzed by SEM. The GCD on the left side is prepared by direct collection, the GCD on the right side with an intermediate dispersion step. Each dot represents a single particle. Reproduced with permission of Springer Nature from [47].

As shown in Figure 11, the particle distribution on planchets prepared with an intermediate dispersion step is much more homogeneous than on planchets with directly collected particles.

3.3 Isotopic abundance measurements using SIMS

The uranium isotopic abundance measurements of the microparticles were carried out at the HIP laboratory of the Institute of Earth Sciences, Heidelberg University. The laboratory is equipped with a CAMECA IMS 1280-HR, an LG-SIMS of the second generation [97]. At the time of the measurements for this thesis, the HIP was equipped with a Cs_2CO_3 primary source for the production of Cs^+ primary ions (mainly used for stable isotope measurements such as oxygen) and a duoplasmatron source capable of producing positive and negative oxygen ions. The sample mounts have a diameter of one inch (2.54 cm) and are usually coated with a conductive layer (mostly Au or C). In this case, sample coating could be skipped due to the use of conductive GCD substrates and the very small microparticle diameter of $\sim 1.2 \mu\text{m}$. The SIMS was kept in ultrahigh vacuum of $\sim 3.5 \times 10^{-7}$ Pa in the sample chamber and $\sim 1.6 \times 10^{-6}$ Pa in the detector chamber (projection). The magnet radius is 585 mm, which enables a very high transmission up to an MRP of ~ 6000 . The SIMS can be operated in direct ion microscope mode imaging secondary ions location-dependent from the sample surface on a channel plate or a resistive anode encoder. Scanning ion imaging is possible with electron multiplier (EM) detectors. It is equipped with a multicollection (MC) array of five moveable trolleys (L2, L1, C, H1 and H2) that can fit EM or Faraday cups (FC). Figure 12 shows the MC array in the projection section of the IMS 1280-HR. The MC array allows the simultaneous measurement of up to five ion species in the same mass region.

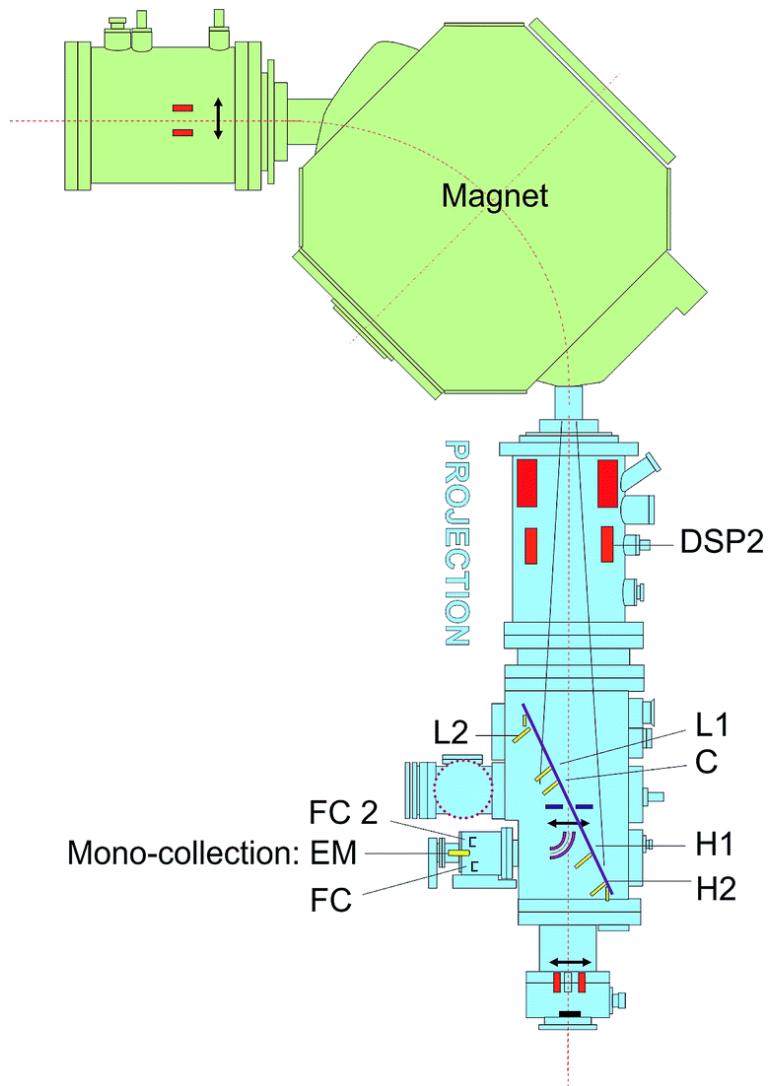


Figure 12: CAMECA IMS 1280-HR ion optics. The DSP2 octopole is a stigmator and a deflector that can be used to increase the mass dispersion. EM, FC and FC 2 are the axial detectors used in mono-collection mode (Hedberg *et al.* [19], [CC BY 3.0](https://creativecommons.org/licenses/by/3.0/)).

The development of a suitable uranium microparticle SIMS measurement setup was a central part of this thesis. Therefore, detailed information about this development process as well as important instrument parameters in the respective development step can be found in the Results and Discussion part of this thesis in chapter 4.1.

3.3.1 Microparticle measurements

The measurements of uranium oxide microparticles have been conducted using an O_2^+ primary beam. Although the potential ion yield for O^- or O_2^- is higher [16], the positive primary ions were chosen because of the higher primary beam density and current stability [19]. The minimal distance between the detector trolleys on the MC array is only sufficient to resolve whole masses up until the mass range of Pb. Therefore, the mass dispersion has to be increased in order to simultaneously measure the ^{234}U , ^{235}U , ^{236}U , ^{238}U and $^{238}U^1H$ ion species. This was achieved by applying a voltage to the DSP2 stigmator (Figure 12).

For the identification of uranium particles, the SIMS was used in ion microprobe mode. A focused primary ion beam with a current of >1 nA was used in scanning mode with a raster of 500×500 μm and the sample stage was moved. The ion image of the species with the highest expected signal (usually ^{238}U) was used to identify sample areas containing uranium particles. An area with an identified particle was enlarged using a smaller rastered beam. When the raster size was decreased, the beam current was lowered accordingly to keep the intensity of the impinging ions on the EM below 100,000 counts per second (cps). The sputtered area was reduced until a single particle measurement could be executed. The exact measurement parameters were different for each approach and can be found in chapters 4.1.1 and 4.1.2.

Using the multicollection setup for a simultaneous ion species measurement introduces the necessity of regular yield measurements between the different multicollection detectors. The detectors are usually exposed to widely varying intensities and will therefore show dissimilar ageing [19], that had to be monitored on a daily basis and corrected, if necessary. There is also an instrumental mass bias effect reported for the measurement of uranium microparticles [15]. This effect needed to be defined and corrected on a daily basis as well. Both the detector yield and the mass bias were determined using the NBL CRM U series reference materials, namely CRM U010, CRM U100, CRM U500 and CRM U930 [20].

The ionization process in SIMS leads to the formation of hydride species. The hydride formation is measured as a ratio of the hydride and the uranium isotope the hydride is derived from (for example $^{238}U^1H/^{238}U$), which is typically in the range of $2 \times 10^{-3} - 2 \times 10^{-4}$ [16]. This leads to significant interference from $^{235}U^1H$ derived from the major isotope ^{235}U on the minor isotope ^{236}U , that cannot be resolved by mass resolution and needed to be corrected for [15; 19; 85]. Although there is also an influence from $^{234}U^1H$ on ^{235}U , this is usually not significant and therefore not corrected. It is assumed that the hydride formation ratio is equal for all isotopes. Therefore, the $^{238}U^1H/^{238}U$ -ratio was directly measured and used for the correction of ^{236}U in the equation

$$\frac{^{236}\text{U}}{^{238}\text{U}} = \frac{^{236}\text{U} + ^{235}\text{U}^1\text{H}}{^{238}\text{U}} - \frac{^{235}\text{U}}{^{238}\text{U}} \times \frac{^{238}\text{U}^1\text{H}}{^{238}\text{U}} \quad (1)$$

This hydride correction significantly increases the measurement uncertainties and therefore the ^{236}U detection limits. In addition, the influence of the hydride correction is larger for samples containing more ^{235}U [16].

3.3.2 Automated Particle Measurement (APM)

Microparticle screening measurements were conducted using the CAMECA-developed APM software [85; 86]. This software package was implemented at the HIP in 2021 for the characterization of the entirety of microparticles on a sample planchet and to reliably identify the major isotopic composition of single particle outliers or of whole particle populations.

The software is divided into data acquisition and data processing. In the acquisition phase, the sample surface was divided into fields of $500 \times 500 \mu\text{m}$. One field was measured rastering a primary beam with a relatively high current (exact parameters used are described in chapter 4.1.4) for a short time and counting with all five MC detectors simultaneously to identify the same ion species as in the microparticle measurements. This created ion images of the selected sample surface area for all measured ion species. After the measurement was completed, the sample stage was moved to the next field and a new measurement was started. When all of the selected sample areas were measured, the beam was turned off and the measurement was saved.

In the processing phase, the recorded images were analyzed and boundaries of identified particles were identified using preselected thresholds. The ion images of the single fields were combined to a mosaic image resembling the whole selected analysis area of the sample. Every identified particle was assigned a unique ID, X- and Y-coordinates on the sample planchet and a preliminary isotopic composition. The calculated particles could be sorted by size, ion intensity, isotopic composition and position. Depending on the requirements for the characterization, single particles could be selected from the list to perform precise microparticle measurements.

3.4 Shelf-life investigation

3.4.1 Storage conditions

To investigate the stability of the uranium oxide microparticles produced with a VOAG, a comprehensive shelf-life investigation was launched. It was separated in two parts: (A) Atmospheric shelf-life study and (B) Dispersion shelf-life study.

3.4.1.1 Atmospheric shelf-life study

The particles used for the atmospheric shelf-life study were treated like possible reference materials as being shipped to the analytical laboratories. They were produced in September 2021 using the CRM NBL 129-A as described in chapter 3.1 and underwent a dispersion step as described in chapter 3.2.2 for a more homogeneous particle distribution. Subsequently, they were shipped as four GCD plachets containing the particles in a water-free argon atmosphere.

Because an influence of water was anticipated due to previous observations [48], the particles were stored under three conditions that minimize H₂O exposure and can be implemented easily for long-term storage prior to their potential use in analytical laboratories .

(a) Laboratory air with silica gel as desiccant: The first GCD containing the microparticles was stored in a desiccator with silica gel underneath. The desiccator remained closed between the analyses and was placed beneath a closed fume hood.

(b) Commercial pure argon (99.9999 %) with silica gel: The second GCD was stored in a desiccator with silica gel. The desiccator was flooded with argon and the oxygen level was checked with a PreSens Microx 4 oxygen meter. An oxygen level below 0.5 % was deemed reasonable, the desiccator was sealed air-tight and placed under the same fume hood.

(c) Laboratory air with silica gel at 90 °C: The third GCD was placed in a ceramic tray containing silica gel. The tray was placed in a laboratory furnace heated to 90 °C and covered with aluminum foil.

An additional test plachet was stored in a water saturated atmosphere for comparison:

(d) H₂O-saturated: The fourth GCD was placed in a desiccator filled with water. The GCD did, however, not touch the water surface and was stored on a ceramic plate above the water level. The desiccator was also placed under a fume hood.

When the samples were extracted from their respective storage conditions for analyses, the storage timer was stopped and they were placed in an intermediate storage desiccator filled with laboratory air and silica gel. The counting of storage time was continued after the storage conditions were restored.

3.4.1.2 Dispersion shelf-life study

The purpose of the second part of the shelf-life investigation was to monitor the stability of uranium oxide microparticles in alcoholic dispersions. The microparticles used were derived from the same production batch as the ones for the atmospheric shelf-life study in September 2021. Instead of the dispersion step as described in chapter 3.2.2, the particles were detached from their production planchets after 60 min of collection using four different alcohols as potential long-term storage media: (1) ethanol (99.9 %, Merck KGaA), (2) 2-propanol (99.5 %, Sigma-Aldrich), (3) *n*-butanol (99.8 %, Sigma-Aldrich) and (4) *tert*-butanol (99.5 %, Carl Roth). A comprehensive description of the procedure can be found in Potts *et al.* [49]. A dispersion using 5 ml of each alcoholic storage medium was prepared by Shannon Potts at FZJ and one aliquot of each with 1 ml dispersion was sent to the Institute of Earth Sciences in Heidelberg for investigation. The vessels containing the dispersions were stored in a desiccator with silica gel under water-free argon atmosphere.

For each analysis session, new planchets were prepared with the particle dispersions. The vessels with the dispersions were extracted from the desiccator and treated in an ultrasonic bath for 30 s to prevent particle accumulation at the bottom. Subsequently, the vessels were opened inside a beaker flooded with argon. 300 μ l of the dispersion was extracted with an Eppendorf pipette and brought onto a GCD. The following procedure was consistent with the dispersion step described in chapter 3.2.2. During the sample heating, the vessels with the remaining dispersions were closed under argon atmosphere and placed in the storage desiccator.

3.4.2 Scanning Electron Microscopy

For both the samples from the atmospheric as well as the dispersion shelf-life study, the particles' shape, size and surface appearance was investigated using SEM. Secondary electron (SE) images were generated using the JEOL FEG-SEM JSM IT800 SEM at the Institute of Earth Sciences,

Heidelberg University. The SEM is equipped with a field emission cathode that allows for the recording of high-resolution SE images [98; 99].

The particles were either placed on Si-wafers or GCDs. Just like the SIMS samples, both substrates are conductors. Combined with the fact, that the microparticles have a diameter of only $\sim 1.2 \mu\text{m}$, charge build up is mitigated by the conducting substrate, which renders a coating obsolete. The SEM was operated at a pressure of $\sim 2 \times 10^{-4}$ Pa at a high voltage (HV) of 10 – 15 kV and working distances of 5 – 8 mm. The HV range is necessary, because the uranium oxide microparticles themselves are poor conductors and a higher HV would lead to sample charging resulting in imaging artifacts. A lower HV would, however, reduce the achievable lateral resolution. This resulted in a typical magnification of 70,000 – 80,000 for images of field of view-filling particles. The public domain software ImageJ (version 1.53k) was used for image processing [100].

3.4.3 μ -Raman spectroscopy

The structural investigation and the possible qualitative determination of uranium phase alteration in the uranium oxide microparticles was done using a WITec Alpha 300R μ -Raman spectroscope at the Institute of Earth Sciences, Heidelberg University. The Raman spectrometer is equipped with a green 532 nm doubled Nd:YAG (neodymium-doped yttrium aluminum garnet) laser with a maximum power of 75 mW and a UHTS 300 VIS-NIR (visible to near-infrared) spectrometer with a grating of 1200 grooves/mm used for particle analyses.

For particle identification and focusing, the microscope was operated using 10 \times and 50 \times magnification objectives. The single particle measurements were carried out using an objective with 100 \times magnification. The diameter of the laser beam using the 100 \times objective is listed as 721 nm, which results in a spatial resolution of 361 nm. The spectra were recorded using a laser power of 1 mW with a duration of 60 s for a single iteration. These conditions were selected to mitigate possible particle dehydration and potential re-formation of uranium oxides, whereby the low laser power was compensated by the comparatively long integration time. The spectra were recorded using the WITec Control 5.3 software and processed with WITec Project 5.3. For an advanced spectrum fit, the Fityk (version 1.3.1) software package was used [101]. The single peak fit as well as the cumulative fit were calculated using a Levenberg-Marquardt algorithm from MPFIT.

4 Results and Discussion

4.1 SIMS measurements

LG-SIMS like the CAMECA IMS 1280-HR have been regularly used to measure isotopic abundances of uranium microparticles. However, prior to this study, this field of work was new to the HIP laboratory. One of the main tasks in this work was the implementation of a working microparticle measurement setup at the HIP. The following chapters illustrate the developing process of the implementation.

4.1.1 First steps using a mixed EM and FC detector setup

The HIP operates a state-of-the-art LG-SIMS instrument capable of simultaneous detection of masses between ~ 6 and 238 (i.e. lithium to uranium) at single atomic mass unit separation. Seven movable detectors are available in addition to the axial detector, and they comprise EM and FC detectors. The instrument is usually used for a variety of cosmo- and geochemical applications. Among these applications, stable isotope analyses (e. g. $\delta^{18}\text{O}$) play an important role. Compared to other measurements, these analyses usually yield very high intensities. Just like uranium isotope measurements, those measurements are usually performed in MC mode (see chapter 3.3). However, stable isotope analyses exceed the maximum intensities recommended for EMs. Hence, some of the MC detectors are FCs in their default configuration. While the usage of EMs for intensities of more than $\sim 1.500.000$ cps leads to rapid degradation and ageing, an FC detector is capable of counting much higher intensities. In an FC the impinging ions are transferred into a current that is amplified via a feedback resistor circuit and then measured as an electric current. An electrode with a negative repeller voltage in front of the FC prevents the charge loss of escaping secondary electrons.

For the measurement of uranium microparticles, much lower intensities than usually measured with FCs are to be expected. Unfortunately, the modification from FC to EM detectors is very time consuming and requires several days of evacuating the detection unit of the ion probe to achieve an acceptable vacuum for subsequent measurements. In addition, the detector modification has to be reversed after every measurement campaign. Therefore, in practice the frequency of detector changes is minimized by binning the applications according to their respective detector configuration.

Moreover, FCs usually have a much worse signal-to-noise ratio than EMs when it comes to relatively low intensities. Reliable measurements of intensities in the low thousand cps are impossible, and intensities between 10^3 and 10^5 cps are imprecise. Considering this, the only uranium isotopes where a measurement with FCs is remotely feasible are the major isotopes ^{235}U and ^{238}U . At the HIP, MC detectors L2, L1, C and H2 are EMs in their default configuration, which makes H1 the only FC in the detection array. Fortunately, H1 is the detector used for ^{238}U in the approach of Hedberg *et al.* [15; 19].

Therefore, the initial approach for measuring uranium microparticles in a MC setup at the HIP is the simultaneous measurement of all isotopes with a mix of FC and EM detectors based on the measurement setup suggested by Hedberg *et al.* [15; 19]. A drawing of the approach is shown in Figure 13.

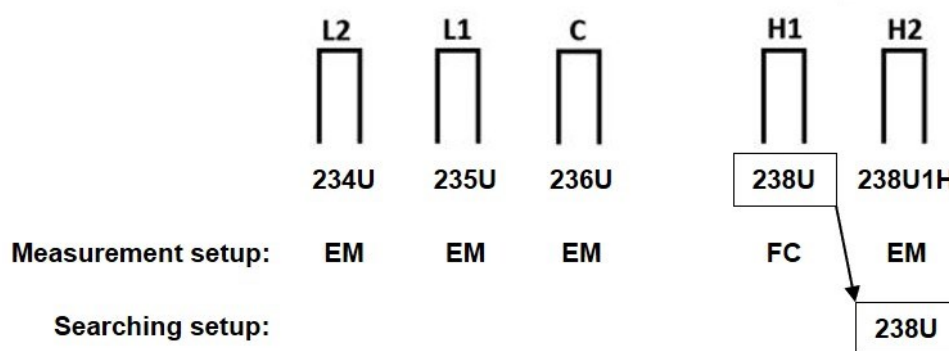


Figure 13: MC detector setup for an approach with FC on the H1 detector and EMs on the other detectors. Measurement setup and particle searching setup are distinguished. Modified after Hedberg *et al.* [1], [CC BY 4.0](#).

However, this approach generates some problems for the image generation of the microparticles. Usually uranium microparticles are identified using a scanning ion image of the isotope with the highest abundance. This is usually ^{238}U . However, an ion image of the sample surface can only be obtained by using EM detectors. In this setup ^{238}U is measured with an FC detector and an ion image can therefore not be used to identify uranium microparticles. The intensity of ^{235}U as the major isotope with the next higher abundance in natural samples is less than $1/100^{\text{th}}$ of ^{238}U and is therefore not suitable to create an ion image, at least for low enriched samples.

To solve this issue, the signal of ^{238}U has to be detected on a neighboring EM detector. This can be achieved by either changing the magnet field or by deflecting the secondary ion beam of $^{238}\text{U}^+$ ions after passing the magnet. In this case, the DSP2_X quadrupole was used to deflect the signal of ^{238}U into the H2 EM detector. This is the particle searching setup (Figure 13).

When calculating ratios derived from intensities from both EMs and FCs, the detector yields will not behave in a similar way over time. EMs will age over time, which requires the EM HV to be increased to achieve the same detection efficiency. Ageing does not affect FCs in the same way,

especially with relatively low intensities. Additionally, the baseline of the FC detector has to be determined periodically. While EMs also have a background, this is many times lower than the baseline of the FC (< 3 counts per minute (cpm) according to CAMECA specs). To correct for the detector drift, yield measurements between the EMs and the FC were performed on a regular basis. As an evaluation of the magnitude of yield variation over the course of a day, VOAG-produced uranium microparticles derived from a solution of CRM NBL 129-A which resemble natural isotopic abundances were measured repeatedly. The particles were directly collected on a silicon wafer in 2020 and have a typical size of ~ 1.2 μm . Particles were located using the ^{238}U signal on the H2 detector. For these test measurements an O^- primary ion beam of ~ 150 pA was used. As indication for the magnitude of yield variation, the results were compared to data from Hedberg *et al.* [15]. The results of these measurements are shown in Figure 14.

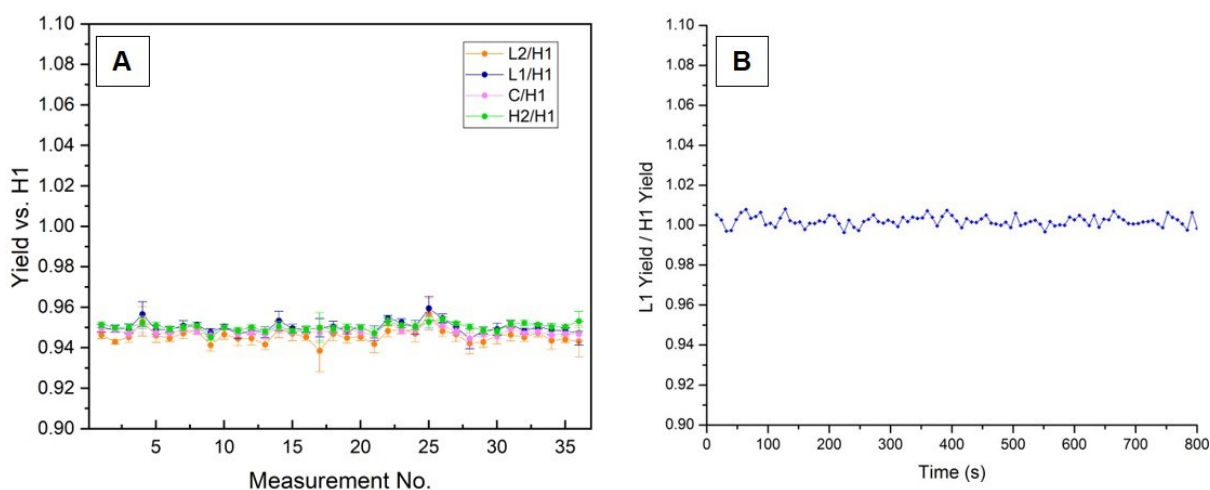


Figure 14: A) Measured yield of EM detectors vs. H1 FC in several measurements over the course of a day. B) Yield of 2 EM detectors over the course of a single measurement. Data shown in B) from Hedberg *et al.* [1], [CC BY 4.0](#).

For the yield measurements, ^{238}U was measured sequentially on all 5 detectors. For sequential measurements, the intensity on each detector may vary due to a different number of sputtered ions over the time of the measurement because of particle sputtering and therefore has to be corrected [102]. The measured intensity on the EM detectors is corrected to resemble an interpolated intensity between the cycles that corresponds to the same measurement time ^{238}U is measured on the H1 FC detector. By doing this, intensity variations caused by the consumption of the measured particles are prevented. The measurement time on each EM was 2 s, and on the H1 FC 5 s. In Figure 14A), the ratios of the EM intensities vs. H1 FC intensity are shown. These ratios are the mean of 10 measurement cycles per measurement. Typically, the 4 EM detectors reach only $\sim 95\%$ of the FC yield, because low voltage pulses are filtered out by the discriminator. The effect decreases, when a shorter waiting time is applied, because the FC responds with a delay compared to the EMs. Empirical observation has shown, that a waiting time of 3 s in each cycle is

a reasonable compromise between lost intensity on the FC and wasted sputtered ions from each particle.

Nonetheless, the yield variation over the course of a day for each detector is in the range of $\sim 2\%$. Compared to the data of Hedberg *et al.* [15] in Figure 14B) from a single measurement, this variation is in the same range. Overall, the yield variation can be monitored at high confidence for this setup, if enough verification measurements are performed.

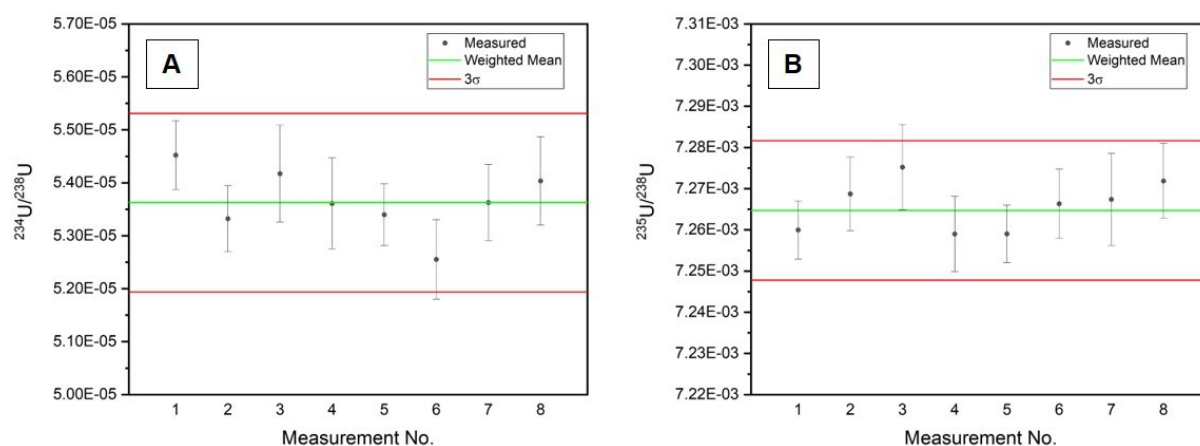


Figure 15: $^{234}\text{U}/^{238}\text{U}$ ratios and $^{235}\text{U}/^{238}\text{U}$ ratios of Uranium microparticles resembling natural Uranium. The measured ratios are corrected for detector yield, but no mass bias correction was applied.

For the same sample and primary beam presets, the isotopic ratios for $^{234}\text{U}/^{238}\text{U}$ (Figure 15A) and $^{235}\text{U}/^{238}\text{U}$ (Figure 15B) were measured to verify the reproducibility of this setup. Eight particle measurements were conducted. At the time of these measurements in October 2020, standard materials to determine the mass bias were unavailable. Therefore, the measured isotopic ratios differ from the ratios from the certificate of CRM NBL 129-A. There was also no hydride correction for $^{235}\text{U}^1\text{H}$ applied. Thus, no $^{236}\text{U}/^{238}\text{U}$ -ratio was calculated. The measurements are exclusively meant for verification of reproducibility. The H1 FC detector was corrected for its baseline and subsequently the detector yields for the EMs were corrected. Note that in this configuration no pixel based dead time correction for the EMs was used. Instead the dead time correction was applied to the average secondary ion signal.

Repeated measurements of $^{234}\text{U}/^{238}\text{U}$ and $^{235}\text{U}/^{238}\text{U}$ ratios agree within stated uncertainties. For $^{234}\text{U}/^{238}\text{U}$, the relative standard deviation (RSD) is 1.13%, for $^{235}\text{U}/^{238}\text{U}$ the RSD is 0.08%. These results are comparable to the reproducibility of the measured isotopic abundances from Hedberg *et al.* in 2018 [15] and in 2015 [19] with RSDs for ^{234}U of 0.54% (2015: 0.50%) and for ^{235}U of 0.06% (2015: 0.11%). Note that Hedberg *et al.* used NBL CRM U100, a reference material containing more ^{234}U and ^{235}U .

Although the results overall look promising, a measurement setup with a mix of EM and FC detectors has some serious downsides. A highly enriched sample with very low amounts of ^{238}U would lead to a very bad signal-to-noise ratio on the H1 FC and would therefore not be measurable. Additionally, the continuous measurement of the FC baseline and the yield measurements are very time consuming. The identification of particles on the sample planchet takes more time as well, because the mass of ^{238}U has to be deflected to the H2 EM.

The most important disadvantage for the mixed setup is the fact that particle samples cannot be screened using the APM software. For the APM software to identify particle boundaries and to determine isotope ratios in them, all the measured isotopes have to be detected by EMs. Therefore, although it is a promising approach for single particle measurements, a mixed detector setup is impractical for routine uranium microparticle characterization with SIMS. Hence, a different setup with 5 EM detectors was used in all following sessions.

4.1.2 Full EM detector setup

To allow for reliable results of single particle measurements as well as for the application of the APM software, a full-EM detector setup as suggested by Hedberg *et al.* [15; 19] was applied and tested on the same particles that were used before for the mixed setup. To keep the results as comparable as possible to previously reported analytical set-ups, an O_2^+ primary beam was used. The analytical conditions are based on the IAEA protocol, which also uses the conditions suggested by Hedberg *et al.* [15]. They can be found in Table 1.

Table 1: SIMS analytical conditions for single particle measurements.

Operating conditions

Primary ions	O ₂ ⁺
Primary acceleration voltage	+15 kV
Secondary acceleration voltage	+8 kV
Total incident energy	7 keV
Raster	10 × 10 μm
Optical mode	Circular
Primary ion currents	~100-150 pA
Image field for transfer optics	80 μm
Dynamic Transfer Optical System	On
Contrast aperture	400 μm
Field aperture	5000 μm
Entrance slit	174 μm
Exit slit	500 μm
Mass resolution	~2000
Energy bandwidth	30 eV

Although overall comparable, the exit slit is 500 μm in contrast to 350 μm as suggested by Hedberg *et al.* [15]. This is due to the fact, that the exit slit width for the multi-collection is not continuously adjustable like for the axial single detector, but has to be chosen out of three fixed exit slits. In Heidelberg, the three exit slit options are 500, 250 and 100 μm. Because in this study only synthetic particles were examined, interfering PbAl or PbSi molecules [14; 15] that can occur in environmental samples are unlikely, an MRP of ~2000 is suitable. To retain a flat-top peak at high transmission, the 500 μm exit slit was chosen.

In contrast to the mixed FC/EM detector setup, the all-EM setup allows the use of a pixel-based dead time correction for the EMs. With this correction applied, a larger area around the single particles (10 × 10 μm) can be sputtered by the primary ion beam. This means an overall higher number of secondary ions, because during the sputtering process, some sputtered uranium atoms are redeposited on the sample surface next to the microparticles and can be ionized by the scanned primary ion beam with a raster.

Before starting any test measurements, the EM detector gain, i.e. the yield of impinging ions detected, was optimized. For this, the EM high voltage for each EM detector was adjusted by measuring ^{238}U with an intensity of $\sim 50.000\text{-}60.000$ cps. As described by Hedberg *et al.* [19], there is a long-term alteration of the first dynode of EM detectors when exposed to sustained high intensities. This effect can be mitigated by shifting the ion beam along the Y axis using the DSP2_Y octopole. For each detector, the maximum intensity while scanning DSP2_Y was measured and then the octopole was adjusted to a value, that provided reasonable intensities for each detector (generally the arithmetic mean of the maximum values for the respective detectors). Afterwards the detector background was determined by starting a measurement for 40 minutes while the primary beam was turned off. It was aimed for a detector background of less than 1 cpm, although this is lower than the CAMECA specs.

Detector backgrounds depend on the setting of a discriminator voltage. As a secondary ion strikes the first dynode of the EM, secondary electrons are emitted that are accelerated and multiplied through the following dynodes of the EM. The produced charge pulse is converted into a voltage pulse and amplified. However, this amplitude is not constant but can be shown in a pulse height distribution (PHD) as can be seen in Figure 16.

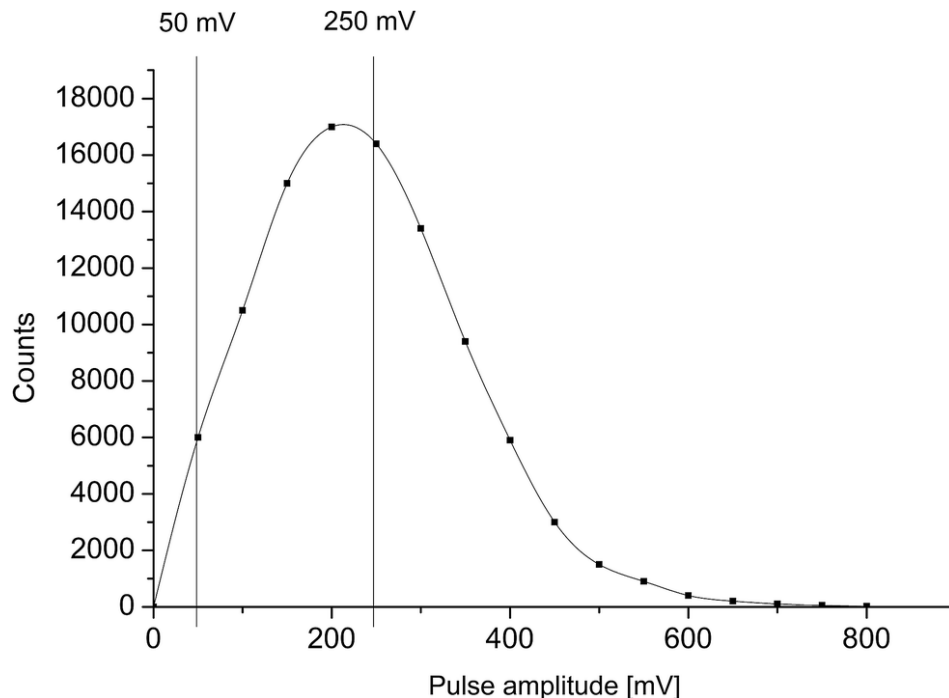


Figure 16: Typical detector pulse height distribution (PHD) from a Hamamatsu EM detector (Hedberg *et al.* [2], [CC BY 3.0](#)).

Sometimes not only impinging secondary ions but also other events can cause the emission of a charge pulse (background). However, the PHD for events that are part of the ordinary background

looks different from a normal impinging secondary ion event. Hence, there are lower and upper detection thresholds to cut off the system noise. In the Hamamatsu EMs that are used in the multi-collection array of the HIP, the default setting for the lower threshold (Thr1) is 50 mV and for the upper threshold (Thr2) 250 mV (Figure 16). A raise of Thr1 will discriminate more induced charge pulses in the lower spectrum of the PHD that may resemble background noise.

This discrimination was used for the adjustment of EM background noise. Initial results for an EM discriminator threshold of 50 mV only partially satisfied the criterion of low noise. Although detectors L2, L1 and H2 yielded results of less than 1 cpm, H1 with 1.07 cpm and especially C with 5.51 cpm were outside the limit (Figure 17). For the second background measurement, Thr1 was raised to 70 mV. The result was a noticeable lower background for all EM detectors (L2: 0.50 cpm; L1: 0.15 cpm; C: 0.55 cpm; H1: 0.30 cpm; H2: 0.20 cpm). With the new settings, all EM detectors are below the maximum limit of 1 cpm.

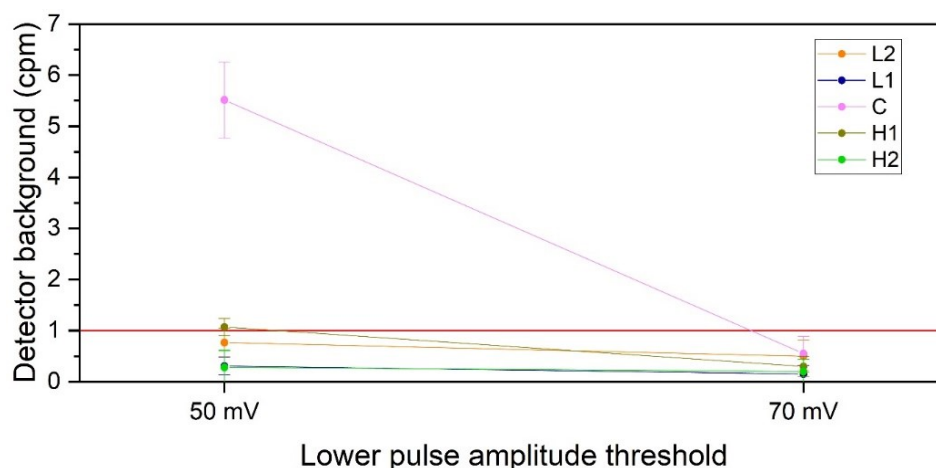


Figure 17: Detector background for EMs with different lower pulse amplitude thresholds (Thr1). Red limit at 1 cpm.

EM HV was adjusted for all detectors with the new lower threshold, and test measurements of ^{238}U on the same particles with the same primary ion current yielded $\sim 50,000\text{-}60,000$ cps, which leads to the conclusion, that raising the lower pulse amplitude threshold does not affect the transmission in a significant magnitude.

As described by Hedberg *et al.* [19], short term drift of the EM detectors can affect the quality of uranium isotope abundance measurements. However, EM detectors with an advanced age, i.e. that were exposed to high intensities before, are less vulnerable to short term drift. New Hamamatsu EMs typically start with a voltage of about 1600 V which changes during the aging process up to 2200–2400 V due to carbon deposition on the last dynodes [103].

To investigate the age and stability of the Hamamatsu multicollection EMs at the HIP, stability measurements were performed. The primary ion beam was shut down and all EMs were rested for ~ 16 hours. ^{238}U was measured with an intensity of $\sim 100,000$ cps on all detectors sequentially by exposing them to the signal directly after the resting interval. The measurements were stopped, when the intensity dropped below 50,000 cps when the measured particle was becoming exhausted. Each measurement cycle was set to 4 s. After each measurement cycle, EM HV adjustment for the detector was performed and the detector voltage recorded. The results are shown in Figure 18.

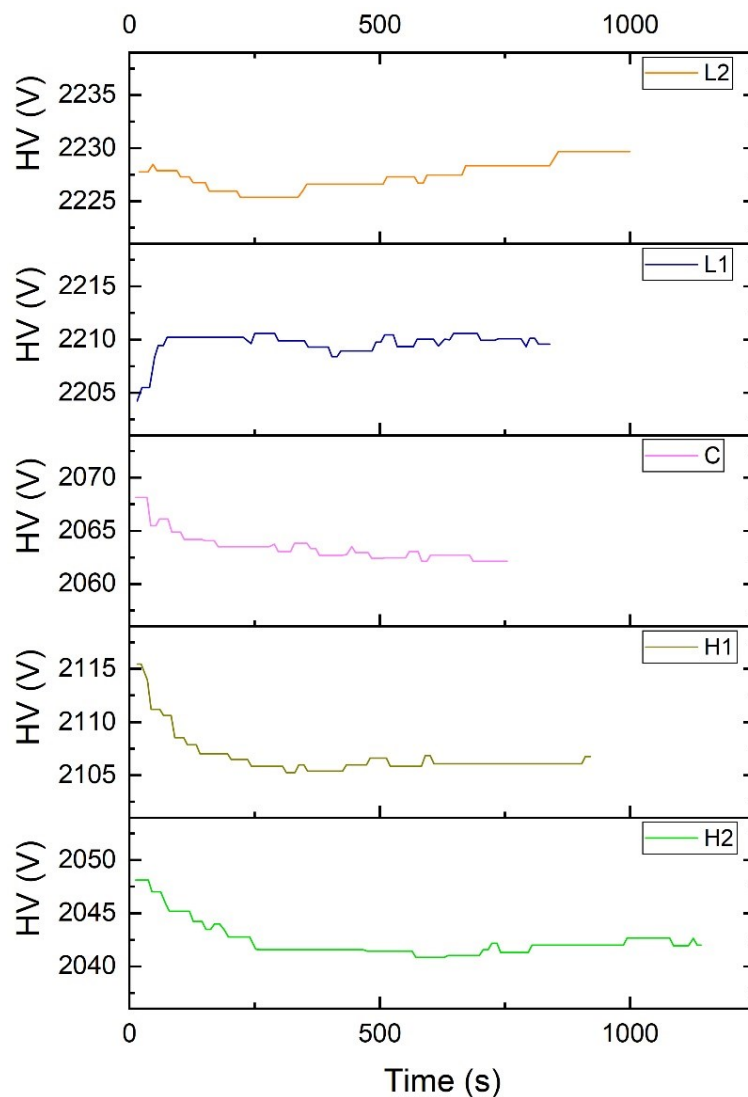


Figure 18: HV adjustment of EMs during particle measurements in December 2021.

Overall, the EM detectors are set to voltages between ~ 2000 and 2250 V. Compared to the data reported by Hedberg *et al.* [19], this suggests an advanced detector age. Therefore, the detectors should not be very prone to short term drift. The drift patterns for L2, C, H1 and H2 match the data from Hedberg *et al.* with a rapid voltage drop in the beginning of the measurement and then

a phase of detector stabilization. However, detector L1 shows a voltage increase instead of a drop and then stabilizes afterwards. Several stability measurements over a time period of 1.5 years confirmed this behavior. Detector L2 also shows signs of a slight voltage increase before the drop, but overall the drift pattern looks more like the ones recorded by Hedberg *et al.* Although this reaction is unexpected and anomalous, this does not seem to affect the stability phase when compared to the other EM detectors.

For all detectors, the voltage fluctuation is below 10 V. Compared to these results, the voltage decrease described by Hedberg *et al.* is much larger. This can be explained by the advanced detector age. In summary, the stability of the detectors should allow for reliable isotopic abundance measurements.

For the whole duration of a measurement session, the detector yield was closely monitored. Therefore, several yield measurements were performed at different times on every measurement day. These yield measurements were similar to those performed with the mixed FC/EM setup. ^{238}U was measured on every EM detector sequentially and a drift time correction was applied [102]. The yield measurements were performed with an intensity of $\sim 50,000\text{--}60,000$ cps to prevent the introduction of increased short-term detector drift by putting high intensity ion beams on the minor isotope detectors L2, C and H2 [19; 104]. Figure 19 shows the detector yield of each EM detector over a period of 10 days as ratio of measured intensity against the measured intensity for H1 on the left side. Each data point resembles a single measurement of 25 cycles with a counting time of 4 s on each detector. At the start and the end of each measurement, an EM HV adjustment was performed on each detector. The corresponding HV values for each detector are on the right side in Figure 19.

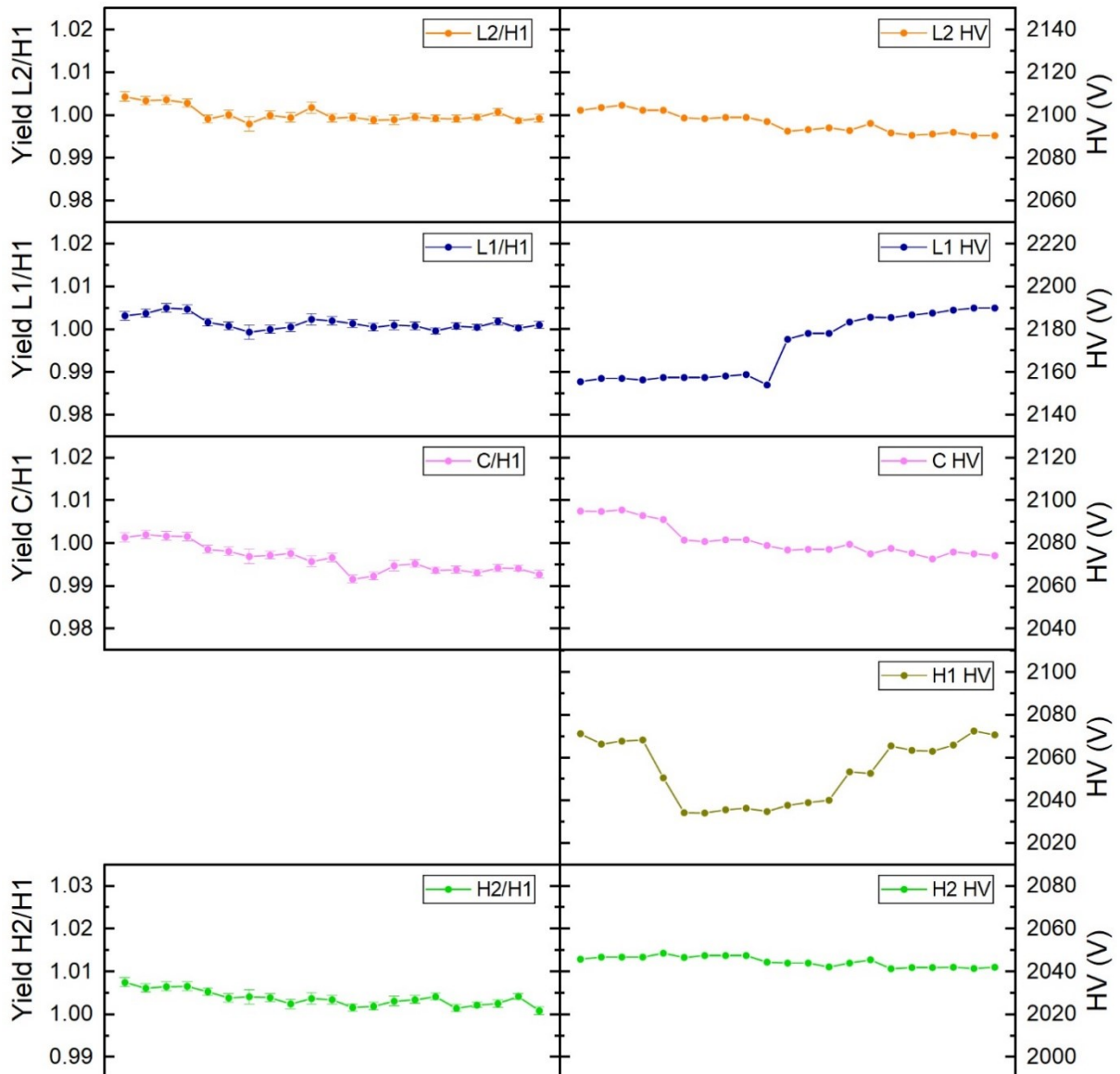


Figure 19: EM detector yield and HV over a period of 10 days in October 2021. Yield is calibrated against H1 detector.

For all EM detectors, the yield variations are less than $\pm 1\%$ over a period of 10 days. This leads to the conclusion, that the EM detector yield is overall stable. The detectors for the minor isotopes L2, C and H2 display only slight changes in detector HV, while the detectors for the major isotopes L1 and H1 are clearly running with higher HV towards the end of the measurement campaign. This confirms the accelerated aging of detectors that are exposed to higher intensities [103].

To get accurate results for ^{236}U , a hydride correction for $^{235}\text{U}^1\text{H}$ has to be applied. The factor was estimated by measuring the $^{238}\text{U}^1\text{H}/^{238}\text{U}$ -ratio [16].

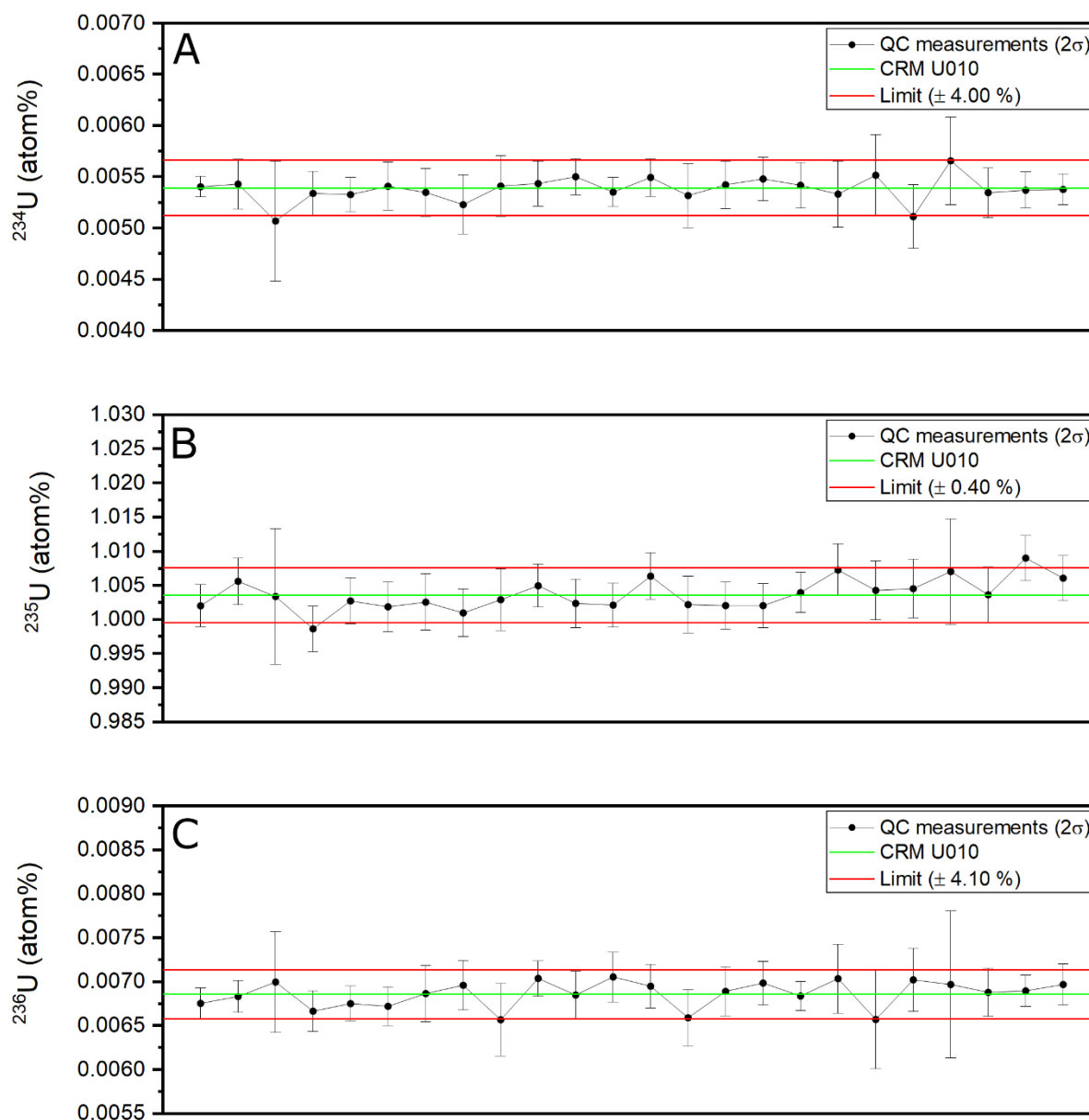


Figure 20: Quality Control (QC) measurements of CRM U010 over the period of 10 days. Shown are ^{234}U (A), ^{235}U (B) and ^{236}U (C). Control limits for this CRM are set due to empirical value and agree with IAEA protocol.

For mass calibration and determination of mass bias, NBL CRMs U010 with $\sim 1\%$ ^{235}U , U100 with $\sim 10\%$ ^{235}U and U500 with $\sim 50\%$ ^{235}U were used. Figure 20 shows isotope abundance measurements of CRM U010 performed over a time span of 10 days as quality control measurements. Nearly all of the measurements plot within the empirical control limits for CRM U010 adapted from the IAEA measurement protocol. These quality control measurements are used to calculate the mass bias which is usually 0.1-0.4 % per atomic mass unit (amu) [15; 16]. In this study, a mass bias of -0.21 % per amu was calculated. This means, that the isotopically lighter isotopes are preferably detected and intensities have to be corrected for this factor. The physical reasons for this mass bias could be preferred sputtering of lighter isotopes, better transmission or higher detection efficiency.

Isotopic abundance measurements were carried out following the IAEA measurement protocol for dynamic multi-collection measurements [19] as shown in Figure 21.

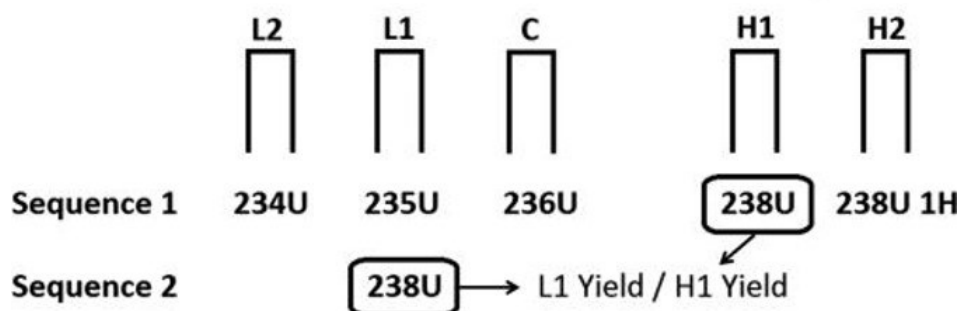


Figure 21: MC detector setup for dynamic multi-collection measurements as described by Hedberg *et al.* [1].

EM HV adjustment prior to the measurement was applied for detectors L1 and H1. Yield for detector L1 was calculated using the ^{238}U intensity on H1 in sequence 1 and on L1 on sequence 2, while isotopic abundance was calculated using all the intensities from sequence 1. Hedberg *et al.* [15] suggest a short counting time of 4 s for sequence 1 and 1 s for sequence 2 with 100 cycles per measurement. However, this approach wastes a lot of measurement time while switching between the sequences. A total evaporation measurement where particles are completely sputtered with a primary ion beam current of ~ 100 pA was performed to measure the time it takes to consume a typical VOAG-produced uranium microparticle with a size of ~ 1.2 μm (Figure 22). The results lead to the conclusion, that a single particle is mostly consumed after 12–15 min of sputtering. To avoid wasting too much time for the adjustment of the magnet field for the respective sequences in each cycle (which means loss of valuable intensity), the counting times for isotope abundance measurements and the number of cycles per measurement were changed. The counting time for sequence 1 was set to 16 s, for sequence 2 to 2.5 s while only using 25 cycles per measurement which leads to a total measurement time of ~ 11 min. This provides a better yield of total counted ions and therefore better counting statistics.

The uncorrected intensities of the total evaporation measurement in Figure 22 show the typical intensity development of single particle measurements. While the intensities of ^{234}U , ^{235}U and ^{238}U increase in the first seconds, form a plateau and then decrease until the particle is consumed, the intensity of ^{236}U decreases from the beginning. This leads to the conclusion, that the ions counted at mass 236 are in fact mostly hydrides from ^{235}U [16], in agreement with the very low amount of 9.7 ppm ^{236}U reported for CRM NBL 129-A [90] that is below the LG-SIMS detection limit for ^{236}U in uranium microparticles as defined by Ranebo *et al.* [16].

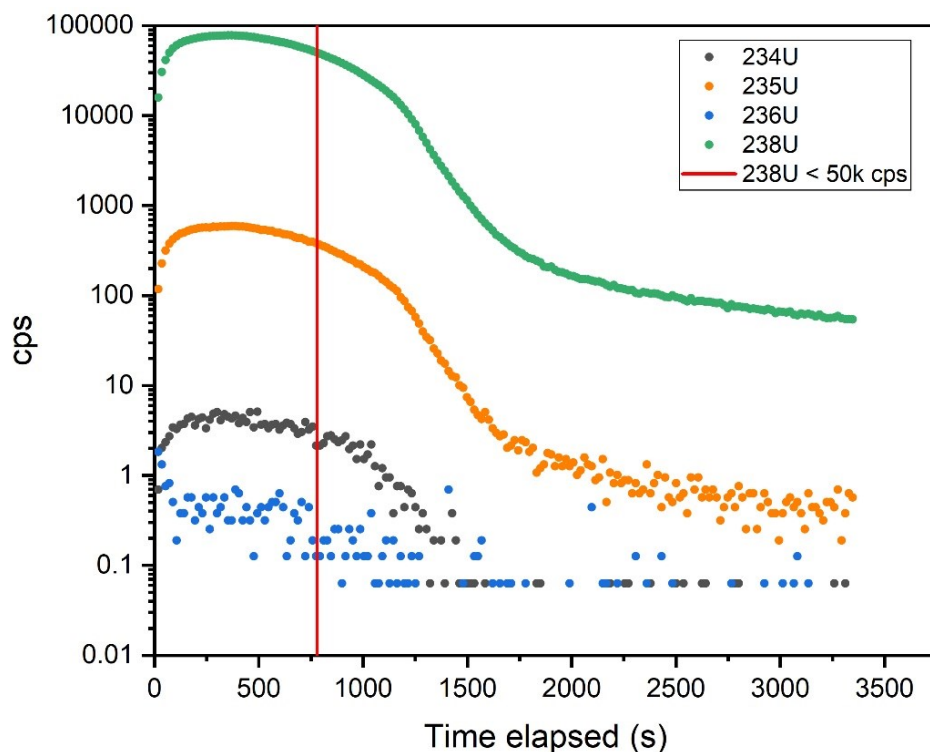


Figure 22: Total evaporation measurement of a typical VOAG-produced uranium microparticle measured with a primary ion beam current of ~ 100 pA. 50,000 cps ^{238}U is an empirically set lower limit for reasonable counting statistics.

The isotopic abundances of the measured CRM NBL129-A particles agree with the empirically determined limits for the certificate value of CRM NBL 129-A within their 1σ uncertainties (Figure 23). The relative standard deviation for ^{234}U is 2.91 %, for ^{235}U 0.22 % and for ^{236}U 106.44%, which is due to the fact that CRM NBL 129-A contains very low amounts of ^{236}U (less than 1 ppm of all U atoms). Overall the relative standard deviation of the isotope abundance values is within the limits recommended for LG-SIMS measurement protocols as suggested by the IAEA (Hedberg *et al.* [15]). In conclusion, these tests demonstrate that an adequate precision and accuracy for isotopic abundance measurements of uranium microparticles can be achieved with the HIP.

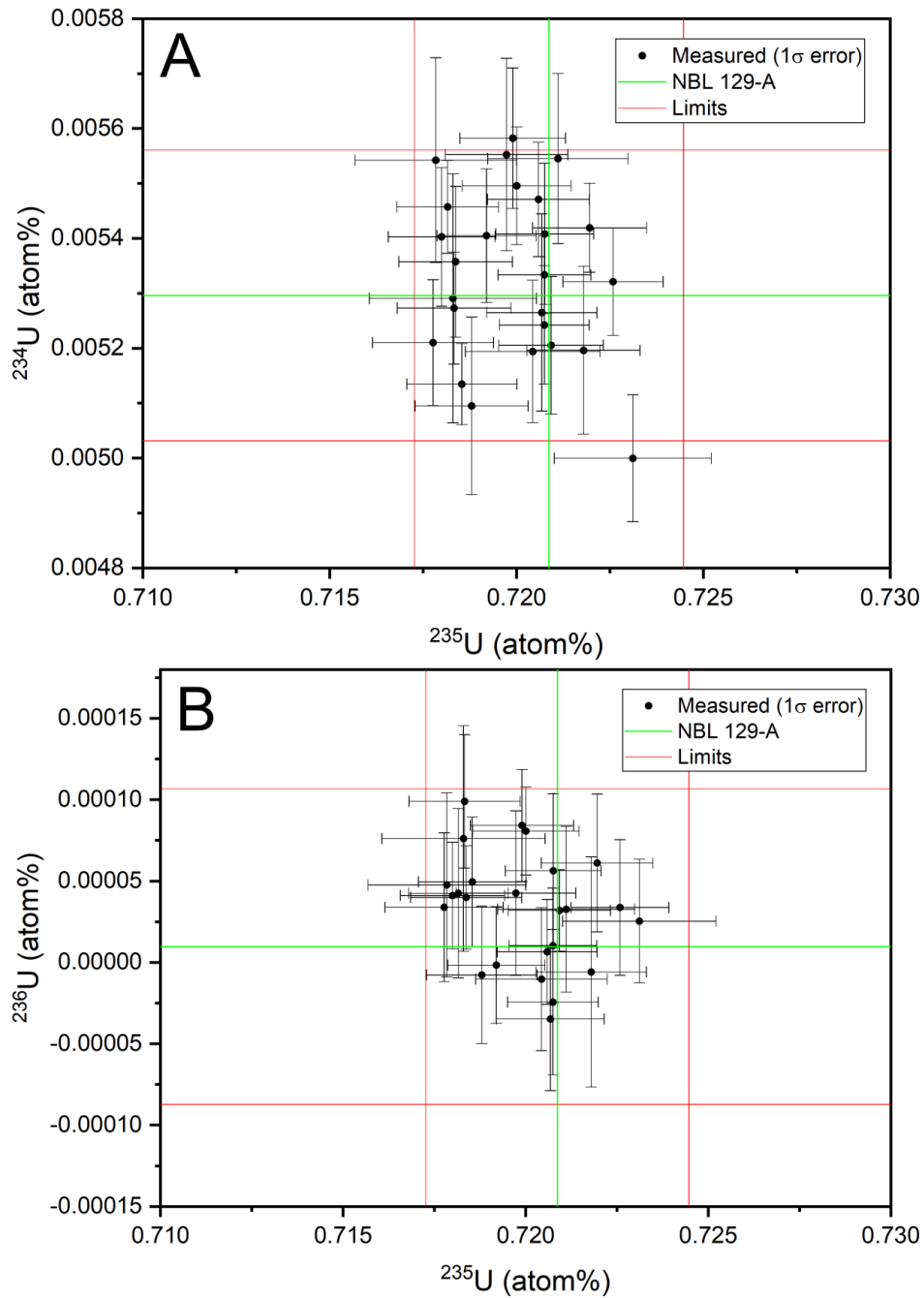


Figure 23: Isotopic abundance measurements of particles produced with CRM NBL 129-A. (A) is ^{234}U vs. ^{235}U and (B) is ^{236}U vs. ^{235}U . All values are atom%. Certificate value and empirical limits close to IAEA standards are shown as green and red lines.

4.1.3 Uranium isotopic composition of *Lanthanide*-doped microparticles

As reference materials for the IAEA, composite materials of U-Th and U-Pu microparticles are of particular interest [105]. To investigate the production of mixed uranium microparticles with the VOAG in the FZJ, lanthanide-doped (*Ln*-doped) microparticles were produced. The process is described by Kegler *et al.* for Nd-doped particles [48].

The question arises whether this doping process affects the uranium isotopic composition and could lead to a fractionation process. To investigate this, mixed uranium microparticles derived from CRM NBL 129-A with 10 atom% Ce were measured with the established microparticle measurement setup and compared to pure uranium microparticles produced using the same CRM.

As shown in Figure 24, the particles agree in their uranium isotopic abundance. Although the ^{234}U mean values for both the undoped and the doped particles are $\sim 1.5\%$ lower than the certificate value, this effect attributed to a bias in the EM detector yield adjustment rather than isotopic fractionation, and hence can be neglected. For ^{236}U , both particle populations show slightly raised values due to the low overall abundance of ~ 9.7 ppm ^{236}U in CRM NBL 129-A [90]. It can be concluded that Ce-doping of VOAG-produced uranium microparticles up to 10 atom% does neither affect the U isotopic composition of the particles nor the ability to measure said composition with the established measurement setup.

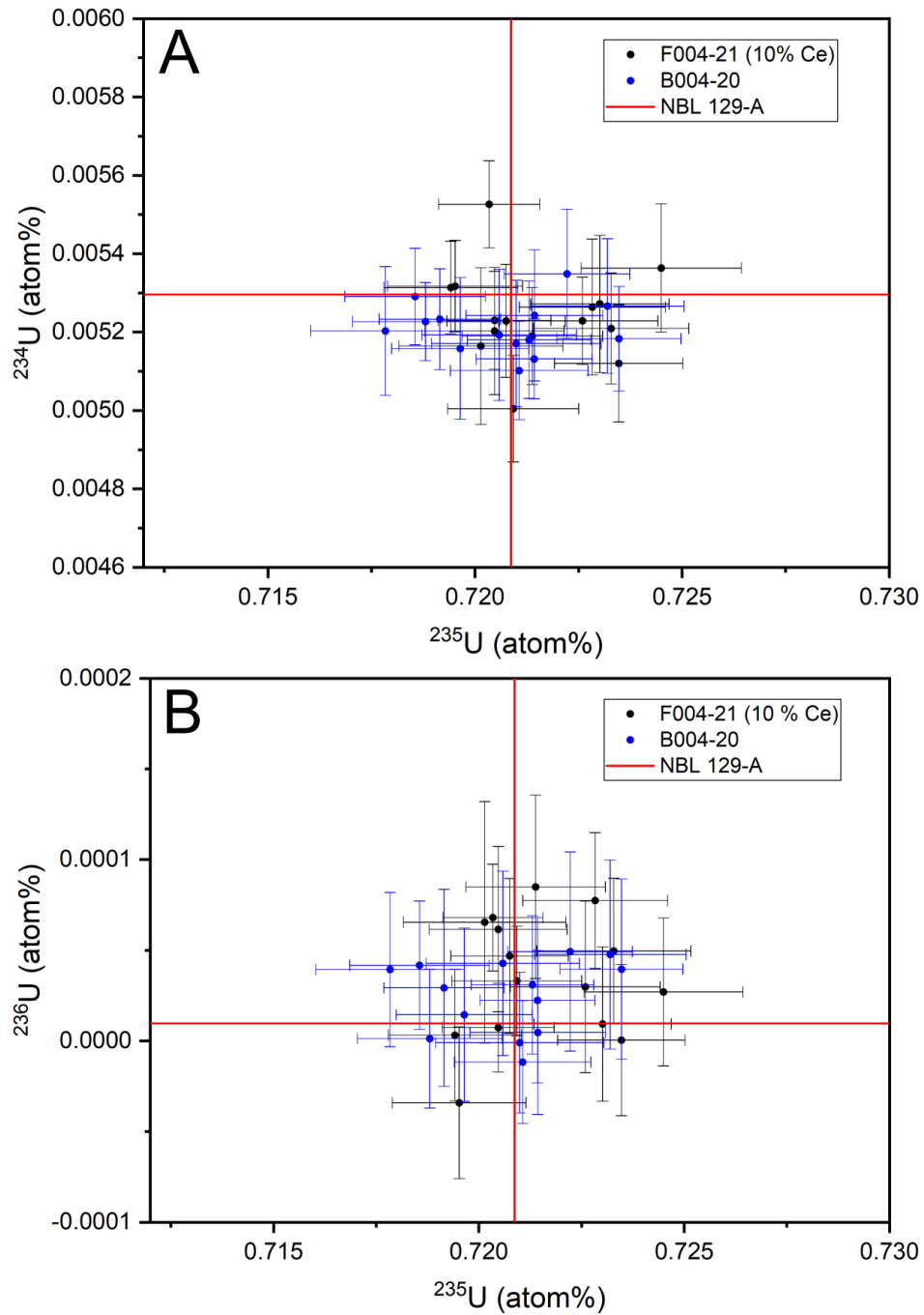


Figure 24: Uranium isotopic abundance of pure U microparticles compared to U microparticles doped with 10 atom% Ce with 1σ uncertainties and certificate values of CRM NBL 129-A. (A) is ^{234}U vs. ^{235}U and (B) is ^{236}U vs. ^{235}U .

4.1.4 APM verification

One of the main requirements for uranium microparticles to qualify as reference materials is the homogeneity of the particles. A valuable tool to assess the isotopic homogeneity of microparticles and to identify particles with divergent isotopic abundance within the entirety of microparticles on a sample planchet is the so-called APM software introduced in 2008 [85].

Table 2: SIMS analytical conditions for APM measurements.

Operating conditions APM	
Primary ions	O ₂ ⁺
Primary acceleration voltage	+15 kV
Secondary acceleration voltage	+8 kV
Total incident energy	7 keV
Raster	500 × 500 μm
Optical mode	Circular
Primary ion currents	~30-100 nA
Image field for transfer optics	80 μm
Dynamic Transfer Optical System	On
Contrast aperture	400 μm
Field aperture	12000 μm
Entrance slit	174 μm
Exit slit	500 μm
Mass resolution	~2000
Energy bandwidth	30 eV

The APM software was installed in the HIP in December 2021. A test planchet resembling a real field sample was provided by the IAEA to verify the setup for APM measurements. The setup was mainly adapted from the single particle measurements and modified according to Hedberg *et al.* [15; 85] and Peres *et al.* [86]. The exact parameters can be found in Table 2. In this case, a relatively high primary ion beam current of ~100 nA was used, because a low particle concentration and small particle size was expected. A relatively high primary beam current promises sufficient intensities for the APM software.

The particles on the sample were deposited using a vacuum impactor. With this technique, particles are usually deposited on a surface area with a radius of ~8 mm. Therefore, a circular

area with a radius of 10 mm was split into fields of $500 \times 500 \mu\text{m}$. Each measured $500 \times 500 \mu\text{m}$ field of the sample surface was pre-sputtered for 10 s and then counted for 30 s. This equals a total acquisition time of ~ 10 h. The measurement is completely automated and was conducted during the night.

The latest auto-threshold calculation mode by CAMECA was used to calculate the uranium particle boundaries. This approach promises the best results over earlier calculation methods [86].

The calculation algorithm was set to the following parameters: Threshold exclusion at 10 %, smoothing average of 3×3 pixels, minimum particle size of 20 pixels and maximum particle size of 5000 pixels (to exclude measurement artifacts). For this test, no minimum ^{235}U intensity was applied and no particles on the field edged were excluded.

The APM software calculated 2933 particles. The majority of the calculated particles shows an enrichment of ~ 30 % ^{235}U (Figure 25). However, there are some particles with a lower total intensity that yield ^{235}U enrichment values of less than 1 %. These particles resemble natural uranium. The shape of the particle enrichment distribution is very typical for APM measurements of uranium microparticles [85; 86; 106]. The particles are distributed relatively even over the sample surface (Figure 26) and show a slightly denser populated central and rim area, which is typical for the preparation using a vacuum impactor. The calculated enrichment of the particles deviates from the actual enrichment depending on the total intensity. Hence, the particles that scatter in the lower part of the APM graph yielding low intensities below 10 cps deviate from the known isotopic abundance of the particles. In fact, their deviation from the real particle enrichment level can be directly correlated to their high uncertainties and is therefore an artifact from very low counting statistics.

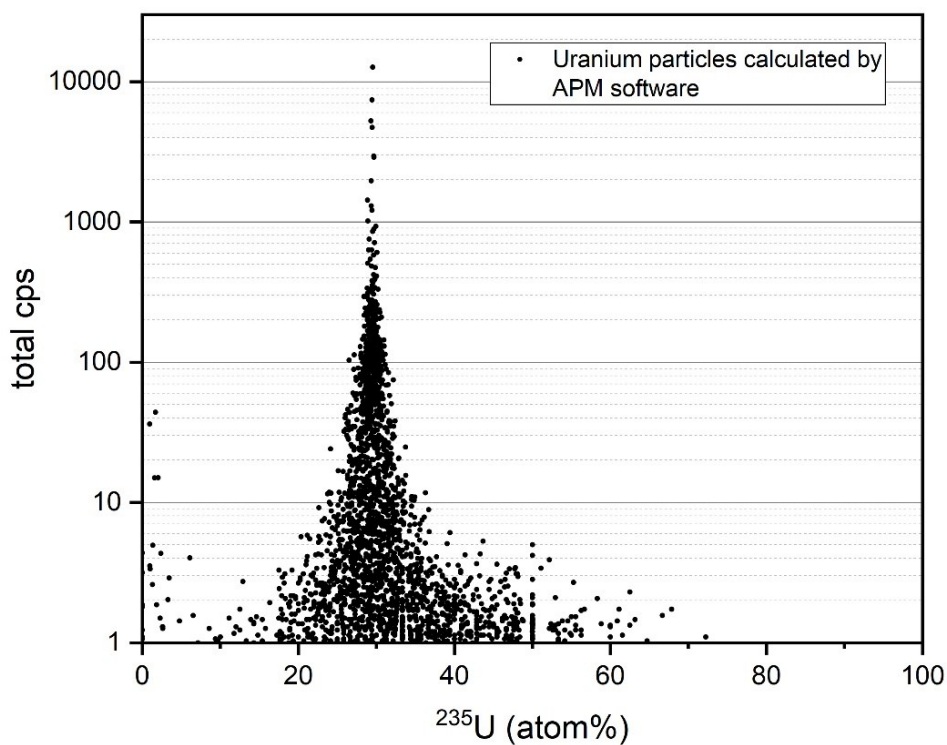


Figure 25: Results of APM performed on the simulated field sample provided by the IAEA. Total intensity is plotted vs. ^{235}U enrichment of the calculated particles.

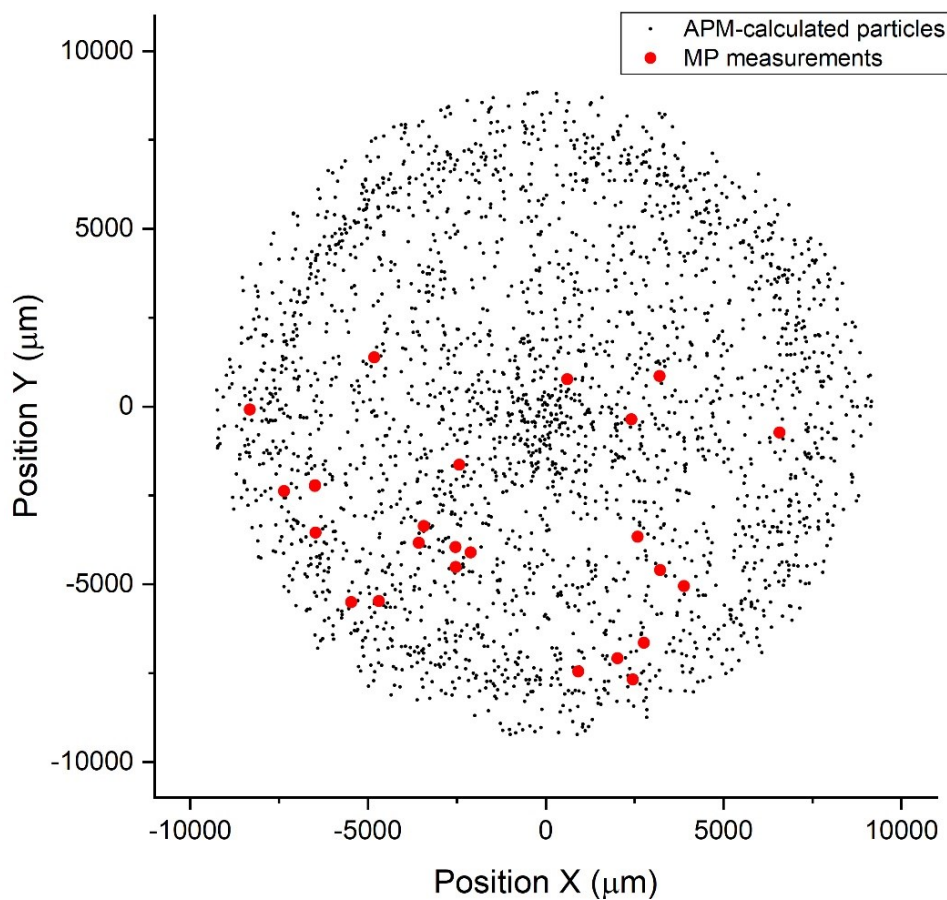


Figure 26: Position of the APM calculated microparticles on the sample planchet (black) and of the particles measured with microbeam analyses.

To verify the presence of two different particle populations, microparticle measurements for the particles with the highest total intensities resembling the populations with $\sim 30\%$ ^{235}U enrichment and less than 1% ^{235}U enrichment were performed (Figure 27). The results confirm the presence of a particle population of natural uranium with $\sim 0.72\%$ ^{235}U and a low abundance of minor isotopes and a population with $\sim 29.12\%$ ^{235}U and a higher enrichment in minor isotopes.

The APM measurement and subsequent calculation of the uranium particles on the simulated IAEA field sample successfully detected the presence of two different particle populations. This leads to the conclusion that the APM software is correctly implemented and ready to be used to exclude any contamination in newly produced microparticle reference materials and to confirm their homogeneity.

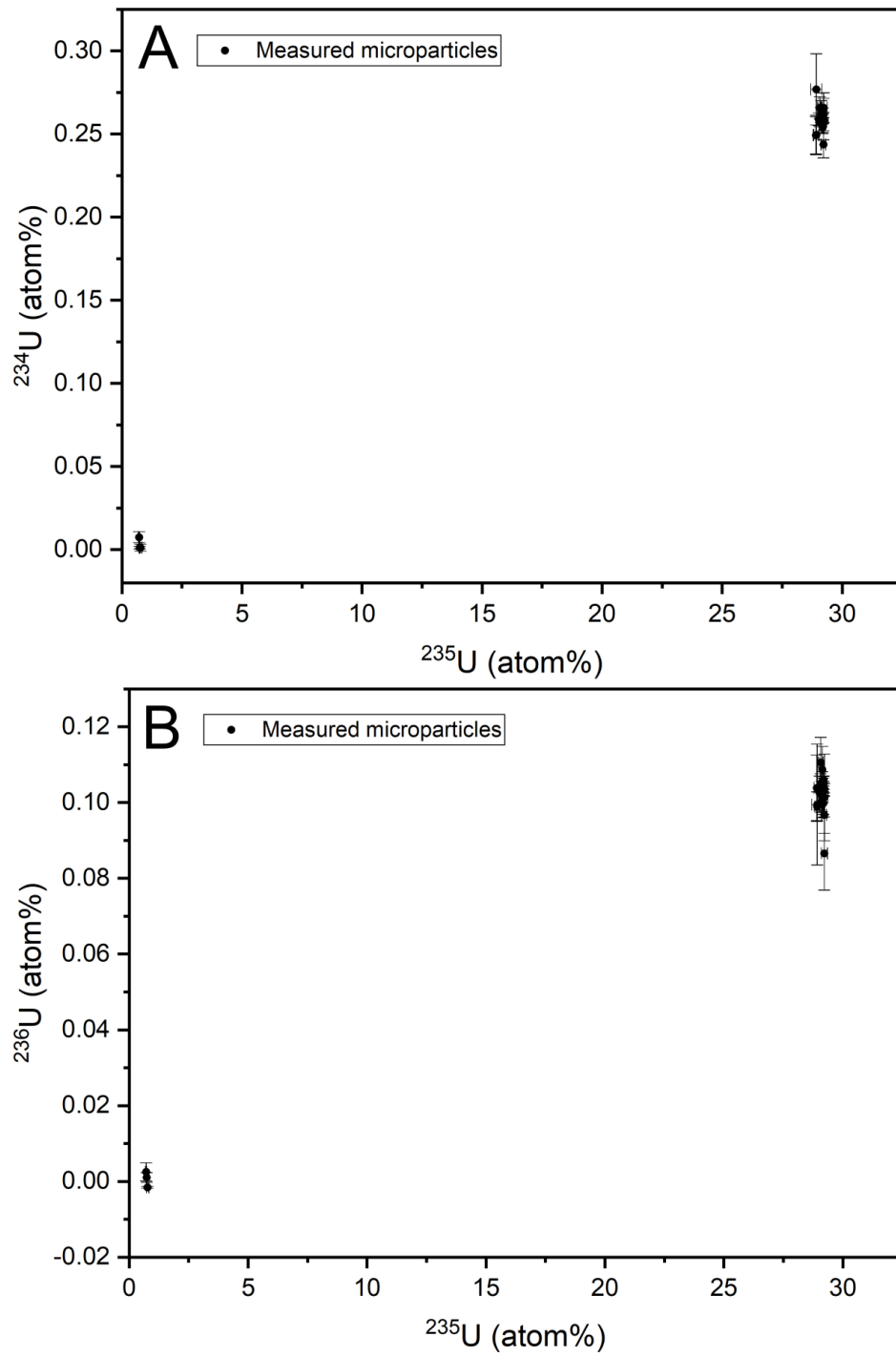


Figure 27: Isotopic abundance microparticle measurements of particles calculated by APM on the simulated IAEA field sample resembling two different particle populations. (A) is ^{234}U vs. ^{235}U and (B) is ^{236}U vs. ^{235}U .

4.2 SIMS characterization of IAEA-requested uranium microparticles

After the establishment of a working measurement protocol at the HIP, three IAEA-requested particle productions were characterized. Two of them will be described in the following chapters, while the isotopic abundance of the third production is currently part of a non-disclosure agreement (NDA). This production is expected to be used for an ILC between the NWAL labs, and its isotopic composition should therefore not be publicized at this time.

An IAEA-requested reference material has to match a pre-defined isotopic composition. For both of the following particle productions, feeding solutions of the IRMM-3000 series produced by European Commission JRC Geel were chosen [95; 107]. Further requirements are a (1) defined particle size and their size distribution, (2) a defined number and homogeneous distribution of particles on a planchet, (3) a certain number of samples produced and finally (4) the produced particles have to meet certain, pre-defined analytical acceptance criteria [94].

Both particle productions were carried out using the VOAG in the FZJ safeguards laboratories in 2022 and 2023 with the same well-established process as used before for the production of reference materials IRMM-2329P and IRMM-2331P [26; 45; 48; 94]. For each production, two particle batches with different mean particle diameter of $\sim 0.9 \mu\text{m}$ and $\sim 1.4 \mu\text{m}$ were requested. An additional dispersion step was applied to guarantee homogeneous particle distribution on the planchet surface [47].

As an editorial note, the official names of the particle productions presented are FZJ-30XXP/1 and FZJ-30XXP/2. The use of a slash in sample names may cause problems with some programs used for data processing. Therefore, the sample names were changed to FZJ-30XXP-1 and FZJ-30XXP-2 in some figures. Both naming conventions represent the same samples.

4.2.1 Glassy Carbon Disk blank

To exclude the possibility of contamination at the HIP, a freshly produced, unused GCD planchet (Seishin Trading Co., Ltd., Kobe, Japan) was analyzed using the APM software. To measure even the slightest traces of uranium, a relatively high primary ion beam of 100 nA was used. Each field had an integration time of 20 s. For this special contamination measurement all calculated particles were included. The results of the APM are shown in Figure 28.

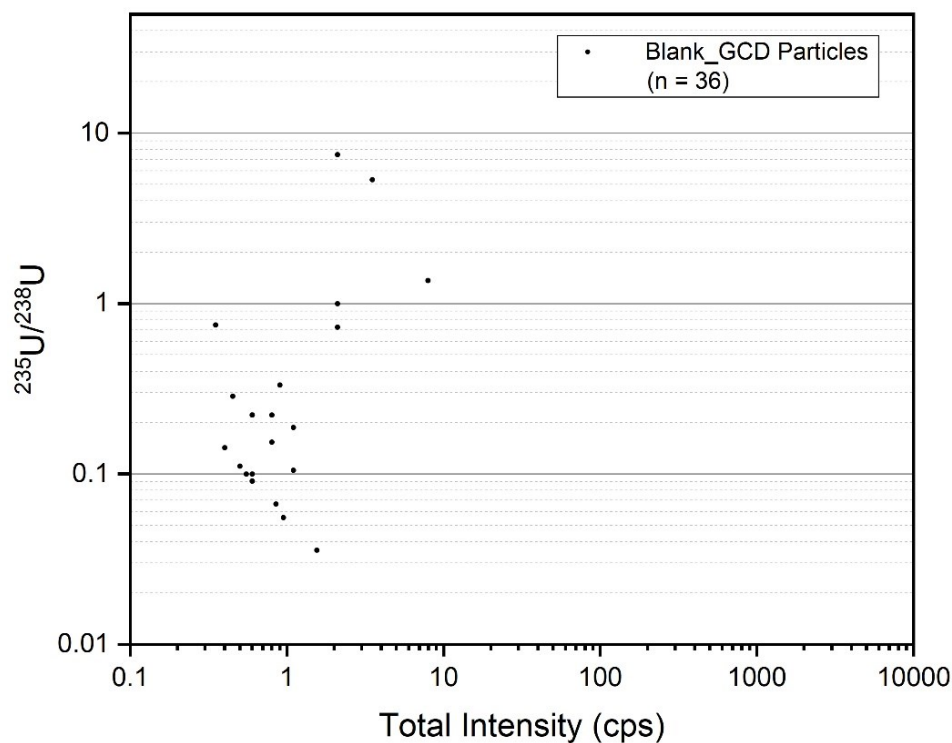


Figure 28: Results of APM performed on Blank_GCD. Total intensity is plotted vs. $^{235}\text{U}/^{238}\text{U}$ -ratio of the calculated particles.

A total of 36 particles were calculated by the APM software. However, closer examination of the calculated particles showed that all of them are in fact APM artifacts and no particles could be identified for microanalysis. Therefore, it can be concluded that there is no contamination, neither on the freshly produced GCD plachets nor in the HIP LG-SIMS that could lead to wrong results in follow-up measurements.

4.2.2 LG-SIMS measurements of FZJ-3050P

The first potential reference particles should have an enrichment of approximately 50 atom% ^{235}U . Therefore, IRMM-3050 was chosen as feeding solution for this particle production [95]. The smaller particles with an intended size of $\sim 0.9\ \mu\text{m}$ were labelled as FZJ-3050P/1, the bigger particles with an intended size of $\sim 1.4\ \mu\text{m}$ were labelled as FZJ-3050P/2.

For the characterization of the FZJ-3050P uranium oxide microparticles, LG-SIMS measurements were performed at the HIP in September 2022. The overall measurement setup and protocol is based on the protocol used by the IAEA-SGAS in the ESL in Seibersdorf. The measurement process was divided into two parts: Measurement of single microparticles and characterization of the

microparticle entirety using APM. For both parts of the characterization, the IAEA expressed some requirements, that will be defined in the respective chapters.

4.2.2.1 Microparticle measurements

For the characterization of the isotopic composition of the individual particles, a randomly chosen population of 40 microparticles per planchet had to be taken into consideration. The RSD of ^{235}U content in atom% should not be larger than 0.1 %. The minor isotopes should be consistent with certified values within normal LG-SIMS working uncertainties.

The values given in Table 3 and Table 4 represent the weighted mean of the measured isotopic abundance of 40 single particles analyzed. The uncertainties for the measured mean values represent the expanded uncertainty at a 95 % level of confidence. The standard uncertainty of the mean value derived from the variance of the weighted mean is multiplied with the Student's t-factor to provide uncertainties at a 95 % level of confidence [108].

FZJ-3050P/1

Table 3: Mean isotopic abundance of the particles on FZJ-3050P/1 with IRMM-3050 certificate values [107].

<i>Isotopic Abundance</i>	^{234}U	^{235}U	^{236}U	^{238}U
<i>Atom Fraction (atom%)</i>	0.001006	50.5759	0.001807	49.4209
<i>Uncertainty (95% confidence level)</i>	± 0.000021	± 0.0141	± 0.000153	± 0.0115
<i>RSD (%)</i>	5.662	0.043	30.141	0.044
<i>Certificate Values (atom%)</i>	0.0009838	50.5814	0.0019615	49.4157
	± 0.0000063	± 0.0044	± 0.0000060	± 0.0044

The RSD of ^{235}U is significantly lower than the required 0.1 %. For the minor isotopes, the relatively large RSD for ^{234}U can be explained by the small amount of ^{234}U in the FZJ-3050P particles. The large RSD for ^{236}U is a result of the massive influence of $^{235}\text{U}^1\text{H}$ and therefore the great impact of the hydride correction on the measured ^{236}U .

FZJ-3050P/2

Table 4: Mean isotopic abundance of the particles on FZJ-3050P/2 with IRMM-3050 certificate values [107].

<i>Isotopic Abundance</i>	^{234}U	^{235}U	^{236}U	^{238}U
<i>Atom Fraction (atom%)</i>	0.000996	50.5808	0.001883	49.4163
<i>Uncertainty (95% confidence level)</i>	± 0.000015	± 0.0135	± 0.000123	± 0.0108
<i>RSD (%)</i>	4.690	0.060	16.367	0.061
<i>Certificate Values (atom%)</i>	0.0009838	50.5814	0.0019615	49.4157
	± 0.0000063	± 0.0044	± 0.0000060	± 0.0044

The RSD of ^{235}U is also significantly lower than the required 0.1 %. The RSDs for the minor isotopes can be explained in the same way as for the FZJ-3050P/1.

Figure 29 shows the isotopic abundance of ^{234}U vs. ^{235}U (top) and ^{236}U vs. ^{235}U (bottom) of the single particles measured as well as the weighted mean for each sample planchet. The measured mean isotopic abundance values for both FZJ-3050P/1 and FZJ-3050P/2 is in good agreement with the certificate values of the feeding solution IRMM-3050 [107]. The overall uncertainties of the smaller FZJ-3050P/1 particles are between 5 – 30 % higher than the uncertainties of the bigger FZJ-3050P/2 particles. This effect can be expected due to the higher number of sputtered ions and therefore better counting statistics for bigger particles. For the major isotopes, the measured ^{235}U value of FZJ-3050P/1 is ~ 0.01 % lower than the certificate value of IRMM-3050. To check if this deviation is significant, a t-test can be performed [109]. The t-statistics can be calculated using the following equation:

$$T = \sqrt{n} \times \frac{(\bar{x} - \mu_0)}{SD} \quad (2)$$

n = number of measurements

\bar{x} = calculated weighted mean of the sample

μ_0 = expected value (certificate value)

SD = standard deviation of the sample

Using the values for the measured ^{235}U in equation (2), the calculated absolute t-value is $T = 1.598$. For a significance test, a critical t value has to be defined. The t-value is given by Student's t-distribution. For this case, a confidence interval of 95 % in a two-tailed t-distribution was chosen. Given the number of degrees of freedom by the number of measurements minus one

is 39, the relevant critical t-value is $T_{\text{crit}} = 2.023$. Given that $T < T_{\text{crit}}$, the null hypothesis cannot be rejected. This means, that it can be stated within a confidence level of 95 % that the deviation of the measured ^{235}U is not significant and therefore within normal uncertainties of the certificate value. The measured ^{235}U value of FZJ-3050P/2 is a slightly higher than for the smaller particles and nearly on point when compared to the certificate value of the feeding solution at 50.5814 atom% ^{235}U [107].

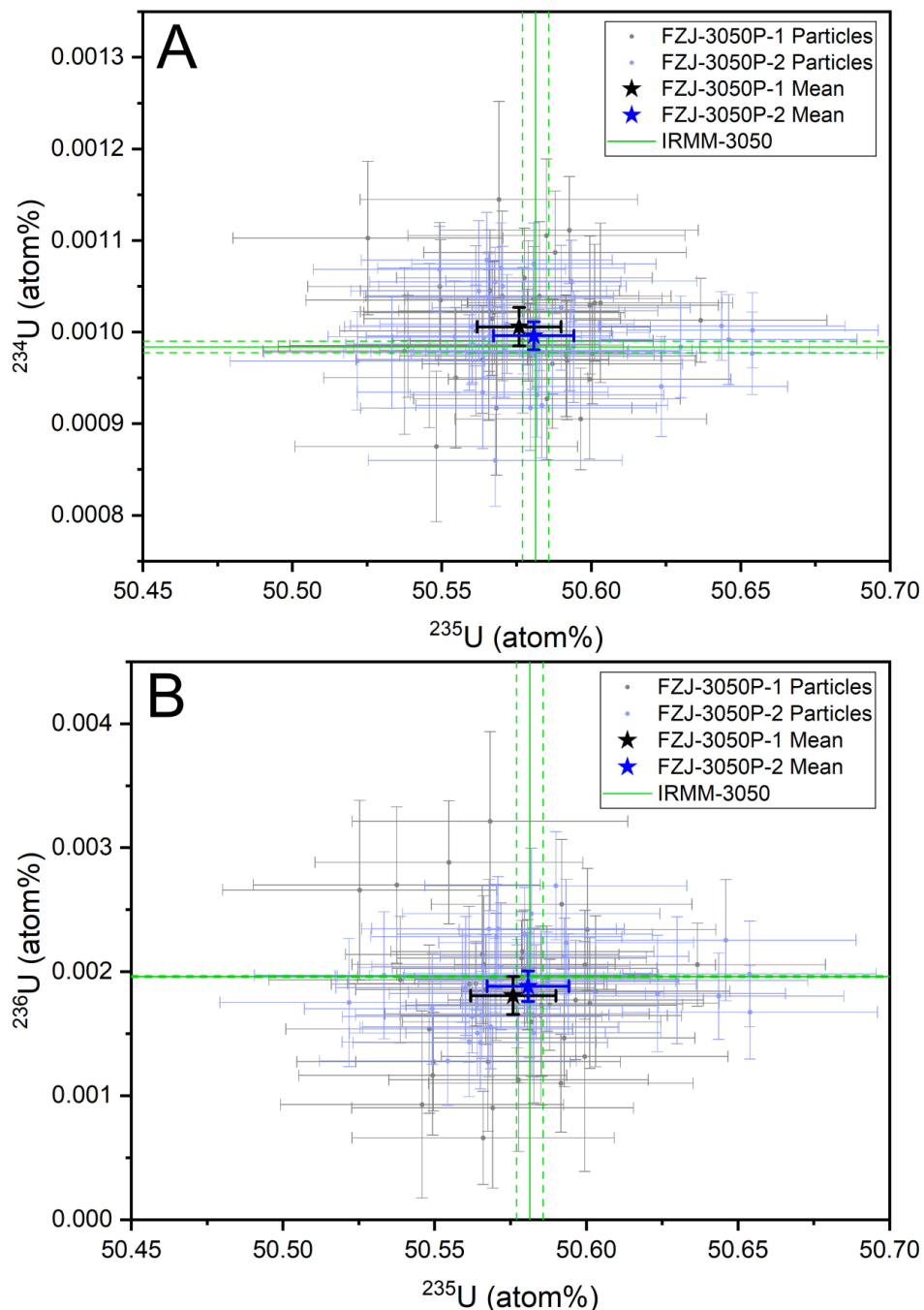


Figure 29: Isotopic abundance of the particles on FZJ-3050P/1 and FZJ-3050P/2 with weighted mean values. Panel A shows ^{234}U vs. ^{235}U and panel B ^{236}U vs. ^{235}U .

4.2.2.2 APM measurements

APM measurements were performed to exclude unintended U isotopic composition (contamination). They are also used as an indicator for the particle loading on the planchet. The IAEA's requirements for LG-SIMS APM measurements for the FZJ-3050P are, that less than 0.1% (1:1000) of the APM ^{235}U results deviate more than 4σ from the weighted mean. All particles with more than 100 ^{235}U counts should be taken into consideration. The number of particles on the planchet should be between 500 and 10,000 (nominal 3,000–5,000).

FZJ-3050P/1

The APM Software calculated 9309 U particles on the planchet. There was no evidence for the presence of more than one particle population on the planchet. As shown in Figure 30, 1 particle had a major U isotopic composition deviating more than 4σ from the weighted mean (0.011%).

FZJ-3050P/2

The APM Software calculated 3493 U particles on the planchet. There was no evidence for the presence of more than one particle population on the planchet. As shown in Figure 31, 2 particles had a major U isotopic composition deviating more than 4σ from the weighted mean (0.057%).

APM measurements of both samples lead to the conclusion that the production process occurred contamination free. The particles are mono-disperse and mono-isotopic for both batches. Additionally, the number of particles is within the specifications requested by the IAEA.

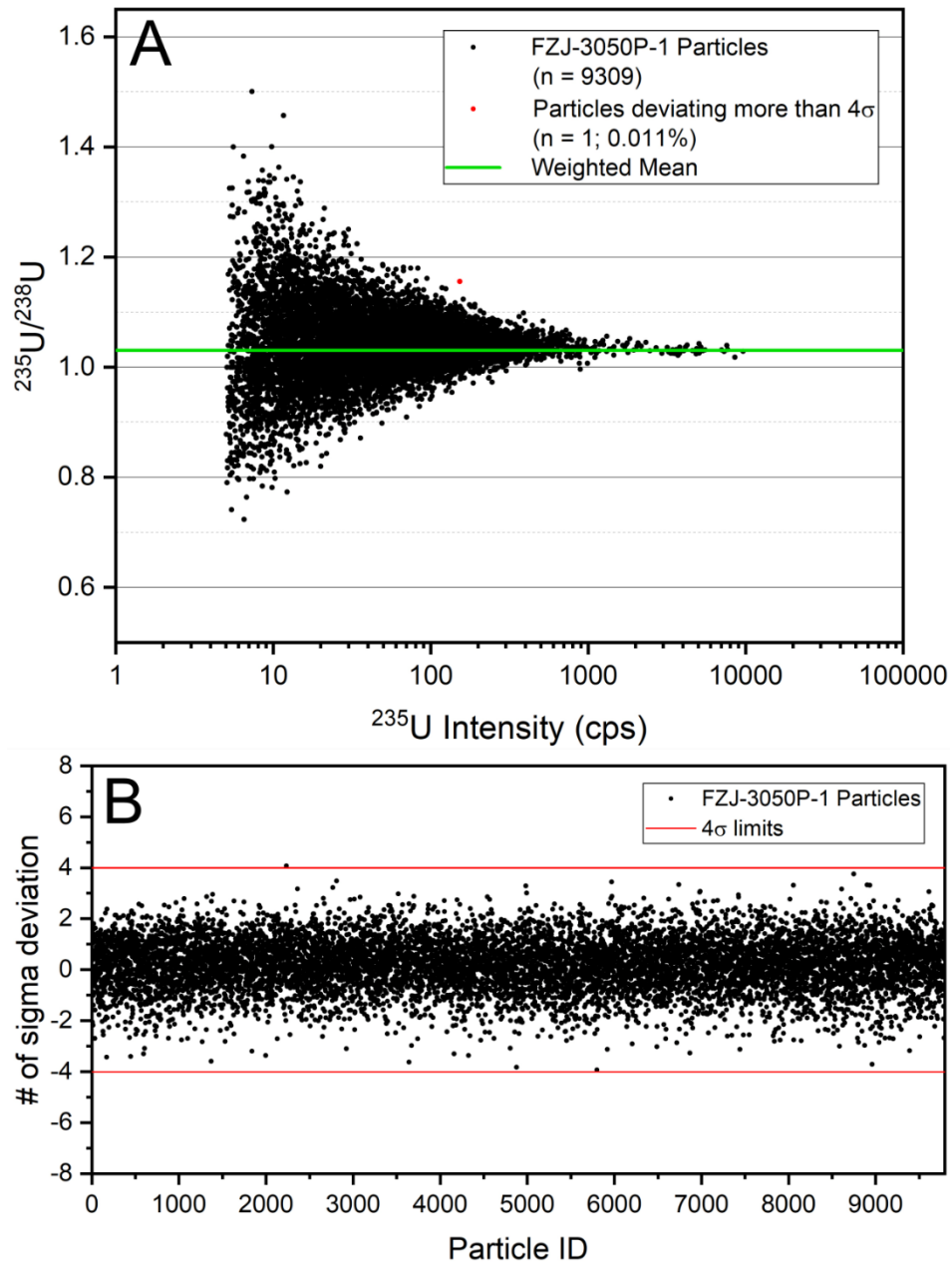


Figure 30: $^{235}\text{U}/^{238}\text{U}$ -ratio vs. ^{235}U intensity (A) and σ deviation (B) of the calculated particles on FZJ-3050P/1.

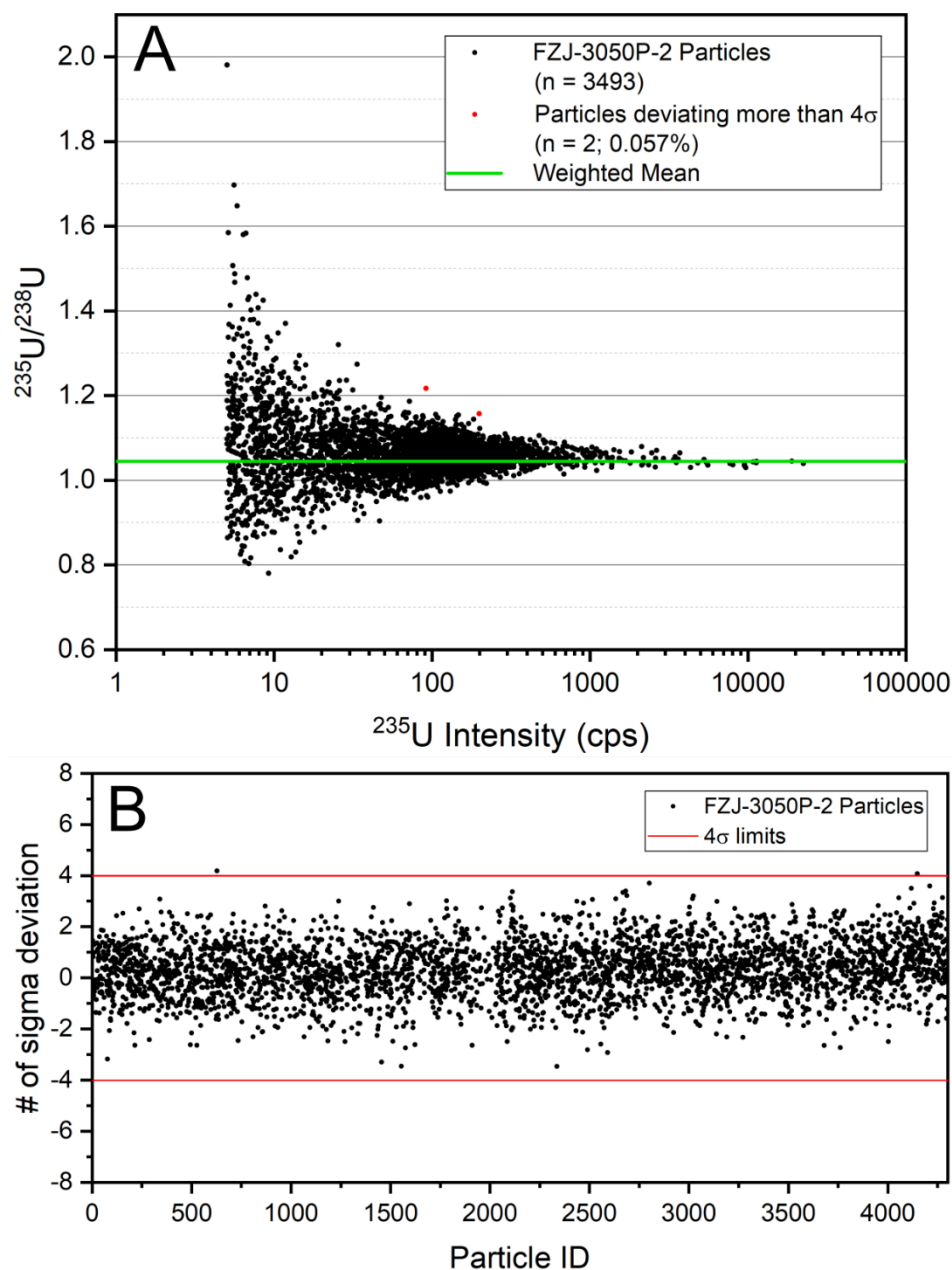


Figure 31: $^{235}\text{U}/^{238}\text{U}$ -ratio vs. ^{235}U intensity (A) and σ deviation (B) of the calculated particles on FZJ-3050P/2.

The particles on both plachets were easy to identify by both APM and for single-particle measurements. Due to the intermediate dispersion step, particle distribution on the GCD was homogeneous and no major particle agglomerations were formed.

The SIMS measurements at HIP lead to the conclusion that both FZJ-3050P/1 and FZJ-3050P/2 are viable options as potential uranium microparticle reference materials. Further use as standard material, research and development (R&D) material or as simulated field samples is up to the IAEA.

4.2.3 LG-SIMS measurements of FZJ-3090P

For the second IAEA-requested particle production derived from the IRMM-3000 series feeding solution, IRMM-3090 with approximately ~ 90 atom% ^{235}U was chosen [95; 107]. Similar to FZJ-3050P, particles with a mean size of ~ 0.9 μm and ~ 1.4 μm were requested. The naming of the sample batches is therefore FZJ-3090P/1 for the smaller and FZJ-3090P/2 for the bigger particles, according to the labelling of FZJ-3050P.

The SIMS measurement of the newly produced FZJ-3090P particles were performed at the HIP in August 2023. The measurement setup was an adjusted version of the IAEA-SGAS protocol. The IAEA requirements for the measurements were similar to the ones for FZJ-3050P.

4.2.3.1 Microparticle measurements

According to the requirements for the SIMS measurements of FZJ-3050P, a randomly chosen population of 40 microparticles per planchet had to be taken into consideration. The RSD of ^{235}U content in atom% should not be larger than 0.15%. Just as before, the minor isotopes should be consistent with certified values within normal LG-SIMS working uncertainties.

The values given in Table 5 and Table 6 represent the weighted mean of the measured isotopic abundance of 40 single particles analyzed. The uncertainties for the measured mean values represent the uncertainty at a 95% level of confidence. The standard uncertainty of the mean value derived from the variance of the weighted mean is multiplied with the Student's t-factor to provide uncertainties at a 95% level of confidence.

FZJ-3090P/1

Table 5: Mean isotopic abundance of the particles on FZJ-3090P/1 with IRMM-3090 certificate values [107].

<i>Isotopic Abundance</i>	^{234}U	^{235}U	^{236}U	^{238}U
<i>Atom Fraction (atom%)</i>	0.001708	86.7892	0.003707	13.2049
<i>Uncertainty (95% confidence level)</i>	± 0.000033	± 0.0160	± 0.000489	± 0.0078
<i>RSD (%)</i>	4.736	0.020	32.818	0.135
<i>Certificate Values (atom%)</i>	0.001685	86.7983	0.0033854	13.1966
	± 0.000011	± 0.0016	± 0.0000046	± 0.0016

The RSD of ^{235}U is significantly lower than the required 0.1%. For the minor isotopes, the relatively large RSD for ^{234}U can be explained by the small amount of ^{234}U in the FZJ-3090P

particles. The large RSD for ^{236}U is a result of the massive influence of $^{235}\text{U}^1\text{H}$ and therefore the great impact of the hydride correction on the measured ^{236}U paired with the poor counting statistics for the $^{238}\text{U}^1\text{H}/^{238}\text{U}$ -ratio that is used as reference for the hydride correction.

FZJ-3090P/2

Table 6: Mean isotopic abundance of the particles on FZJ-3090P/2 with IRMM-3090 certificate values [107].

<i>Isotopic Abundance</i>	^{234}U	^{235}U	^{236}U	^{238}U
<i>Atom Fraction (atom%)</i>	0.001690	86.7990	0.003699	13.1947
<i>Uncertainty (95% confidence level)</i>	± 0.000023	± 0.0153	± 0.000384	± 0.0063
<i>RSD (%)</i>	3.833	0.020	28.085	0.131
<i>Certificate Values (atom%)</i>	0.001685	86.7983	0.0033854	13.1966
	± 0.000011	± 0.0016	± 0.0000046	± 0.0016

The RSD of ^{235}U is also significantly lower than the required 0.1%. The RSDs for the minor isotopes can be explained in the same way as for the FZJ-3090P/1.

Figure 32 shows, that the mean isotopic abundance for both particle sizes is in good agreement with the certificate values of IRMM-3090 [107]. The measured ^{235}U enrichment for the bigger FZJ-3090P/2 particles almost exactly matches the certificate value. It is striking that the measured ^{235}U enrichment of the smaller FZJ-3090P/1 particles is once again lower than for the bigger particles. Using equation (2) in accordance to FZJ-3050P/1 to decide if the deviation is significant, the calculated t-value is $T=3.233$. When the same critical t-value for a confidence interval of 95 % of $T_{\text{crit}}=2.023$ is assumed, that means that $T > T_{\text{crit}}$. This leads to the conclusion, that with an error margin of 5 % it can be assumed, that the deviation of measured ^{235}U in FZJ-3090P/1 from the certificate value and from the calculated results of FZJ-3090P/2 is significant. Nevertheless, they agree with the certificate values within their uncertainties. This observation is discussed in chapter 4.4.3. Consistent with the FZJ-3050P particles, the uncertainties for the smaller particles are a little higher because of the worse counting statistics.

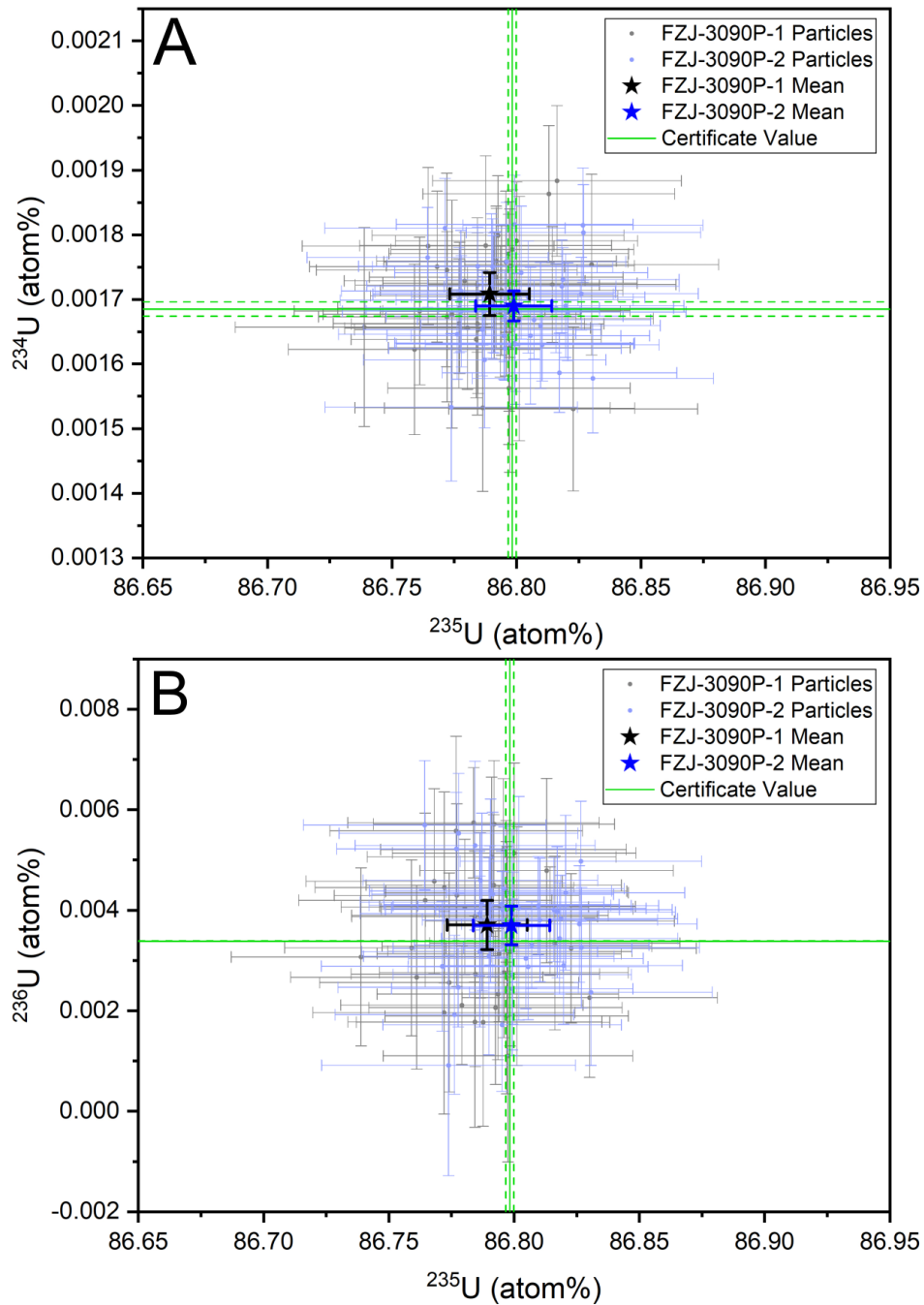


Figure 32: Isotopic abundance of the particles on FZJ-3090P/1 and FZJ-3090P/2 with weighted mean values. Panel A shows ^{234}U vs. ^{235}U and panel B ^{236}U vs. ^{235}U .

4.2.3.2 APM measurements

Like for FZJ-3050P, APM measurements on both FZJ-3090P were performed to exclude unintended U isotopic composition (contamination) and to assess the particle loading on the planchets. The IAEA's requirements for LG-SIMS APM measurements for the FZJ-3090P

concerning deviating isotopic abundance and particle load on the planchets are the same as for FZJ-3050P.

FZJ-3090P/1

The APM Software calculated 2078 U particles on the planchet. As shown in Figure 33, 5 particles had a major U isotopic composition deviating to higher values by more than 4σ from the weighted mean (0.24%). The calculated particles with a deviation of more than 4σ could not be identified as artifacts and therefore not be removed when looking into them in detail. The particles in question are marked red in Figure 33. When looking on the ^{235}U intensity, they are on the higher side. This leads to better counting statistics and therefore lower σ -values of the calculated particles, but also makes it more likely for the particles to cross the 4σ threshold set by the IAEA. Unfortunately, this is a weakness for this way of addressing the quality of the APM measurement. Possible reasons for this higher-than-expected deviation could be the stability of the primary ion source, that turned out to be suboptimal. During the overnight measurements, the primary beam current steadily increased from the target value of 30 nA to ~ 35 nA. We also noticed problems with the Z-axis focusing for some sample holders, that could influence the quality of the measurement and that caused the drift to higher σ deviation for particles with higher IDs, that imply a position on the lower part of the sample planchet (Figure 33). Nevertheless, the particles with more than 4σ deviation are just slightly outside the $+4\sigma/-4\sigma$ -region, and thus that there is insufficient evidence for the presence of more than one particle population on the planchet.

FZJ-3090P/2

The APM Software calculated 1370 U particles on the planchet. As shown in Figure 34, 6 particles had a major U isotopic composition deviating more than 4σ from the weighted mean (0.44%). This is also higher than the target value. The assumed reasons are equivalent to those of the deviation in FZJ-3090P/1. In this case, the primary beam current increased from 30 nA to ~ 33 nA. The drift towards higher σ deviation values for particles with higher ID, i.e. position at the planchet bottom, can also be observed for FZJ-3090P/2 (Figure 34). Nonetheless, there is also no evidence for a second particle population.

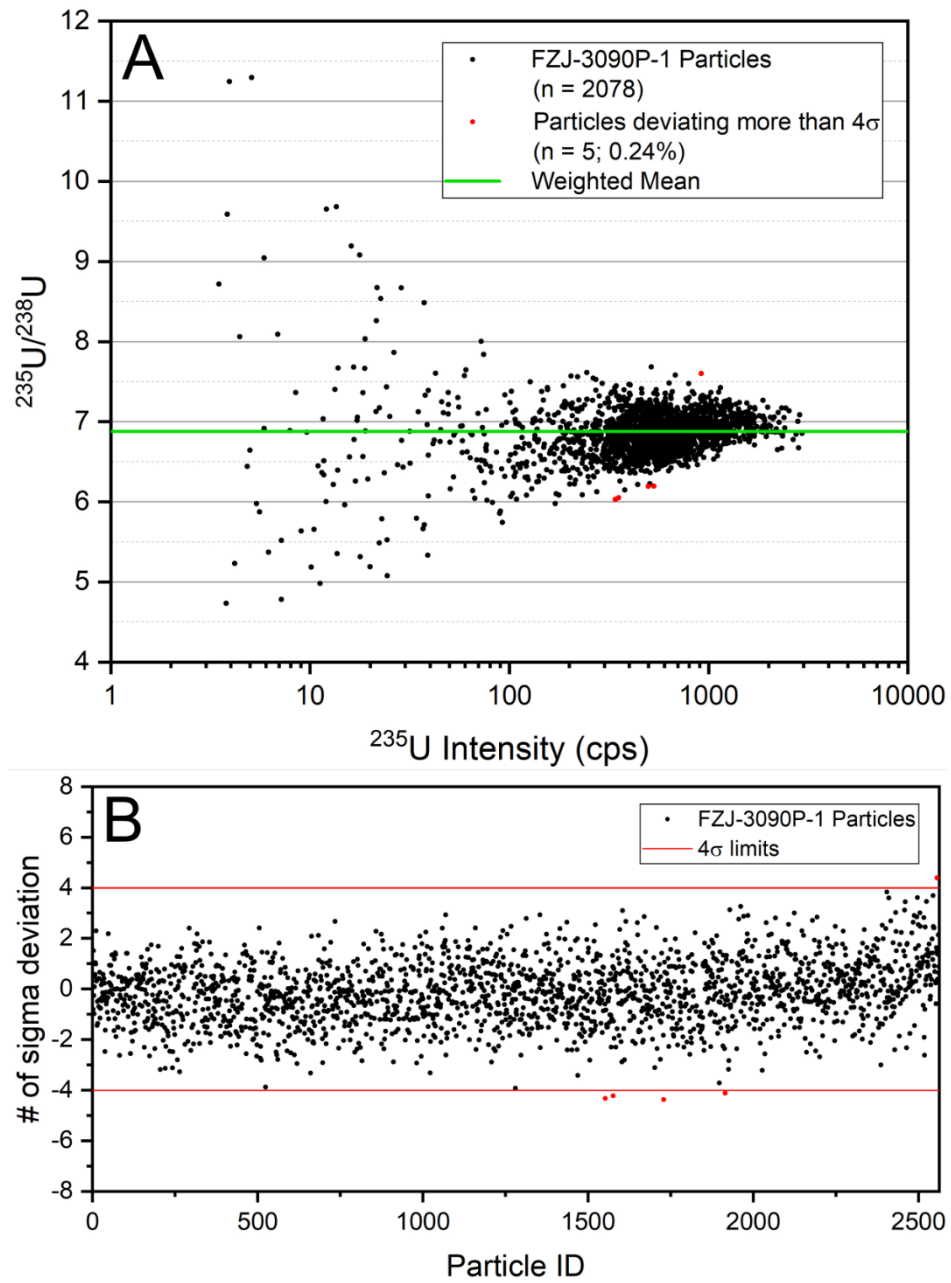


Figure 33: $^{235}\text{U}/^{238}\text{U}$ -ratio vs. ^{235}U intensity (A) and σ deviation (B) of the calculated particles on FZJ-3090P/1.

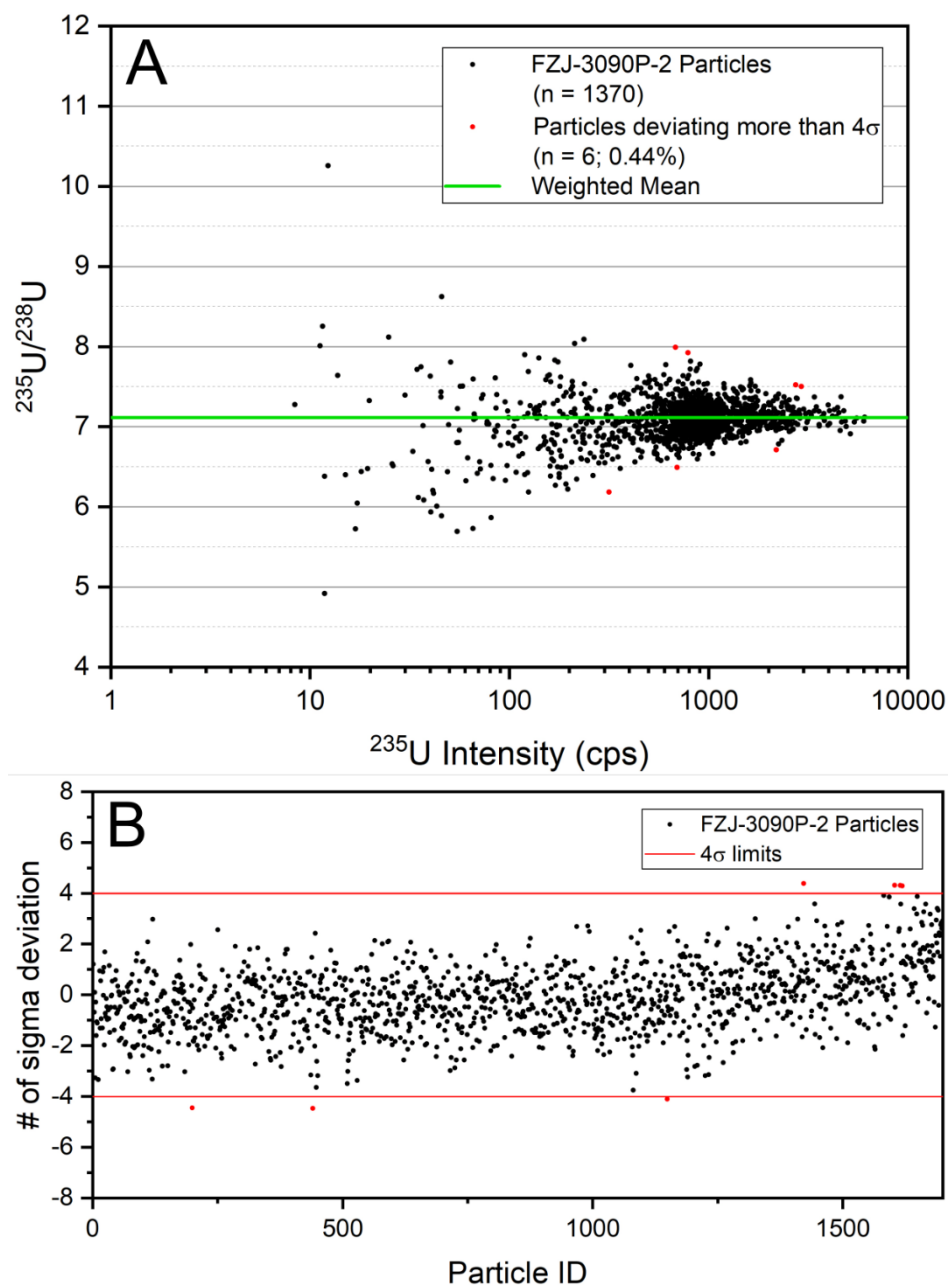


Figure 34: $^{235}\text{U}/^{238}\text{U}$ -ratio vs. ^{235}U intensity (A) and σ deviation (B) of the calculated particles on FZJ-3090P/2.

Again, the particles on both FZJ-3090P/1 and FZJ-3090P/2 were homogeneously distributed on the sample planchets. They could be easily identified by APM and for single-particle measurements. The overall number of particles on both planchets is lower than on FZJ-3050P planchets, but still within IAEA requirements.

Like for FZJ-3050P, we concluded, that both batches of FZJ-3090P particles seem to be viable as standards, R&D materials or for the production of simulated field samples.

 4.2.4 Cleaning process verification

 4.2.4.1 FZJ-3050P blank

After each particle production in the Safeguards Laboratories in Jülich, the VOAG is cleaned with diluted nitric acid to preclude contamination on planchets in subsequent particle productions. For IAEA-requested particle productions sensible parts of the VOAG such as furnace, orifice, etc. are completely exchanged by default. As an examination of the quality of this cleaning step, a blank was produced after the cleaning all parts of the VOAG following the production of the FZJ-3050P particles. No parts of the VOAG were replaced for this examination. A new planchet was placed in the vacuum impactor while the VOAG was running with ethanol solution for a typical particle collection time. In theory, there should be no uranium oxide particles on the planchet.

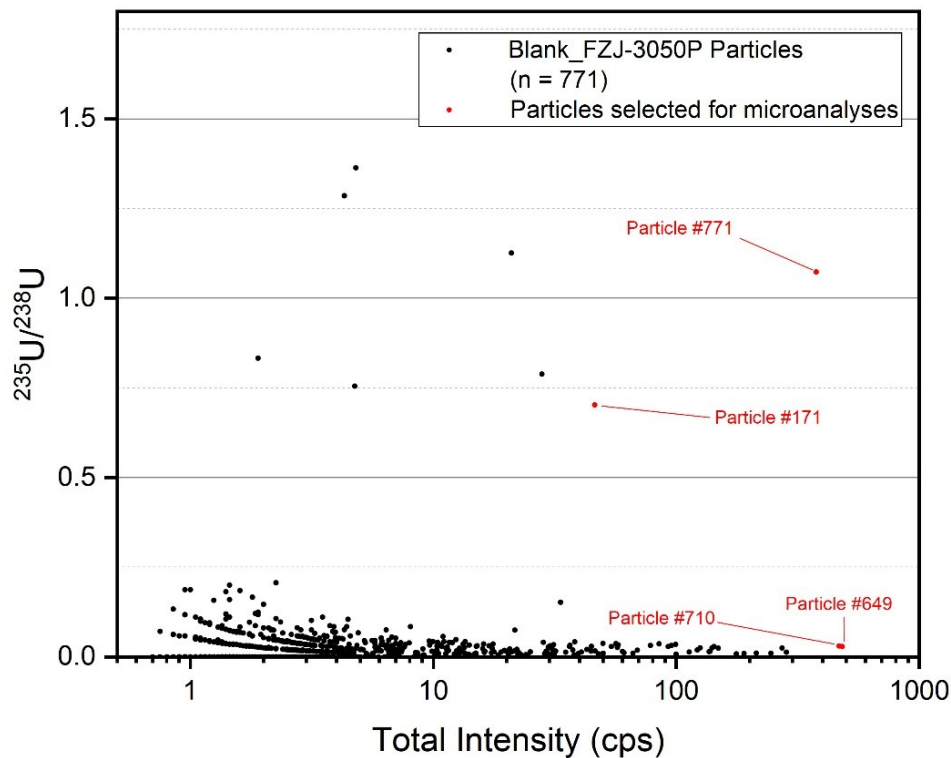


Figure 35: Results of APM performed on Blank_FZJ-3050P. Total intensity is plotted vs. $^{235}\text{U}/^{238}\text{U}$ -ratio of the calculated particles. Red particles were analyzed as single particles using microanalysis.

This planchet – Blank_FZJ-3050P – was measured with the APM Software at the HIP in June 2023. A relatively high primary ion beam of ~ 100 nA was used, because a lack of particles on this planchet was expected. In contrast to APM measurements of IAEA-requested particle productions, no identified particles were excluded. The integration time for every measured field was 20 s. The results of the APM are shown in Figure 35.

The APM calculated a total of 771 particles. All particles were included and therefore APM artifacts are also shown in this figure. Particles with an overall high intensity or divergent isotopic composition were chosen for single-particle microanalysis (red in Figure 35). Other APM-calculated particles with comparable composition to the selected particles were manually checked, but only yielded insufficient signals preventing microanalysis. They are therefore considered to be APM artifacts. If a recorded signal was identified as a real particle and not just an APM artifact, the isotopic composition was expected to be similar to the particles of FZJ-3050P. To verify this assumption, the particles in question were measured in a microbeam analysis.

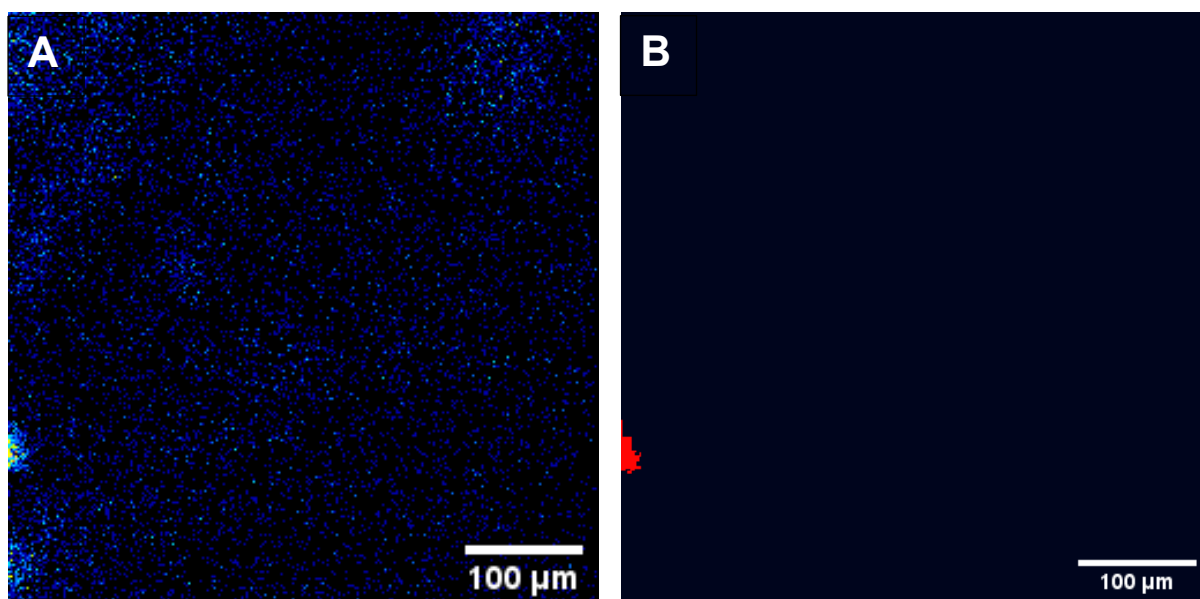


Figure 36: ^{238}U ion image (A) and calculated boundaries (B) of particle #171.

Table 7 shows a list of three of the four analyzed calculated particles with the highest intensity. Isotopic compositions could only be measured for particles #771, #649 and #710. Particle #171 was located at the edge of two measured fields (Figure 36). This can result in an erroneous output from the APM Software. Thus, in an APM measurement of IAEA-requested particle reference material calculated particles at the edge of measured fields would be excluded to prevent misleading results. A microanalysis measurement for particle #171 could not be performed, because no usable signal could be obtained. A possible reason for this is, that the particle was either too small and already consumed by the APM measurement or it was not a real particle but an APM artifact.

The results of particles #649 and #710 (Table 7) show unexpected and unusual isotopic compositions in the range of low enriched uranium (LEU). The calculated amounts of minor isotopes are negative. Measurements of both particles have a very high RSD in ^{235}U . The uncommon results can be explained when looking at the total Intensity of the particles. Compared

to 130,205 cps at #771, both #649 and #710 show very low intensities at 366 cps and 23 cps, respectively. This leads to the conclusion that particles #649 and #710 are in fact also APM artifacts.

Particle #771 shows a common total intensity of ~130,000 cps and the RSD is in the typical range for other measured particles. The isotopic composition points towards FZJ-3050P particles.

Table 7: Isotopic composition of particles #649, #710 and #771. All results are in atom%. Uncertainty is 1σ .

#	^{234}U	<i>unc.</i>	^{235}U	<i>unc.</i>	^{236}U	<i>unc.</i>	^{238}U	<i>unc.</i>	RSD ^{235}U (%)	I_{tot} (cps)
649	-0.0002	0.0001	0.9597	0.0661	-0.0007	0.0002	99.041	0.066	6.886	366
710	-0.0029	0.0020	2.6955	0.5974	-0.0028	0.0019	97.310	0.597	22.164	23
771	0.0020	0.0001	50.4641	0.0428	0.0026	0.0006	49.531	0.035	0.085	130205

In conclusion there was a single particle that can be identified as a microparticle from the FZJ-3050P production. The applied cleaning procedure proved to be suitable to remove nearly all remnants of former particle productions from the VOAG. This procedure seems to be appropriate as standard procedure prior to the production of R&D particles. For particle productions with an intended use as a reference material it is nevertheless recommended to replace as many parts of the VOAG as possible to minimize the risk of possible contamination.

4.2.4.2 Intentional contamination

The cleaning procedure of the VOAG is very time and resource consuming. The question arises, if such a comprehensive step is necessary at all or if the amount of residual “older” particles on a planchet of a new production is negligible even without the cleaning step. To investigate the influence of residual particles in the uncleaned VOAG, a sample planchet of particles derived from a starting solution containing CRM NBL 129-A was prepared after the FZJ-3090P production campaign without performing any cleaning step.

The so called “dirty” sample O001_PP/23/NBL-129A was measured using the APM software in August 2023. The expected particle concentration of the sample was very high, because the particles were collected directly on the sample planchet, and no intermediate dispersion step was performed. Considering this, a relatively low primary beam intensity of ~30 nA was applied. The integration time for every field was 20 s. The same exclusion criteria as for IAEA-requested particles were used. Particles have to provide at least 100 counts ^{235}U , their allowed maximum

size is 5,000 pixels and calculated particles located at the edge of measured fields are excluded. The results of the APM are shown in Figure 37.

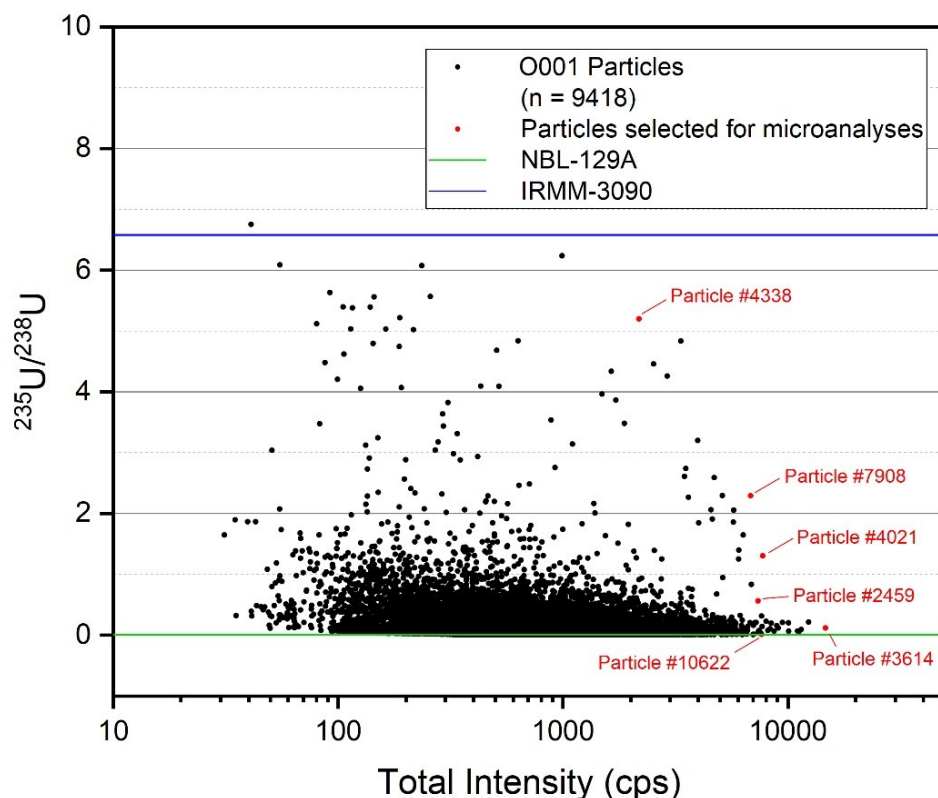


Figure 37: Results of APM performed on O001_PP/23/NBL-129A. Total intensity is plotted vs. $^{235}\text{U}/^{238}\text{U}$ -ratio of the calculated particles. Red particles were analyzed as single particles using microanalysis. Blue and green lines represent certificate values of CRM NBL-129A and IRMM-3090, respectively.

Of the 12,233 particles identified, 2,915 were excluded due to the aforementioned criteria. Of the remaining 9,418 particles shown in Figure 37, 6 particles with a high intensity or suspicious isotopic composition were chosen for microanalysis (red in APM graph). Particles found on the planchet were expected to yield isotopic abundances of either CRM NBL 129-A as source material for the newly produced particles or IRMM-3090 as source material of possibly residual older particles. The $^{235}\text{U}/^{238}\text{U}$ -ratios of both CRMs are shown in Figure 37.

In contrast to the expectations, the particles do neither show the isotopic abundance of a single population, nor of two separated populations. The $^{235}\text{U}/^{238}\text{U}$ -ratios of most of the calculated particles are in between the values of NBL 129-A and IRMM-3090. Although most of the particles clearly point towards the isotopic composition of NBL 129-A, nearly all of them have a higher $^{235}\text{U}/^{238}\text{U}$ -ratio. Due to their calculated ratios, the particles' isotopic composition seems to be a mix of NBL 129-A and IRMM-3090 in various orders of magnitude. The question arises, if the particles do in fact yield a mixed isotopic composition or if the calculation of the APM software

blends the isotopic abundance of neighboring particles with a signature of either NBL 129-A or IRMM-3090. To investigate this, the particles shown in Table 8 were chosen for microanalysis.

Table 8: Isotopic composition of analyzed single particles. All results are in atom%. Uncertainty is 1σ .

#	^{234}U	<i>unc.</i>	^{235}U	<i>unc.</i>	^{236}U	<i>unc.</i>	^{238}U	<i>unc.</i>	<i>RSD</i> ^{^{235}U} (%)
3614	0.0051	0.0001	0.9673	0.0021	0.0001	0.0000	99.0276	0.0020	0.217
10622	0.0050	0.0001	0.9814	0.0018	0.0001	0.0001	99.0135	0.0018	0.185
4337	0.0051	0.0002	1.0098	0.0022	0.0000	0.0001	98.9851	0.0022	0.221
2459	0.0023	0.0001	71.9881	0.2130	-0.0196	0.0025	28.0292	0.2100	0.296
4021	0.0019	0.0001	78.2337	0.4766	-0.0192	0.0052	21.7835	0.4754	0.609
4338	0.0017	0.0001	85.3532	0.2708	-0.0092	0.0018	14.6542	0.2676	0.317
7908	0.0017	0.0002	85.5170	0.0980	-0.0368	0.0091	14.5181	0.0882	0.115

Looking at the isotopic abundance of the single particles measured, no particle matches NBL 129-A (0.72087 % ^{235}U) or IRMM-3090 (86.7983 % ^{235}U). The major isotopic composition of #3614, #10622 and #4337 point in the direction of natural U and therefore NBL 129-A, while #2459, #4021, #4338 and #7908 show a much higher enrichment in ^{235}U . Although the RSD of ^{235}U overall is acceptable and the intensities for the analyzed particles were in a typical range for single particle measurements, the ^{236}U values for the latter group are negative. This leads to the conclusion that the effect of the hydride correction for $^{235}\text{U}^1\text{H}$ is too high. A cause for this problem could be the influence of $^{238}\text{U}^1\text{H}$ from neighboring particles with an isotopic composition of NBL 129-A that may lead to an excessive correction. $500 \times 500 \mu\text{m}$ ion images of ^{235}U and ^{238}U confirm the high particle concentration anticipated (Figure 38).

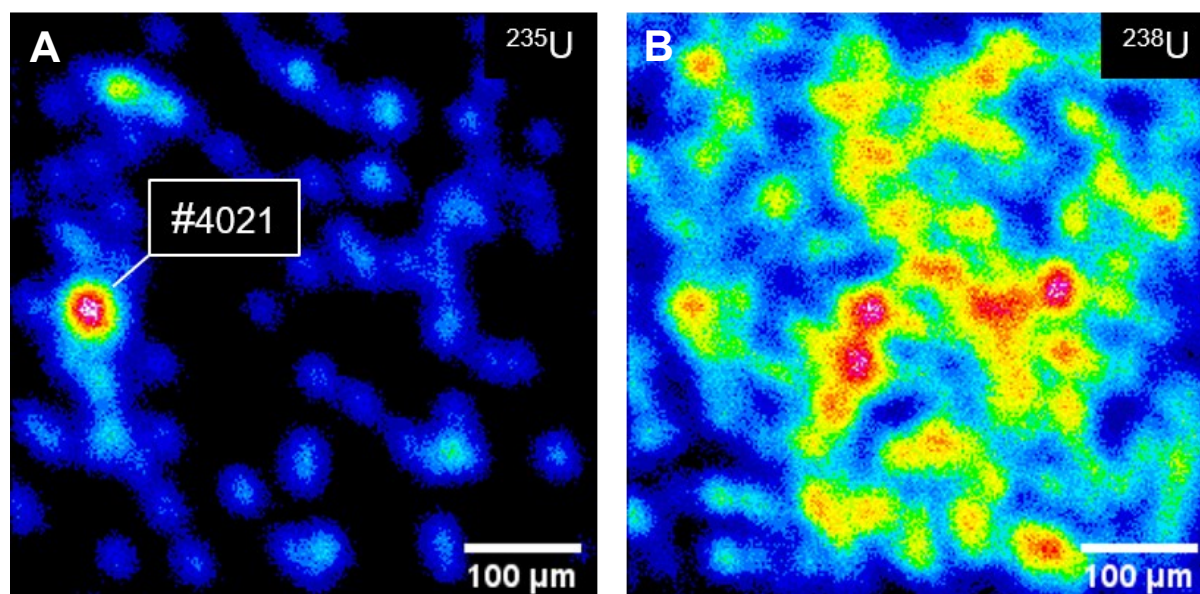


Figure 38: ^{235}U ion image (A) and ^{238}U ion image (B) of the field of particle #4021 on sample plachet O001_PP/23/NBL-129A. The color scheme is based on a rainbow look-up-table (LUT) where white represents the highest relative ion count and black represents low ion count. Most of the particles show a high ^{238}U abundance with low ^{235}U , while particle #4021 has high ^{235}U and lower ^{238}U . The particle concentration is very dense.

Particle #4021 is clearly visible in the ^{235}U image, while the ^{238}U image shows particles with a higher ^{238}U abundance in an overall higher number in different spots of the analyzed field. Nevertheless, there seem to be some low-enriched particles neighboring particle #4021. Considering the fact that a single particle analysis is performed using a rastered primary beam that covers $10 \times 10 \mu\text{m}$ of the sample surface, there is a very high probability of an influence of neighboring particles and therefore a partly mixed analysis. This could explain the measured enrichment of 78.2337 % ^{235}U instead of the expected 86.7983 % ^{235}U of IRMM-3090, the source material for the previously produced particles.

This effect is also visible in areas of the sample plachet, that are not as densely populated as the field shown in Figure 38. Figure 39 shows the field of particles #4337 and #4338. The intensities of the APM in this field were overall lower than in the one containing #4021. This can be caused by defocusing of the primary beam, when the sample is moved out of the Z axis optimum during the APM measurement. Still, this has no influence on the single particle measurement, because the Z axis is manually focused to guarantee maximum transmission. However, even particles analyzed in a sparsely populated field deviated from the exact isotopic abundance as the standards used for the previous production or for the particles in this production. Although the deviation from the standard values is not as large as for particle 4021, they are still clearly divergent (1.0098 % ^{235}U measured in #4337 vs. 0.72087 % ^{235}U in NBL 129-A and 85.3532 % ^{235}U measured in #4338 vs. 86.7983 % ^{235}U in IRMM-3090).

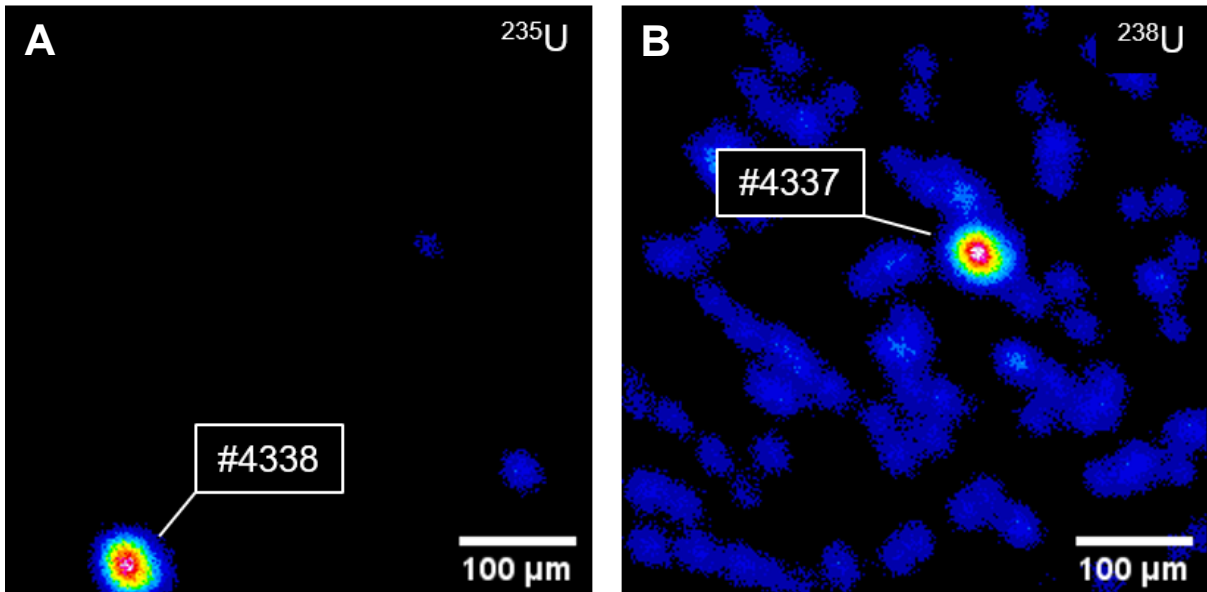


Figure 39: ^{235}U ion image (A) and ^{238}U ion image (B) of the field of particles #4337 and #4338. The same relative rainbow LUT is used. Particle #4337 is typical for NBL 129-A feeding solution, while particle #4338 is a remnant from the FZJ-3090P particle production and represents contamination.

The distribution of particles with high ^{235}U (minority) vs. particles with high ^{238}U (majority) in the ion images is in accordance with the distribution in the APM. However, the ion images of the particle surface reinforce the impression that both the APM data as well as the single-particle microanalyses represent a mix of two particle populations due to the high particle concentration on the planchet.

However, the most important conclusion of these measurements is the fact, that a cleaning step after a particle production is extremely important. The remaining particles of a previous production are not only visible in the APM, they also influence the measurement of the isotopic composition in the APM and for single-particle microanalyses.

4.3 Uranium microparticle shelf-life

To investigate the structural and chemical stability of VOAG-produced uranium microparticles and possible impact of previously reported alteration [48; 49], a systematic shelf-life study (SLS) was launched. In the following chapters, microparticle alteration and possible implications for the application as reference materials are discussed. The observed microparticles were VOAG-produced uranium oxide microparticles derived from a CRM NBL 129-A feeding solution. They are characterized as well-rounded with a diameter of $\sim 1.2 \mu\text{m}$ [26; 45]. The main component of freshly produced microparticles is U_3O_8 with U oxidation states of V and VI, however XANES measurements indicate the presence of at least one uranium oxide with oxidation states of IV and V (e. g. U_4O_9) [48]. The shelf-life investigation in this study is separated in two parts. In the first part, the particles were produced with the VOAG, underwent a dispersion step to deposit them on GCD planchets and were then stored in different atmospheric conditions [23]. These samples were treated as possible reference materials, where the same sample planchets with the same microparticles were used for every shelf-life investigation measurement. The second part covers the stability of VOAG-produced particles in different alcoholic storage media. For these measurements, new sample planchets with new microparticles were prepared for each shelf-life measurement session.

4.3.1 Atmospheric shelf-life investigation

After the preparation of the microparticle planchets in a dispersion step, they were stored in three possible long-term storage conditions: (1) laboratory air with silica gel as desiccant, (2) commercial argon with silica gel and (3) laboratory air with silica gel at 90°C . An additional planchet was stored in a (4) water-saturated atmosphere for comparison. Particles in this study were analyzed after 30, 117, 218 and 454 days under their respective storage conditions.

4.3.1.1 SEM investigation

Figure 40 shows the summarized SEM images of particles from the different samples after a certain amount of time in their respective storage conditions. The image of the particle after 0 days is a reference image. The images after 0 and after 30 days of storage were taken at the SEM of IEK-6 at FZJ, the images after 117, 218 and 454 days at the JEOL FEG-SEM JSM-IT800 at the Institute of Earth Sciences, Heidelberg University.

After 30 days of storage time, the particles in the three potential long-term storage conditions are indistinguishable and retain their original shape. However, the test sample in a humid atmosphere shows first signs of surface roughening comparable to the alteration observed for uranium microparticles stored in ethanol for 4 years [49]. Nevertheless, the test sample particles still retain a well-rounded shape. After 117 days, particles in the water free atmospheres still resemble the shape and texture of freshly produced particles, while the signs of alteration on some particles in the sample intentionally exposed to a water-saturated atmosphere increase. This trend continues over the whole duration of the shelf-life study.

Figure 41 shows more detailed images of particles stored for 218 days. Particles stored in laboratory air (a), argon atmosphere (b) and laboratory air at 90°C (c) remain in their original shape with a smooth surface showing no signs of alteration. However, particles in a water-saturated atmosphere (d) clearly changed in shape and size. Although their initial spherical shape is still visible, their surface is now covered by a microcrystalline secondary phase. The formation of the columnar crystallites leads to a growth in size from $\sim 1.2 \mu\text{m}$ up to $\sim 1.9 \mu\text{m}$ compared to the particles stored in arid conditions. This appears to be a result of the dehydration of a surficial hydrated form that takes place when high vacuum is applied to the sample. Previous studies on the alteration of UO_2 in water have shown similar effects [110].

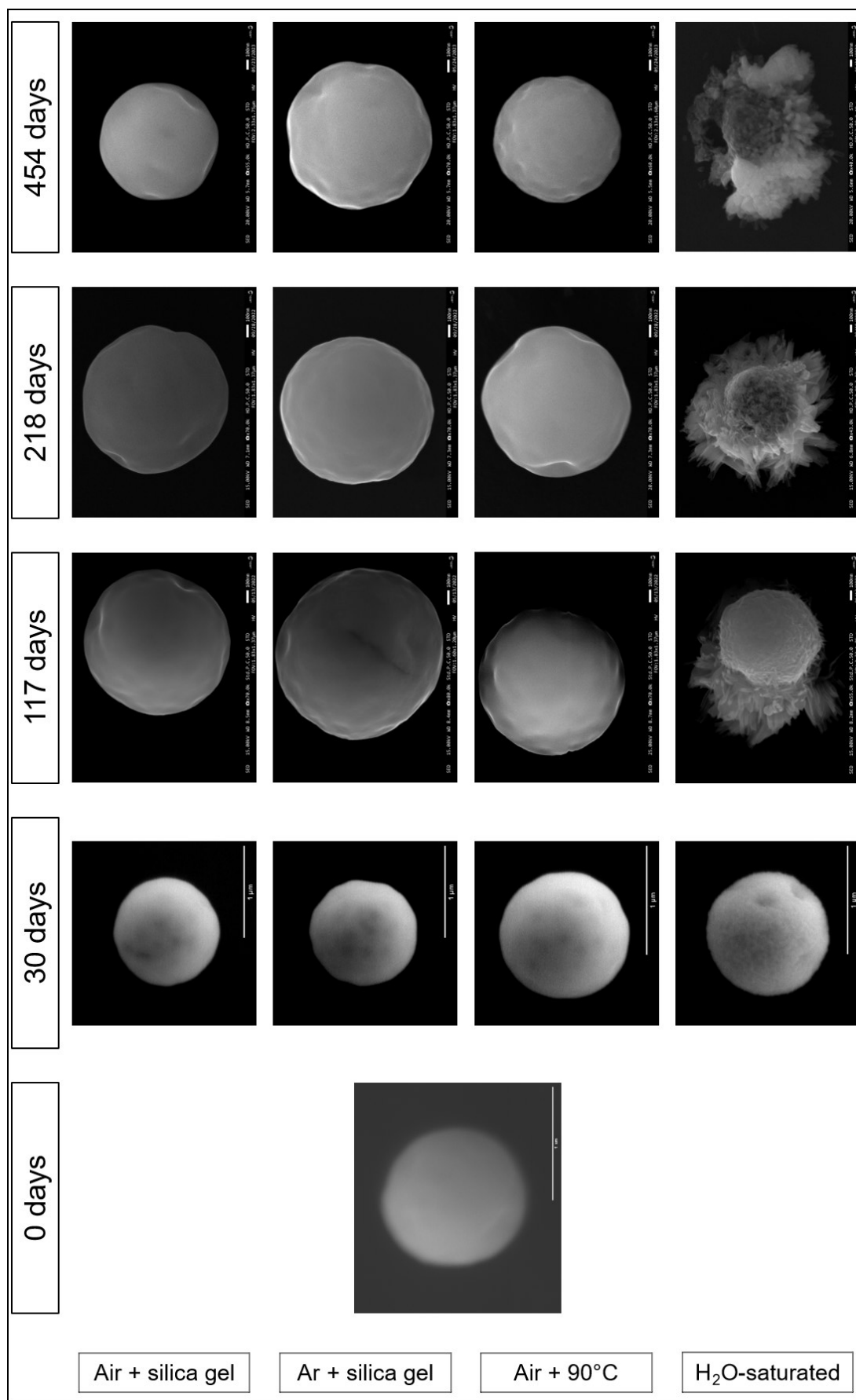


Figure 40: Graphic summary of SEM investigation of microparticles stored in different atmospheric conditions. Extended from Kegler *et al.* [111].

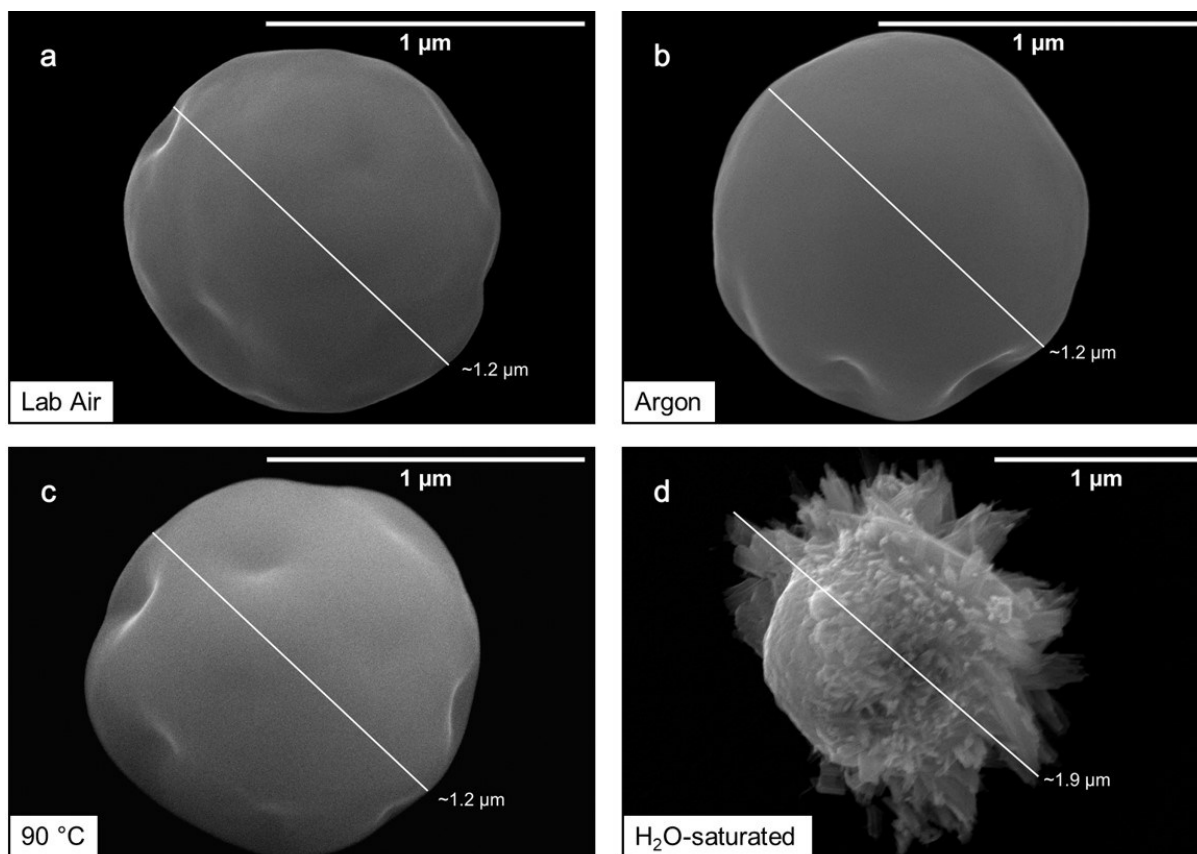


Figure 41: Representative SEM images of particles stored for 218 days in laboratory air (a), argon (b), laboratory air at 90°C (c) and in H₂O-saturated atmosphere (d) (from Hammerich *et al.* [23]).

The last investigation of the particles after 454 days confirmed the previous observations (Figure 40). Now the majority of particles on the water-saturated test sample were completely altered. Although merely observable, particles stored in laboratory air at 90°C started to show initial signs of surface features. However, discussions with Shannon Potts from FZJ who was conducting comparable investigations lead to the conclusion, that these surface features do not resemble the same form of alteration observed for particles stored in water-saturated atmosphere. Overall, the particles in all three potential long-term storage conditions retained their spherical shape and size and could be clearly recognized as VOAG-produced uranium microparticles.

4.3.1.2 μ-Raman spectroscopy

In accordance with the SEM investigation, Raman spectra from single particles were obtained after 30, 117, 218 and 454 days of storage time. All Raman measurements were carried out at the WITec alpha 300R microscope (μ-Raman) at the Institute of Earth Sciences, Heidelberg University. The summarized Raman spectra of representative particles after a certain period of

time in their respective storage conditions is shown in Figure 42. A comprehensive collection of the spectra can be found in appendix 6.1.

Raman spectra after 30 days of storage are indistinguishable for particles stored in room-temperature laboratory air (Figure 43a), argon atmosphere (Figure 43b) and in laboratory air at 90°C (Figure 43c). The intensities and exact positions for the Raman bands vary between particles from samples stored in different storage conditions, however, this effect can also be seen for particles on the same sample planchet and is therefore independent of different storage conditions. All spectra from particles in storage conditions 1-3 verify the presence of U_3O_8 , indicated by the triplet of Raman bands between 300 and 500 cm^{-1} and the clearly visible bands at $\sim 240\text{ cm}^{-1}$ and $\sim 750\text{ cm}^{-1}$ [112]. In addition, there is evidence for the presence of a higher oxidized UO_3 phase indicated by the strong band at $\sim 767\text{ cm}^{-1}$ [113; 114] and the absence of a band at $\sim 800\text{ cm}^{-1}$ that would be typical for U_3O_8 . Although the latter was also described for U_3O_8 before, this was only the case for samples that underwent pressures of at least 9 GPa [115]. The broad band between 640 and 670 cm^{-1} indicates the possibility of the presence of a minor U_4O_9 phase [116]. It has to be noted that even Raman spectra of uranium oxides in macroscopic sizes are very complex and this complexity further increases with smaller samples and therefore smaller laser energies. In contrast to VOAG-produced uranium oxide microparticles investigated by Kegler *et al.* [48], there is no strong Raman band at $\sim 830\text{--}840\text{ cm}^{-1}$, indicating the absence of uranium hydroxides in the particles stored under conditions 1-3 [114; 117]. However, the particles investigated by Kegler *et al.* [48] were already stored for two years before the Raman investigations while the spectra in Figure 43 were recorded on freshly produced particles, that were only stored for 30 days in their respective conditions.

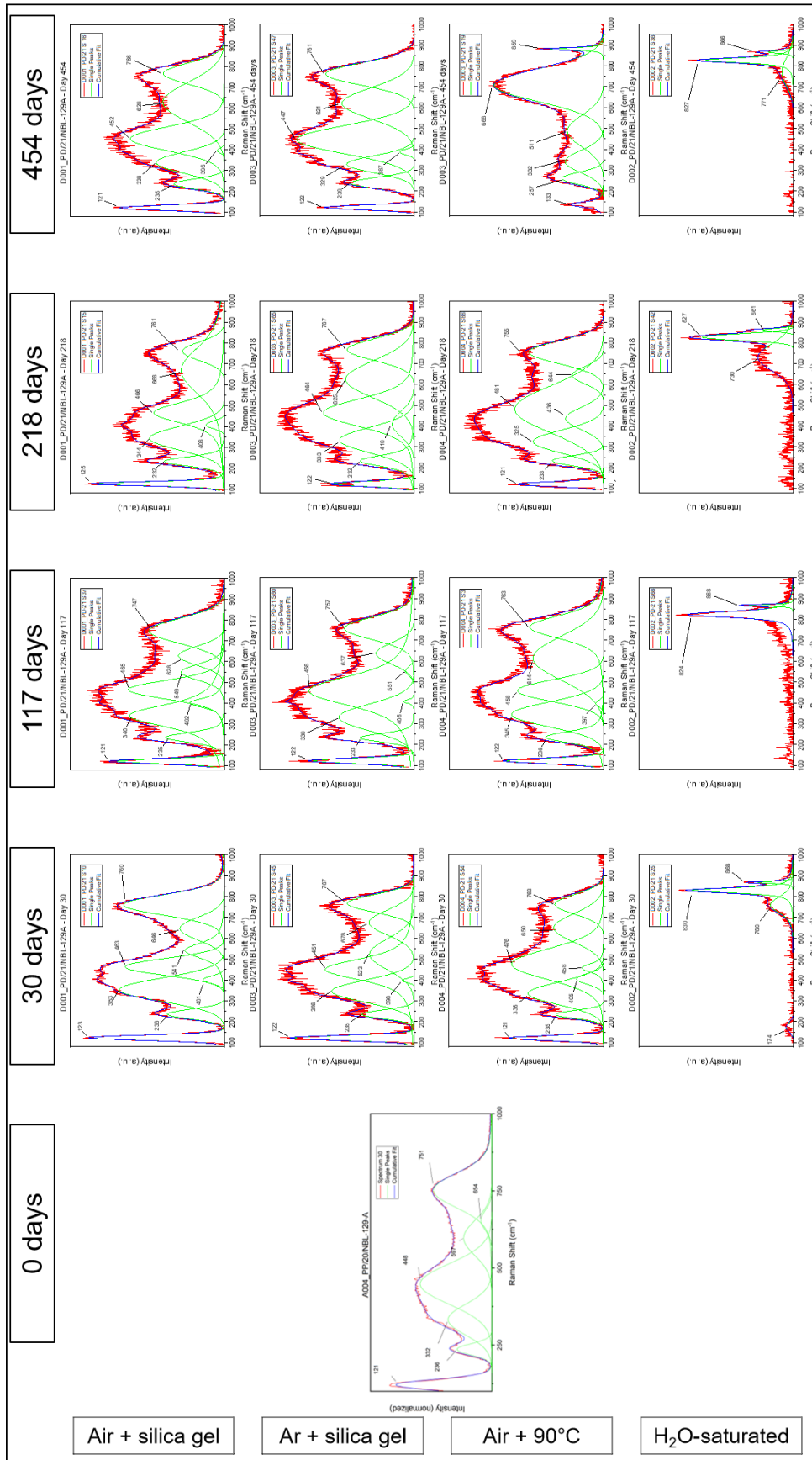


Figure 42: Graphic summary of μ -Raman investigation of microparticles stored in different atmospheric conditions. Extended from Kegler *et al.* [111].

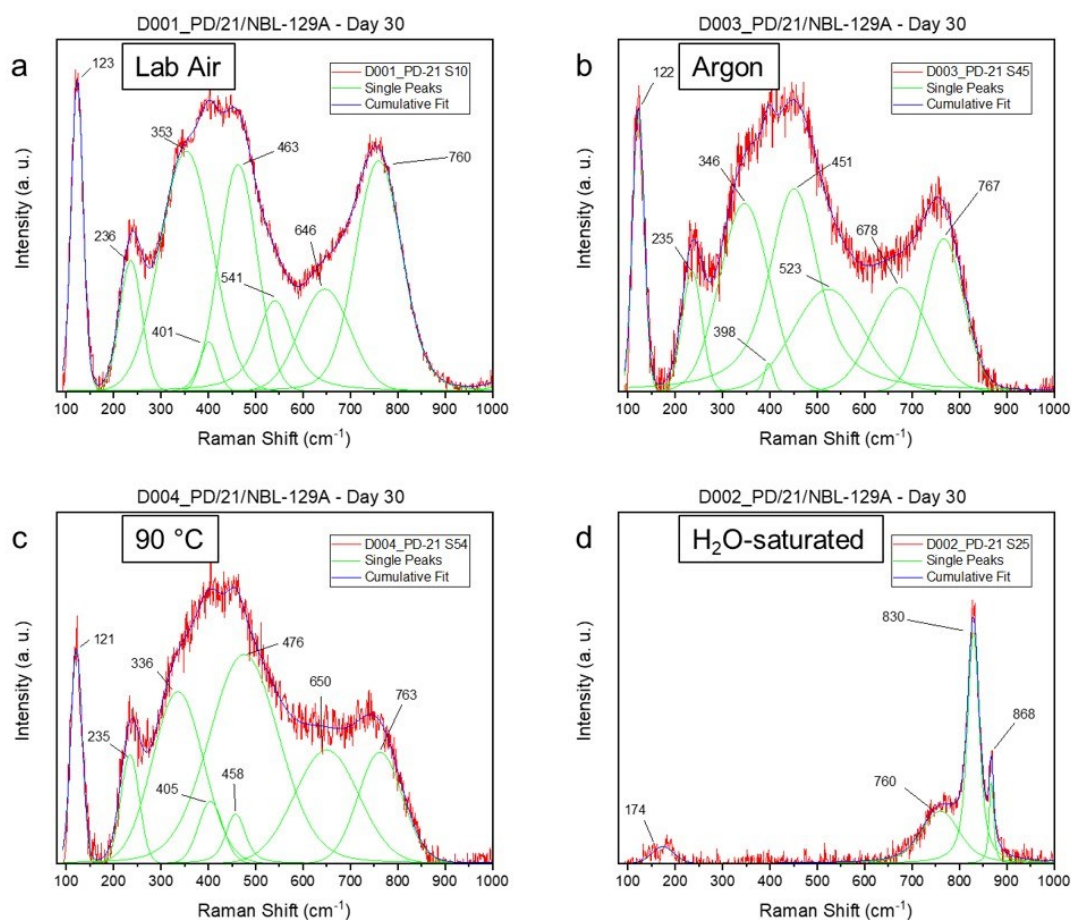


Figure 43: Representative Raman spectra of particles stored for 30 days in laboratory air (a), argon (b), laboratory air at 90°C (c) and in H₂O-saturated atmosphere (d) (from Hammerich *et al.* [23]).

Figure 43d shows the Raman spectrum of one of the particles stored in water-saturated atmosphere for 30 days. It clearly differs from the other spectra. Even after a relatively short storage time of only 30 days, the surface of some of the particles underwent a phase transition that fits the observation of increased surface roughness in the SEM images. A phase transition like this was expected; however, the anticipated alteration phase was schoepite with a typical single Raman band at $\sim 840\text{--}845\text{ cm}^{-1}$. The observed Raman bands at $\sim 830\text{ cm}^{-1}$ (U-O vibration) and $\sim 868\text{ cm}^{-1}$ (O-O vibration) in this sample point towards the formation of (meta-)studtite, a form of uranyl peroxide with the formula $\text{UO}_4 \cdot n\text{H}_2\text{O}$ [118-120]. The observed columnar crystallite structure of the alteration phase (Figure 41) reinforces that (meta-)studtite formed instead of layered schoepite [121; 122].

The measurements after 117 and 218 days of storage time yielded similar results and confirmed the observations made after 30 days of storage. Spectra obtained from particles stored in conditions 1–3 pointed towards complex uranium oxide phases but lack evidence of the formation of uranium hydroxide or uranium hydroperoxide. The more time in water-saturated atmosphere elapsed, the more particles yielded spectra corresponding to (meta-)studtite.

The question arises, why the Raman spectra identify (meta-)studtite as alteration phase instead of expected and schoepite. Previous studies on the alteration of UO_2 in water yielded similar results [123]. However, the formation of studtite is depending on the concentration of H_2O_2 . While both phases can be present at the same time, lower H_2O_2 concentrations lead to the formation of schoepite, while higher concentrations support the formation of studtite. Previous *in-situ* μ -Raman studies have shown, that α irradiation induces the formation of H_2O_2 by water radiolysis [124; 125]. The α irradiation of ^{238}U in the VOAG-produced particles could lead to radiolysis in a boundary layer of H_2O molecules between water-saturated atmosphere and the surface of the microparticles and could therefore support the formation of studtite. However, there is also the possibility of the conversion of dehydrated schoepite into studtite as reported by Forbes *et al.* [126]. Because the samples used for this shelf-life study were treated like potential standards, they were exposed to vacuum for SEM or SIMS measurements multiple times. This was not the case for particles analyzed using Raman spectroscopy by Kegler *et al.* [48]. This conversion could take place because of the application of high vacuum and therefore the possible dehydration of hypothetical schoepite.

While after 454 days of storage time in their respective storage conditions the Raman spectra for particles stored in laboratory air and argon atmosphere were still undistinguishable from spectra of freshly produced particles, some particles stored under laboratory air at 90°C started to show first signs of alteration (Figure 42). In contrast to previously recorded spectra, the Raman band triplet between 300 cm^{-1} and 500 cm^{-1} from those particles was not as visible. In addition, the Raman band at $\sim 750\text{ cm}^{-1}$ shifted to lower wavenumbers and overall broadened. This points towards a more amorphous structure of the particle surface after 454 days of storage in laboratory air at 90°C and can be interpreted as first indication of alteration.

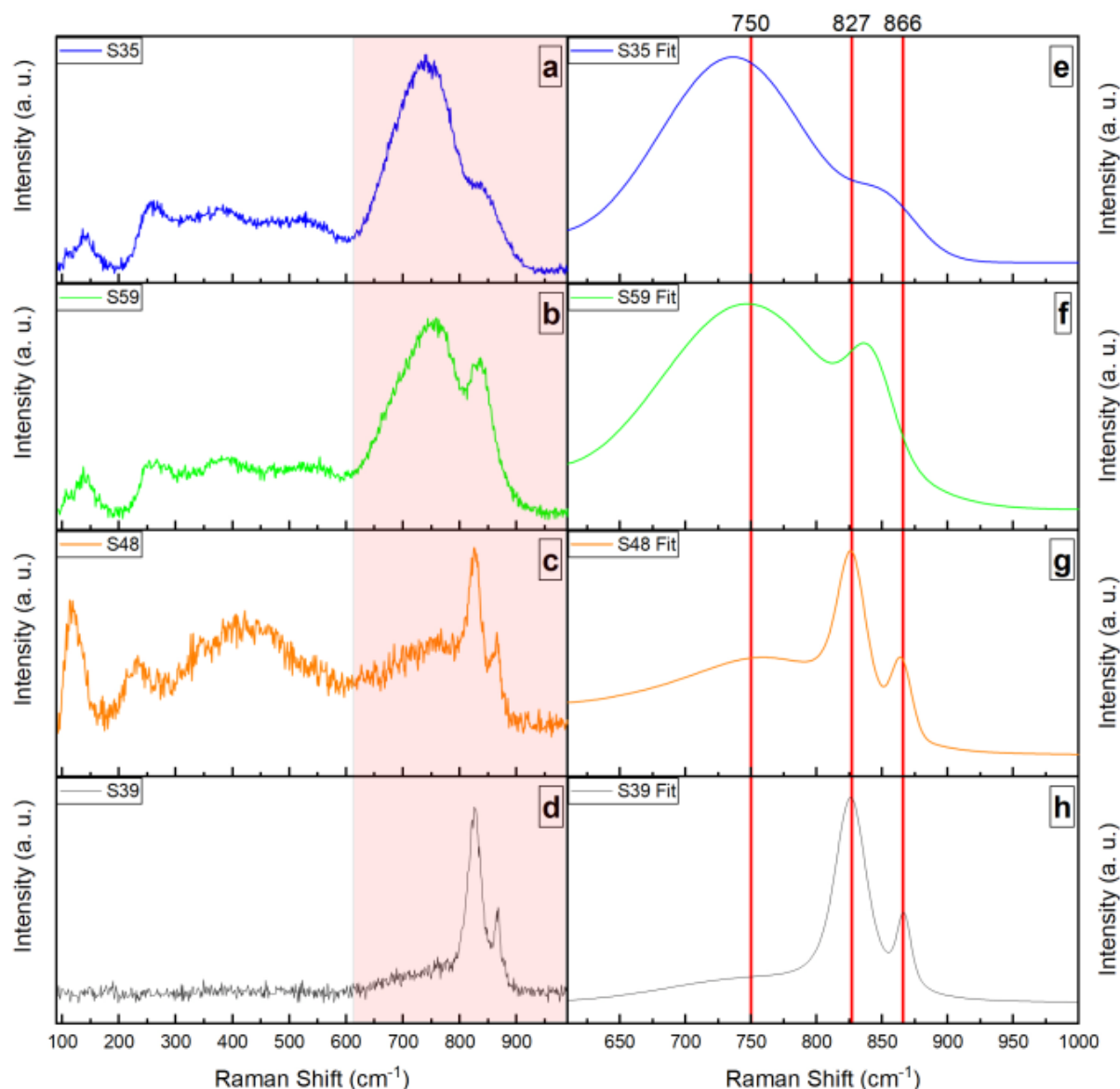


Figure 44: Raman spectra of particles stored in water-saturated atmosphere for 454 days. Complete spectra are shown on the left side (a, b, c, d), the corresponding fits between wavenumbers of 600 cm^{-1} and 1000 cm^{-1} are shown on the right side (e, f, g, h). Typical Raman position of Raman bands for U_3O_8 ($\sim 750 \text{ cm}^{-1}$) and (meta)-studdite ($\sim 827 \text{ cm}^{-1}$ and $\sim 866 \text{ cm}^{-1}$) are highlighted in the fitted spectra. The fitted part of the spectrum is shown in light red on the left side.

After 454 days, the majority of particles analyzed on the water-saturated test sample showed Raman spectra typical for (meta)-studdite. However, spectra of particles in different progression states of alteration could be obtained (Figure 44). The original spectra of 4 particles (S35, S59, S48 and S39) are on the left (a-d) and the relevant part of the corresponding calculated fit of the spectra is on the right side (e-f). Previously recorded spectra of unaltered uranium oxide particles displayed dominant Raman bands at wavenumbers of $\sim 750 \text{ cm}^{-1}$ and previously obtained spectra of altered particles that resemble (meta)-studdite have clearly visible Raman bands at $\sim 827 \text{ cm}^{-1}$ and $\sim 866 \text{ cm}^{-1}$. Reference lines for these relevant peak positions are shown as red lines. Although the spectrum S35 (a, e) already shows first signs of particle alteration and amorphization

comparable to the ones mentioned before for particles stored in laboratory air at 90°C for 454 days like the decline of peaks between 300 cm⁻¹ and 500 cm⁻¹, the recorded main peak is still in the region of ~750 cm⁻¹. The slight shift to lower wavenumbers points towards more amorphous phases. The visible peak shoulder that is starting to form at ~850 cm⁻¹ can be linked to a mix of lower intensity peaks at ~830 cm⁻¹ and ~870 cm⁻¹ that cannot yet be clearly separated. S59 (b, f) shows a decrease in relative intensity for the amorphous peak at ~750 cm⁻¹ and increased intensity for the shoulder that starts to form a single peak at ~840 cm⁻¹. In the lower range, S48 (c, g) has features typical for uranium oxides, however the trend of a declining peak at ~750 cm⁻¹ continues. Now two clearly separated peaks at ~827 cm⁻¹ and ~866 cm⁻¹ resembling the presence of (meta-)studtite are visible.

The indication of uranium oxides in the lower range of the spectrum and the evidence of uranium hydroperoxide in the higher range of the spectrum demonstrate the coexistence of original and alteration phases, that can also be observed in the earlier stages of the alteration process. This can be explained by the fact, that the alteration starts at the contact zone of uranium oxide and water molecules – the particle surface. The penetration depth of the laser and therefore the information obtained from Raman spectrometry depends on the transparency of the analyzed material and the focus depth of the objective [127]. In this case, the uranium oxide microparticles are not transparent. Hence, it can be concluded, that the information gained by Raman spectrometry is only applicable on the particles' surface. SEM observations indicate that not all particles show the same degree of surface alteration. That leads to the conclusion, that the spectra of less altered particles are a mix of uranium hydroperoxide on the particle surface and uranium oxide in the layers beneath the particle surface, similar to the observations made by Kegler *et al.* [48]. S39 (d, e) is a typical spectrum of particles that are in an advanced stage of alteration. Only two main Raman bands at ~827 cm⁻¹ and ~866 cm⁻¹ can be assigned to (meta-)studtite. Although a very broad peak between 600 cm⁻¹ and 900 cm⁻¹ as a remnant of an amorphous phase is still visible, the spectrum points very clearly towards (meta-)studtite as main phase. All in all, the spectra of the 4 analyzed particles are a representative showcase for uranium phase compositions on the particle surface during different stages of the alteration process.

4.3.1.3 SIMS ion images

Complementary to the SEM and μ -Raman investigations, the particles were analyzed using LG-SIMS after the respective storage time. To investigate possible uranium migration, the LG-SIMS was used as an ion microscope. Images of the ^{238}U intensities of the sample surface were recorded with the H1 EM detector. To capture as much of the sample surface area as possible, the largest raster size of $500 \times 500 \mu\text{m}$ was chosen. Figure 45 shows a summary of the ^{238}U ion images.

After 30 days of storage time, particles stored in all conditions showed sharp particle boundaries in the ion images. After 117 days, particles in conditions 1–3 remained clearly separated and could be easily distinguished. In contrast, some particles stored in water-saturated atmosphere presumably started to grow in size (Figure 45). Figure 46 shows a more detailed view, however the image used in Figure 46d is different from the one in Figure 45 and only displays an area of $100 \times 100 \mu\text{m}$. The close-up image reveals, that the ^{238}U intensity is heterogeneous and there is still a visible particle center. However, some particles started to also display a U-rich halo. This leads to the conclusion that uranium oxide particle alteration in water-saturated atmosphere can lead to uranium migration from the original particle onto the sample surface of the GCD.

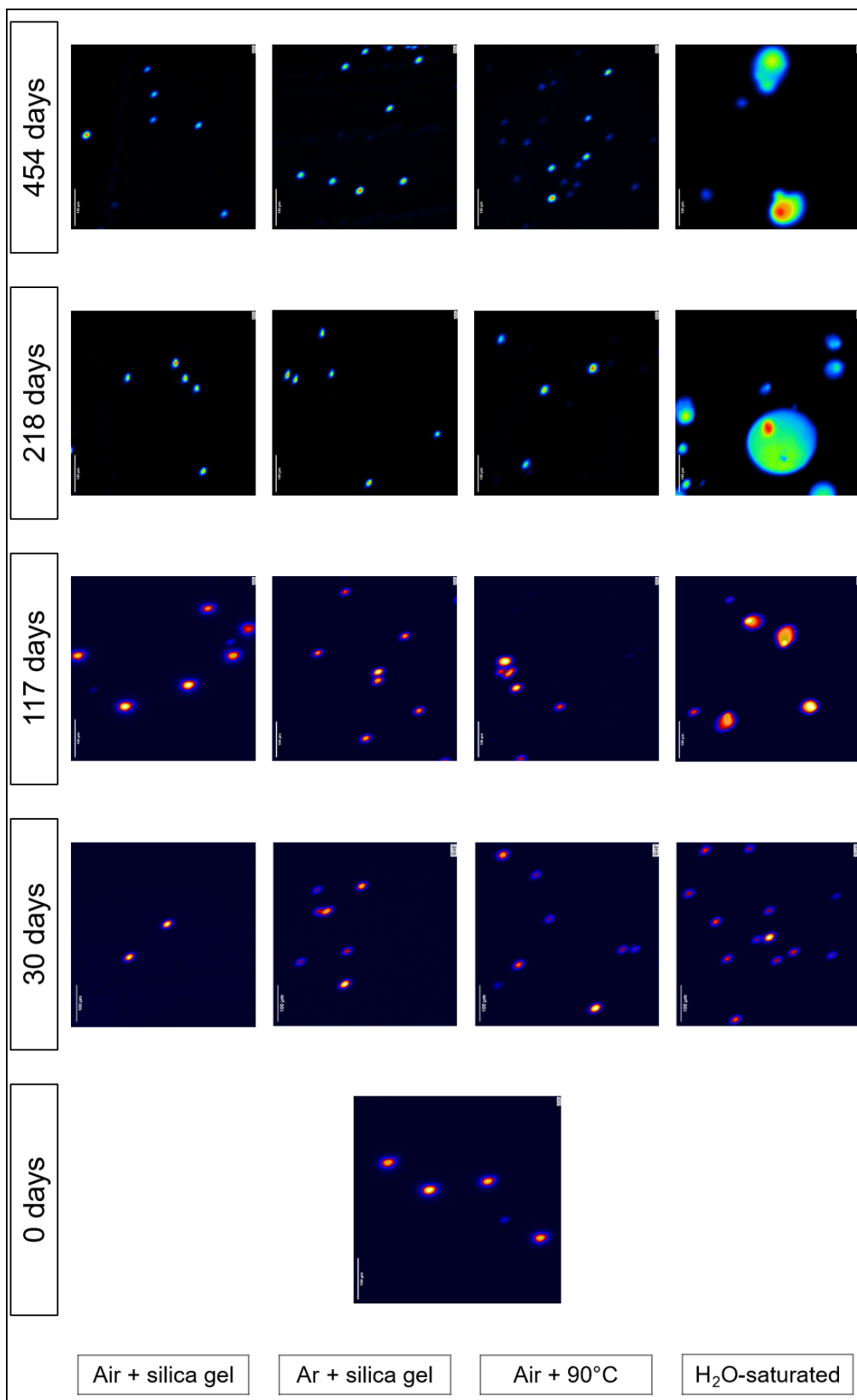


Figure 45: Graphic summary of ^{238}U ion images of microparticles stored in different atmospheric conditions. The white scale bar resembles 100 μm . The color scales are divided between a heat LUT (brighter = higher) up to 117 days and a rainbow LUT with red as maximum and black as minimum ions counted for the other two panels. The colors do not correspond to fixed values but show a relative min-max distribution.

These observations could be confirmed by ion images after 218 and 454 days of storage under the respective conditions. While particles stored in conditions 1–3 are clearly separated and easy to locate, uranium migration intensified for the altered particles with more particles showing uranium halos, that were also larger in size (Figure 45).

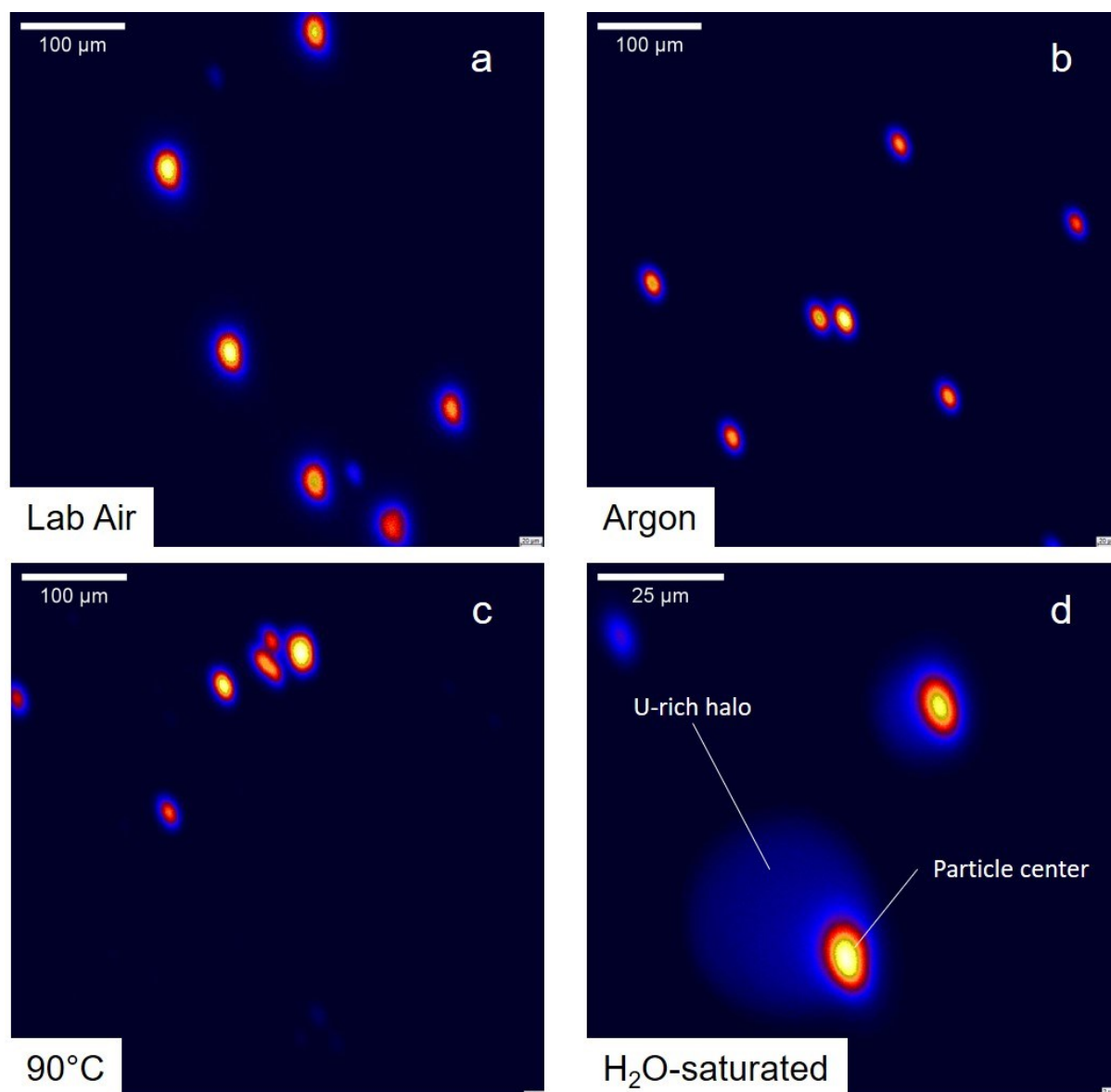


Figure 46: Selected ^{238}U ion images of particles stored for 117 days in laboratory air (a), argon (b), laboratory air at 90°C (c) and in H₂O-saturated atmosphere (d) (from Hammerich et al. [19]). Note that a, b and c display an area of 500 × 500 μm , while the size of d is only 100 × 100 μm . The color scheme is a relative heat LUT with brighter equals more counts.

The formation of uranium halos makes the particles harder to locate in ion imaging and sometimes requires pre-sputtering of the sample surface to remove the undesired, diffuse uranium intensities on the sample surface. This problem was reported before by participants of ILC exercise “Nuclear Signatures Interlaboratory Measurement Evaluation Programme 9” (NUSIMEP-9) organized by the JRC-Geel, Belgium [128]. In this ILC, the participating laboratories

were required to measure the isotopic abundance of VOAG-produced IRMM-2329P particles [129]. Some laboratories reported the observation of uranium halos around the particles, which could be a hint to inappropriate storage conditions.

As an addition to this shelf-life investigation, a sample planchet of IRMM-2329P particles was investigated using LG-SIMS and ^{238}U ion images were taken in December 2021 (Figure 47).

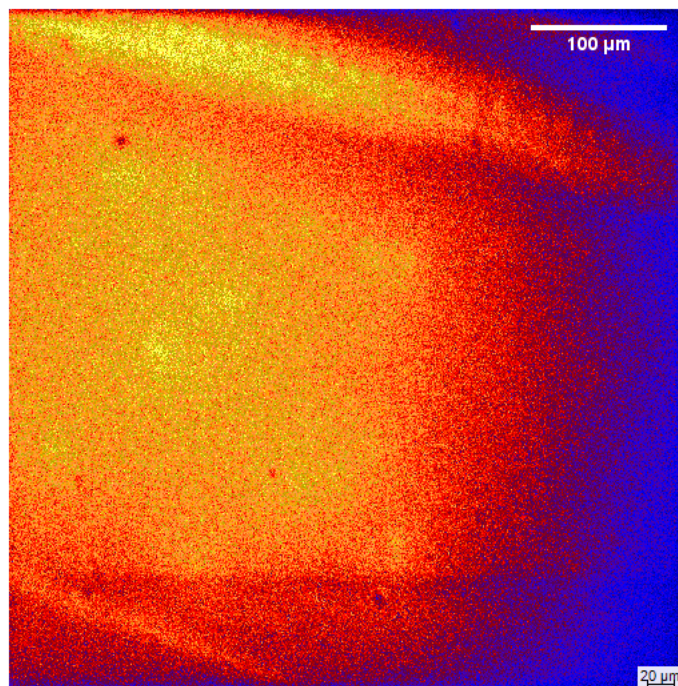


Figure 47: $500 \times 500 \mu\text{m}$ ^{238}U ion image of IRMM-2329P sample surface in December 2021. In the relative heat LUT brighter equals higher ion count.

The observations made in NUSIMEP-9 could be confirmed and sample conditions even worsened. ^{238}U signal is spread across the whole sample surface. This made it impossible to locate single particles and therefore conduct isotopic abundance measurements. When interpreting the uranium intensity across the planchet and comparing it to NUSIMEP-9 results, it is important to note that the IRMM-2329P particles were produced in 2018 and NUSIMEP-9 took place in late 2018 to early 2019 [128]. The IRMM-2329P particle measurements in Heidelberg took place ~ 3 years later. Provided that the formation of uranium halos observed in NUSIMEP-9 had the same cause as in this study, Figure 47 could show late-stage alteration of a uranium oxide microparticle sample that was stored in unsuitable conditions.

4.3.1.4 Uranium isotopic abundance of microparticles stored in different atmospheres

The main requirement for a potential uranium microparticle reference material is a consistent and constant uranium isotopic abundance. SEM images, μ -Raman spectroscopy and SIMS ion images have shown that particle alteration can occur, if the particles are stored incorrectly. The question arises, if this alteration leads to possible uranium isotopic fractionation and can therefore change the isotopic composition of the microparticles or influence the isotopic abundance measurements in a different way. To investigate this possibility, a randomly chosen population of microparticles from each storage condition was measured for their uranium isotopic composition after 30, 117, 218 and 454 days of storage time. The results were then compared to the certificate values for CRM NBL 129-A. Detailed data can be found in appendix 6.2.1.

The uranium isotopic composition of particles stored in all conditions remained invariant up to 117 days. After 218 days, the reliable measurement of single particles stored in water-saturated atmosphere started to get more difficult due to the particle localization problems discussed before. Nonetheless, data from enough particles could be obtained (Figure 48). It was also possible to measure some uranium halos that formed around the particles, however the uncertainties of these measurements are overall higher due to the lower number of sputtered ions and therefore inferior counting statistics.

Particles stored under conditions 1–3 match the certified values of CRM NBL 129-A within their analytical uncertainties. However, isotopic abundance measurements of particles stored in water-saturated atmosphere have a larger variation. Although most measured particles plot in the bulk of particle measurements consistent with the other conditions, there are outliers. For at least two particles lower-than-average ^{235}U values were measured. In absolute values, this means 0.7161 atom% and 0.7163 atom % compared to a certificate value of 0.72087 atom% [90]. A z-score can be calculated using the equation

$$Z = \frac{x - \mu}{S} \quad (3)$$

x = sample value

μ = expected value (certificate value)

S = standard deviation of the sample

The calculated absolute z-score from equation (3) shows a deviation of $\sim 2.6 \sigma$ and respectively $\sim 2.9 \sigma$ from the certificate value. The minor isotopic composition of these two outliers also deviates from the bulk, although there is no clear tendency observable.

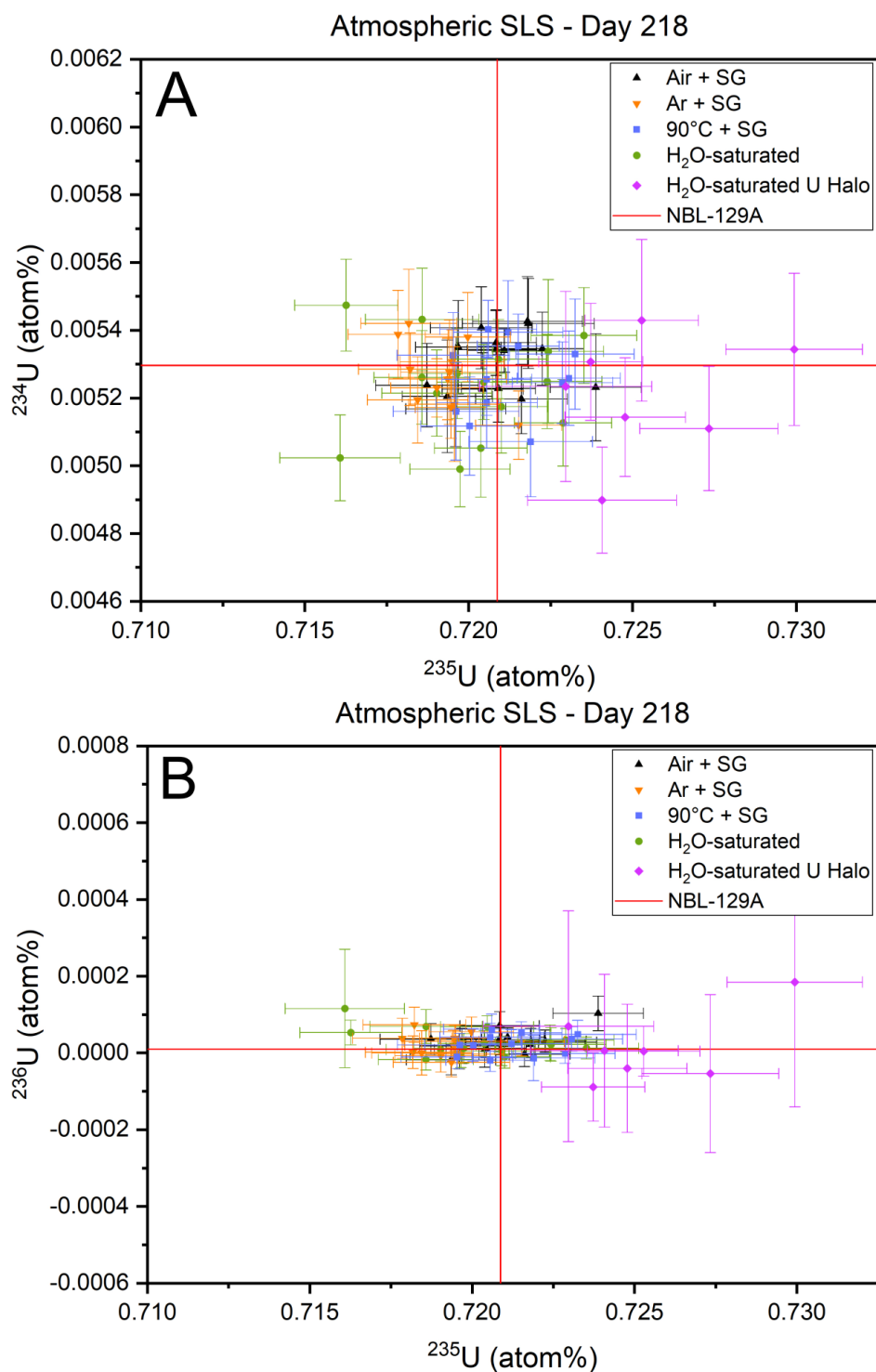


Figure 48: Uranium isotopic abundance of representative particles stored for 218 days in laboratory air, argon, laboratory air at 90°C and in H₂O-saturated atmosphere for the shelf-life study (SLS). Panel A is ^{234}U vs. ^{235}U and panel B is ^{236}U vs. ^{235}U .

Complementary to the particles, measurements of the observed uranium halos yielded higher-than-average ^{235}U values. Although the measurement uncertainties are higher, the deviation to higher ^{235}U values is clearly visible. The average ^{235}U in the halos was ~ 0.005 atom% higher than

the certificate value. In accordance with the results for the particles, the minor isotopes of the measured halos lack a mass dependent deviation. Some measured uranium halos even yield negative ^{236}U values. This can be an artifact of the applied hydride correction. Because of the overall lower intensity of the uranium halos with a fast drop after a short time of sputtering, it is estimated that the uranium that migrated to the GCD surface only forms a very thin layer. The very high surface-to-volume ratio of the measured uranium layer leads to a disproportionately high formation of hydrides and therefore high impact on the calculation of ^{236}U . Hence, the results for the minor isotopes of the uranium halos should not be overvalued.

This general trend could be verified with measurements after 454 days of storage (Figure 49). While particles stored in conditions 1–3 match the composition of the original solution, altered particles tend to yield lower ^{235}U values while their corresponding uranium halos point to higher ^{235}U values. Like after 218 days, the minor isotopes lack any statistically relevant deviations from the expected values. Compared to the observations after 218 days, the absolute difference between the certificate value and the average of the halos are only ~ 0.003 atom%. A reason for this can be the fact that particles after 454 days were harder to locate than those from the 218 days experiment and measurements of both particles and halos are therefore sometimes mixed analyses.

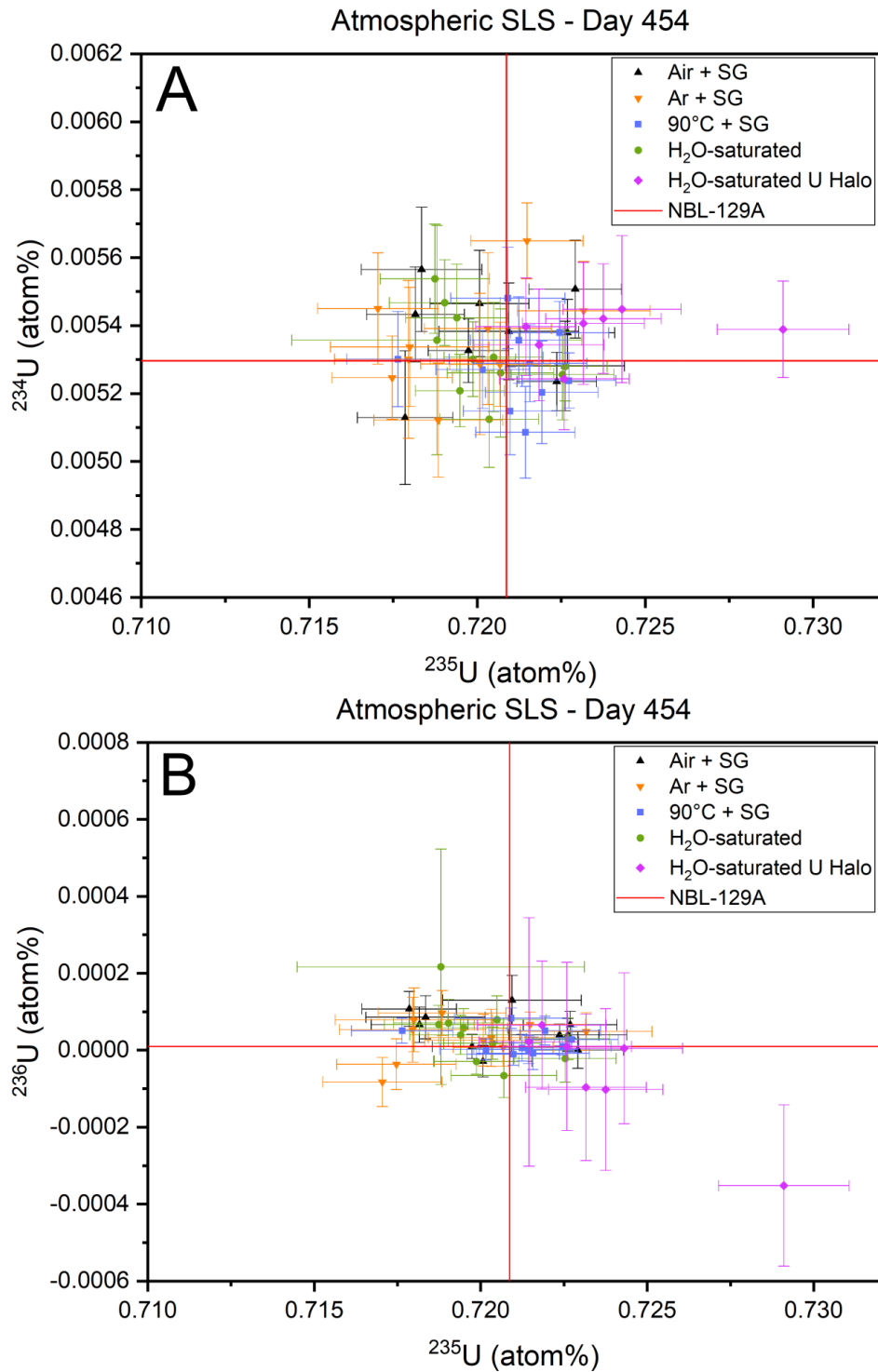


Figure 49: Uranium isotopic abundance of representative particles stored for 454 days in laboratory air, argon, laboratory air at 90°C and in H₂O-saturated atmosphere for the shelf-life study (SLS). Panel A is ^{234}U vs. ^{235}U and panel B is ^{236}U vs. ^{235}U .

The results for samples stored in water-saturated atmosphere suggest that the uranium migration onto the GCD surface may lead to mass dependent fractionation, if only the major isotopes are considered. When compared to unaltered particles, the migrated uranium in the

halos is enriched in the isotopic lighter ^{235}U , while the particle remnants are depleted and therefore enriched in the isotopic heavier ^{238}U .

The question is, if this measured isotopic deviation is a real, physical fractionation or if it is some kind of artifact from the measurement because of the larger size of the measured uranium halos. Preliminary LG-SIMS data from NIST test measurements (Todd Williamson, pers. comm.) on uranium oxides stored in water yielded the same observations and therefore support the conclusion of a real fractionation, especially when considering that the team at the NIST SIMS laboratory uses an unfocused Köhler beam instead of a focused, rastered beam.

In conclusion, the complementary SEM, μ -Raman spectroscopy and SIMS investigations of VOAG-produced uranium oxide microparticles confirm the hypothesis that the microparticle shelf-life heavily depends on the storage conditions. The presence of water triggers the formation of uranyl hydroperoxides, even after a relatively short duration of 30 days. Surficial particle alteration can be observed, where clear changes in their physical form compared to their original shape occur. Continuous exposure to water-saturated atmosphere could eventually make the uranium microparticles impracticable as reference material due to uranium migration and spread of uranium halos that covers the whole sample planchet, obfuscating reliable analysis of individual particles. This confirms previously reported alteration effects from the NUSIMEP-9 ILC. More importantly, the observed uranium migration leads to a significant isotopic deviation, rendering the microparticles unusable as reference material. However, a brief exposure to water-saturated atmospheres is of no concern to the viability as reference material. Three easily implemented storage conditions kept the particles stable for at least one year. However, there is a discussion to be made that first signs of alteration could be observed in laboratory atmosphere at 90°C after 454 days. These possible alteration signs and the results of the water-saturated particles lead to the conclusion that storage in an inert, water-free environment is strongly recommended. For the moment, storage in argon with silica gel as desiccant proves to be the most promising storage approach.

4.3.2 Particle shelf-life in alcoholic dispersion

Complementary to the shelf-life study of particles in different atmospheres, their stability in different alcoholic media was investigated. The particles were stored in ethanol (1), 2-propanol (2), *n*-butanol (3) and *tert*-butanol (4). Aliquots of the same dispersions were investigated at FZJ using SEM, ICP-MS and Focused Ion Beam (FIB). First results are shown in Figure 50. The SEM

investigations suggested, that all four alcoholic solvents are suitable storage media for up to 93 days [49].

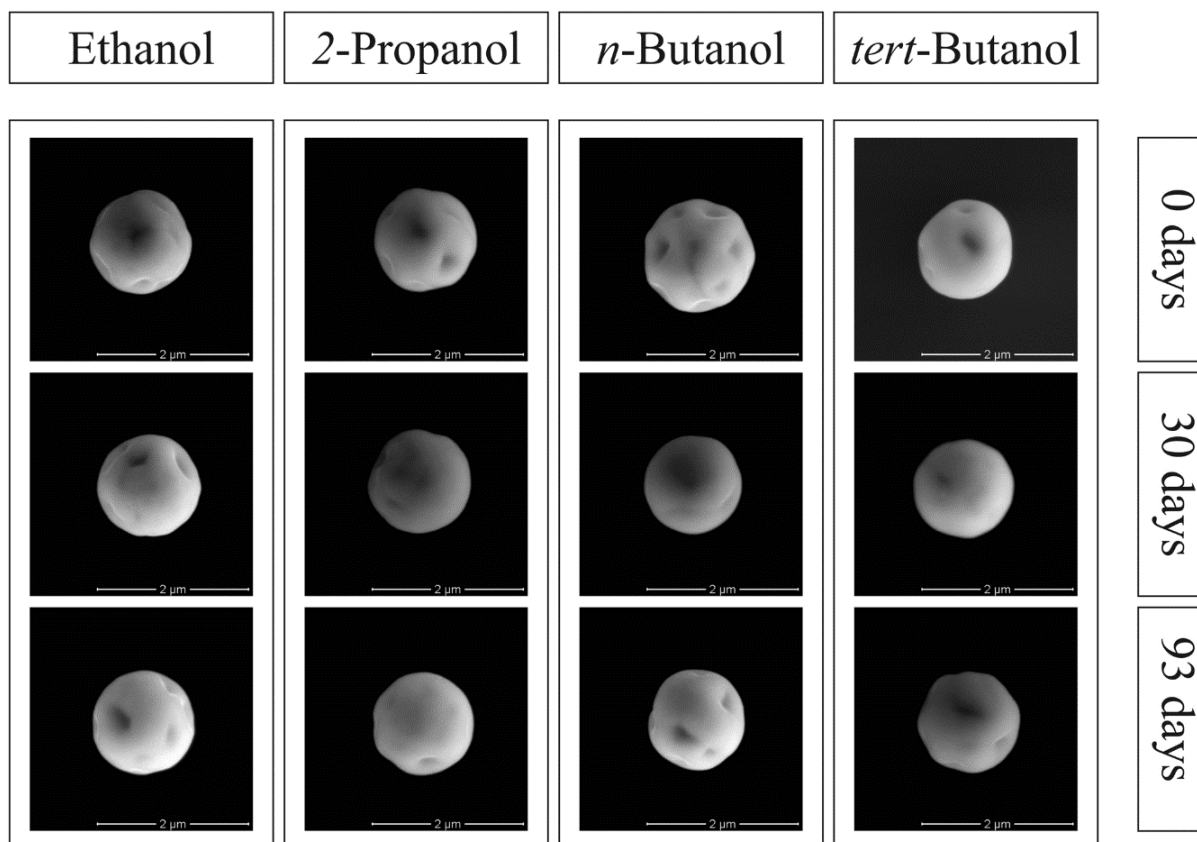


Figure 50: Representative SEM images of uranium oxide particles stored in ethanol, 2-propanol, *n*-butanol and *tert*-butanol after a certain time of storage (from Potts *et al.* [49]).

As a continued investigation of the results obtained by Potts *et al.*, the uranium microparticles in the aliquots shipped to Heidelberg were investigated in the same way as the microparticles in the atmospheric shelf-life study after 163, 337 and 580 days in their respective storage media using μ -Raman spectroscopy and LG-SIMS and after 337 and 580 days of storage using SEM.

4.3.2.1 Ethanol

^{238}U ion images of the uranium particles stored in ethanol show that the particle concentration for each newly prepared sample is very inconsistent (Figure 51). While samples prepared after 163 and 337 days of storage yield a relatively low number of particles, the sample prepared after 580 days shows a much denser particle distribution. The high number of particles sometimes even leads to particle agglomerations. However, even on a densely dispersed sample, the single particles show clear boundaries and can be easily distinguished.

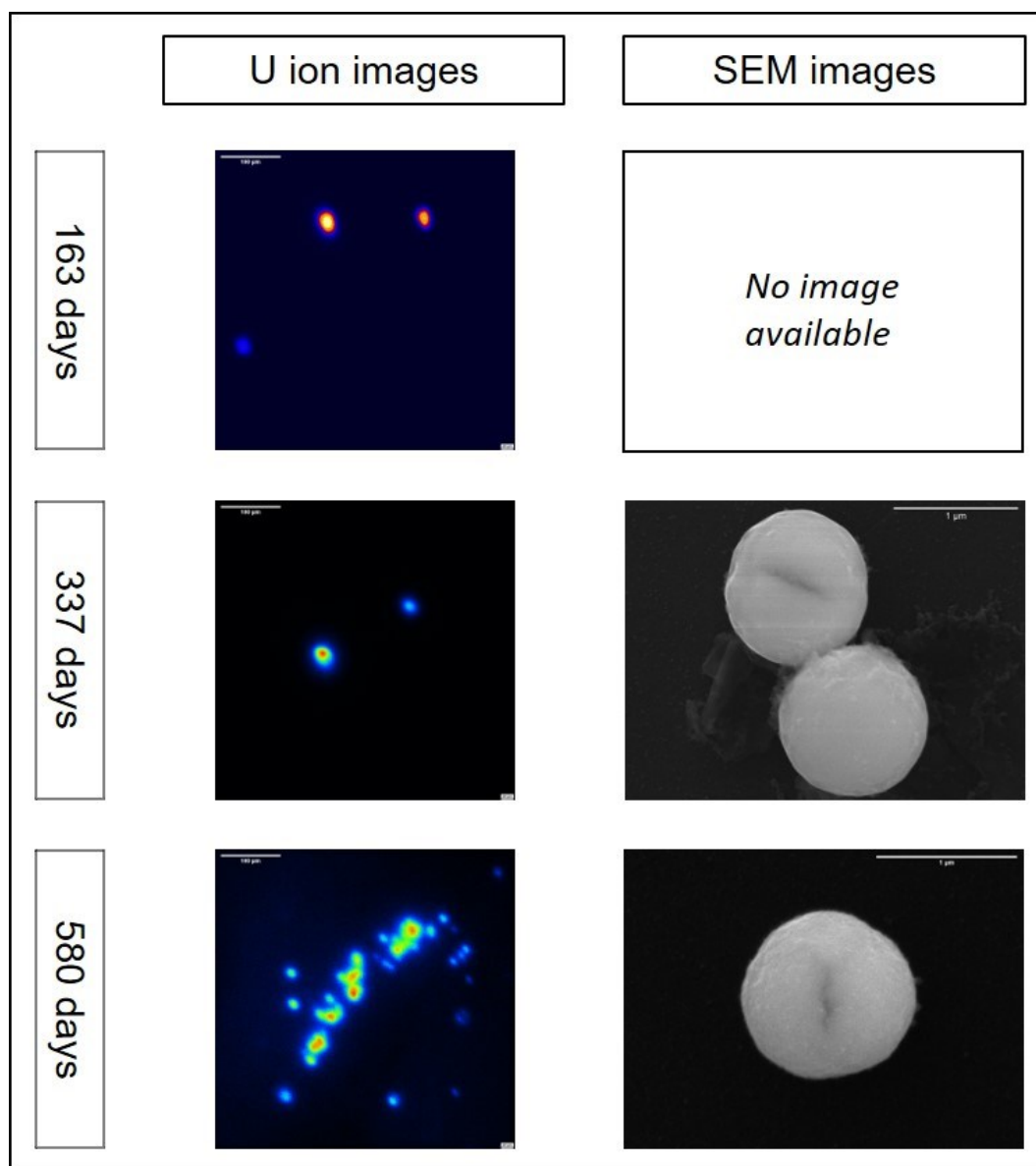


Figure 51: $500 \times 500 \mu\text{m}$ ^{238}U ion images and SEM images of uranium microparticles stored in ethanol for 163, 337 and 580 days. The first ion image uses a heat LUT, the others a rainbow LUT.

The overall lower number of particles on the first two samples can be explained by inefficient detachment from the collection planchet when rinsed in ethanol. Previous studies have shown

that ethanol detaches approximately 50% of the particles collected on the production planchet and brings them into dispersion [49]. Considering the fact that the number of particles in 5 ml dispersion corresponds to ~50% of particles collected in the production of a single GCD with directly collected microparticles after 60 min collection time, and a single aliquot for this study was prepared using 300 μ l of the dispersion, the expected particle concentration is relatively low. An explanation for the fact that the latest sample created has the highest particle concentration is harder to find. One possibility is the insufficient mixing of the dispersion prior to sample preparation. This would lead to particle enrichment in the remaining dispersion and therefore a higher number of particles in the aliquot used to create the last sample. However, longer treatment in the ultrasonic bath is not recommended, because this could damage the particles.

In the SEM images, the particles retain a round shape and an overall smooth surface after 337 days of storage in ethanol. This is in accordance to previous observations [47]. First signs of increased surface roughening can be seen on some particles after 580 days in ethanol. The effect is not as notably as the dissolution phenomena reported by Potts *et al.* [49] after 4 years of storage in ethanol, but it points towards the first signs of alteration observed for particles stored in water-saturated atmosphere discussed before.

It was not possible to obtain Raman spectra of the particles after 163 and 337 days due to their low number. After 580 days of storage, the particles can be divided in two sub-groups. The minority of particles yields spectra like Figure 52. The spectrum is comparable to a freshly produced microparticle and points towards a mixture of uranium oxides as it was discussed before.

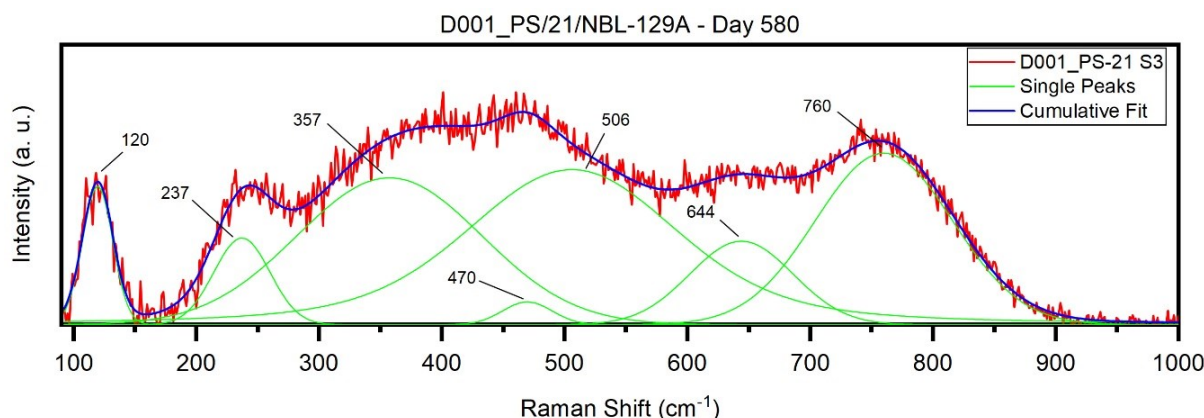


Figure 52: Raman spectrum obtained from minority of particles stored in ethanol for 580 days.

However, the majority of particles yielded spectra like Figure 53. The overall spectrum looks very similar to those recorded for particles stored in water-saturated atmosphere that started to show first signs of alteration (Figure 44a). Although some features typical for uranium oxides like the

Raman bands between 300 and 500 cm^{-1} are still visible, the spectrum points towards amorphization. There is also a peak shoulder visible at $\sim 844 \text{ cm}^{-1}$ that implies the formation of an alteration phase. However, formation of uranium hydroperoxide (e.g., [meta]-studtite) or uranium hydroxide (e.g. schoepite) cannot be unambiguously distinguished. Therefore, the reason for this alteration could be the same as for a water-saturated atmosphere. Ethanol is a reasonable hygroscopic solvent. Although the samples were handled in an argon atmosphere that contained as little water as possible, there is still the possibility of water influx into the dispersion.

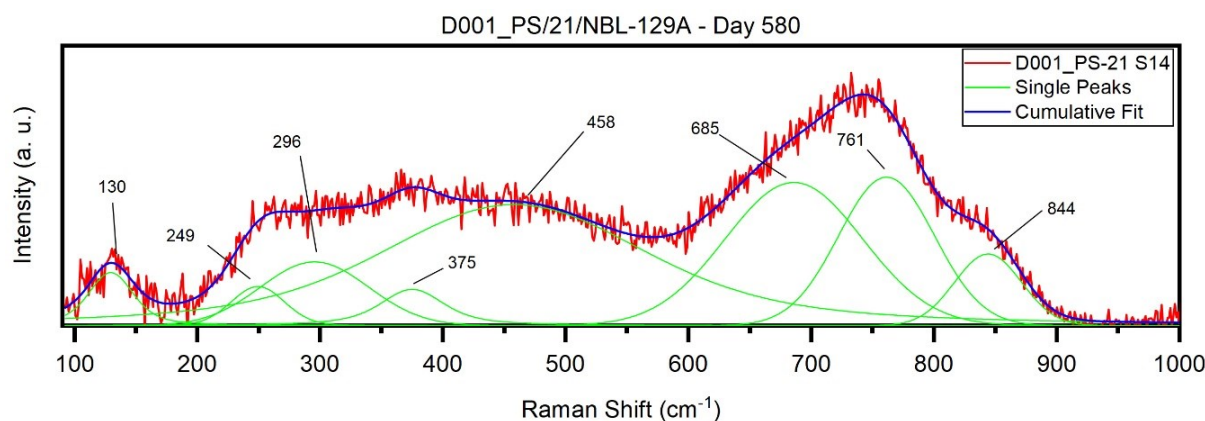


Figure 53: Raman spectrum obtained for majority of particles stored in ethanol for 580 days.

This particle alteration is not very advanced and the particles could still be easily measured by SIMS. However, the observed alteration leads to the conclusion that ethanol, while viable as short-term dispersion medium, is not the perfect solvent for long-term storage of uranium oxide particles.

4.3.2.2 2-Propanol

In contrast to the particles stored in ethanol, ^{238}U ion images obtained for particles stored in 2-propanol display a homogeneous particle distribution after 163, 337 and 580 days of storage (Figure 54). The overall number is consistently low for all prepared samples. These observations are in contrast to the experimental values for the detachment efficiency determined by Potts *et al.* [49], where $\sim 96\%$ of the expected particles on the production sample could be detached and went into dispersion. However, the uncertainty of the calculated detachment efficiency is very high (59%) and the theoretical detachment efficiency of 2-propanol should be lower due to its moderate dynamic viscosity of 2.098 $\text{mPa}\cdot\text{s}$ [130]. Nonetheless, both experimental and theoretical detachment efficiency and therefore number of particles in the dispersion should be higher than in ethanol. The reason for this unexpected observation could be a similar one to the

low number of particles in the first two samples prepared from ethanol dispersion in the form of insufficient mixing before preparation. However, this is very speculative and the reason for the low number of particles remains uncertain.

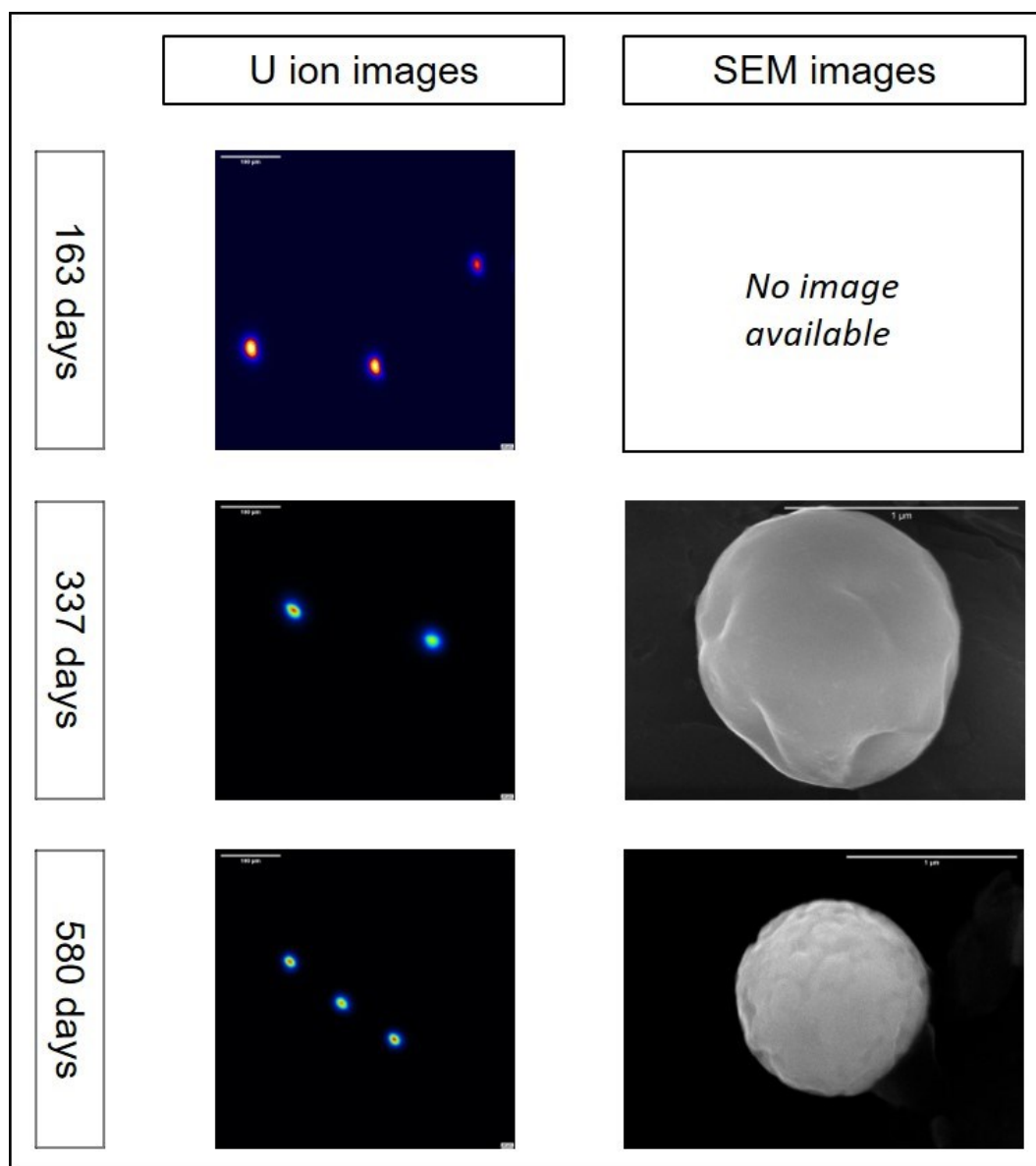


Figure 54: $500 \times 500 \mu\text{m}$ ^{238}U ion images and SEM images of uranium microparticles stored in 2-propanol for 163, 337 and 580 days. The first ion image uses a heat LUT, the others a rainbow LUT.

The SEM images after 337 days show unaltered and well-rounded particles with a smooth surface. After 580 days, an increased surface roughness like the one of particles stored in ethanol can be observed, although this was not the case for all particles.

Due to the consistently low number of particles, the only Raman spectrum recorded is from a particle stored for 163 days (Figure 55). The spectrum shows the typical Raman bands for a U_3O_8 -

dominated mix of uranium oxides indistinguishable from freshly produced microparticles that underwent the dispersion step.

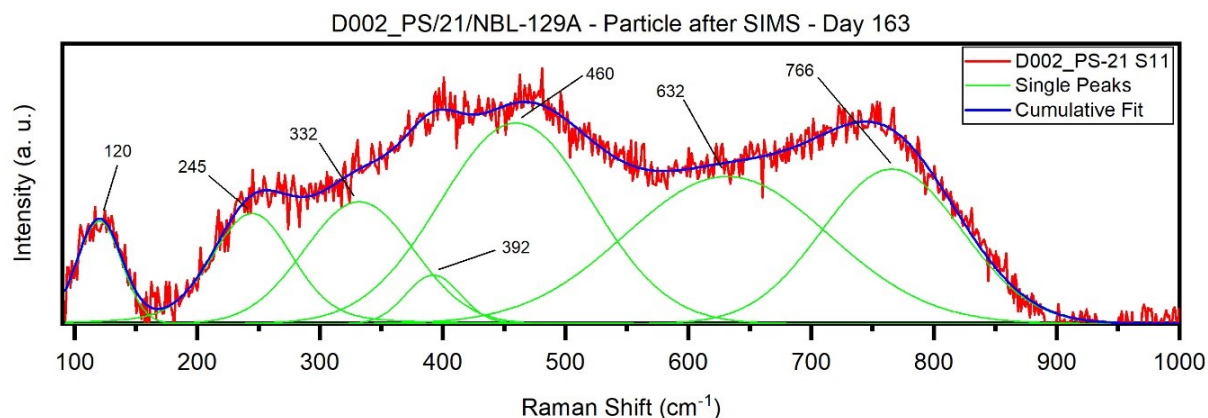


Figure 55: Raman spectrum of a particle stored in 2-propanol for 163 days.

Although no Raman spectra after 337 and 580 days could be recorded to confirm it, the SEM images point towards a beginning alteration after 580 days, that is comparable to the one observed for particles stored in ethanol. Therefore, 2-propanol is not recommended as a long-term storage medium.

4.3.2.3 *n*-Butanol

Comparable to the particles stored in ethanol, ^{238}U ion images of particles stored in *n*-butanol show the inconsistent particle concentration on the samples prepared after the respective storage time (Figure 56). The first two samples prepared yielded a very low number of particles, while the last sample prepared was relatively densely populated. Considering the experimental results of the detachment efficiency observed by Potts *et al.* [49] where only $\sim 20\%$ of the presumably produced particles were detached, the low number of particles on the first two samples prepared is not unexpected. A possible explanation for the comparably high number of particles on the last sample can be the same as for the particles stored in ethanol, indicating unsuitable mixing of the dispersion prior to the preparation of the first two samples and therefore leaving the remaining dispersion used for the last sample enriched in particles.

SEM investigation after 337 days shows, that some particles developed some kind of circular crystallites on the particles' surface. If this can be linked to water-influenced alteration cannot be confirmed, because nothing comparable could be observed before. It is noteworthy, that no particles showing the same kind of surficial phase formation could be discovered after 580 days, although some particles displayed a very slight form of surface roughening. However, the stage

of alteration was not comparable to the alteration found on particles stored in ethanol or 2-propanol.

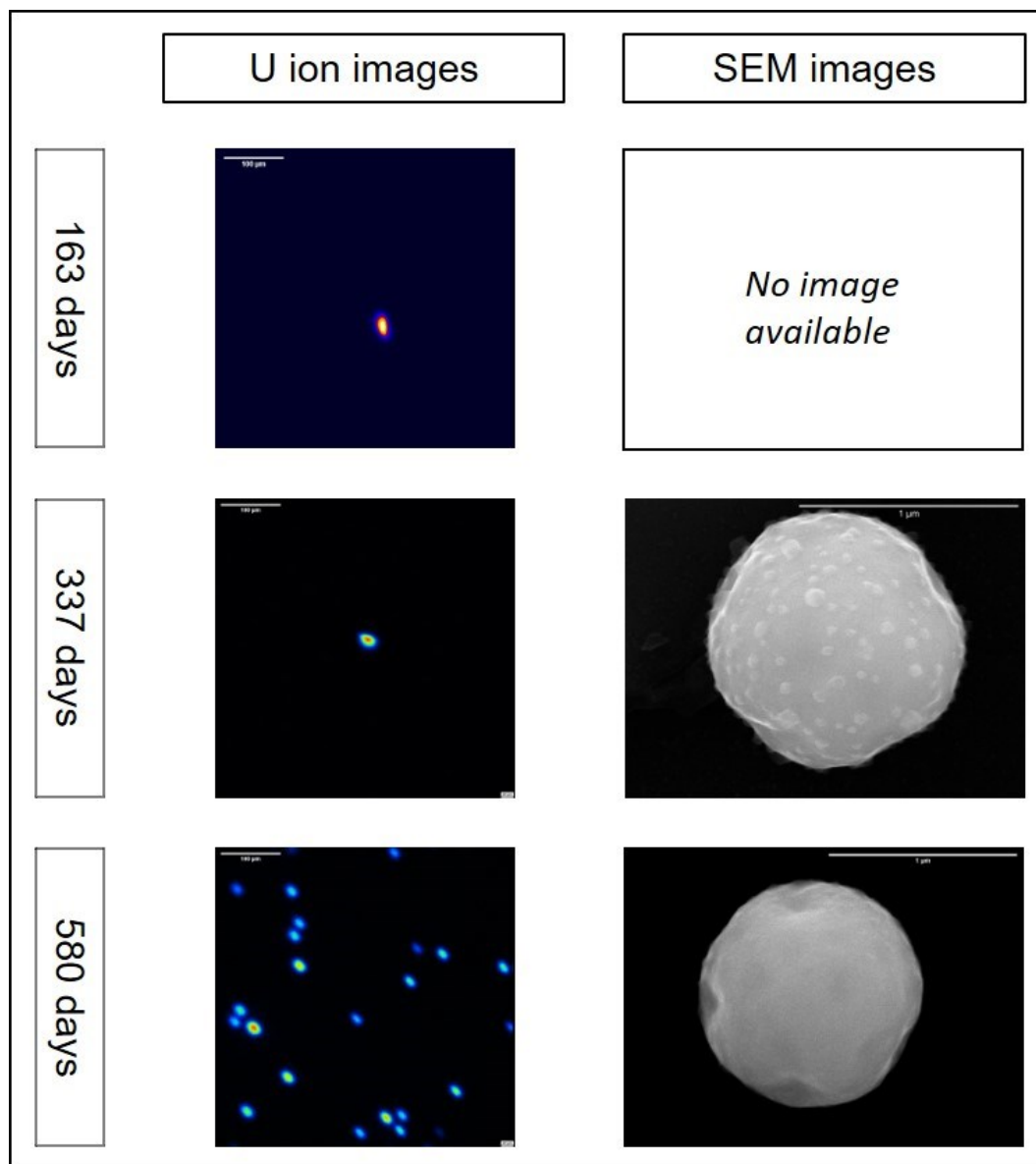


Figure 56: $500 \times 500 \mu\text{m}$ ^{238}U ion images and SEM images of uranium microparticles stored in *n*-butanol for 163, 337 and 580 days. The first ion image uses a heat LUT, the others a rainbow LUT.

Like for the sparsely populated samples before, it was not possible to obtain Raman spectra of particles stored in *n*-butanol for 163 and 337 days. However, after 580 days a large number of particles could be measured using μ -Raman spectroscopy. The majority of particles displayed a typical uranium oxide spectrum (Figure 57).

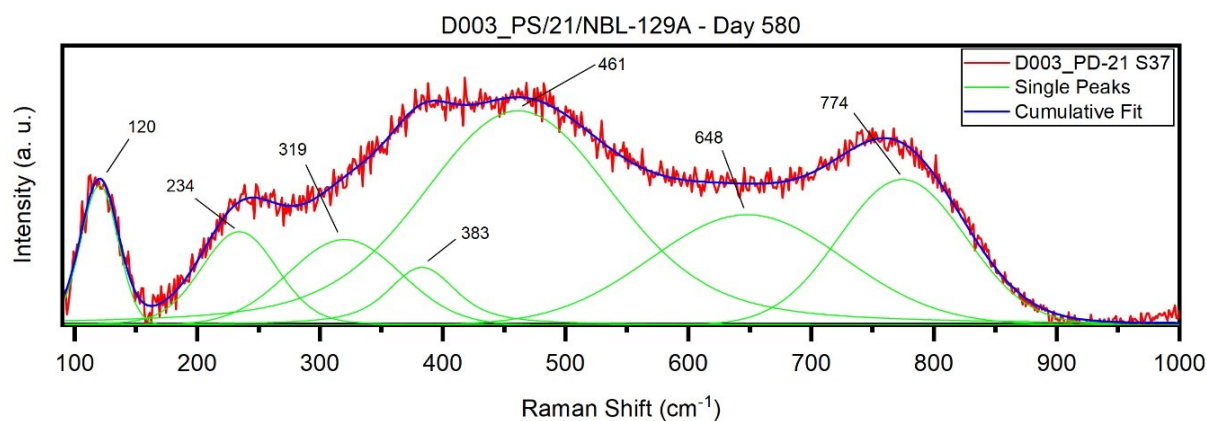


Figure 57: Raman spectrum obtained for majority of particles stored in *n*-butanol for 580 days.

However, there was also a minority of particles showing spectra like Figure 58. There are still features visible that are typical for uranium oxide, but surficial amorphization is already well-advanced and the peak shoulder at ~ 842 cm⁻¹ points towards a beginning formation of uranium hydroxides or uranium hydroperoxides.

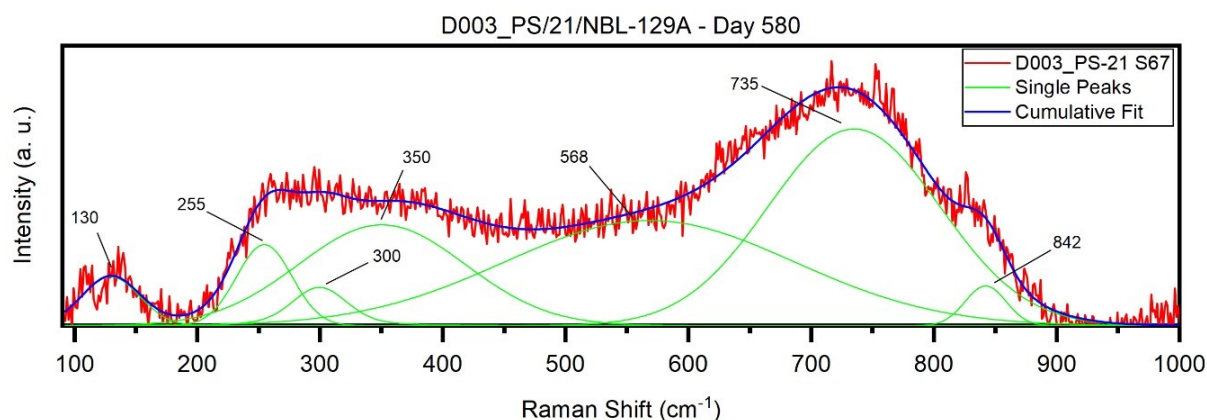


Figure 58: Raman spectrum obtained from minority of particles stored in *n*-butanol for 580 days.

Although the microparticles stored in *n*-butanol were still easily measurable by LG-SIMS and only a small fraction of particles started to show signs of water-influenced alteration, *n*-butanol is not recommended as a long-term storage medium for VOAG-produced uranium oxide microparticles.

4.3.2.4 *tert*-Butanol

The ²³⁸U ion images show, that the overall particle concentration of particles stored in *tert*-butanol is the highest (Figure 59). Although the first sample prepared yields a relatively low number of particles – possibly due to reasons already discussed for particles stored in the other three alcoholic solvents – both the second and the third samples prepared are densely populated.

This observation, indicating that the *tert*-butanol dispersion contains the highest number of particles, is not in accordance to the experimental results for the detachment efficiency, but fits the theoretical expectations [49]. The particles can be easily located and do not tend to form agglomerations.

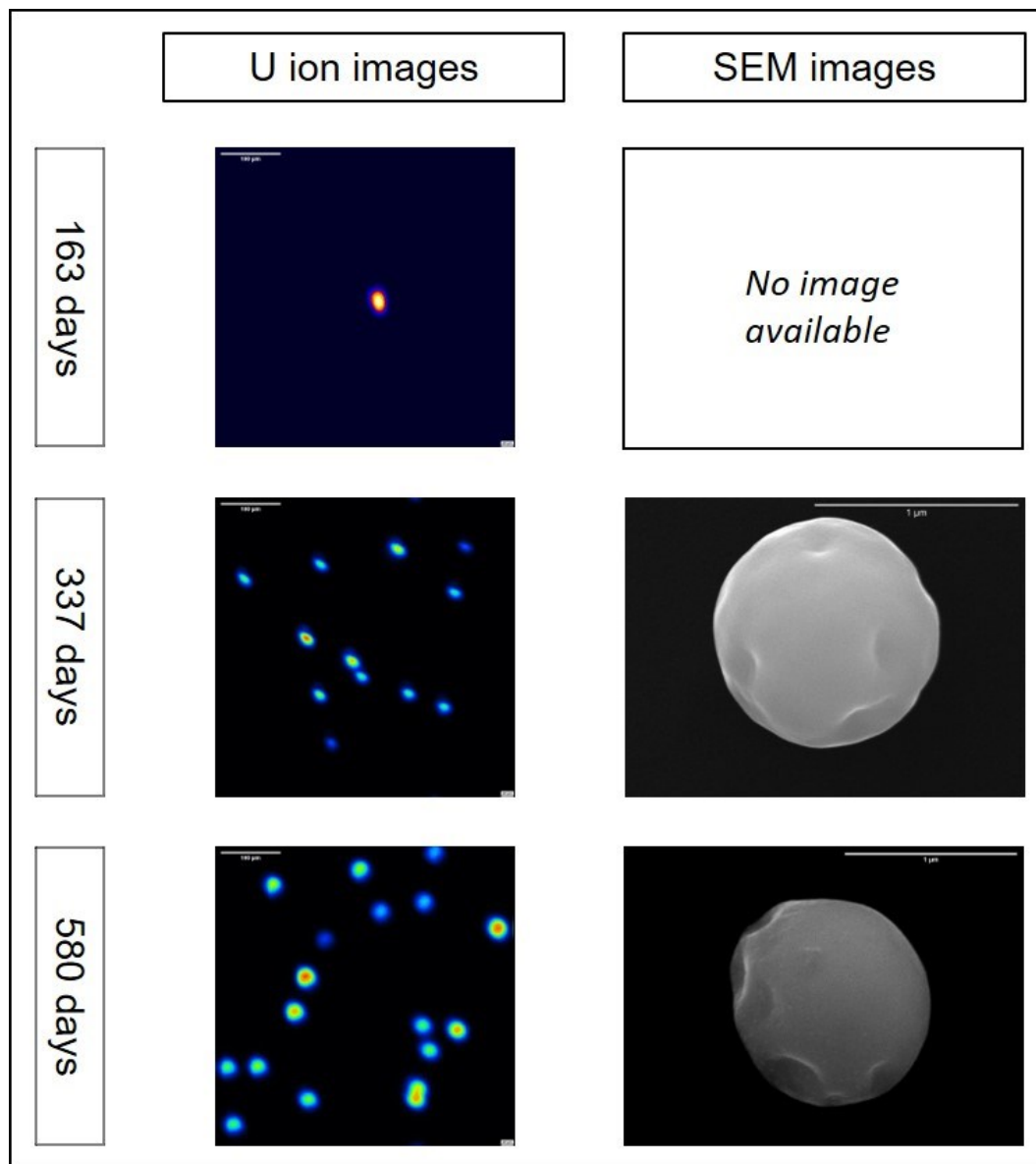


Figure 59: $500 \times 500 \mu\text{m}$ ^{238}U ion images and SEM images of uranium microparticles stored in *tert*-butanol for 163, 337 and 580 days. The first ion image uses a heat LUT, the others a rainbow LUT.

Particles investigated with SEM display a round shape and smooth surface equal to freshly produced particle productions both after 337 and 580 days. No signs of alteration could be identified. These observations match the obtained Raman spectra after 163, 337 and 580 days. Figure 60 shows a representative Raman spectrum of a uranium microparticle obtained after 580 days of storage in *tert*-butanol. It indicates the typical mix of uranium oxides with U_3O_8 as a main phase and does not point to the presence of any kind of water-induced alteration phases.

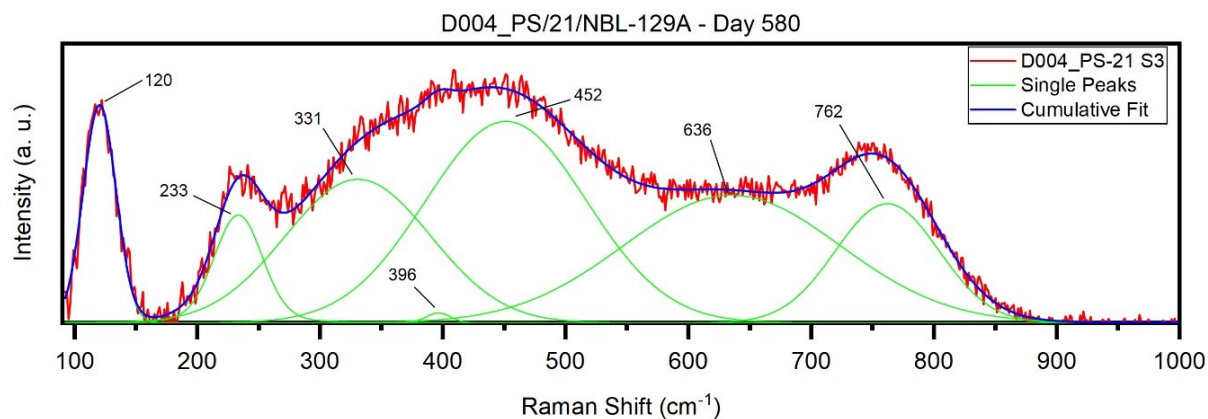


Figure 60: Representative Raman spectrum obtained from particles stored in *tert*-butanol for 580 days.

The absence of alteration phenomena and the relatively high particle yield make *tert*-butanol a promising long-term storage medium for uranium microparticles.

4.3.2.5 Uranium isotopic abundance of microparticles stored in different alcoholic solvents

SEM images and Raman spectra indicated the beginning of particle alteration in ethanol, 2-propanol and n-butanol comparable to the very early stages of water-induced alteration in an H₂O-saturated atmosphere. The most important question for possible intermediate storage in these solvents is if this slight alteration has any kind of influence on the uranium isotopic composition of the particles and therefore their viability as reference materials. To investigate this, a randomly chosen population of microparticles from each storage medium was analyzed in SIMS microparticle measurements after 163, 337 and 580 days.

The isotopic composition of particles out of the four storage media remained invariant over 580 days. Figure 61 shows the uranium isotopic abundance of the measured particles after 580 days. The variations of the single particle measurements are within normal range and particles from all different alcoholic storage dispersion lack any deviation from the expected values. The SIMS microparticle measurements after 163 and 337 days confirm this and can be found in appendix 6.2.2.

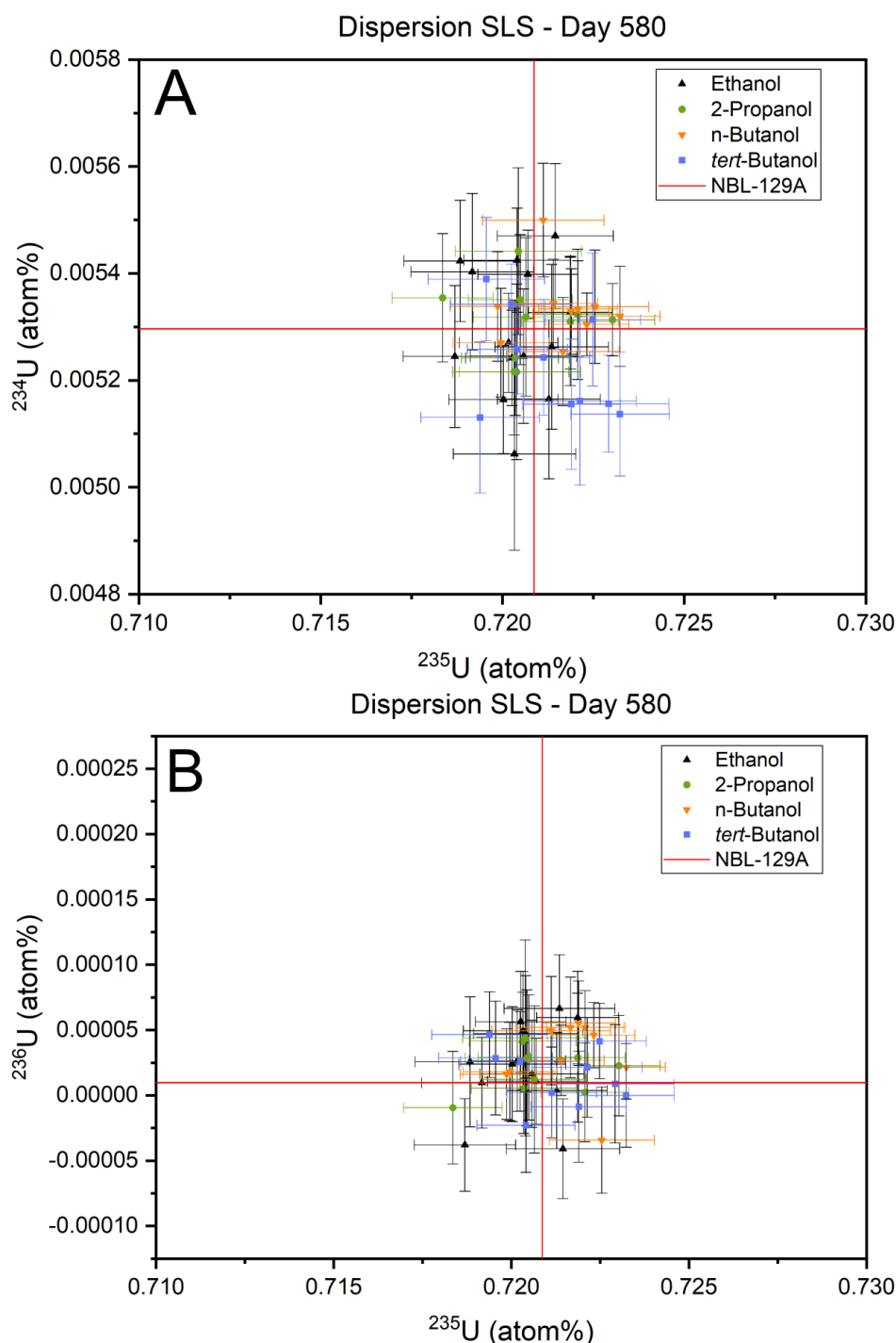


Figure 61: Uranium isotopic abundance of representative particles stored for 580 days in ethanol, 2-propanol, *n*-butanol and *tert*-butanol. Panel A is ^{234}U vs. ^{235}U and panel B is ^{236}U vs. ^{235}U .

The fact that after 580 days of storage time, particles from all alcoholic dispersions investigated could be easily located and measured using LG-SIMS, and their isotopic abundance is equivalent to the certificate value of CRM NBL 129-A demonstrates that the VOAG-produced uranium microparticles are stable in the different alcoholic solvents. Hence, they remain viable as reference materials over the durations investigated. However, particles in three of the four possible long-term storage media showed first signs of alteration. The most promising candidate

as a long-term storage medium for VOAG-produced uranium oxide microparticles is *tert*-butanol. Dispersion on the sample planchet after storage in *tert*-butanol yielded the highest number of particles and the particles retained their structure and shape. High detachment efficiency and high particle stability are strong arguments for *tert*-butanol as long-term storage medium. In addition, it is also highly recommended to store the dispersion vessels and also conduct sample preparation in H₂O-free atmospheres, e.g. argon, to preclude any influx of water and therefore possible particle alteration.

4.4 Insights for SIMS measurement setup

During the implementation of the uranium microparticle measurement setup, the results of the analyses provided some new insights that lead to adjustments recommended for future SIMS analysis of uranium reference materials and potential field samples.

4.4.1 Secondary ion beam aberrations

The first measurements during the characterization of the potential reference materials FZJ-3050P/1 and FZJ-3050P/2 in September 2022 with the established microparticle measurement setup based on the IAEA-SGAS protocol after Hedberg *et al.* [15] showed that unexpectedly high intensities were recorded on the L2 detector measuring ²³⁴U. A mass scan using all 5 detectors reveals that the shape of the recorded mass peak is uncommon and covers a higher mass range than the peaks for the other masses (Figure 62). Certificate values for the IRMM-3050 solution, which was used to produce the FZJ-3050P particles, show a very low ²³⁴U amount of 0.0009838 atom%. Test measurements on NBS CRM U010 and CRM U100 used for instrument calibration lacked this unusual peak form. Mass scans on CRM U500 with a comparable amount of ²³⁵U had the same broad intensity recorded by L2, however, the intensity at the mass center was overlaid by the intensity of a typically shaped ²³⁴U mass peak. The higher mass peak can be explained by the higher isotopic abundance of ²³⁴U in CRM U500 (0.5181 atom%). This leads to the conclusion, that the recorded intensity on L2 for FZJ-3050P particles is not a result of real ²³⁴U⁺ ion impingement, but of deflected secondary ion intensity of an unknown source. The fact that this was not recorded on reference materials with a lower amount of ²³⁵U points towards deflected ²³⁵U⁺ ions as origin of this unintended intensity. Secondary ion beams of masses in the same range have a similar shape. The recorded ²³⁸U intensity on the H1 detector is in the same range as the recorded ²³⁵U intensity on L1 (Figure 62). To check for possibly deflected ²³⁸U⁺ ions, this effect

was investigated with a mass scan of mass 237 and its vicinity, where usually no impinging ions are expected. The scan showed the same kind of atypically shaped intensity at mass 237. This leads to the conclusion that the secondary ion beams of all isotopes measured are responsible for obscure intensities one mass lower than their actual mass peak proportional to the amount of actual impinging ions.

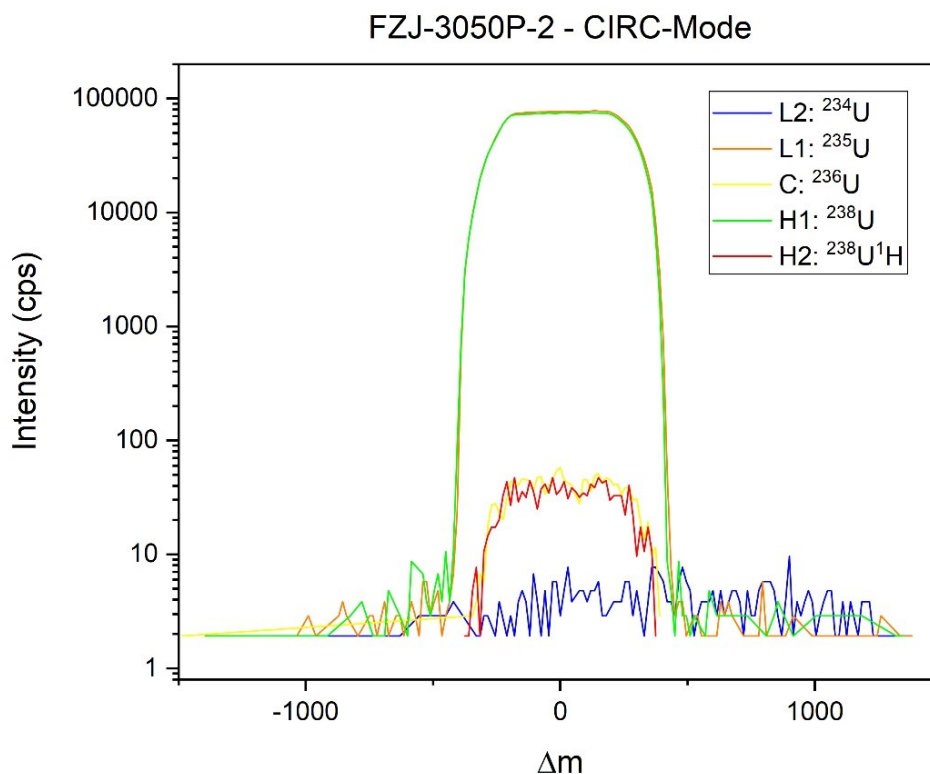


Figure 62: Mass peaks for uranium isotopes measured with all 5 EM detectors using CIRC-mode for an FZJ-3050P/2 particle.

A possible reason for the deflection can be aberrations in the secondary ion beam. CAMECA implemented a mode to focus the ion beam Y axis into one level. This mode is called XY-mode (in contrast to the usually used and previously for particle analysis recommended CIRC-mode). After changing to XY-mode, the calibration standards needed to be remeasured and correction parameters for detector yield and calculated mass bias had to be readjusted. A mass scan of FZJ-3050P particles in the same range displays that the unintended intensity recorded on the L2 detector disappeared (Figure 63) and the remaining ions counted correspond to a realistic number of $^{234}\text{U}^+$ ions.

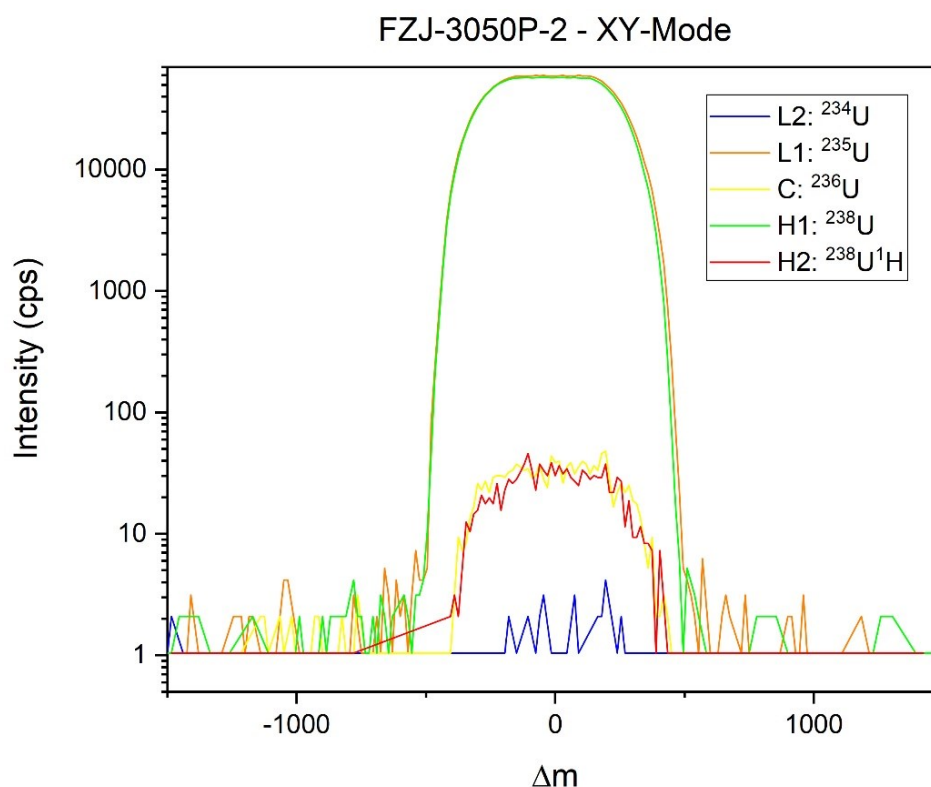


Figure 63: Mass peaks for uranium isotopes measured with all 5 EM detectors using XY-mode for an FZJ-3050P/2 particle.

Comparative isotopic abundance measurements of the particles show the influx of the adjustment to XY-mode (Figure 64). While the unintended intensity on the L2 detector in CIRC-mode leads to results that deviate from the certificate values for IRMM-3050 in ^{234}U and to a lower extent in ^{235}U , results of the adjusted measurement setup using XY-mode are in accordance with the IRMM-3050 certificate. Later measurements of the FZJ-3090P particles confirmed these observations and did also show increased ^{234}U values for measurements in CIRC-mode.

The problem using CIRC-mode will only occur for samples with a very high $^{235}\text{U}/^{234}\text{U}$ -ratio. For samples with a low amount of ^{235}U , the number of deflected ions is too low to create a considerable intensity on the L2 detector. On the other hand, highly ^{235}U enriched samples that also contain a reasonable amount of ^{234}U (e. g. CRM U500) are also safe to be measured using CIRC-mode, because the influence of deflected $^{235}\text{U}^+$ ions is very low compared to the actual ^{234}U intensity. The added number of ions counted is within normal measurement uncertainties. However, if the minor isotopic composition of the standard used to calibrate the instrument varies in several orders of magnitude from the measured sample, it is necessary to use XY-mode. For samples like these, reshaping the secondary ion beam using the XY-mode mitigates the problem and seems to be a viable solution. However, this is highly case-dependent and for different samples the CAMECA-recommended CIRC-mode might be the better solution.

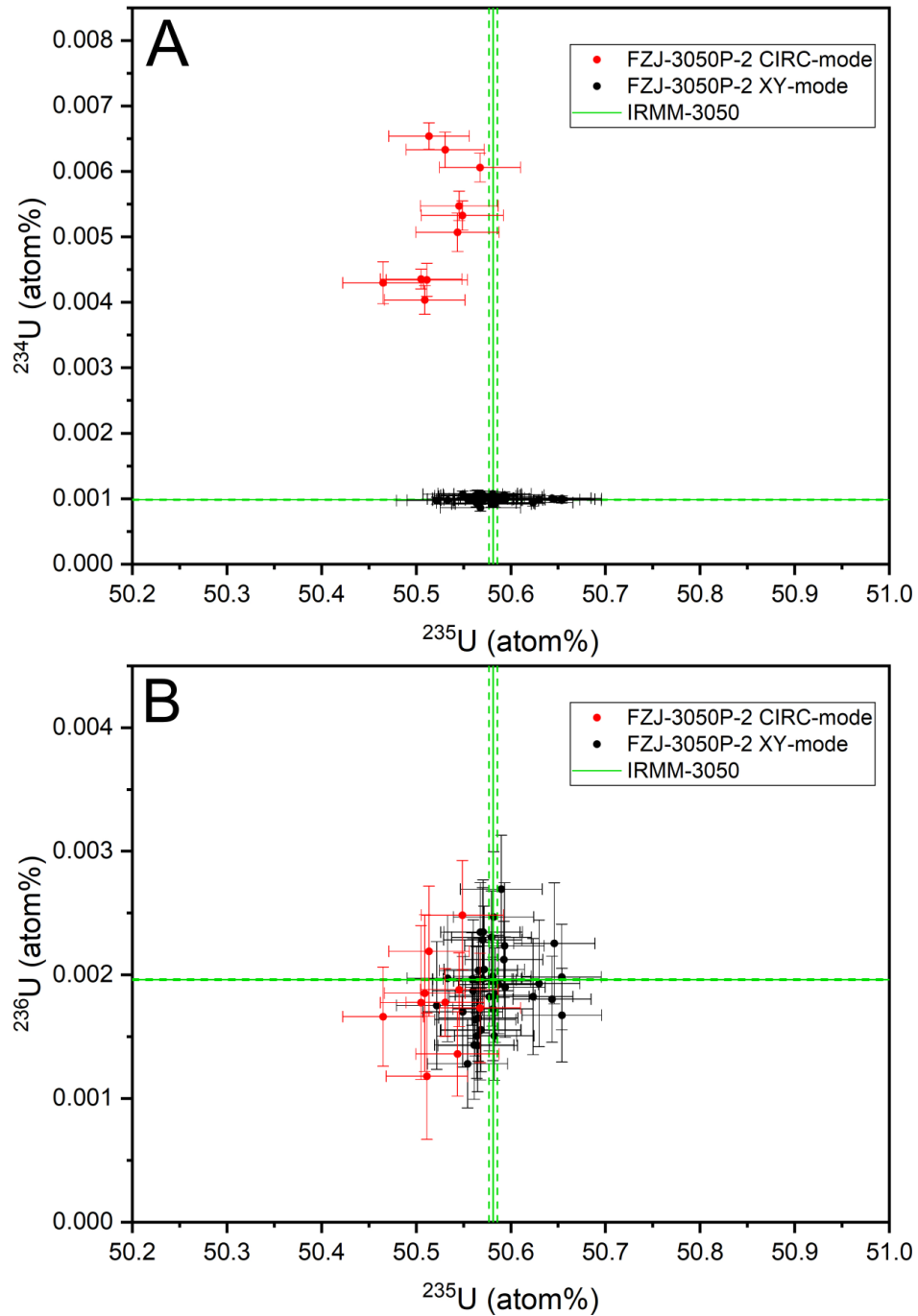


Figure 64: Uranium isotopic abundance of FZJ-3050P/2 particles using CIRC-mode and XY-mode. Panel A is ^{234}U vs. ^{235}U and panel B is ^{236}U vs. ^{235}U .

4.4.2 Influence of Z-axis centering on APM measurements

For every single microparticle measurement, the primary ion beam has to be focused on the sample surface by centering the Z axis of the sample. For small scale single particles, this centering is done manually to guarantee the highest secondary ion transmission. APM measurements are usually in a larger scale. A high-energy primary beam with a larger size is used to cover an area of $500 \times 500 \mu\text{m}$ instead of the $10 \times 10 \mu\text{m}$ of a microparticle measurement. In addition, the field aperture is opened to $12,000 \mu\text{m}$ to prevent cutting off signal. A manual correction of the Z axis during the APM measurement is not possible on the CAMECA IMS 1280-HR at HIP. The newer IMS 1300-HR model is equipped with a motorized Z axis. For the IMS 1280-HR, the primary beam is focused on a central spot on the sample planchet.

During the APM measurements of an IAEA-requested sample IAEA-1, the Z score of the APM-calculated particles showed a wide range. In contrast to normal deviation, there was a clear trend apparent. Figure 65 shows the Z score of the calculated particles depending on their position on the sample planchet for IAEA-1 (top) compared to the previously APM-measured and discussed sample FZJ-3050P/2. While the Z score deviation of the FZJ-3050P/2 particles is homogeneously distributed across the sample planchet, the IAEA-1 Z score distribution shows a clear trend depending on the Y position of the particles on the sample planchet. Particles in the upper half of the planchet tend to show a negative deviation and therefore lower $^{235}\text{U}/^{238}\text{U}$ -ratio than the average while particles in the lower half tend to show a positive deviation meaning higher-than-average $^{235}\text{U}/^{238}\text{U}$ -ratio.

The APM measurement was later repeated with a different sample holder. The results were comparable to the ones of FZJ-3050P/2 with no systematic isotopic deviation trend. This leads to the conclusion, that the observed Z score deviation of the first measurement is not a result of an actual tilted sample planchet, but connected to the used sample holder.

The reason for a mass-dependent fractionation caused by a tilted sample plane needs to be discussed in the future. Oxygen isotope measurements not connected to this work confirmed the influence of an insufficiently centered Z axis due to sample plane tilt on measured isotopic ratios. For now, it is recommended to check the sample holders for perfect flatness and to review APM results for position-dependent trends to identify possible sample plane tilt.

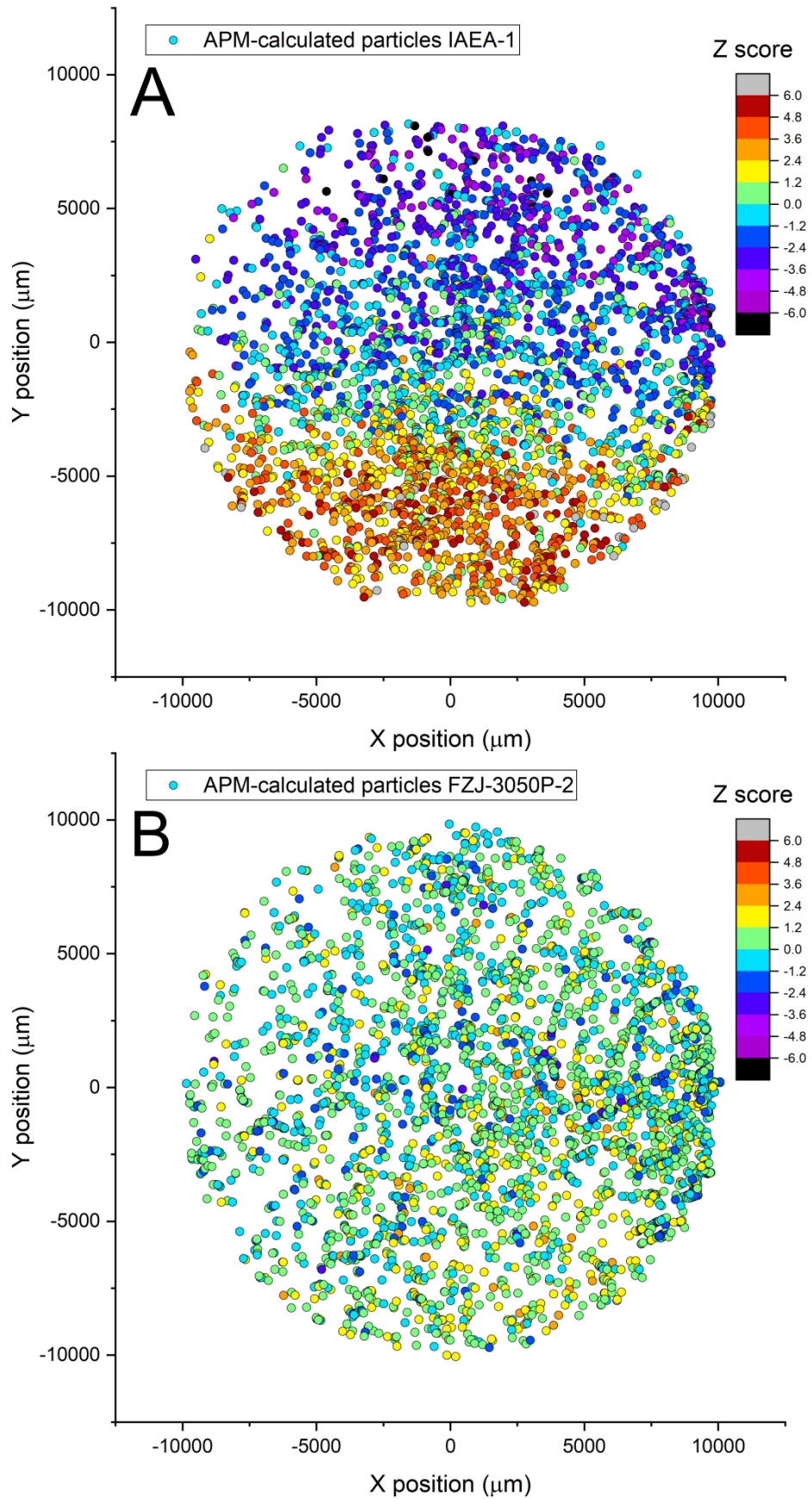


Figure 65: Z score of APM-calculated uranium microparticles of sample IAEA-1 (A) and FZJ-3050P/2 (B) depending on their position on the planchet.

4.4.3 Signal size in sputtered area

It is noticeable that in the characterization measurements of both the FZJ-3050P and the FZJ-3090P particles, the mean ^{235}U values of the smaller particles were lower than the ^{235}U value of the larger particles. At least for the FZJ-3090P particles, the smaller particles deviated significantly from the certificate values (Figure 32). As a comparison for *Ln*-doped particles, the uranium isotopic composition of natural uraninite grains from the Happy Jack Mine, UT, USA, [91; 92] was measured with the same measurement setup used for single particle measurements of uranium microparticles. An important difference between particle measurement and uraninite grain measurements is the area size of uranium signal obtained. The uranium microparticles are only $\sim 1.2\ \mu\text{m}$ in diameter while the sputtered sample surface area is $10 \times 10\ \mu\text{m}$. Hence, most of the area sputtered by the primary ion beam is free of uranium. The measured Happy Jack uraninite grains have a size of $\sim 100\text{--}200\ \mu\text{m}$. Thus, the uraninite grains cover the whole area sputtered, leading to an even distribution of uranium signal. However, the mass bias used to calculate the $^{235}\text{U}/^{238}\text{U}$ -ratio was determined with the NBS CRM U010, CRM U100 and CRM U500 standard materials. These standard materials are distributed as U_3O_8 powders with single grains of about the same size as the default uranium microparticles ($\sim 1.2\ \mu\text{m}$). The results of the uranium isotopic abundance measurements and the literature value for Happy Jack uraninite reported by Dorais *et al.* [91] are shown in Figure 66. The large deviation from the literature values, especially in ^{235}U , is remarkable. Measured ^{235}U is consistently $\sim 2.5\ \%$ higher than the previously reported value.

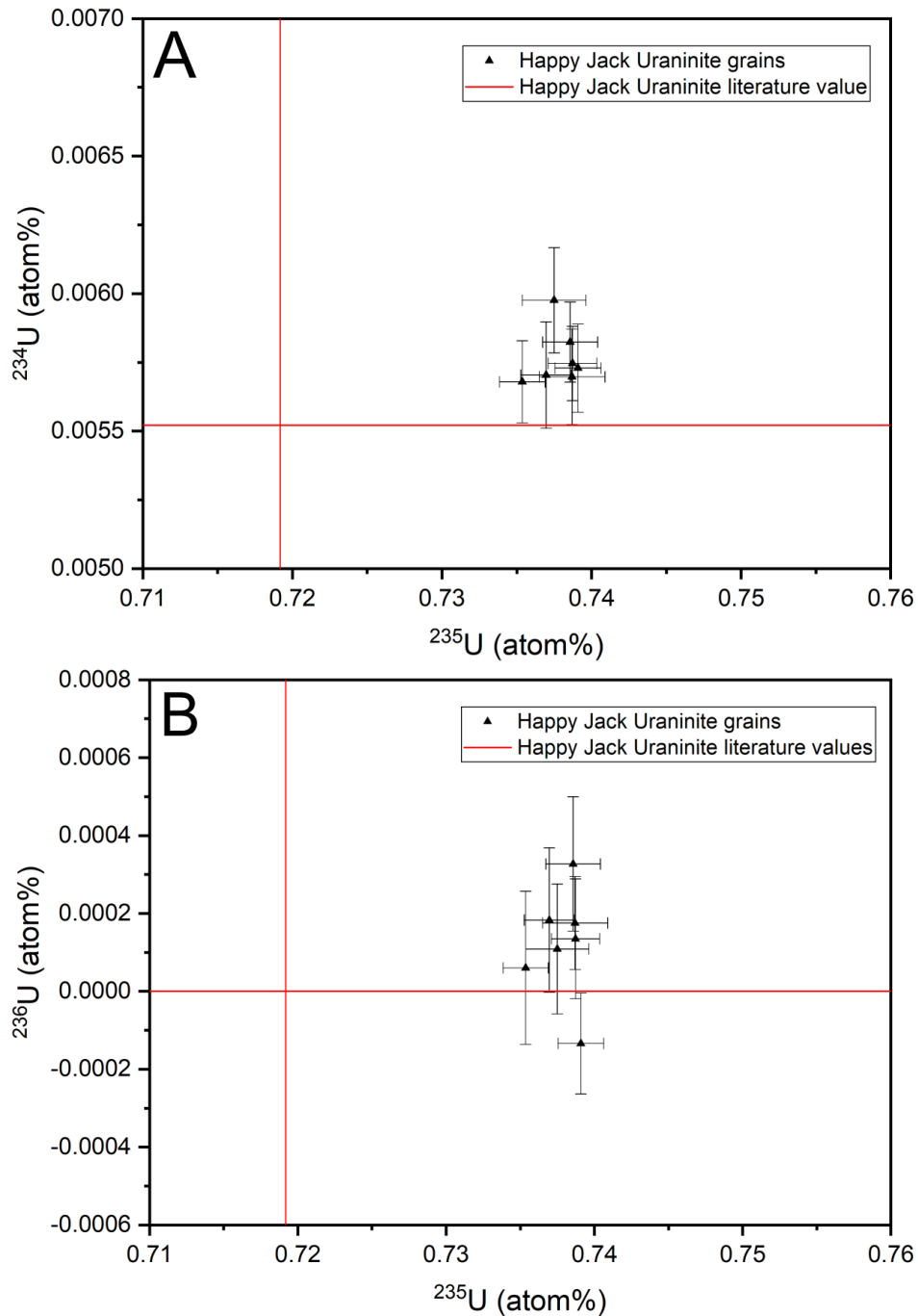


Figure 66: Measured uranium isotopic abundance of Happy Jack uraninite grains particles using NBS CRM particle standard materials for calibration. Panel A is ^{234}U vs. ^{235}U and panel B is ^{236}U vs. ^{235}U .

These results combined with the observations for particles of different size made during the measurements of FZJ-3050P and FZJ-3090P particles suggest that the size of the sputtered area containing uranium plays a significant role in the determination of the mass bias used to correct the measured $^{235}\text{U}/^{238}\text{U}$ -ratio. This kind of matrix effect for the calculation of uranium mass bias and relative sensitivity factor for inter-element measurements was previously recorded and confirmed by observations made by Williamson *et al.* [131; 132] with a measurement setup using

a Köhler beam and not using the pixel-based dead time correction. Thus, it is very unlikely, that these observations are linked to dead-time correction or spot size.

This conclusion leads to the question, if the observed uranium isotopic fractionation during the uranium halo formation of altered particles (Figure 48, Figure 49) can actually be attributed to the same process. While it may play a role in the measurements of the uranium halos, the lower-than-expected ^{235}U values of the remaining altered particles cannot be explained by this effect, considering the altered particles are also observed to be larger in size than freshly produced particles (Figure 41). It is therefore assumed that alteration can fractionate uranium isotopes.

The influence of matrix effects on the calculated mass bias is best minimized by using standards that are comparable in size and structure to the samples analyzed. This fact further highlights the essential need of a broad range of uranium microparticle reference materials and confirms the usefulness of easy and fast VOAG production of uranium microparticles.

5 Conclusion and Outlook

The work presented in this thesis illustrates the process to implement a measurement setup for uranium oxide microparticles in an LG-SIMS lab, evaluate the measurement process until approval by the IAEA is achieved and subsequently use this implemented measurement setup to characterize two IAEA-requested uranium oxide microparticle productions for the use as potential reference materials. Besides the isotopic characterization of the potential reference materials, special emphasis is placed on the investigation of the stability in different storage conditions.

Although a first SIMS measurement approach using a mixed MC detector setup provided promising and reproducible results for the isotopic abundance of VOAG-produced uranium oxide microparticles, the practical use proved to be questionable. This setup is limited to the measurement of natural uranium or LEU samples. Samples enriched in ^{235}U lead to lower intensities outside the H1 FC detectors reliable counting range. The mixed detector setup also excludes the possibility of APM measurements of all uranium isotopes simultaneously due to the necessity of ion imaging to calculate the microparticles' location. Consequently, the full EM detector setup modified after Hedberg *et al.* [15] is identified as the more practical approach. Test measurements of uranium microparticles produced in the safeguards laboratories of the FZJ resembling natural uranium composition and of IAEA-provided powder particles derived from certified reference materials of the NBL CRM U series are consistent and confirm the measurement capabilities of the implemented setup.

Consequential, three IAEA-requested uranium microparticle productions from FZJ were characterized in the HIP lab for later use as reference materials or in ILCs. The characterization included the verification of the isotopic abundance of both single particles and bulk. Outliers and contamination could be excluded using the APM software developed for the purpose of nuclear forensics. The characterization results confirmed the requested isotopic composition and other IAEA requirements for the production in the safeguards labs of FZJ. As further process QC, the used GCDs were investigated for contamination and the VOAG cleaning process was examined. The used substrates proved to be suitable. The comparison of microparticles on GCD planchets produced with and without an intermediate cleaning step gave clear evidence for the effectiveness of the applied cleaning process and highlights the ability of FZJs VOAG-based process to produce reliable reference particles.

Measurements of the IAEA-requested particle productions FZJ-3050P and FZJ-3090P revealed additional challenges. Certain isotopic abundances of samples or reference materials can affect

the quality of results especially for the minor isotopes. When faced with these kind of challenges, the measurement setup has to be adjusted to guarantee the generation of accurate measurement results. Problems like the Z axis focusing can lead to deviations for APM measurements for older LG-SIMS generations. CAMECA's latest LG-SIMS version IMS 1300-HR SIMS will probably not face the same challenges, because of the automatic Z axis adjustment.

The stability and recommended storage conditions for the VOAG-produced uranium oxide microparticles were investigated in both atmospheric and dispersion shelf-life studies. The investigations have shown that it heavily depends on the atmospheric storage conditions. Even after relatively short periods, the presence of water leads to alteration processes including the formation of uranyl hydroperoxides. SEM investigations revealed clearly visible changes to the particles' physical form compared to their original form and to particles stored in water-free atmospheres. Sustained storage in water-saturated conditions lead to uranium mobilization and increasingly complex particle location for SIMS measurements. Moreover, the alteration can lead to deviation in the isotopic composition. However, a brief water exposure does not seem to affect their use as reference materials. Nevertheless, the microparticles can be kept in three easily implemented storage conditions for at least one year. Storage in an inert, water-free atmosphere such as argon is strongly recommended.

After almost two years of storage time in four different alcoholic media, the particles can be easily measured with SIMS and are suitable as potential reference materials. However, particles in three potential long-term storage media showed first signs of alteration. Over the duration of the investigation, particles stored in *tert*-butanol retained their original structure, shape and isotopic composition. Therefore, *tert*-butanol is the recommended storage medium, if particle dispersions are requested.

LG-SIMS measurements with the current setup yield varying results depending on the signal size of the sputtered area. This raises the question, if the assumed occurrence of a mass bias is an actual bias or just an artifact of the measurement setup. For now, it is not clear if this phenomenon can be replicated using a different measurement approach. A possibility for future investigations is to repeat the measurements using a Köhler beam instead of a focused beam.

Further developments of the measurement process could include the measurement of mixed oxide particles. The IAEA is very interested in the development and characterization of mixed U-Pu oxide particles. Still, there is currently no well-developed process for simultaneous measurement of uranium and plutonium isotopes. Lanthanide-doped uranium particles are already successfully produced as surrogates for U-Pu particles [105]. Further developments are required for the setup of a reliable SIMS measurement process.

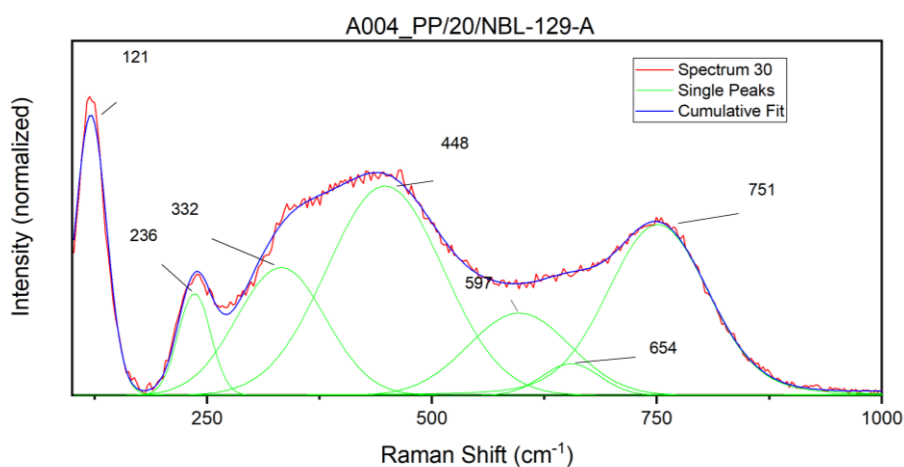
As one last future development, a reliable dating process for the uranium microparticles is desirable. Many NWAL member laboratories are already working on a solution for microparticle dating. The IAEA encourages associated labs to develop new processes for dating methods. It remains to be seen, if this is also a reasonable purpose for the capacities at the HIP.

6 Appendices

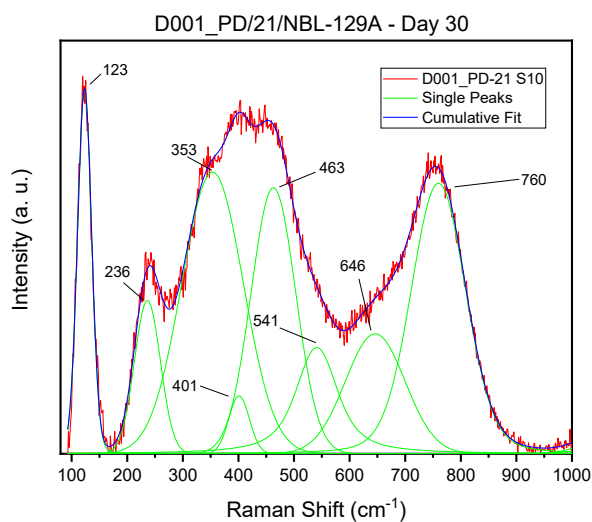
In these appendices additional spectra and isotopic abundance graphs are included. Further supplementary data can be provided by the author on reasonable request.

6.1 Detailed μ -Raman spectra

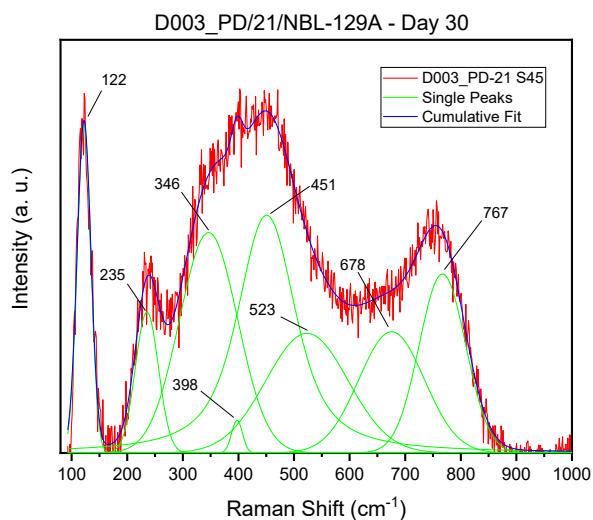
The following figures show the spectra from Figure 42 in better resolution.



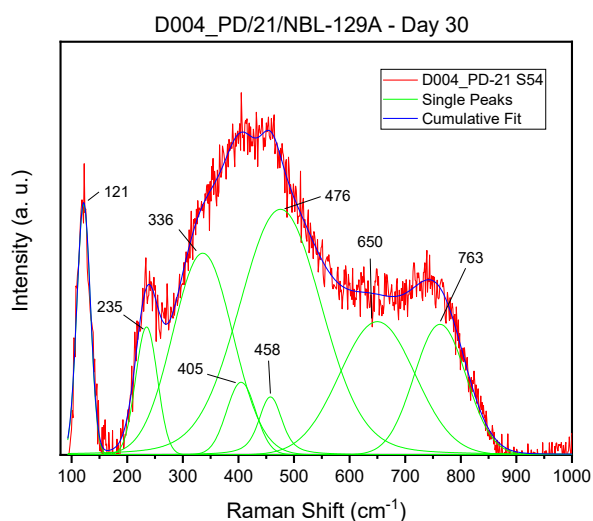
App.-Figure 6-1: μ -Raman spectrum of freshly produced uranium oxide microparticle.



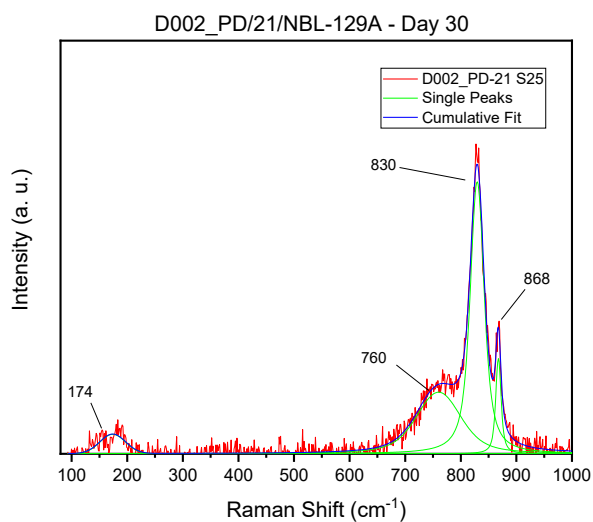
App.-Figure 6-2: μ -Raman spectrum of uranium oxide microparticle after 30 days in lab air.



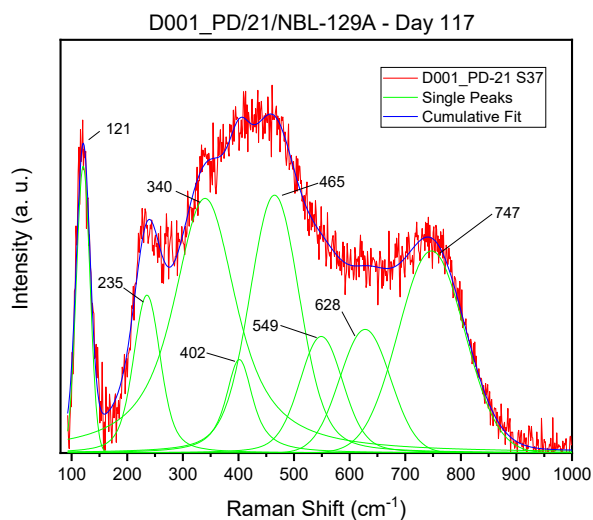
App.-Figure 6-3: μ -Raman spectrum of uranium oxide microparticle after 30 days in Ar.



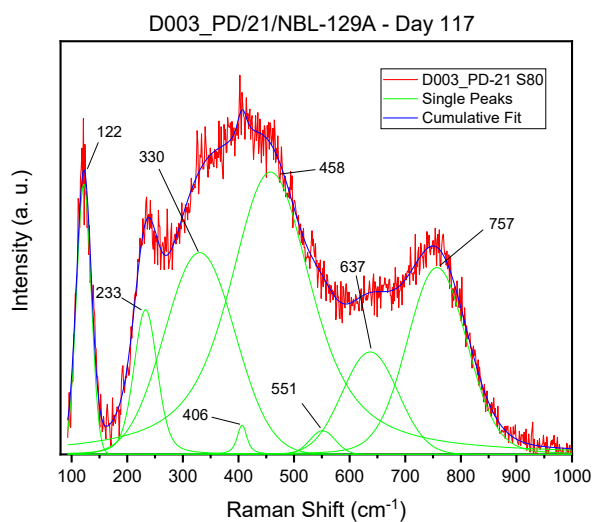
App.-Figure 6-4: μ -Raman spectrum of uranium oxide microparticle after 30 days at 90°C.



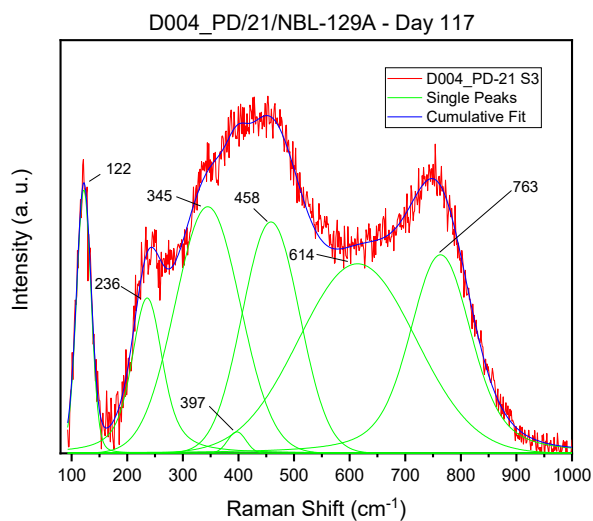
App.-Figure 6-5: μ -Raman spectrum of uranium oxide microparticle after 30 days in water-saturated atmosphere.



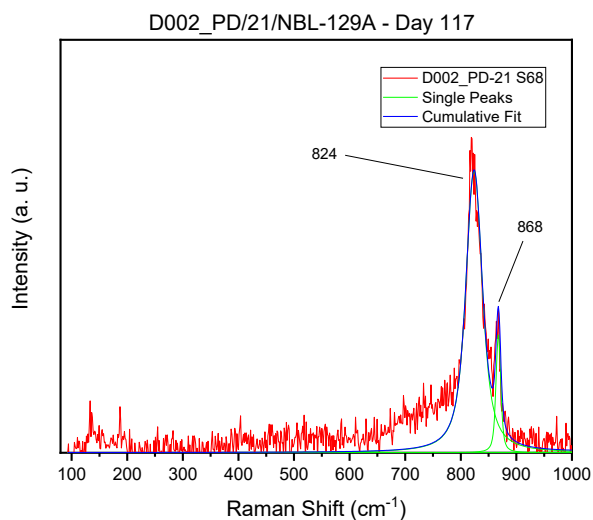
App.-Figure 6-6: μ -Raman spectrum of uranium oxide microparticle after 117 days in lab air.



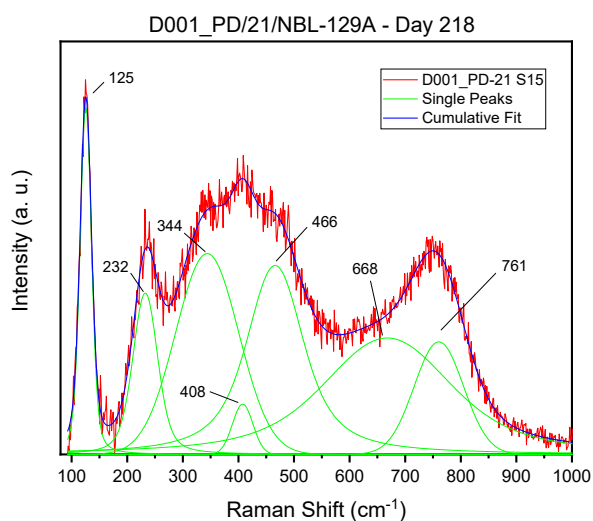
App.-Figure 6-7: μ -Raman spectrum of uranium oxide microparticle after 117 days in Ar.



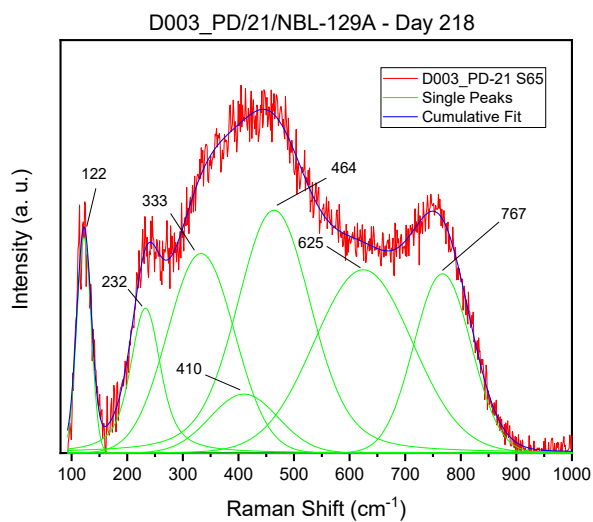
App.-Figure 6-8: μ -Raman spectrum of uranium oxide microparticle after 117 days at 90°C.



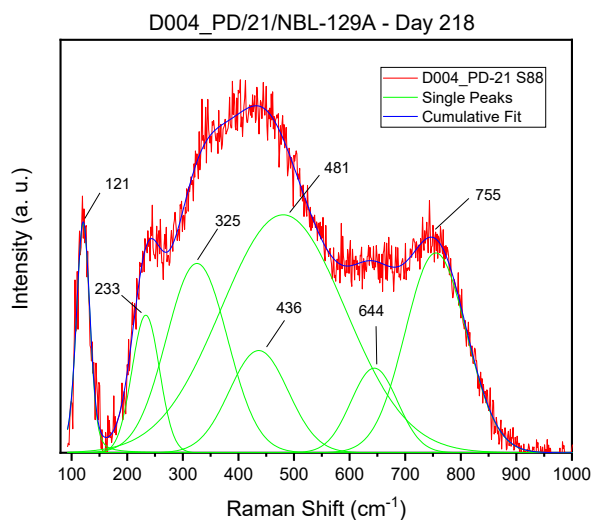
App.-Figure 6-9: μ -Raman spectrum of uranium oxide microparticle after 117 days in water-saturated atmosphere.



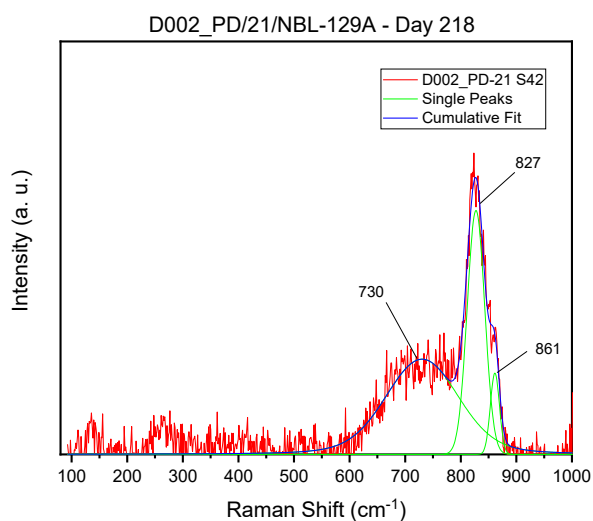
App.-Figure 6-10: μ -Raman spectrum of uranium oxide microparticle after 218 days in lab air.



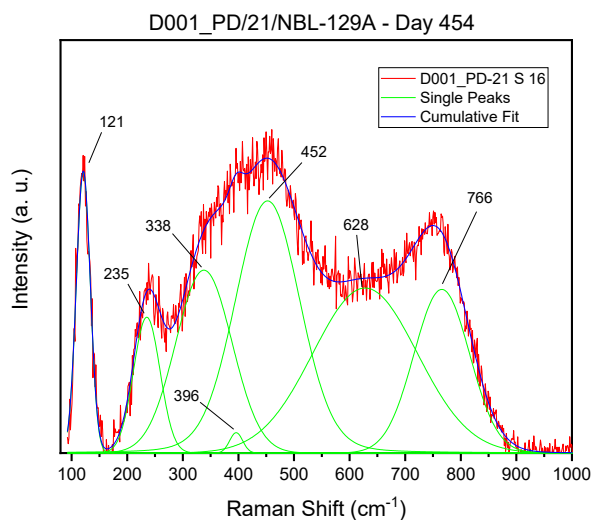
App.-Figure 6-11: μ -Raman spectrum of uranium oxide microparticle after 218 days in Ar.



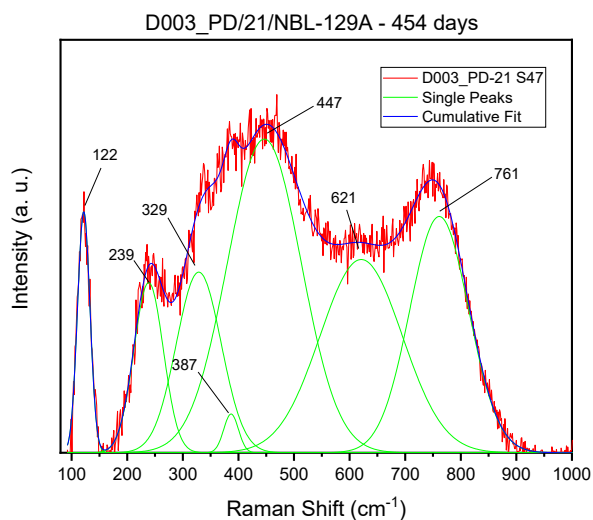
App.-Figure 6-12: μ -Raman spectrum of uranium oxide microparticle after 218 days at 90°C.



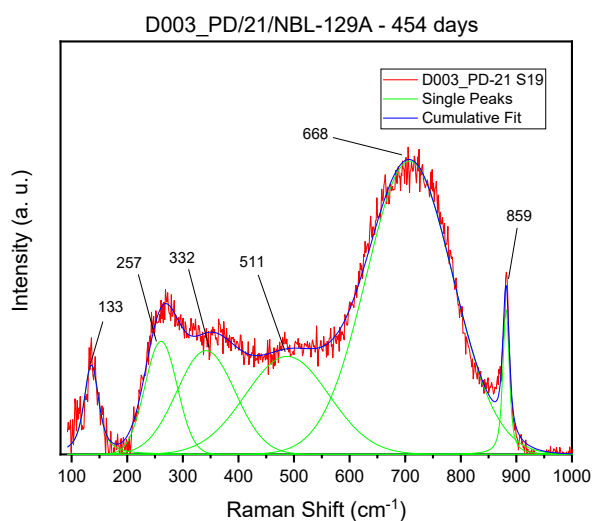
App.-Figure 6-13: μ -Raman spectrum of uranium oxide microparticle after 218 days in water-saturated atmosphere.



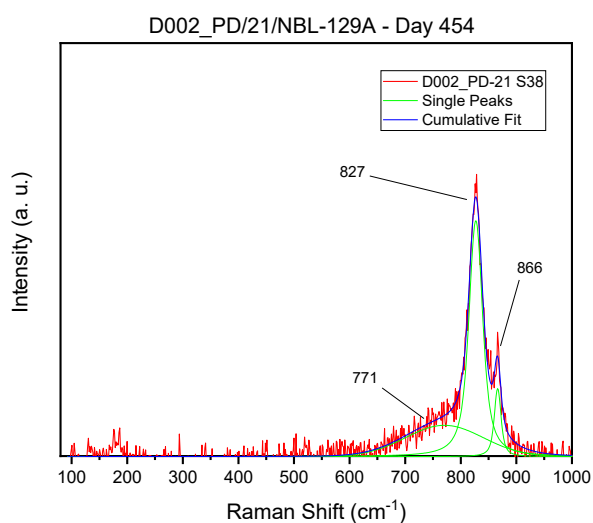
App.-Figure 6-14: μ -Raman spectrum of uranium oxide microparticle after 454 days in lab air.



App.-Figure 6-15: μ -Raman spectrum of uranium oxide microparticle after 454 days in Ar.



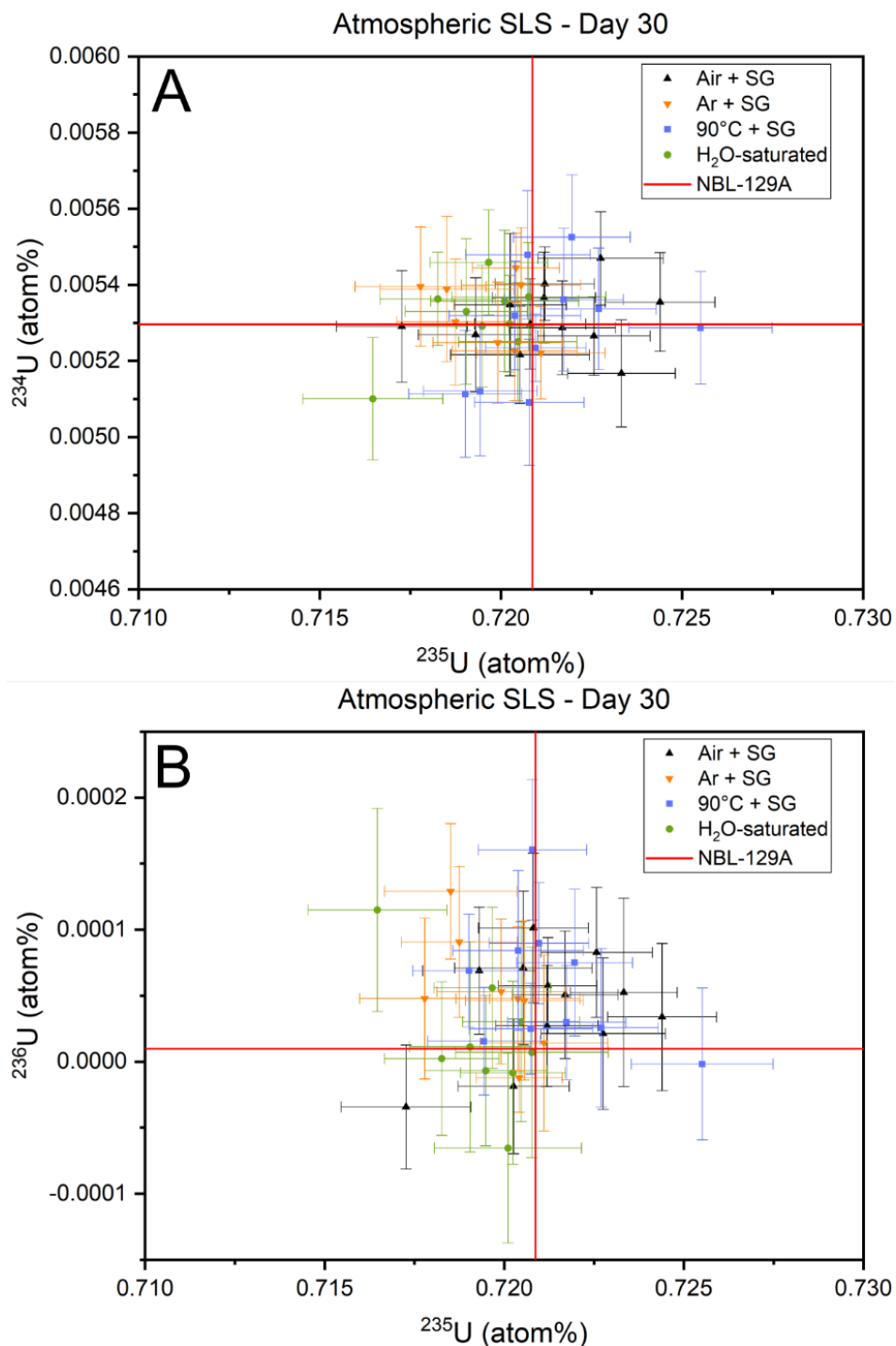
App.-Figure 6-16: μ -Raman spectrum of uranium oxide microparticle after 454 days at 90°C.



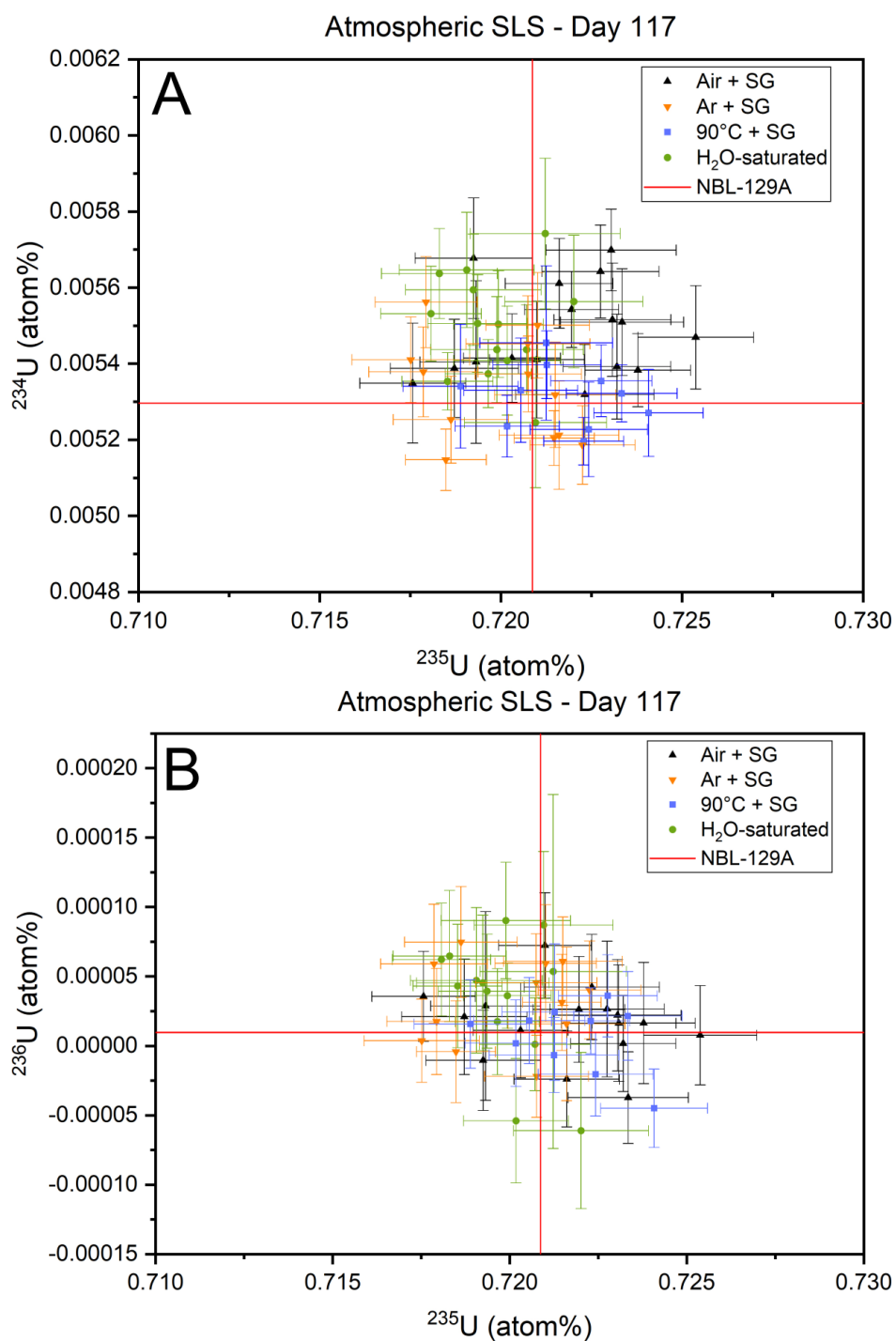
App.-Figure 6-17: μ -Raman spectrum of uranium oxide microparticle after 454 days in water-saturated atmosphere.

6.2 Additional Isotopic Abundance Measurements

6.2.1 Atmospheric Shelf-Life Investigation

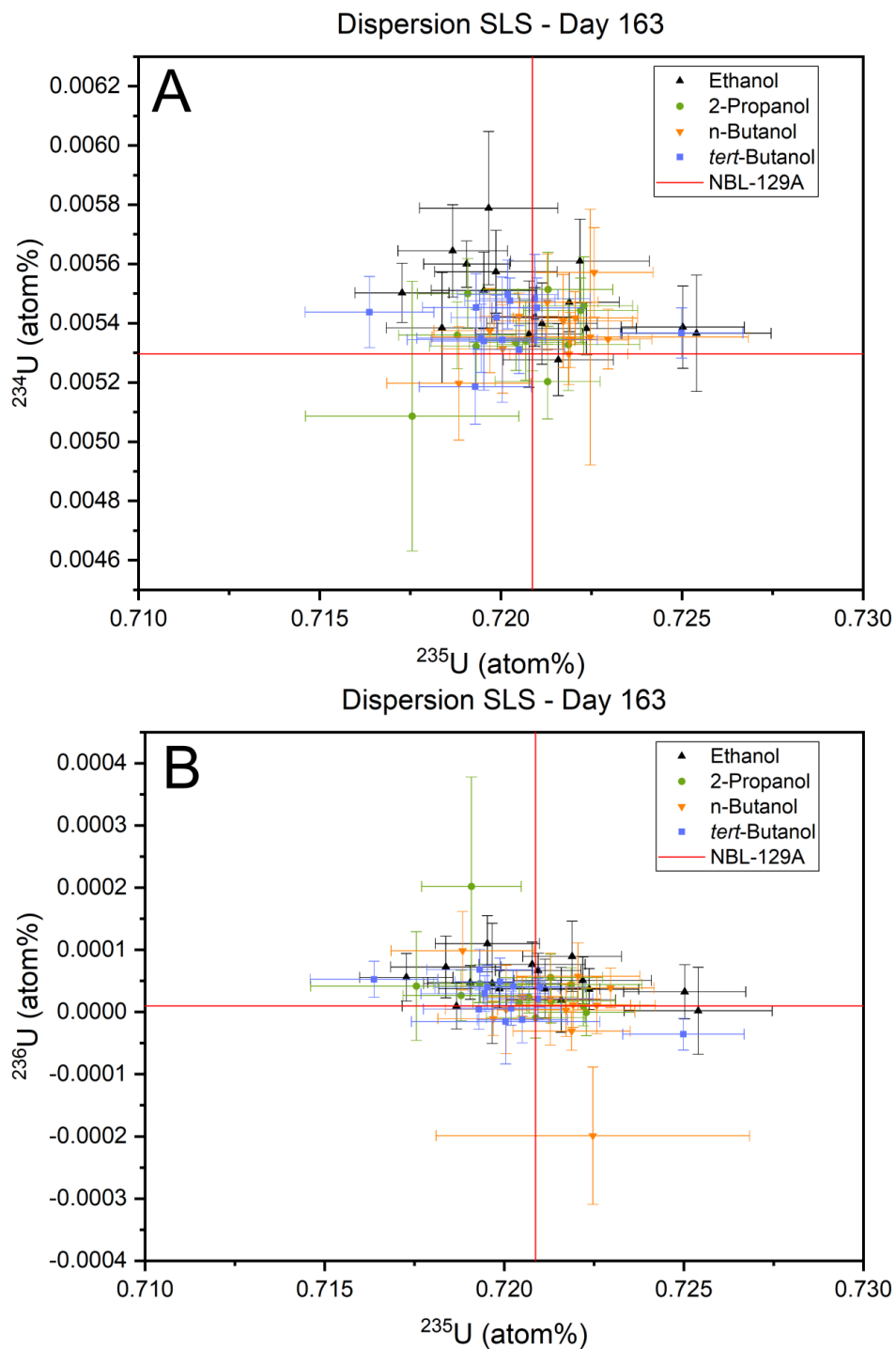


App.-Figure 6-18: Uranium isotopic abundance of representative particles stored for 30 days in laboratory air, argon, laboratory air at 90°C and in H₂O-saturated atmosphere for the shelf-life study (SLS). Panel A is ^{234}U vs. ^{235}U and panel B is ^{236}U vs. ^{235}U .

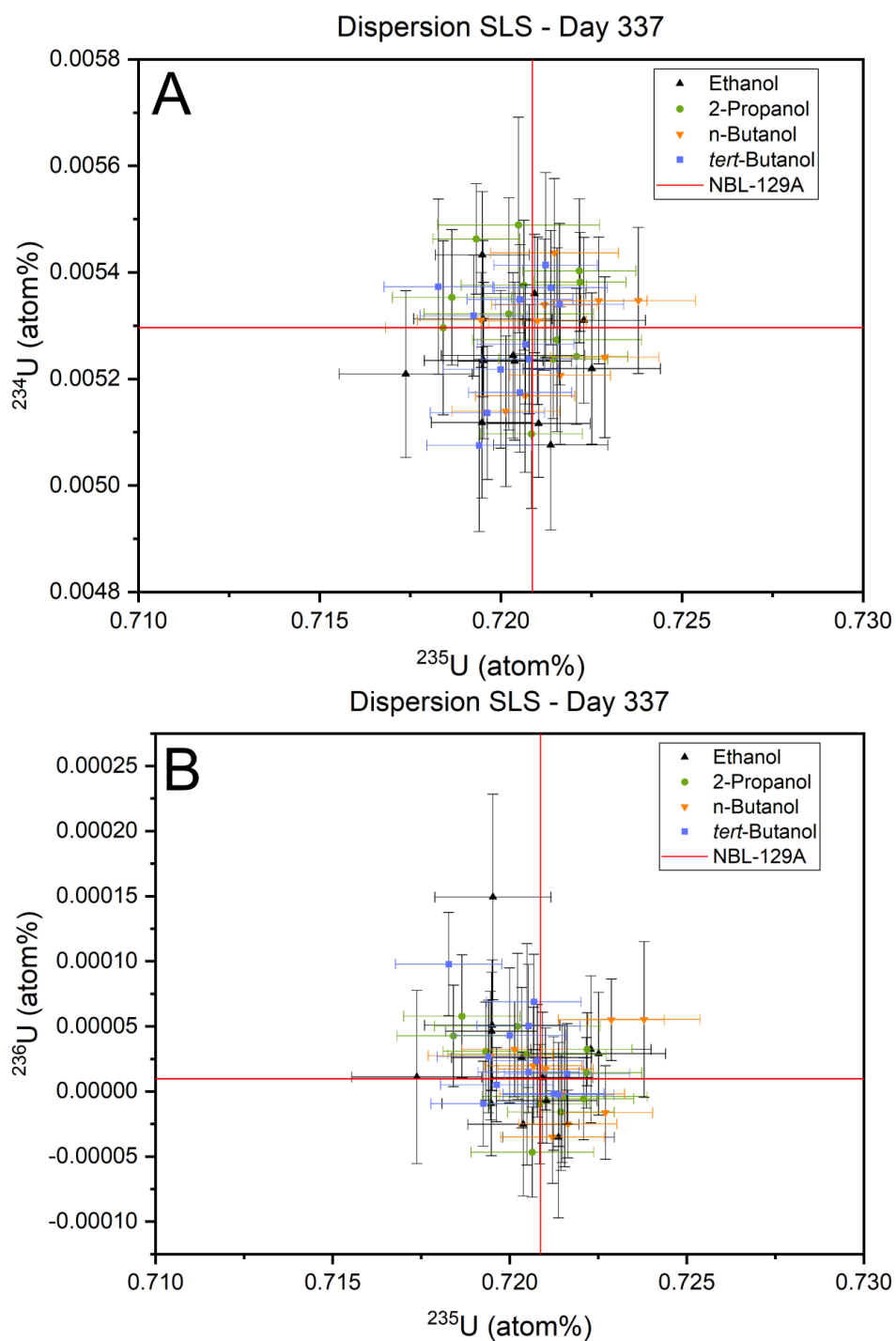


App.-Figure 6-19: Uranium isotopic abundance of representative particles stored for 117 days in laboratory air, argon, laboratory air at 90°C and in H₂O-saturated atmosphere for the shelf-life study (SLS). Panel A is ^{234}U vs. ^{235}U and panel B is ^{236}U vs. ^{235}U .

6.2.2 Dispersion Shelf-Life Investigation



App.-Figure 6-20: Uranium isotopic abundance of representative particles stored for 163 days in ethanol, 2-propanol, *n*-butanol and *tert*-butanol. Panel A is ^{234}U vs. ^{235}U and panel B is ^{236}U vs. ^{235}U .



App.-Figure 6-21: Uranium isotopic abundance of representative particles stored for 337 days in ethanol, 2-propanol, *n*-butanol and *tert*-butanol. Panel A is ^{234}U vs. ^{235}U and panel B is ^{236}U vs. ^{235}U .

List of Tables

Table 1: SIMS analytical conditions for single particle measurements.....	32
Table 2: SIMS analytical conditions for APM measurements.....	44
Table 3: Mean isotopic abundance of the particles on FZJ-3050P/1 with IRMM-3050 certificate values [107].....	51
Table 4: Mean isotopic abundance of the particles on FZJ-3050P/2 with IRMM-3050 certificate values [107].....	52
Table 5: Mean isotopic abundance of the particles on FZJ-3090P/1 with IRMM-3090 certificate values [107].....	57
Table 6: Mean isotopic abundance of the particles on FZJ-3090P/2 with IRMM-3090 certificate values [107].....	58
Table 7: Isotopic composition of particles #649, #710 and #771. All results are in atom%. Uncertainty is 1σ	65
Table 8: Isotopic composition of analyzed single particles. All results are in atom%. Uncertainty is 1σ	67

List of Figures

Figure 1: Inspectors taking a swipe sample at a nuclear facility. Photo: IAEA Department of Safeguards, Copyright IAEA, 2016 [9].	2
Figure 2: Schematic overview of the microparticle production system using spray pyrolysis. Reprinted with permission from [45]. Copyright 2017, American Chemical Society.	7
Figure 3: SEM images of U-oxide microparticles distributed on a glassy carbon substrate with high-resolution SEM image included. Inset: Particle size distribution of collected particles showing highest abundance at $\sim 1.2 \mu\text{m}$. Image reprinted from Kegler <i>et al.</i> [48], CC BY 4.0.	9
Figure 4: Raman spectra of microparticles produced using uranyl nitrate (UN), uranyl acetate (UA) and uranyl chloride (UC) compared to the spectrum of a micrometer-sized U_3O_8 particle and the spectrum of a uranium ore concentrate (UOC) from South Dakota. The line at $\sim 521 \text{ cm}^{-1}$ is an interference from the Si substrate. Reprinted with permission from [45]. Copyright 2017, American Chemical Society.	9
Figure 5: Background subtracted Raman spectrum of an individual uranium oxide particle stored for two years under laboratory atmosphere. Image reprinted from Kegler <i>et al.</i> [48], CC BY 4.0.	10
Figure 6: Normalized U M_4 HR-XANES spectra of uranium microparticles in comparison to uranium reference compounds. Image reprinted from Kegler <i>et al.</i> [48], CC BY 4.0.	11
Figure 7: Schematic flow chart for widely used analytical procedures for nuclear safeguards samples showing the area of application for different measurement techniques. Image reprinted from Song <i>et al.</i> [75], CC BY-NC 4.0.	12
Figure 8: Laminar flow bench for the preparation of uranyl nitrate feeding solutions for the VOAG in the FZJ safeguards laboratories.	16
Figure 9: VOAG in the FZJ safeguards laboratories. The syringe with the feeding solution is placed on the top left side, the vacuum impactors with the substrates are on the right side of the drying column.	17
Figure 10: Vacuum impactor containing a substrate (left) within the VOAG setup of the FZJ safeguards laboratories. Bypass for substrate change is on the right.	18
Figure 11: Distribution of uranium oxide microparticles on GCDs analyzed by SEM. The GCD on the left side is prepared by direct collection, the GCD on the right side with an intermediate dispersion step. Each dot represents a single particle. Reproduced with permission of Springer Nature from [47].	19
Figure 12: CAMECA IMS 1280-HR ion optics. The DSP2 octopole is a stigmator and a deflector that can be used to increase the mass dispersion. EM, FC and FC 2 are the axial detectors used in mono-collection mode (Hedberg <i>et al.</i> [19], CC BY 3.0).	21
Figure 13: MC detector setup for an approach with FC on the H1 detector and EMs on the other detectors. Measurement setup and particle searching setup are distinguished. Modified after Hedberg <i>et al.</i> [1], CC BY 4.0.	28
Figure 14: A) Measured yield of EM detectors vs. H1 FC in several measurements over the course of a day. B) Yield of 2 EM detectors over the course of a single measurement. Data shown in B) from Hedberg <i>et al.</i> [1], CC BY 4.0.	29
Figure 15: $^{234}\text{U}/^{238}\text{U}$ ratios and $^{235}\text{U}/^{238}\text{U}$ ratios of Uranium microparticles resembling natural Uranium. The measured ratios are corrected for detector yield, but no mass bias correction was applied.	30

Figure 16: Typical detector pulse height distribution (PHD) from a Hamamatsu EM detector (Hedberg et al. [2], CC BY 3.0).....	33
Figure 17: Detector background for EMs with different lower pulse amplitude thresholds (Thr1). Red limit at 1 cpm.	34
Figure 18: HV adjustment of EMs during particle measurements in December 2021.....	35
Figure 19: EM detector yield and HV over a period of 10 days in October 2021. Yield is calibrated against H1 detector.	37
Figure 20: Quality Control (QC) measurements of CRM U010 over the period of 10 days. Shown are ^{234}U (A), ^{235}U (B) and ^{236}U (C). Control limits for this CRM are set due to empirical value and agree with IAEA protocol.	38
Figure 21: MC detector setup for dynamic multi-collection measurements as described by Hedberg et al. [1].	39
Figure 22: Total evaporation measurement of a typical VOAG-produced uranium microparticle measured with a primary ion beam current of ~ 100 pA. 50,000 cps ^{238}U is an empirically set lower limit for reasonable counting statistics.	40
Figure 23: Isotopic abundance measurements of particles produced with CRM NBL 129-A. (A) is ^{234}U vs. ^{235}U and (B) is ^{236}U vs. ^{235}U . All values are atom%. Certificate value and empirical limits close to IAEA standards are shown as green and red lines.....	41
Figure 24: Uranium isotopic abundance of pure U microparticles compared to U microparticles doped with 10 atom% Ce with 1σ uncertainties and certificate values of CRM NBL 129-A. (A) is ^{234}U vs. ^{235}U and (B) is ^{236}U vs. ^{235}U	43
Figure 25: Results of APM performed on the simulated field sample provided by the IAEA. Total intensity is plotted vs. ^{235}U enrichment of the calculated particles.....	46
Figure 26: Position of the APM calculated microparticles on the sample planchet (black) and of the particles measured with microbeam analyses.....	46
Figure 27: Isotopic abundance microparticle measurements of particles calculated by APM on the simulated IAEA field sample resembling two different particle populations. (A) is ^{234}U vs. ^{235}U and (B) is ^{236}U vs. ^{235}U	48
Figure 28: Results of APM performed on Blank_GCD. Total intensity is plotted vs. $^{235}\text{U}/^{238}\text{U}$ -ratio of the calculated particles.....	50
Figure 29: Isotopic abundance of the particles on FZJ-3050P/1 and FZJ-3050P/2 with weighted mean values. Panel A shows ^{234}U vs. ^{235}U and panel B ^{236}U vs. ^{235}U	53
Figure 30: $^{235}\text{U}/^{238}\text{U}$ -ratio vs. ^{235}U intensity (A) and σ deviation (B) of the calculated particles on FZJ-3050P/1.....	55
Figure 31: $^{235}\text{U}/^{238}\text{U}$ -ratio vs. ^{235}U intensity (A) and σ deviation (B) of the calculated particles on FZJ-3050P/2.....	56
Figure 32: Isotopic abundance of the particles on FZJ-3090P/1 and FZJ-3090P/2 with weighted mean values. Panel A shows ^{234}U vs. ^{235}U and panel B ^{236}U vs. ^{235}U	59
Figure 33: $^{235}\text{U}/^{238}\text{U}$ -ratio vs. ^{235}U intensity (A) and σ deviation (B) of the calculated particles on FZJ-3090P/1.....	61
Figure 34: $^{235}\text{U}/^{238}\text{U}$ -ratio vs. ^{235}U intensity (A) and σ deviation (B) of the calculated particles on FZJ-3090P/2.....	62
Figure 35: Results of APM performed on Blank_FZJ-3050P. Total intensity is plotted vs. $^{235}\text{U}/^{238}\text{U}$ -ratio of the calculated particles. Red particles were analyzed as single particles using microanalysis.....	63

Figure 36: ^{238}U ion image (A) and calculated boundaries (B) of particle #171.....	64
Figure 37: Results of APM performed on O001_PP/23/NBL-129A. Total intensity is plotted vs. $^{235}\text{U}/^{238}\text{U}$ -ratio of the calculated particles. Red particles were analyzed as single particles using microanalysis. Blue and green lines represent certificate values of CRM NBL-129A and IRMM-3090, respectively.....	66
Figure 38: ^{235}U ion image (A) and ^{238}U ion image (B) of the field of particle #4021 on sample planchet O001_PP/23/NBL-129A. The color scheme is based on a rainbow look-up-table (LUT) where white represents the highest relative ion count and black represents low ion count. Most of the particles show a high ^{238}U abundance with low ^{235}U , while particle #4021 has high ^{235}U and lower ^{238}U . The particle concentration is very dense.....	68
Figure 39: ^{235}U ion image (A) and ^{238}U ion image (B) of the field of particles #4337 and #4338. The same relative rainbow LUT is used. Particle #4337 is typical for NBL 129-A feeding solution, while particle #4338 is a remnant from the FZJ-3090P particle production and represents contamination.....	69
Figure 40: Graphic summary of SEM investigation of microparticles stored in different atmospheric conditions. Extended from Kegler <i>et al.</i> [111].....	72
Figure 41: Representative SEM images of particles stored for 218 days in laboratory air (a), argon (b), laboratory air at 90°C (c) and in H ₂ O-saturated atmosphere (d) (from Hammerich <i>et al.</i> [23]).....	73
Figure 42: Graphic summary of μ -Raman investigation of microparticles stored in different atmospheric conditions. Extended from Kegler <i>et al.</i> [111].....	75
Figure 43: Representative Raman spectra of particles stored for 30 days in laboratory air (a), argon (b), laboratory air at 90°C (c) and in H ₂ O-saturated atmosphere (d) (from Hammerich <i>et al.</i> [23]).....	76
Figure 44: Raman spectra of particles stored in water-saturated atmosphere for 454 days. Complete spectra are shown on the left side (a, b, c, d), the corresponding fits between wavenumbers of 600 cm ⁻¹ and 1000 cm ⁻¹ are shown on the right side (e, f, g, h). Typical Raman position of Raman bands for U ₃ O ₈ (~750 cm ⁻¹) and (meta-)studdite (~827 cm ⁻¹ and ~866 cm ⁻¹) are highlighted in the fitted spectra. The fitted part of the spectrum is shown in light red on the left side.	78
Figure 45: Graphic summary of ^{238}U ion images of microparticles stored in different atmospheric conditions. The white scale bar resembles 100 μm . The color scales are divided between a heat LUT (brighter = higher) up to 117 days and a rainbow LUT with red as maximum and black as minimum ions counted for the other two panels. The colors do not correspond to fixed values but show a relative min-max distribution.....	81
Figure 46: Selected ^{238}U ion images of particles stored for 117 days in laboratory air (a), argon (b), laboratory air at 90°C (c) and in H ₂ O-saturated atmosphere (d) (from Hammerich <i>et al.</i> [19]). Note that a, b and c display an area of 500 \times 500 μm , while the size of d is only 100 \times 100 μm . The color scheme is a relative heat LUT with brighter equals more counts.	82
Figure 47: 500 \times 500 μm ^{238}U ion image of IRMM-2329P sample surface in December 2021. In the relative heat LUT brighter equals higher ion count.....	83
Figure 48: Uranium isotopic abundance of representative particles stored for 218 days in laboratory air, argon, laboratory air at 90°C and in H ₂ O-saturated atmosphere for the shelf-life study (SLS). Panel A is ^{234}U vs. ^{235}U and panel B is ^{236}U vs. ^{235}U	85

Figure 49: Uranium isotopic abundance of representative particles stored for 454 days in laboratory air, argon, laboratory air at 90°C and in H ₂ O-saturated atmosphere for the shelf-life study (SLS). Panel A is ²³⁴ U vs. ²³⁵ U and panel B is ²³⁶ U vs. ²³⁵ U.....	87
Figure 50: Representative SEM images of uranium oxide particles stored in ethanol, 2-propanol, <i>n</i> -butanol and <i>tert</i> -butanol after a certain time of storage (from Potts <i>et al.</i> [49]).....	89
Figure 51: 500 × 500 μm ²³⁸ U ion images and SEM images of uranium microparticles stored in ethanol for 163, 337 and 580 days. The first ion image uses a heat LUT, the others a rainbow LUT.....	90
Figure 52: Raman spectrum obtained from minority of particles stored in ethanol for 580 days.....	91
Figure 53: Raman spectrum obtained for majority of particles stored in ethanol for 580 days.....	92
Figure 54: 500 × 500 μm ²³⁸ U ion images and SEM images of uranium microparticles stored in 2-propanol for 163, 337 and 580 days. The first ion image uses a heat LUT, the others a rainbow LUT.....	93
Figure 55: Raman spectrum of a particle stored in 2-propanol for 163 days.....	94
Figure 56: 500 × 500 μm ²³⁸ U ion images and SEM images of uranium microparticles stored in <i>n</i> -butanol for 163, 337 and 580 days. The first ion image uses a heat LUT, the others a rainbow LUT.....	95
Figure 57: Raman spectrum obtained for majority of particles stored in <i>n</i> -butanol for 580 days.....	96
Figure 58: Raman spectrum obtained from minority of particles stored in <i>n</i> -butanol for 580 days.....	96
Figure 59: 500 × 500 μm ²³⁸ U ion images and SEM images of uranium microparticles stored in <i>tert</i> -butanol for 163, 337 and 580 days. The first ion image uses a heat LUT, the others a rainbow LUT.....	97
Figure 60: Representative Raman spectrum obtained from particles stored in <i>tert</i> -butanol for 580 days.....	98
Figure 61: Uranium isotopic abundance of representative particles stored for 580 days in ethanol, 2-propanol, <i>n</i> -butanol and <i>tert</i> -butanol. Panel A is ²³⁴ U vs. ²³⁵ U and panel B is ²³⁶ U vs. ²³⁵ U.....	99
Figure 62: Mass peaks for uranium isotopes measured with all 5 EM detectors using CIRC-mode for an FZJ-3050P/2 particle.....	101
Figure 63: Mass peaks for uranium isotopes measured with all 5 EM detectors using XY-mode for an FZJ-3050P/2 particle.....	102
Figure 64: Uranium isotopic abundance of FZJ-3050P/2 particles using CIRC-mode and XY-mode. Panel A is ²³⁴ U vs. ²³⁵ U and panel B is ²³⁶ U vs. ²³⁵ U.....	103
Figure 65: Z score of APM-calculated uranium microparticles of sample IAEA-1 (A) and FZJ-3050P/2 (B) depending on their position on the planchet.....	105
Figure 66: Measured uranium isotopic abundance of Happy Jack uraninite grains particles using NBS CRM particle standard materials for calibration. Panel A is ²³⁴ U vs. ²³⁵ U and panel B is ²³⁶ U vs. ²³⁵ U.....	107

List of Abbreviations

amu	atomic mass unit
AP	Additional Protocol
APM	Automated Particle Measurement
CEA	Commissariat à l'Énergie Atomique
cpm	counts per minute
cps	counts per second
CRM	Certified Reference Material
CSA	Comprehensive Safeguards Agreement
DoE	Department of Energy
EDS	Energy Dispersive X-ray Spectroscopy
EM	Electron Multiplier
ESL	Environmental Sampling Laboratory
FC	Faraday Cup
FIB	Focused Ion Beam
FZJ	Forschungszentrum Jülich
GCD	Glassy Carbon Disk
HIP	Heidelberg Ion Probe
HR-XANES	High Resolution X-Ray Absorption Near-Edge Structure Spectrometry
HV	High Voltage
IAEA	International Atomic Energy Agency
ICSM	Institut de Chimie Séparative de Marcoule
ID-TIMS	Isotope Dilution-Thermal Ionization Mass Spectrometry
IEK-6	Institute of Energy and Climate Research – Nuclear Waste Management and Reactor Safety

List of Abbreviations

ILC	Interlaboratory Comparison
IAEA	Japanese Atomic Energy Agency
JRC-IRMM	Joint Research Centre – Institute for Reference Materials and Measurements
JRC-ITU	Joint Research Centre – Institute for Transuranium Elements
LA-ICP-MS	Laser Ablation-Inductively Coupled Plasma-Mass Spectrometry
LEU	Low Enriched Uranium
LG-SIMS	Large Geometry-Secondary Ion Mass Spectrometer
<i>Ln</i>-doped	Lanthanide-doped
LUT	look-up table
MC	Multi-Collection
MRP	Mass Resolution Power
NBL	New Brunswick Laboratory
NDA	Non-Disclosure Agreement
Nd:YAG	Neodymium-doped Yttrium Aluminum Garnet
NIST	National Institute of Standards and Technology
NML	Nuclear Material Laboratory
NPT	Treaty on Non-Proliferation of Nuclear Weapons
NUSIMEP	Nuclear Signatures Inter-Laboratory Measurement Evaluation Programme
NWAL	Network of Analytical Laboratories
PHD	Pulse Height Distribution
PNNL	Pacific Northwest National Lab
QC	Quality Control
R&D	Research and Development
RSD	Relative Standard Deviation
SE	Secondary Electrons
SEM	Scanning Electron Microscope

SGAS	Safeguards Analytical Services
SG-SIMS	Small Geometry-Secondary Ion Mass Spectrometry
SLS	Shelf-Life Study
UA	Uranyl Acetate
UC	Uranyl Chloride
UCLA	University of California, Los Angeles
UN	Uranyl Nitrate
UOC	Uranium Ore Concentrate
VIS-NIR	Visible to Near Infrared
VOAG	Vibrating Orifice Aerosol Generator
VTT	Technical Research Center of Finland

Acknowledgements

This work was conducted as part of the Joint Programme on the Technical Development and Further Improvement of IAEA Safeguards between the Federal Ministry for the Environment, Nature Conservation, Nuclear Safety and Consumer Protection and the IAEA (Task C.45/A 1961).

Over the course of the past four and a half years, I have worked with countless people that contributed in a direct or indirect way to this research and the resulting thesis.

First, I want to express my deepest gratitude to my supervisors Prof. Dr. Axel Schmitt and Prof. Dr. Mario Trieloff for giving me the unique opportunity to pursue a PhD in a field that is not exactly part of the usual Earth Sciences. I am very thankful for your support and guidance through the different stages of my project. Both of you have always had good and helpful advice, sometimes even from the other side of the world. Moreover, you gave me the freedom and time I needed to successfully finish this work.

I would also like to thank the remaining members of the committee, Prof. Dr. Lucie Tajčmanová and Prof. Dr. Frank Keppler, for their time and interest in this work.

This project would not exist without Dr. Stefan Neumeier and Dr. Philip Kegler of FZJ. I am remarkably thankful for your help and guidance as well as your exceptional scientific work that led to this successful cooperation. You were always very open and supported me, be it a good advice for a difficult scientific problem or a having beer as two Trekkies in a Star Wars bar in Boston to fight jet lag. The same applies to my PhD candidate colleague in Jülich, Shannon Kimberly Potts. I am very thankful for the great work that you contributed to this thesis, the fun experiences we shared in Vienna and Boston and especially for your great support during my time at FZJ. I would like to extend my gratitude to Dr. Irmie Niemeyer as coordinator of the support program and Dr. Thomas Krieger for his very appreciated help.

I would like to thank the scientific staff at the Institute of Earth Sciences in Heidelberg, especially Thomas Ludwig for his invaluable support at the Ion Probe. I dare not estimate how many hours you spent on this project. Thank you! My sincere appreciation to Dr. Jens Hopp and Dr. Winfried Schwarz for their support on countless occasions concerning administrative issues, radiation protection, laser microscopy, Raman spectroscopy and ion probe problems. Thanks to Dr. Alexander Varychev for his assistance at the SEM and Dr. Sonja Storm for her help preparing SIMS mounts. And of course, a big thank you to Dr. Andreas Hertwig for the fruitful discussions, valuable insights and dedicated help at the ion probe, sometimes even late in the evening.

Special thanks to my PhD colleagues in Heidelberg, Anne Sturm and Carlos Angeles de la Torre. It was a pleasure working with you and exchanging our experiences. I would also like to thank the (former) members of the Isotope Geology and Petrology group, namely Dr. Maren Kahl, Dr. Shuang-Qing Li, Dr. Christian Bergemann, Dr. Gülin Korkmaz, Dr. Rezvaneh Jamali Ashtiani and Dr. Katharina Cionoiu as well as Dr. Sebastian Cionoiu, Dr. Philip Groß and Alexander Blum from the 6th floor.

Additionally, I want to thank all the students I had the pleasure to meet and work with during my PhD journey: Jan Schmitt, Daniel Mahr, Cara Nicholson, Fabian Schmitt and Sebastian Schmidt.

Thanks to the institute staff and members of different groups for their help concerning administrative and technical issues: Torsten Hoffmann, Petra Fuchs, Stefan Johäntgen, Ilse Glass, Francisco Cueto, Dr. Moritz Schroll and Dr. Marcus Schneider.

I want to acknowledge the tremendous support I received from IAEA ESL staff, especially Johannes Grimm and Dr. Laure Sangely. Thank you so much for your help and advice concerning SIMS measurements both on-site and remote and provision of reference materials.

I want to thank the members of the particle community I had the pleasure to meet and to discuss problems and challenges with. Thank you for your valuable insights, Dr. Nicolas Clavier (ICSM), Dr. Todd Williamson (NIST), Dr. Matthew Wellons (SRNL), Dr. Travis Tenner and Dr. Ning Xu (both LANL).

Many thanks to my colleagues at my new position at Studsvik GmbH & Co. KG Otávio Ribeiro, Thomas Dahl-Jacobsen, Dr. Alina Scheklaikov and Patrik Konneus as well as Savvas Kosmidis from Nuvia for their patience and consideration.

Of course, this work did not only require scientific but also personal support. My deepest thanks for their invaluable encouragement to my parents Martina and Thomas, my grandma Christel, my brother Lukas with Magdalena as well as the rest of my family. Of course, I also want to thank my extended family Jutta and Manfred and Antonia with Sebastian and Eliano.

The time of a PhD does not only consist of academia. I'm very happy to have my friends to remind me of that! Thanks to the "Kuscheltiere" Andreas, Karoline, Matti, Eliana, Chris, Urs, Mario, Patrycja, Nils, Susanne and Tobias, thanks to Stephen and Max and thanks to Kilian, Michael, Moritz, René, Yannick, Maximilian and Adrian and everyone I might have forgotten.

Finally, I want to thank the two most important people in my life: Susanne, I cannot express how thankful I am for your endless support and patience and everything else. I am also proud of and thankful for my youngest supporter, my son Marlon. I know, right now you are not yet interested in uranium microparticles, but who knows what the future might bring?

Literature

- [1] IAEA Statute, (1956).
- [2] Treaty on the Non-Proliferation of Nuclear Weapons, (1970).
- [3] IAEA. *Non-Proliferation Treaty (NPT)*. Retrieved 02.08.2024 from <https://www.iaea.org/topics/non-proliferation-treaty>
- [4] *Legal Framework for IAEA Safeguards*. (2013). INTERNATIONAL ATOMIC ENERGY AGENCY. <https://www.iaea.org/publications/10388/legal-framework-for-iaea-safeguards>
- [5] IAEA. *Verification and other safeguards activities*. Retrieved 03.08.2024 from <https://www.iaea.org/topics/verification-and-other-safeguards-activities>
- [6] IAEA. *Department of Safeguards*. Retrieved 03.08.2024 from <https://www.iaea.org/about/organizational-structure/department-of-safeguards>
- [7] Donohue, D., & Zeisler, R. (1993). Analytical chemistry in the aftermath of the Gulf War. *Analytical Chemistry*, 65(7), 359A-368A.
- [8] IAEA. *Additional Protocol*. Retrieved 03.08.2024 from <https://www.iaea.org/topics/additional-protocol>
- [9] IAEA. (2016). *Swipe Check: Collecting and Analysing Environmental Samples for Nuclear Verification*. Retrieved 03.08.2024 from <https://www.iaea.org/newscenter/news/swipe-check-collecting-and-analysing-environmental-samples-nuclear-verification>
- [10] IAEA. (2021). *How Environmental Sampling Helps Verify the Peaceful Use of Nuclear*. Retrieved 03.08.2024 from <https://www.iaea.org/newscenter/news/how-environmental-sampling-helps-verify-the-peaceful-use-of-nuclear>
- [11] Donohue, D. L. (1998). Strengthening IAEA safeguards through environmental sampling and analysis. *Journal of Alloys and Compounds*, 271-273, 11-18.
- [12] Donohue, D. L. (2002). Peer Reviewed: Strengthened Nuclear Safeguards. *Analytical Chemistry*, 74(1), 28 A-35 A.
- [13] Boulyga, S., Konegger-Kappel, S., Richter, S., & Sangély, L. (2015). Mass spectrometric analysis for nuclear safeguards [10.1039/C4JA00491D]. *Journal of Analytical Atomic Spectrometry*, 30(7), 1469-1489.
- [14] Hedberg, P., Ingeneri, K., Watanabe, M., & Kuno, Y. (2005). Isotopic measurements of U particles by secondary ion mass spectrometry~ SIMS. Institute of Nuclear Materials Management Annual Meeting,
- [15] Hedberg, P., Peres, P., Fernandes, F., Albert, N., & Vincent, C. (2018). Latest improvements in isotopic uranium particle analysis by large geometry~secondary ion mass spectrometry for nuclear safeguards purposes. *Journal of Vacuum Science & Technology B, Nanotechnology and Microelectronics: Materials, Processing, Measurement, and Phenomena*, 36(3), 03F108.
- [16] Ranebo, Y., Hedberg, P., Whitehouse, M., Ingeneri, K., & Littmann, S. (2009). Improved isotopic SIMS measurements of uranium particles for nuclear safeguard purposes. *Journal of Analytical Atomic Spectrometry*, 24(3), 277-287.
- [17] IAEA. *Verification and Monitoring in Iran*. Retrieved 03.08.2024 from <https://www.iaea.org/newscenter/focus/iran>
- [18] IAEA. (2012). *The IAEA Safeguards Analytical Laboratories*. Retrieved 03.08.2024 from <https://www.iaea.org/sites/default/files/safeguardslab.pdf>
- [19] Hedberg, P., Peres, P., Fernandes, F., & Renaud, L. (2015). Multiple ion counting measurement strategies by SIMS—a case study from nuclear safeguards and forensics. *Journal of Analytical Atomic Spectrometry*, 30(12), 2516-2524.
- [20] NBL. (2002). *NBL Certified Reference Materials Catalog*. Retrieved 03.08.2024 from <https://www.nrc.gov/docs/ML0512/ML051220501.pdf>
- [21] Inn, K. G., Johnson, C. M., Oldham, W., Jerome, S., Tandon, L., Schaaff, T., Jones, R., Mackney, D., MacKill, P., & Palmer, B. (2013). The urgent requirement for new radioanalytical certified reference materials for nuclear safeguards, forensics, and consequence management. *Journal of Radioanalytical and Nuclear Chemistry*, 296(1), 5-22.

- [22] Inn, K. G. W., LaMont, S., Jerome, S., Essex, R., Johnson, C. M., Morrison, J., Frechou, C., Branger, T., & Dion, H. (2016). Roadmap for radioanalytical reference and performance evaluation materials for current and emerging issues. *Journal of Radioanalytical and Nuclear Chemistry*, 307(3), 2529-2538.
- [23] Hammerich, S., Potts, S. K., Kegler, P., Neumeier, S., Schmitt, A. K., & Trieloff, M. (2023). Shelf-life of uranium oxide microparticle reference materials and possible implications for the identification of optimal storage conditions. *MRS Advances*, 8(6), 290-295.
- [24] Knott, A., Roth, G., & Bosbach, D. (2017). *Production and characterization of monodisperse uranium particles for nuclear safeguards applications*. Fachgruppe für Rohstoffe und Entsorgungstechnik.
- [25] Middendorp, R. (2018). *Synthesis and Stability Assessment of Uranium Microparticles: Providing Reference Materials for Nuclear Verification Purposes*. Nukleare Entsorgung und Reaktorsicherheit.
- [26] Neumeier, S., Middendorp, R., Knott, A., Dürr, M., Klinkenberg, M., Pointurier, F., Sanchez, D. F., Samson, V.-A., Grolimund, D., & Niemeyer, I. (2018). Microparticle production as reference materials for particle analysis methods in safeguards. *MRS Advances*, 3(19), 1005-1012.
- [27] Raptis, K., Ingelbrecht, C., Wellum, R., Alonso, A., De Bolle, W., & Perrin, R. (2002). The preparation of uranium-doped glass reference materials for environmental measurements. *Nuclear Instruments and Methods in Physics Research Section A: Accelerators, Spectrometers, Detectors and Associated Equipment*, 480(1), 40-43.
- [28] Kappel, S., Boulyga, S. F., & Prohaska, T. (2012). Direct uranium isotope ratio analysis of single micrometer-sized glass particles. *Journal of Environmental Radioactivity*, 113, 8-15.
- [29] Kips, R. (2008). *Development of uranium reference particles for nuclear safeguards and non-proliferation control*.
- [30] Kips, R., Leenaers, A., Tamborini, G., Betti, M., Van den Berghe, S., Wellum, R., & Taylor, P. (2007). Characterization of Uranium Particles Produced by Hydrolysis of UF₆ Using SEM and SIMS. *Microscopy and Microanalysis*, 13(3), 156-164.
- [31] Kips, R., Kristo, M. J., Hutcheon, I. D., Wang, Z., Johnson, T. J., Gerlach, D. C., Amonette, J. E., Olsen, K. B., & Stefaniak, E. (2011). Measuring fluorine in uranium oxyfluoride particles using secondary ion mass spectrometry for nuclear forensics. *Proceedings in Radiochemistry*, 1(1), 7-11.
- [32] Kips, R., Pidduck, A. J., Houlton, M. R., Leenaers, A., Mace, J. D., Marie, O., Pointurier, F., Stefaniak, E. A., Taylor, P. D. P., Van den Berghe, S., Van Espen, P., Van Grieken, R., & Wellum, R. (2009). Determination of fluorine in uranium oxyfluoride particles as an indicator of particle age. *Spectrochimica Acta Part B: Atomic Spectroscopy*, 64(3), 199-207.
- [33] Pope, T. R., Arey, B. W., Zimmer, M. M., II, M., Bronikowski, M. G., Kuhne, W., Baldwin, A. T., Padilla-Cintron, C., Anheier, N. C., & Warner, M. G. (2019). Production of particle reference and quality control materials. *ESARDA*, 29.
- [34] Bergin, R. A., Swindle, A. R., Naes, B. E., Tenner, T. J., Mayberry, D., Pope, T., Stene, R., & Scott, S. M. (2023). *R&D Outcomes of Surrogate Environmental Swipe Manufacturing Technique Method Development for Arms Control and Treaty Verification Applications*. <https://www.osti.gov/biblio/2202359>
- [35] Trillaud, V., Maynadié, J., Manaud, J., Hidalgo, J., Meyer, D., Podor, R., Dacheux, N., & Clavier, N. (2018). Synthesis of size-controlled UO₂ microspheres from the hydrothermal conversion of U(IV) aspartate [10.1039/C8CE01352G]. *CrystEngComm*, 20(48), 7749-7760.
- [36] Manaud, J., Maynadié, J., Mesbah, A., Hunault, M. O. J. Y., Martin, P. M., Zunino, M., Meyer, D., Dacheux, N., & Clavier, N. (2020). Hydrothermal Conversion of Uranium(IV) Oxalate into Oxides: A Comprehensive Study. *Inorganic Chemistry*, 59(5), 3260-3273.
- [37] Asplanato, P., Zannouh, W., Fauré, A. L., Imbert, P. H., Lautru, J., Cornaton, M., Dacheux, N., Pointurier, F., & Clavier, N. (2023). Hydrothermal synthesis of homogenous and size-controlled uranium-thorium oxide micro-particles for nuclear safeguards. *Journal of Nuclear Materials*, 573, 154142.
- [38] Tushingham, J. (1998). *The Preparation for a Low-enriched Uranium Particle Standard for Environmental Analysis*. AEA Technology.

- [39] Erdmann, N., Betti, M., Stetzer, O., Tamborini, G., Kratz, J. V., Trautmann, N., & van Geel, J. (2000). Production of monodisperse uranium oxide particles and their characterization by scanning electron microscopy and secondary ion mass spectrometry. *Spectrochimica Acta Part B: Atomic Spectroscopy*, 55(10), 1565-1575.
- [40] Stetzer, O., Betti, M., van Geel, J., Erdmann, N., Kratz, J.-V., Schenkel, R., & Trautmann, N. (2004). Determination of the ²³⁵U content in uranium oxide particles by fission track analysis. *Nuclear Instruments and Methods in Physics Research Section A: Accelerators, Spectrometers, Detectors and Associated Equipment*, 525(3), 582-592.
- [41] Ranebo, Y., Niagolova, N., Erdmann, N., Eriksson, M., Tamborini, G., & Betti, M. (2010). Production and Characterization of Monodisperse Plutonium, Uranium, and Mixed Uranium–Plutonium Particles for Nuclear Safeguard Applications. *Analytical Chemistry*, 82(10), 4055-4062.
- [42] Kraiem, M., Richter, S., Erdmann, N., Kühn, H., Hedberg, M., & Aregbe, Y. (2012). Characterizing uranium oxide reference particles for isotopic abundances and uranium mass by single particle isotope dilution mass spectrometry. *Analytica Chimica Acta*, 748, 37-44.
- [43] Ould-Dada, Z., Shaw, G., & Kinnersley, R. (2003). Production of radioactive particles for use in environmental studies. *Journal of Environmental Radioactivity*, 70(3), 177-191.
- [44] Park, Y. J., Lee, M. H., Pyo, H. Y., Kim, H. A., Sohn, S. C., Jee, K. Y., & Kim, W. H. (2005). The preparation of uranium-adsorbed silica particles as a reference material for the fission track analysis. *Nuclear Instruments and Methods in Physics Research Section A: Accelerators, Spectrometers, Detectors and Associated Equipment*, 545(1), 493-502.
- [45] Middendorp, R., Dürr, M., Knott, A., Pointurier, F., Ferreira Sanchez, D., Samson, V., & Grolimund, D. (2017). Characterization of the Aerosol-Based Synthesis of Uranium Particles as a Potential Reference Material for Microanalytical Methods. *Analytical Chemistry*, 89(8), 4721-4728.
- [46] Middendorp, R., Dürr, M., & Bosbach, D. (2016). The Stability of Uranium Microspheres for Future Application as Reference Standard in Analytical Measurements. *Procedia Chemistry*, 21, 285-292.
- [47] Middendorp, R., Klinkenberg, M., & Dürr, M. (2018). Uranium oxide microparticle suspensions for the production of reference materials for micro-analytical methods. *Journal of Radioanalytical and Nuclear Chemistry*, 318(2), 907-914.
- [48] Kegler, P., Pointurier, F., Rothe, J., Dardenne, K., Vitova, T., Beck, A., Hammerich, S., Potts, S., Faure, A.-L., & Klinkenberg, M. (2021). Chemical and structural investigations on uranium oxide-based microparticles as reference materials for analytical measurements. *MRS Advances*, 6(4), 125-130.
- [49] Potts, S. K., Kegler, P., Hammerich, S., Klinkenberg, M., Niemeyer, I., Bosbach, D., & Neumeier, S. (2022). Long-term stability of uranium-oxide-based microparticle reference materials: Shelf-life in alcoholic suspension and storage media. *MRS Advances*, 7(7), 134-139.
- [50] Deegan, R. D., Bakajin, O., Dupont, T. F., Huber, G., Nagel, S. R., & Witten, T. A. (2000). Contact line deposits in an evaporating drop. *Physical Review E*, 62(1), 756-765.
- [51] Jain, S., Skamser, D. J., & Kodas, T. T. (1997). Morphology of Single-Component Particles Produced by Spray Pyrolysis. *Aerosol Science and Technology*, 27(5), 575-590.
- [52] Kozlova, R. D., Matyukha, V. A., & Dedov, N. V. (2007). Mechanism and kinetics of thermal decomposition of uranyl nitrate hexahydrate under the nonisothermal conditions. *Radiochemistry*, 49(2), 130-134.
- [53] Stefaniak, E. A., Pointurier, F., Marie, O., Truyens, J., & Aregbe, Y. (2014). In-SEM Raman microspectroscopy coupled with EDX – a case study of uranium reference particles [10.1039/C3AN01872E]. *Analyst*, 139(3), 668-675.
- [54] Lin, D. H. M., Manara, D., Varga, Z., Berlizov, A., Fanghänel, T., & Mayer, K. (2013). Applicability of Raman spectroscopy as a tool in nuclear forensics for analysis of uranium ore concentrates. *Radiochimica Acta*, 101(12), 779-784.
- [55] Popa, K., Prieur, D., Manara, D., Naji, M., Vigier, J.-F., Martin, P. M., Dieste Blanco, O., Scheinost, A. C., Prüßmann, T., Vitova, T., Raison, P. E., Somers, J., & Konings, R. J. M. (2016). Further insights into the chemistry of the Bi–U–O system [10.1039/C6DT00735J]. *Dalton Transactions*, 45(18), 7847-7855.

- [56] Vitova, T., Pidchenko, I., Fellhauer, D., Bagus, P. S., Joly, Y., Pruessmann, T., Bahl, S., Gonzalez-Robles, E., Rothe, J., Altmaier, M., Denecke, M. A., & Geckeis, H. (2017). The role of the 5f valence orbitals of early actinides in chemical bonding. *Nature Communications*, 8(1), 16053.
- [57] Wood, S. H., & Prather, K. A. (1998). Time-of-flight mass spectrometry methods for real time analysis of individual aerosol particles. *TRAC Trends in Analytical Chemistry*, 17(6), 346-356.
- [58] Prather, K. A., Nordmeyer, T., & Salt, K. (1994). Real-time characterization of individual aerosol particles using time-of-flight mass spectrometry. *Analytical Chemistry*, 66(9), 1403-1407.
- [59] Weiss, M., Verheijen, P. J. T., Marijnissen, J. C. M., & Scarlett, B. (1997). On the performance of an on-line time-of-flight mass spectrometer for aerosols. *Journal of Aerosol Science*, 28(1), 159-171.
- [60] Hinz, K.-P., Kaufmann, R., & Spengler, B. (1994). Laser-induced mass analysis of single particles in the airborne state. *Analytical Chemistry*, 66(13), 2071-2076.
- [61] Carson, P. G., Neubauer, K. R., Johnston, M. V., & Wexler, A. S. (1995). On-line chemical analysis of aerosols by rapid single-particle mass spectrometry. *Journal of Aerosol Science*, 26(4), 535-545.
- [62] Murphy, D. M., & Thomson, D. S. (1995). Laser Ionization Mass Spectroscopy of Single Aerosol Particles. *Aerosol Science and Technology*, 22(3), 237-249.
- [63] Yang, M., Dale, J. M., Whitten, W. B., & Ramsey, J. M. (1995). Laser desorption mass spectrometry of a levitated single microparticle in a quadrupole ion trap. *Analytical Chemistry*, 67(6), 1021-1025.
- [64] Esaka, K. T., Esaka, F., Inagawa, J., Iguchi, K., Lee, C.-G., Sakurai, S., Watanabe, K., & Usuda, S. (2004). Application of Fission Track Technique for the Analysis of Individual Particles Containing Uranium in Safeguard Swipe Samples. *Japanese Journal of Applied Physics*, 43(7A), L915.
- [65] Lee, M. H., Douglas, M., & Clark, S. B. (2005). Development of in situ fission track analysis for detecting fissile nuclides in contaminated solid particles. *Radiation Measurements*, 40(1), 37-42.
- [66] Lee, C. G., Iguchi, K., Inagawa, J., Suzuki, D., Esaka, F., Magara, M., Sakurai, S., Watanabe, K., & Usuda, S. (2007). Development in fission track-thermal ionization mass spectrometry for particle analysis of safeguards environmental samples. *Journal of Radioanalytical and Nuclear Chemistry*, 272(2), 299-302.
- [67] Park, Y. J., Song, K., Pyo, H. Y., Lee, M. H., Jee, K. Y., & Kim, W. H. (2006). Investigation on the fission track analysis of uranium-doped particles for the screening of safeguards environmental samples. *Nuclear Instruments and Methods in Physics Research Section A: Accelerators, Spectrometers, Detectors and Associated Equipment*, 557(2), 657-663.
- [68] Wimpenny, J., & Samperton, K. (2021). *Characterization of U Isotope Ratios by Laser Ablation MC-ICP-MS for IAEA Safeguards*. <https://www.osti.gov/biblio/1893591>
- [69] Godoy, M. L. D. P., Godoy, J. M., Roldão, L. A., & Tauhata, L. (2009). Determination of total content and isotopic compositions of plutonium and uranium in environmental samples for safeguards purposes by ICP-QMS. *Journal of Environmental Radioactivity*, 100(8), 613-625.
- [70] Marin, R. C., Sarkis, J. E. S., & Nascimento, M. R. L. (2013). The use of LA-SF-ICP-MS for nuclear forensics purposes: uranium isotope ratio analysis. *Journal of Radioanalytical and Nuclear Chemistry*, 295(1), 99-104.
- [71] Baxter, D. C., Rodushkin, I., & Engström, E. (2012). Isotope abundance ratio measurements by inductively coupled plasma-sector field mass spectrometry [10.1039/C2JA30153A]. *Journal of Analytical Atomic Spectrometry*, 27(9), 1355-1381.
- [72] Bürger, S., Riciputi, L. R., Bostick, D. A., Turgeon, S., McBay, E. H., & Lavelle, M. (2009). Isotope ratio analysis of actinides, fission products, and geolocators by high-efficiency multi-collector thermal ionization mass spectrometry. *International Journal of Mass Spectrometry*, 286(2), 70-82.
- [73] Jakopič, R., Richter, S., Kühn, H., Benedik, L., Pihlar, B., & Aregbe, Y. (2009). Isotope ratio measurements of pg-size plutonium samples using TIMS in combination with “multiple ion

- counting” and filament carburization. *International Journal of Mass Spectrometry*, 279(2), 87-92.
- [74] Kraiem, M., Richter, S., Kühn, H., Stefaniak, E. A., Kerckhove, G., Truyens, J., & Aregbe, Y. (2011). Investigation of Uranium Isotopic Signatures in Real-Life Particles from a Nuclear Facility by Thermal Ionization Mass Spectrometry. *Analytical Chemistry*, 83(8), 3011-3016.
- [75] Kyuseok, S., Jong-Ho, P., Chi-Gyu, L., & Sun-Ho, H. (2016). Recent Developments in Nuclear Forensic and Nuclear Safeguards Analysis Using Mass Spectrometry. *Mass Spectrometry Letters*, 7(2), 31-40.
- [76] Tamborini, G., Betti, M., Forcina, V., Hiernaut, T., Giovannone, B., & Koch, L. (1998). Application of secondary ion mass spectrometry to the identification of single particles of uranium and their isotopic measurement. *Spectrochimica Acta Part B: Atomic Spectroscopy*, 53(9), 1289-1302.
- [77] Betti, M., Tamborini, G., & Koch, L. (1999). Use of Secondary Ion Mass Spectrometry in Nuclear Forensic Analysis for the Characterization of Plutonium and Highly Enriched Uranium Particles. *Analytical Chemistry*, 71(14), 2616-2622.
- [78] Tamborini, G., & Betti, M. (2000). Characterisation of Radioactive Particles by SIMS. *Microchimica Acta*, 132(2), 411-417.
- [79] Stoffel, J. J., Briant, J. K., & Simons, D. S. (1994). A particulate isotopic standard of uranium and plutonium in an aluminosilicate matrix. *Journal of the American Society for Mass Spectrometry*, 5(9), 852-858.
- [80] Esaka, F., & Magara, M. (2014). Secondary ion mass spectrometry combined with alpha track detection for isotope abundance ratio analysis of individual uranium-bearing particles. *Talanta*, 120, 349-354.
- [81] Ranebo, Y., Eriksson, M., Tamborini, G., Niagolova, N., Bildstein, O., & Betti, M. (2007). The Use of SIMS and SEM for the Characterization of Individual Particles with a Matrix Originating from a Nuclear Weapon. *Microscopy and Microanalysis*, 13(3), 179-190.
- [82] Pointurier, F., Pottin, A.-C., & Hubert, A. (2011). Application of Nanosecond-UV Laser Ablation–Inductively Coupled Plasma Mass Spectrometry for the Isotopic Analysis of Single Submicrometer-Size Uranium Particles. *Analytical Chemistry*, 83(20), 7841-7848.
- [83] Simons, D., Gillen, J., Zeissler, C., Fleming, R., & McNitt, P. (1998). Automated SIMS for Determining Isotopic Distributions in Particle Polutations. In: Wiley, Hoboken, NJ.
- [84] de Chambost, E. (2011). Chapter 1 - A History of Cameca (1954–2009). In P. W. Hawkes (Ed.), *Advances in Imaging and Electron Physics* (Vol. 167, pp. 1-119). Elsevier.
- [85] Hedberg, P. M. L., Peres, P., Cliff, J. B., Rabemananjara, F., Littmann, S., Thiele, H., Vincent, C., & Albert, N. (2011). Improved particle location and isotopic screening measurements of sub-micron sized particles by Secondary Ion Mass Spectrometry [10.1039/C0JA00181C]. *Journal of Analytical Atomic Spectrometry*, 26(2), 406-413.
- [86] Peres, P., Hedberg, P., Walton, S., Montgomery, N., Cliff, J., Rabemananjara, F., & Schuhmacher, M. (2013). Nuclear safeguards applications using LG-SIMS with automated screening capabilities. *Surface and Interface Analysis*, 45(1), 561-565.
- [87] Poths, J., Sangely, L., Bildstein, O., Kitao, T., Schwanhäusser, A., Hosoya, M., & Tanpraphan, T. (2011). Improved Uranium Particle Analysis Using Large-geometry SIMS–Proceedings 33rd ESARDA Conference. In: Budapest.
- [88] Groopman, E. E., Williamson, T. L., & Simons, D. S. (2022). Improved uranium particle analysis by SIMS using O3– primary ions [10.1039/D2JA00231K]. *Journal of Analytical Atomic Spectrometry*, 37(10), 2089-2102.
- [89] Truyens, J., Stefaniak, E. A., & Aregbe, Y. (2013). NUSIMEP-7: uranium isotope amount ratios in uranium particles. *Journal of Environmental Radioactivity*, 125, 50-55.
- [90] NBL. (2008). Certificate of Analysis CRM 129-A. In.
- [91] Dorais, C., Simonetti, A., Corcoran, L., Spano, T. L., & Burns, P. C. (2020). Happy Jack Uraninite: A new reference material for high spatial resolution analysis of U-rich matrices. *Geostandards and Geoanalytical Research*, 44(1), 125-132.
- [92] Zhou, L., Riegler, T., Bonnetti, C., McClenaghan, S., & Kamber, B. (2022). Revisiting the Happy Jack Uraninite Reference Material: A Combined Electron Beam and Laser Ablation In Situ Study. *Geostandards and Geoanalytical Research*, 46(4), 735-749.

- [93] Neumeier, S., Kegler, P., Potts, S., Richter, S., Hammerich, S., Zoriy, M., Hexel, C., Manard, B., Schmitt, A., Trieloff, M., Bosbach, D., & Niemeyer, I. (2024). Production of Uranium Oxide-based Reference Microparticles at FZJ – Current Status and New Developments. INMM – 65th Annual Meeting, Portland, Oregon.
- [94] Neumeier, S., Kegler, P., Richter, S., Hammerich, S., Zoriy, M., Hexel, C., Manard, B., Schmitt, A., Trieloff, M., & Potts, S. (2023). Production and analyses of uranium oxide microparticulate reference standards: current status and outlook. Proceedings of the INMM & ESARDA—joint annual meeting, Vienna/Austria.
- [95] Richter, S., Hennessy, C., Truyens, J., Jacobsson, U., Venchiarutti, C., Bujak, R., & Aregbe, Y. (2024). 50 Years of uranium isotopic reference materials at JRC-Geel. *Journal of Radioanalytical and Nuclear Chemistry*, 333(2), 825-840.
- [96] Esaka, F., Watanabe, K., Fukuyama, H., Onodera, T., Esaka, K. T., Magara, M., Sakurai, S., & Usuda, S. (2004). Efficient Isotope Ratio Analysis of Uranium Particles in Swipe Samples by Total-Reflection X-ray Fluorescence Spectrometry and Secondary Ion Mass Spectrometry. *Journal of Nuclear Science and Technology*, 41(11), 1027-1032.
- [97] HIP. (2022, 04.02.2022). *Cameca IMS 1280-HR*. Retrieved 11.08.2024 from https://www.geow.uni-heidelberg.de/HIP/cameca_en.html
- [98] de Jonge, N., Lamy, Y., Schoots, K., & Oosterkamp, T. H. (2002). High brightness electron beam from a multi-walled carbon nanotube. *Nature*, 420(6914), 393-395.
- [99] Houdellier, F., de Knoop, L., Gatel, C., Masseboeuf, A., Mamishin, S., Taniguchi, Y., Delmas, M., Monthieux, M., Hÿtch, M. J., & Snoeck, E. (2015). Development of TEM and SEM high brightness electron guns using cold-field emission from a carbon nanotip. *Ultramicroscopy*, 151, 107-115.
- [100] Collins, T. J. (2007). ImageJ for Microscopy. *BioTechniques*, 43(sup1), S25-S30.
- [101] Wojdyr, M. (2010). Fityk: a general-purpose peak fitting program. *Journal of Applied Crystallography*, 43(5 Part 1), 1126-1128.
- [102] Coakley, K. J., Simons, D. S., & Leifer, A. M. (2005). Secondary ion mass spectrometry measurements of isotopic ratios: correction for time varying count rate. *International Journal of Mass Spectrometry*, 240(2), 107-120.
- [103] Cutter, A., Hunter, K., Paterson, P., & Stresau, R. (1994). The “aging” mechanism in electron multipliers and operating life. 42nd ASMS Conference on Mass Spectroscopy and Allied Topics, Chicago, Illinois.
- [104] Hoffmann, D. L., Richards, D. A., Elliott, T. R., Smart, P. L., Coath, C. D., & Hawkesworth, C. J. (2005). Characterisation of secondary electron multiplier nonlinearity using MC-ICPMS. *International Journal of Mass Spectrometry*, 244(2), 97-108.
- [105] Potts, S. K., Kegler, P., Modolo, G., Hammerich, S., Niemeyer, I., Bosbach, D., & Neumeier, S. (2022). Structural incorporation of lanthanides (La, Eu, and Lu) into U₃O₈ as a function of the ionic radius. *MRS Advances*, 7(7), 128-133.
- [106] Scott, S., Naes, B., Christian, J., Foley, B., Tenner, T., Kuhne, W., Wurth, K., Shehee, T., Lawson, S., & Ajo, H. (2023). New Particle Working Standards for NWAL Particle Laboratory Calibration and Quality Control-Operational Engineering for an Aerosol-Based Production Platform for the Synthesis of Plutonium-Containing Reference Particulate Materials. Proc. INMM & ESARDA-Joint Annual Meeting, Vienna.
- [107] Aregbe, Y., Richter, S., Hexel, C., Venchiarutti, C., & Hennessy, C. (2021). Preparation and Certification of Highly Enriched Uranium Nitrate Solutions IRMM-3000 Series.
- [108] BIPM, I., IFCC, ILAC, ISO, IUPAC, IUPAP, and OIML. (2008). *Evaluation of measurement data — Guide to the expression of uncertainty in measurement*. Joint Committee for Guides in Metrology, JCGM 100:2008.
- [109] Mishra, P., Singh, U., Pandey, C. M., Mishra, P., & Pandey, G. (2019). Application of Student's t-test, Analysis of Variance, and Covariance. *Annals of Cardiac Anaesthesia*, 22(4).
- [110] Sattonnay, G., Ardois, C., Corbel, C., Lucchini, J. F., Barthe, M. F., Garrido, F., & Gosset, D. (2001). Alpha-radiolysis effects on UO₂ alteration in water. *Journal of Nuclear Materials*, 288(1), 11-19.
- [111] Kegler, P., Potts, S., Hammerich, S., Niemeyer, I., Bosbach, D., & Neumeier, S. (2024). Long-term Experiments for the Determination of the Influence of Storage Media and Storage

- Conditions on the Alteration of Uranium Oxide Microparticle Reference Materials to Identify Optimal Storage Conditions. INMM – 65th Annual Meeting, Portland, Oregon.
- [112] Miskowicz, A., Niedziela, J. L., Spano, T. L., Ambrogio, M. W., Finkeldei, S., Hunt, R., & Shields, A. E. (2019). Additional complexity in the Raman spectra of U₃O₈. *Journal of Nuclear Materials*, 527, 151790.
- [113] Sweet, L. E., Blake, T. A., Henager, C. H., Hu, S., Johnson, T. J., Meier, D. E., Peper, S. M., & Schwantes, J. M. (2013). Investigation of the polymorphs and hydrolysis of uranium trioxide. *Journal of Radioanalytical and Nuclear Chemistry*, 296(1), 105-110.
- [114] Berlizov, A., Ho, D., Nicholl, A., Fanghänel, T., & Mayer, K. (2016). MRS Advances Assessing hand-held Raman spectrometer FirstDefender RM for nuclear safeguards applications. *Journal of Radioanalytical and Nuclear Chemistry*, 307(1), 285-295.
- [115] Lipp, M., Jenei, Z., Park-Klepeis, J., & Evans, W. (2011). Raman investigation of the uranium compounds U₃O₈, UF₄, UH₃ and UO₃ under pressure at room temperature.
- [116] Desgranges, L., Baldinozzi, G., Simon, P., Guimbretière, G., & Canizares, A. (2012). Raman spectrum of U₄O₉: a new interpretation of damage lines in UO₂. *Journal of Raman Spectroscopy*, 43(3), 455-458.
- [117] Frost, R. L., Čejka, J., & Weier, M. L. (2007). Raman spectroscopic study of the uranyl oxyhydroxide hydrates: becquerelite, billietite, curite, schoepite and vandendriesscheite. *Journal of Raman Spectroscopy: An International Journal for Original Work in all Aspects of Raman Spectroscopy, Including Higher Order Processes, and also Brillouin and Rayleigh Scattering*, 38(4), 460-466.
- [118] Lin, D. H. M., Manara, D., Lindqvist-Reis, P., Fanghänel, T., & Mayer, K. (2014). The use of different dispersive Raman spectrometers for the analysis of uranium compounds. *Vibrational Spectroscopy*, 73, 102-110.
- [119] Pointurier, F., & Marie, O. (2010). Identification of the chemical forms of uranium compounds in micrometer-size particles by means of micro-Raman spectrometry and scanning electron microscope. *Spectrochimica Acta Part B: Atomic Spectroscopy*, 65(9-10), 797-804.
- [120] Pointurier, F., Lin, D. H. M., Manara, D., Marie, O., Fanghänel, T., & Mayer, K. (2019). Capabilities of micro-Raman spectrometry for the identification of uranium ore concentrates from analysis of single particles. *Vibrational Spectroscopy*, 103, 102925.
- [121] Burns, P. C., & Hughes, K.-A. (2003). Studtite, [(UO₂)(O₂)(H₂O)₂](H₂O)₂: The first structure of a peroxide mineral. *American Mineralogist*, 88(7), 1165-1168.
- [122] Sheldrick, G. (1997). SHELXL-97. *Program for crystal structure refinement*.
- [123] Schlegel, M. L., & Jegou, C. (2022). Uraninite alteration by H₂O₂ solutions and formation of secondary phases: An in situ microRaman spectroscopy and synchrotron X-ray diffraction study. *Journal of Nuclear Materials*, 572, 154056.
- [124] Guimbretière, G., Canizares, A., Simon, P., Tobon-Correa, Y. A., Ammar, M. R., Corbel, C., & Barthe, M. F. (2011). In-Situ Raman Observation of the First Step of Uranium Dioxide Weathering Exposed to Water Radiolysis. *Spectroscopy Letters*, 44(7-8), 570-573.
- [125] Canizarès, A., Guimbretière, G., Tobon, Y., Raimboux, N., Omnée, R., Perdicakis, M., Muzeau, B., Leoni, E., Alam, M. S., & Mendes, E. (2012). In situ Raman monitoring of materials under irradiation: study of uranium dioxide alteration by water radiolysis. *Journal of Raman Spectroscopy*, 43(10), 1492-1497.
- [126] Forbes, T. Z., Horan, P., Devine, T., McInnis, D., & Burns, P. C. (2011). Alteration of dehydrated schoepite and soddyite to studtite, [(UO₂)(O₂)(H₂O)₂](H₂O)₂. *American Mineralogist*, 96(1), 202-206.
- [127] Tuschel, D. (2016). Selecting an excitation wavelength for Raman spectroscopy.
- [128] Venchiarutti, C., Richter, S., Middendorp, R., & Aregbe, Y. (2019). NUSIMEP-9: Uranium isotope amount ratios and uranium mass in uranium micro-particles. *Publications Office of the European Union, Luxembourg*.
- [129] Richter, S., Truyens, J., Venchiarutti, C., Aregbe, Y., Middendorp, R., Neumeier, S., Kegler, P., Klinkenberg, M., Zoriy, M., & Stadelmann, G. (2022). Certification of the First Uranium Oxide micro-particle reference materials for Nuclear Safety and Security, IRMM-2329P and IRMM-2331P. *Journal of Radioanalytical and Nuclear Chemistry*, 1-5.

-
- [130] Canosa, J., Rodríguez, A., & Tojo, J. (1998). Dynamic Viscosities of (Methyl Acetate or Methanol) with (Ethanol, 1-Propanol, 2-Propanol, 1-Butanol, and 2-Butanol) at 298.15 K. *Journal of Chemical & Engineering Data*, 43(3), 417-421.
- [131] Sharp, N., Fassett, J. D., & Simons, D. S. (2016). Uranium ion yields from monodisperse uranium oxide particles. *Journal of Vacuum Science & Technology B*, 34(3).
- [132] Williamson, T., Simons, D. S., & Fassett, J. D. (2021). MULTI-COLLECTOR CONFIGURATION CONSIDERATIONS AND SUBSTRATE RELATIVE SENSITIVITY FACTOR EFFECTS FOR AGE-DATING MEASUREMENTS OF PARTICLES BY LARGE GEOMETRY SECONDARY ION MASS SPECTROMETRY.